Nanoporous Materials from ABAC Tetrablock Terpolymers

A DISSERTATION
SUBMITTED TO THE FACULTY OF THE GRADUATE SCHOOL
OF THE UNIVERSITY OF MINNESOTA
BY

Elizabeth Ashley Jackson

IN PARTIAL FULFILLMENT OF THE REQUIREMENTS
FOR THE DEGREE OF

Doctor of Philosophy

Marc A. Hillmyer, Advisor

July, 2013

Acknowledgements

I would like to thank all of the many people who have supported and encouraged throughout my academic career. I am thankful for all of the professors and teachers who have shared their passion and knowledge with me. I am especially grateful to my advisor Marc Hillmyer for his encouragement, patient guidance and his contagious passion for polymer chemistry. I am grateful for all of the helpful criticism that has allowed me to improve both as a scientist and as a person over the past few years.

I owe many thanks to the polymer group for their mentoring, advice and helpful conversations during my time at the University of Minnesota. First, I would like to thank my co-conspirator, Youngmin Lee, for being a great teammate on parts of this project. I am grateful for his advice, encouragement and friendship. I am grateful to Adam Meuler and Mike Bluemle for sharing their extensive knowledge on multiblock terpolymers. I am grateful to Mark Amendt, Louis Pitet and William Phillip for their helpful advice related to nanoporous materials. I am grateful to Marc Rodwogin for teaching me anionic synthesis. I am also thankful to the following group members for helpful advice and conversations: Andrew Baruth, Ligeng Yin, Mark Martello, Grayce Theryo, Josh Speros, Ben Hamilton, Justin

Kennemur, Morgan Schulze, Paula Delgado, Henry Martinez, Arthur Bertrand, Jingwen Zhang, Ameara Mansour, and Guillermo Alfonzo.

I would also like to thank the helpful and talented staff in the UMN characterization facility. Specifically I would like to thank Chris Frethem, Bob Hafner, Greg Haugstad and Fang Zhou for all of their assistance in imaging polymer samples. Also, I am grateful for the opportunity to work in the coatings lab of Dr. Lorraine Francis. I appreciate the help and guidance provided by her and also Dr. Wieslaw Suszynski. I am also grateful for the collaboration and funding from the Pall Corporation. I received plenty of helpful guidance related to filtration membranes and gained industrial experience working the scientists at Pall.

Dedication

To my family.

Abstract

This dissertation describes efforts towards the preparation of tough nanoporous membranes from ABAC tetrablock terpolymers. This architecture was strategically chosen to combine an etchable C block, PLA, with a mechanically tough ABA triblock into one ABAC terpolymer. Multiple series of poly(styrene-*b*-isoprene-*b*-styrene-*b*-lactide) (PS-PI-PS-PLA) tetrablock terpolymers were synthesized. Morphological behavior was characterized for terpolymers containing both a 50:50 and 30:70 PS:PI ratio with between 0 and ~20% PLA by volume. Observed bulk morphologies include hexagonally packed cylinders (HEX), core(PLA)-shell(PS) cylinders (CSC), and a PLA sphere in cylinder morphology. Mechanical properties of PS-PEEP-PS-PLA tetrablocks were also investigated. All materials exhibited mechanical properties characteristic of tough thermoplastic elastomers.

Composite membranes were prepared from a thin film of PS-PI-PS-PLA terpolymer and a macroporous polyethersulfone support. Described within are the efforts related to the fabrication and filtration performance of these nanoporous PS-PI-PS composite membranes. As part of this process, solvent casting and annealing conditions were varied to investigate effects on tetrablock thin film morphology. Optimum conditions were determined to achieve PS-PI-PS-PLA films with perpendicular PLA cylinder orientation. These conditions included use of a mixed solvent system and the addition of a small amount of homopolymer PLA. Highly ordered films with vertically oriented nanopores were obtained.

Table of Contents

List of Tables

List of Figures

Chapter 1

Chapter 2

Chapter 3

Chapter 4

Appendix A

List of Schemes

Chapter 1

Introduction to Nanoporous Materials from Ordered Block Polymers*

* Portions of this chapter were modified from Jackson, E. A.; Hillmyer, M. A. *ACS Nano*, **2010**, *4*, 3548-3553.

1.1 Introduction

Materials that contain small voids up to 100 nm in size are generally referred to as "nanoporous".[1] Numerous technologies have benefitted from the incorporation of nanoporous materials. Catalysis, controlled separations, drug delivery, templating and nanoparticles are just some technologies whose successes are due mostly to the nanoporous materials employed.[2] This is due in part to the nanoscale feature sizes but also to the enhanced properties and physical phenomena that occur in the nanosize range (<100 nm). Nanoporous materials have been prepared from organic, polymeric, and inorganic systems.[2] Some commercial nanoporous materials have been inspired by nature, such as biological nanopores or nanochannels.[3,4,5]

Polymeric materials have found increasing utility in applications where inorganic and others have fallen short. Filtration and liquid chromatography are just some technological arenas in which the utility of nanoporous polymeric materials has outshined inorganic materials.[2] Also, nanolithography of polymeric materials has meant tremendous success for semiconductors, microelectromechanical system (MEMS) devices and advancements in many other nanolithography related applications.[6] In many of these applications, block polymers have been the leading workhorse material used to create nanoporous materials with ordered domains and controlled feature size.

Block copolymers are a class of fascinating, self-assembling soft materials that are composed of macromolecules with long, covalently connected segments

(blocks) of two or more distinct repeating units (**Figure 1.1**).[7] These hybrid molecules combine the physical attributes of the different polymer blocks and can form ordered structures with nanoscopic heterogeneities. Block copolymers have received much attention over the last five decades as property-enhancing additives, adhesives, and thermoplastic elastomers. Since the 1990s, the versatility of block copolymers has dramatically increased; many researchers have exploited the exquisite nanostructures formed in block copolymers for use in various advanced technologies.[8]

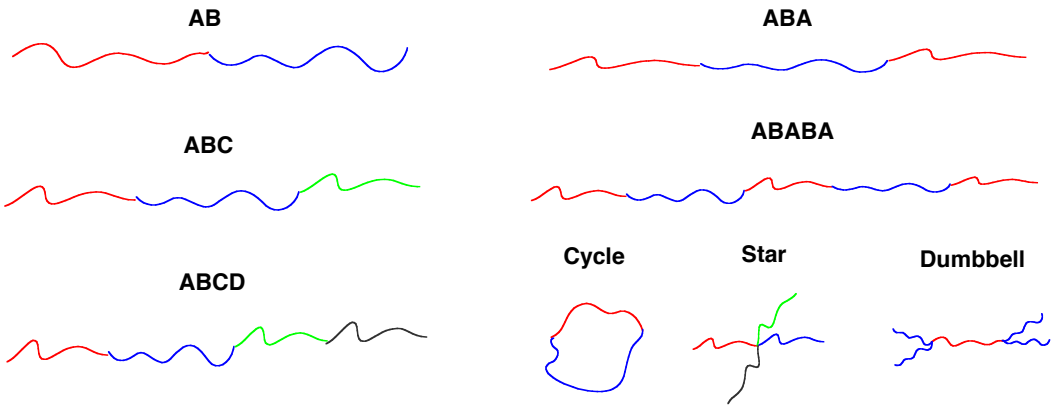

Figure 1.1. Block polymers with different number of blocks and architectures.

Effectively capitalizing on the technological capacity of block copolymers requires control of composition, molecular weight, and architecture. Nowadays, controlled polymerization methods provide access to virtually limitless chemical and architectural variety in block copolymers. Combining new synthetic methods with an understanding of phase behavior enables researchers to target a wide range of chemical, mechanical, thermal, optical, and electrical properties. The ultimate utility of block copolymers has been recognized for demanding, size-dependent

applications ranging from nanolithography to controlled drug delivery to energy applications.[8,9]

Nanoporous materials derived from block copolymers are being pursued as desirable materials for controlled separation membranes due to their pore-size tunability, narrow pore size distributions, and ability for selective functionalization. A block copolymer, which is made of at least one type of polymer covalently bonded to another polymer, can undergo microphase separation where the component blocks separate into distinct microdomains (for some examples, see **Figure 1.2**).[10] Nanoporous materials are made from selectively etching out one polymer block from a self-assembled block copolymer.[11,12,13,14] The self-assembly process of block polymers creates a narrow distribution of domain sizes. Removal of etchable domains can produce a porous membrane capable of highly selective filtration due to the narrow distribution of pore sizes.[11]

Nanoporous materials from block polymers are also attractive because of their tunable material properties. The chemical properties, mechanical properties, pore sizes and pore shapes can all be controlled to fit different applications. Control over innate material properties is accomplished by synthesizing block polymers with necessary block chemistries, block sizes and chain architectures. The basic factors that govern the process of self-assembly are discussed in **Section 1.2**.

1.2 Introduction to Block Polymers

1.2.1 AB Diblock Copolymers

The ability to make well-ordered structures through self-assembly is a central motivation for using block copolymers in nanoporous and membranes for applications including liquid and gas separations, catalysis and other nanofabrications.[10,15] Understanding of phase behavior is crucial to be able to synthesize well-ordered nanoporous materials. The following section will address some basics of block copolymer self-assembly.

To understand block copolymer microphase separation, a brief overview of homopolymer macrophase separation is first necessary. A mixture of homopolymer A and homopolymer B will macrophase separate to an extent governed by the Gibbs free energy of mixing of the two polymers.[10,16] In homopolymer A plus homopolymer B mixtures, the driving force that determines the degree to which blocks mix or segregate depends on both the enthalpic penalty for unlike polymers to mix and the entropic gain for the polymer chains to spread out into the least configurational entropy constrained conformation. The combination of these forces results in the free energy of mixing ΔG_{mix} for two homopolymers.[17] Equation 1.1 shows a basic relation between the enthalpy and entropy of mixing for two homopolymers, A and B:

$$\Delta G_{mix} = kT\left\{\frac{\phi_A}{N_A}\ln\phi_A + \frac{\phi_B}{N_B}\ln\phi_B + \chi\phi_A\phi_B\right\} \qquad \textbf{(1.1)}$$

In this equation, ϕ_A and ϕ_B represent the volume fractions of components A and B; and N_A and N_B represent the degree of polymerization for block A and block B. The first two terms in equation (1) represent the combinatorial entropy of mixing, ΔS_{mix}. Since ΔS_{mix} always favors mixing, the degree of segregation of the two polymers and therefore their resulting morphology depends on χ, ϕ_A and ϕ_B.[17] Mixing is enthalpically unfavorable when $\chi > 0$. This term represents the energetic price of placing one polymer "unit" (one polymerized monomer) into a pot of another polymer "units".[17]

Unlike an A/B homopolymer mixture, an AB diblock cannot macrophase separate due to the covalent bond linking the two blocks. Instead of macrophase separation, AB diblock copolymers microphase separate. The morphology that results from microphase separation comes from the block copolymers preference to minimize unfavorable surface energy at the interface between blocks but also minimize entropically unfavorable chain stretching.

The morphology adopted by block copolymers during self-assembly can be controlled synthetically by altering the size and components of the block copolymer (**Figure 1.2**).[16] The three main factors that govern phase behavior of block copolymers are the volume fractions, *f,* of each component block, the energetic interaction between the specific blocks, χ, and the degree of polymerization of the overall polymer, *N.*[16] The five observed equilibrium morphologies for AB diblocks are lamellar (LAM), cylinders (Cyl), spheres (S), gyroid (G) (**Figure 1.2)** and the orthorhombic O^{70} network (**Figure 1.3)**.[17,18]

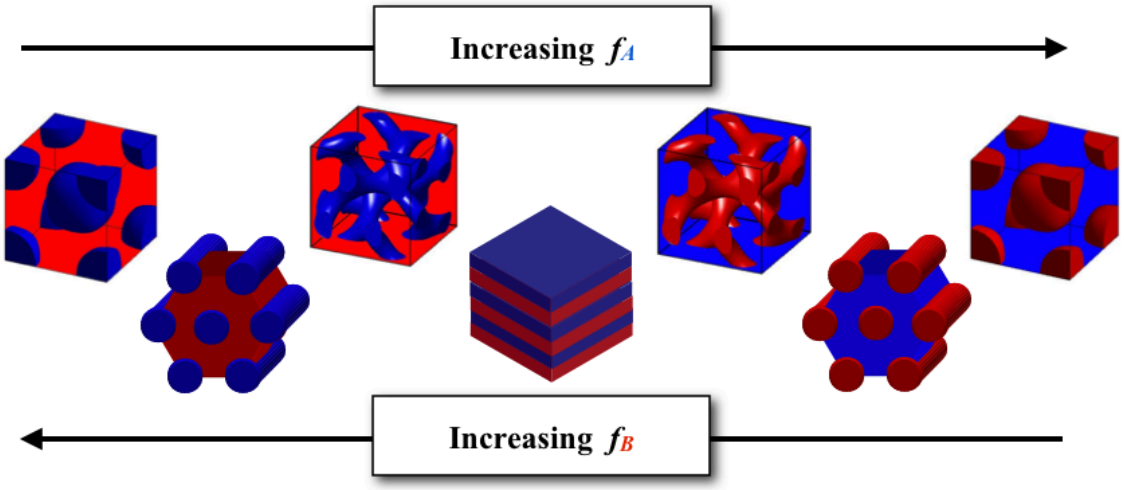

Figure 1.2. The drawings show experimentally observed equilibrium morphologies for AB diblock copolymers: spheres on a body-centered cubic lattice (BCC), hexagonal-packed cylinders, gyroid, and lamellar. Morphologies change upon increasing volume fraction of each component.

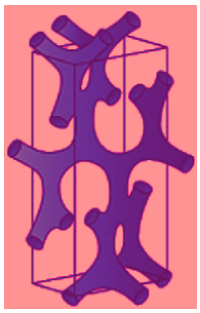

Figure 1.3. The O^{70} *Fddd* network phase for diblock copolymers. Image adapted from Reference 19.

Microphase separation of the blocks increases with increasing immiscibility, which is described by χ.[17] A disordered AB diblock can be forced to microphase separate by decreasing the temperature (Equation 1.2). Here $z\Delta w$ represents the combination of the number of nearest neighbor interactions (z) and the energy increment per polymer-polymer interaction (Δw).[17]

$$\chi = \frac{z\Delta w}{kT} \tag{1.2}$$

The degree of polymerization can also have a significant effect on the degree of segregation and order in self-assembled block copolymer.[16] Thermodynamics predicts that a larger degree of polymerization will result in a more ordered self-assembled structure because longer chains should require less energy to stretch than shorter chains.[20] However, kinetics limits the ordering process when the degree of polymerization becomes large. Large chains require more time to adopt favorable positions and conformations.[21]

1.2.2 ABA Triblock Copolymers

The simplest example of a physically cross-linkable block copolymer is the ABA triblock copolymer. ABA block copolymers, whose microphase separation is similar to that of AB block copolymers, exhibit physical cross-linking (**Figure 1.3**).[22] In ABA block copolymers the B block can serve as a bridge between two different A domains if the A chains each separate into different domains.[22] This is not possible in AB diblocks. This cross-linking can significantly enhance the mechanical properties compared with microphase separated AB block copolymers. ABA block copolymers are more resilient with increased elasticity than AB diblock copolymers.[26,24] The amount of cross-linking is limited though due to the looping of some chains back into the same domain (**Figure 1.4**).[23,24]

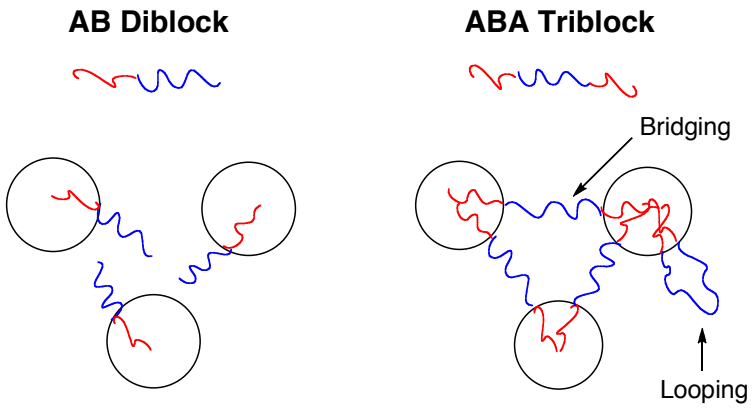

Figure 1.4. The AB, ABA block copolymers drawn here have different mechanical properties due to their block architecture. Red represents A blocks and blue represents B blocks. Circles represent generic domains such as spheres or cylinders.

A specific class of ABA block copolymers where the A component is glassy and the B component is rubbery are called thermoplastic elastomers. They exhibit the toughness and processability of thermoplastics with the resilience and elasticity common in vulcanized rubber.[22-26] These properties are apparent in ABA copolymers when the rubbery B blocks is surrounded by two glassy A blocks.[24,25,26] Combining a glassy polymer with a rubbery polymer into the ABA architecture can decrease brittleness compared to a glassy homopolymer and increase the toughness of the soft rubbery material.[24,25]

Some common commercially available ABA thermoplastic elastomers are poly(styrene-*b*-isoprene-*b*-styrene) (PS-PI-PS) and poly(styrene-*b*-butadiene-*b*-styrene) PS-PB-PS block copolymers. The PS-PI-PS "Kraton D" block copolymer is one example of a commercially available ABA thermoplastic elastomer.[27] This Kraton polymer, which contains about 40 % PS by volume, has a tensile strength of 28 MPa and can withstand greater than 1000 % elongation.

1.2.3 ABC Triblock Terpolymers

ABC terpolymers are attractive due to the additional functionality provided by the additional block and the diverse morphologies available with three blocks. ABC microphase separation depends on the similar enthalpic and entropic factors that govern AB copolymer self-assembly. Microphase separation of ABC terpolymers (**Figure 1.5**) is more complicated than AB copolymers due to the larger number of blocks and therefore larger number of phase behavior parameters to consider. Over 30 morphologies have been observed in ABC block terpolymers (**Figure 1.5**).[28,29,30] ABC and other more complicated systems are not as well understood but recent research has provided evidence for a diverse set of morphologies.[31]

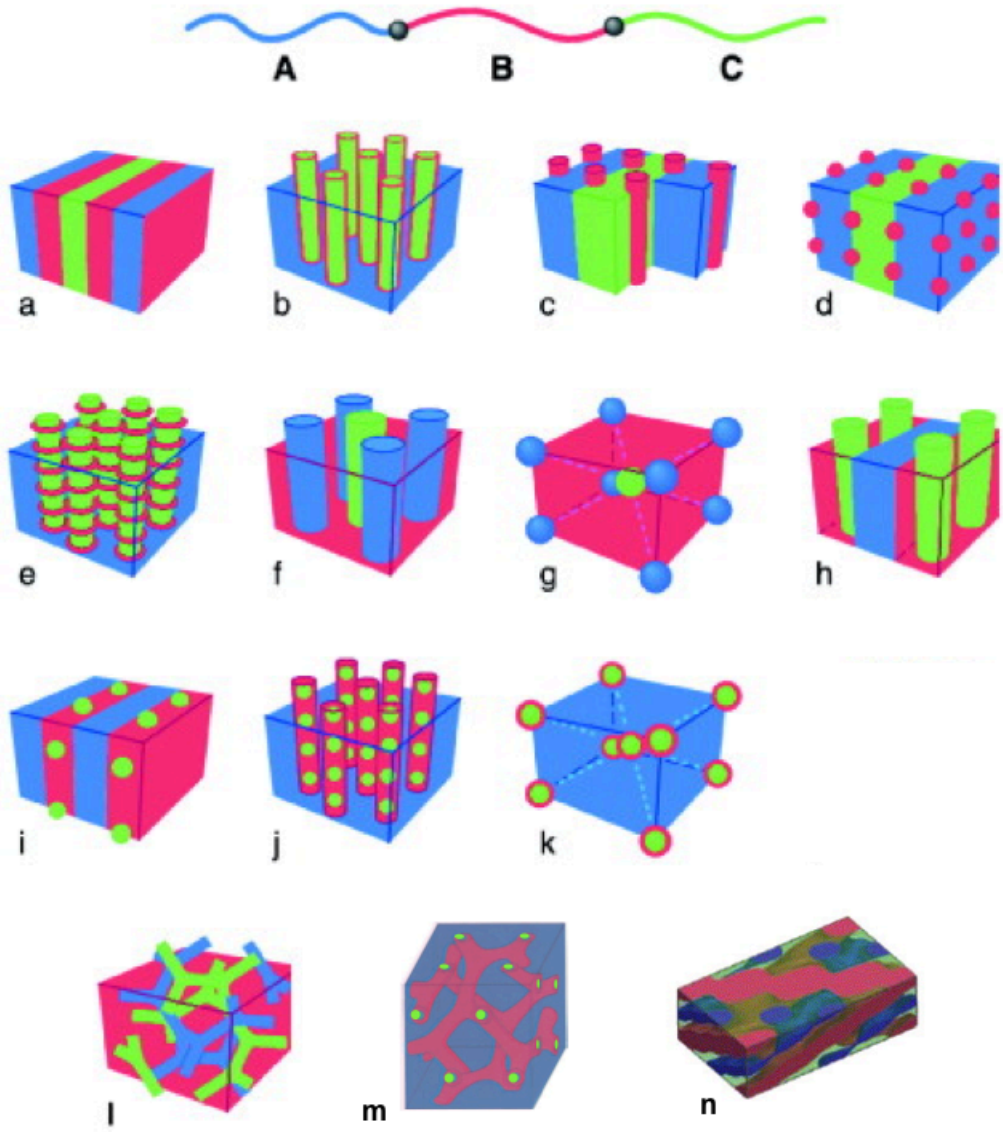

Figure 1.5. ABC terpolymer chain with subset of ABC morphologies: Three phase Lamella (LAM_3), a; core-shell cylinders (CSC), b; cylinders in lamellae, c; spheres in lamellae, d; cylinders with rings, e; alternating cylinders, f; alternating spheres, h; spheres in lamella, I; spheres in cylinders, j; core-shell spheres, k; alternating gyroid (Q^{214}), l; core-shell gyroid (CSG or Q^{230}), m; tricontinuous orthorhombic network (O^{70}), n. Network morphologies shown in images l-n (bicontinuous gyroid, l, core-shell gyroid, m, O^{70} network, n). Images a-l originally from Ref. [7]. Image m modified from Shefelbine *et al.*[32] Image n taken from Castelleto *et al.*[33]

In linear ABC triblock terpolymers there are three different interfaces: A/B; B/C and A/C (**Figure 1.6**). Each of these interfaces has an interaction parameter associated with the contact of the two blocks ($\chi_{A\text{-}B}$, $\chi_{A\text{-}C}$, and $\chi_{B\text{-}C}$). Due to the interior bonds between the A and B block and the B and C blocks, the A/B and B/C interfaces are required. The A/C interface, however, is not forced into contact since A and C blocks are not directly bonded to each other. The possible combinations which can result from variations upon these parameters are another reason why ABC phase behavior is much more complicated than AB diblock copolymer phase behavior.[34]

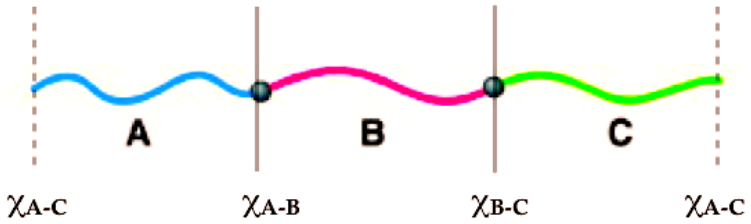

Figure 1.6. ABC chain with interfaces. Solid lines mark the required interfaces. Dashed line marks interface that is not forced into contact. Polymer chains adapted from Ref. [33].

Bailey *et al.* have simplified the ABC systems by classifying them into three main classes based on the binary interaction parameters for each interface ($\chi_{A\text{-}B}$, $\chi_{A\text{-}C}$, and $\chi_{B\text{-}C}$).[35] The classes are organized based on their level of "frustration". The first class, termed "non-frustrated" and labeled F^0, occurs when $\chi_{A\text{-}C}$ is much greater than $\chi_{B\text{-}C}$ and $\chi_{A\text{-}B}$. It is "non-frustrated" since the blocks with the highest incompatibility (A and C) are not required to make contact. The second class, F^1, has one frustrated interface. In this system one interior interface is most

unfavorable. This polymer is frustrated since the blocks that would like least to be in contact are forced to contact. The final system, F^2, occurs when both interior interfaces are highly incompatible while the A/C interface is most compatible. The three frustration classes are listed in **Table 1.1** along with the ABC polymer systems that have been studied. The morphological behavior of each system has been studied to varying degrees. The results from many ABC systems indicate that the phase behavior can depend greatly on the amount of frustration.

Table 1.1. Classes of ABC Terpolymer "Frustration"

Class[35]	Interfacial Relationships	Description[34]	Bulk ABC Systems Studied Experimentally
F^0	$\chi_{A\text{-}C} \geq \chi_{A\text{-}B} \cong \chi_{A\text{-}B}$	No A/C contacts, A/B and B/C interfaces will not have a high degree of curvature	PI-PS-P2VP[44,45,46] PI-PS-PEO[32,47,48,49] PI-PS-PLA[50] PCHE-PEE-PE[51] PS-PI-PDMS[39]
F^1	$\chi_{B\text{-}C} > \chi_{A\text{-}C} > \chi_{A\text{-}B}$ (also: $\chi_{A\text{-}B} > \chi_{A\text{-}C} > \chi_{B\text{-}C}$)	B/C interfaces have high degree of curvature to avoid contact, A/C interfaces are possible	PS-PI-PEO[36] PS-PI-PLA[37] PI-PS-PDMS[32] PS-PB-PV[38] PS-PI-PV[39]
F^2	$\chi_{A\text{-}B}, \chi_{B\text{-}C} > \chi_{A\text{-}C}$	A/B and B/C interfaces have a high degree of curvature to avoid contact, A/C interfaces are possible	PS-PB-PMMA[40,41,42] PS-PEB-PMMA[43]

The remaining discussion of ABC terpolymers will focus on the non-frustrated class since they are most relevant to the polymers studied in this dissertation. To read about the other systems, please refer to the references listed in **Table 1.1**. Non-frustrated systems (F^0) that have been studied experimentally

include: poly(isoprene-*b*-styrene-*b*-2-vinylpyridine) (PI-PS-P2VP)[44,45,46] poly(isoprene-*b*-styrene-*b*-ethylene oxide) (PI-PS-PEO)[32,47,48,49] poly(isoprene-*b*-styrene-*b*-d,l-lactide) (PI-PS-PLA)[50], poly(cyclohexylethylene-*b*-ethylethylene-*b*-ethylene) (PCHE-PEE-PE)[51], and poly(styrene-*b*-isoprene-*b*-dimethylsiloxane) (PS-PI-PDMS).[52] The most comprehensive studies have been on the PI-PS-P2VP and PI-PS-PEO systems.

PI-PS-PEO terpolymers were thoroughly studied across a large compositional space. Three phase morphologies observed in PI-PS-PEO polymers include BBC spheres, core-shell cylinders (CSC), core-shell gyroid (CSG or Q^{230}), alternating Gyroid (Q^{214}), perforated lamella (PL) and an orthorhombic network morphology, O^{70} (see **Figure 1.5**).[53] Hexagonal cylinders were observed along a 70:30 PI:PS volumetric isopleth. The core-shell gyroid structure was observed in some samples with majority PEO and minority PI. A triply continuous *Fddd* orthorhombic network (O^{70}) existed across a broad range of PEO composition along a 50:50 PI:PS isopleth. This non-classical orthorhombic network phase (O^{70}) has been observed in PI-PS-PEO, PCHE-PEE-PE and PS-PI-PDMS terpolymers. A cartoon for this structure is shown in **Figure 1.5n**.

1.2.4 Morphologies for Nanoporous Materials

Some morphologies adopted by block copolymers have nearly ideal attributes for liquid separations, making them attractive candidates for use as ultrafiltration (UF) membranes. The most common implementation involves

selective removal of the minority component in a thin film of block copolymer having hexagonally packed cylinders oriented perpendicular to the membrane surface (**Figure 1.7**).[9]

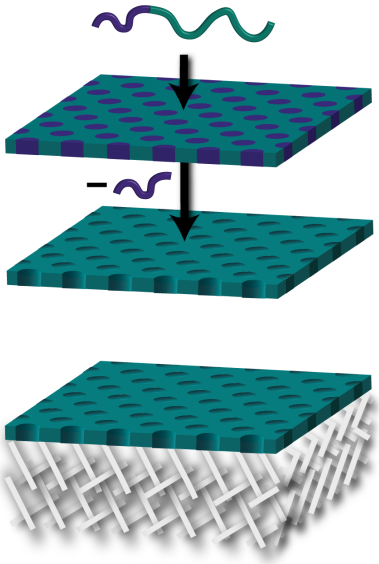

Figure 1.7. (Top) Schematic representation of a cylinder-forming diblock copolymer thin film and the corresponding nanoporous thin film [green] obtained after selective etching of the minority domains [purple]. (Bottom) Composite membrane with nanoporous selective layer on a macroporous support.

ABC terpolymer morphologies with a continuous etchable domain are also desirable as precursors for nanoporous polymers. For ABC terpolymers, phases that meet that requirement are core-shell cylinders (CSC), core-shell gyroid, (CSG), alternating gyroid (Q^{214}), alternating cylinders, perforated lamellar (PL) and the O^{70} network morphology. The next section provides examples of both AB and ABC block polymers used to prepare nanoporous materials.

1.3 Applications for Nanoporous Block Polymers

Nanoporous materials derived from block copolymers are being pursued as desirable materials for controlled separations membranes due to their pore-size tunability, narrow pore size distributions, and ability for selective functionalization. The following section describes extensive research on nanoporous block polymers used for drug delivery and filtration membranes.

1.3.1 Drug Delivery

Currently, the long-term controlled release of therapeutic proteins is an immense challenge. Patients who require, for example, interferon, erythropoietin, or human growth hormone (hGH) rely on multiple weekly injections.[54] Implantable long-term controlled drug release systems, which relieve patients of this hardship, are attractive for improved patient compliance and convenience. Furthermore, much smaller doses should be necessary with controlled-release devices because they offer the potential for localized and continuous release; reduction of toxic side effects or immune reactions associated with high-dose injections may be realized. Patients could see huge benefits from such devices.

Yang *et al*. demonstrate the outstanding potential of nanoporous membranes from block copolymers for controlled drug release.[55] They show how pore sizes can be tailored to slow the passage of or completely reject different proteins. Such control over diffusion on the nanoscale is also beneficial for other technically demanding separation processes (*e.g.*, water purification).

Significant attention has been focused on the use of nanotechnology for controlled, long-term protein-delivery systems. Yang *et al.* have demonstrated a successful strategy for achieving long-term controlled release of protein drugs by incorporating a nanoporous membrane into a drug-eluting device. The enabling membrane contained an 80-nm-thick selective layer of gold-coated nanoporous polystyrene, prepared using a poly(styrene-*b*-methylmethacrylate) (PS-PMMA) copolymer film, laid on a microporous polysulfone supporting membrane. By exploiting a single-file diffusion (SFD) mechanism through the resulting cylindrical nanochannels, they obtained long-term controlled drug release of both bovine serum albumin (BSA) and hGH as model protein drugs with different sizes (their hydrodynamic diameters being about 8 nm and 3 nm, respectively) for at least two months *in vitro*.

The SFD mechanism is predicted to occur when the pore diameter is no larger than two times the hydrodynamic diameter of the passing solute. Under these circumstances, solute molecules cannot pass each other in the pore and move "single-file" at a constant rate regardless of the concentration gradient.

Using zeolite membranes, Kukla *et al.* demonstrated this rate-controlling mechanism in 1996.[56] More recently, Martin and colleagues observed SFD-like behavior for the release of BSA from a drug-eluting device containing 13-nm-wide slits in silicon.[57] These particular nanoporous membranes enabled controlled release of BSA *in vivo* over 50 days. However, true SFD was never fully demonstrated in this device, presumably due to the anisotropic slit structure.

The work by Yang *et al.* is one of the first examples of a functioning device in which a controlled diffusion process was successfully implemented. They tailored their pore sizes to achieve SFD of BSA or the smaller hGH by varying the thickness of a gold layer deposited onto the composite membrane. The gold coating also prevented surface fouling—a critical issue for biological separations and *in vivo* applications. Although this gold-coating strategy was successful, the development of new block copolymers that inherently exhibit even smaller feature sizes than those described by Yang are attractive targets for this and other applications.[58] Yang *et al.* also tuned the rate of SFD by varying the selective layer thickness. Importantly, the hGH was not denatured during elution; results from the *in vivo* pharmokinetics demonstrated constant release of hGH over a three-week period. Their system is promising for the treatment of a variety of diseases and has the potential to be cost effective, simple to fabricate, and fouling resistant.

Nuxoll *et al.* recently demonstrated another related size-selective, mechanically robust composite membrane.[59] They prepared a nanoporous membrane on top of a modified macroporous silicon support. Their selective layer, which contained perpendicularly oriented cylindrical channels, was prepared by first spin casting a poly(styrene-*b*-isoprene-*b*-lactide) (PS-PI-PLA) triblock terpolymer onto a silicon support followed by etching the PLA with dilute base to give a mechanically robust nanoporous film. While small molecules could easily pass through, the diffusion of the large macromolecule dextran blue was hindered. Furthermore, the PI block had the potential to be chemically modified and thus

impart specific pore-wall functionality.[37] Uehara and colleagues demonstrated controlled diffusion of BSA and glucose in a series of tough and flexible nanoporous polyethylene membranes.[60] Their membrane was prepared by fuming nitric acid etching of polystyrene from a poly(ethylene-*b*-styrene) (PE-PS) copolymer. Controlling the PS etching time resulted in controlled pore sizes and allowed selective transport of glucose over BSA. The controlled selectivity and robust mechanical properties of these membranes highlight their potential for improved glucose or other biosensing devices. Collectively, these results exemplify the versatility of block-copolymer-derived membranes for size-selective separations with biomedical relevance and will pave the way for other important separation processes such as water purification.

1.3.2 Filtration Membranes

Providing access to clean water is a global challenge that will ultimately require improvements in the current state of water filtration systems.[61] Improvements in the technology of filtration systems could provide more affordable clean water for all through industrial, municipal, or small-scale filtrations. Ultrafiltration (UF) is just one of the current technologies that could realize significant improvements in separation efficacy from the incorporation of nanoporous membranes prepared using block copolymers.

Typical UF membranes are either quite permeable and not very selective, as in the case of phase-inversion type membranes, or selective and not that permeable,

as in the case of track-etched membranes (**Figure 1.8**).[62] To compete successfully in the UF arena, four main criteria are typically needed: high selectivity, high permeability, mechanical integrity, and resistance to fouling.[63] Nanoporous membranes derived from block copolymers have tremendous promise to fulfill all four of those requirements due to their narrow pore size distributions (high selectivity), high porosity (high permeability), and tunable chemical and physical properties, yet research in the science and engineering of such membranes is needed to combine all of these attributes into practical systems. Because flux is inversely proportional to thickness and costs are directly related to amount of material used, separation membranes containing thin, selective block copolymer layers are most desirable.[64]

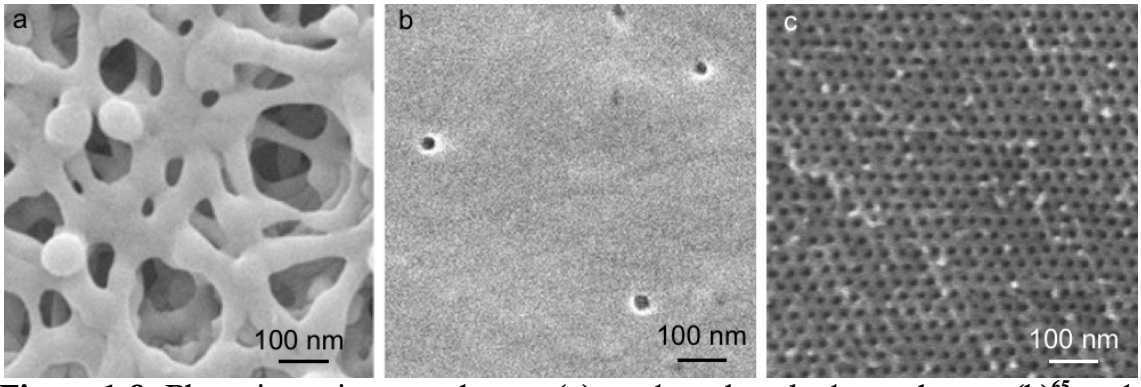

Figure 1.8. Phase inversion membrane, (a), and track-etched membrane, (b)[65] and nanoporous block polymer, (c).[37] Images (a) and (b) reproduced from Ref. 65. Image (c) borrowed from Ref. [37].

Creative strategies, such as that demonstrated by Yang *et al.*, are needed to produce selective membranes that are mechanically stable and compatible with application-specific chemical, thermal, and biological environments. Furthermore,

fabrication hurdles such as achieving proper pore alignment and scalable fabrication steps must also be overcome. The following section will highlight recent progress made toward other block-copolymer-derived nanoporous separation membranes and some of the obstacles that still remain.

In important early work, Liu *et al.* showed that water permeable nanoporous films could be made from poly(*tert*-butyl acrylate-*b*-2-cinnamoylethyl methacrylate) (PtBA-PCEMA) block copolymers.[66] Hydrolysis of the PtBA block left the films with water-compatible poly(acrylic acid) (PAA) cylinders, and pores were effectively formed by soaking the films in high or low pH solutions. They noted that the permeability of their films was comparable to that of PAA-grafted, track-etched membranes and suggested higher permeabilities would have been possible if all channels had been oriented perpendicular to the film surface. In 2006, Cooney *et al.* studied the diffusion of water through a 2-mm-thick nanoporous monolith they prepared from a PLA-etched, channel-die aligned poly(styrene-*b*-polylactide) (PS-PLA) diblock copolymer.[67] Unlike Liu *et al.*, they observed good orientation of PLA cylindrical domains and complete etching of the PLA phase. After wetting of the pores, the expected steady state flux was observed. Also in 2006, Phillip *et al.* estimated that both higher separation factors and higher permeabilities than are currently possible with commercially available membranes could be achieved using related hydrophilic, nanoporous poly(styrene-*b*-dimethylacrylamide) (PS-PDMA).[68] In 2009, Phillip *et al.* showed that high selectivity could be achieved from newly

developed, mechanically robust, nanoporous membranes derived from block copolymers.[69,70]

To compete with phase-inversion membranes, highly selective block-copolymer membranes must also provide high flux. Strategies for creating composite membranes—like those described by Yang *et al.*—that combine a thin block-copolymer selective layer on top of a porous support layer are important research targets for high-flux membranes (**Figure 1.9**). Similar composite membranes for water filtration are also highly desirable but can be more demanding due to the high degree of mechanical integrity needed. Improving mechanical strength of nanoporous films is necessary during fabrication processes and for durability in devices requiring high pressures. For example, Yang and colleagues prepared a composite membrane intended for virus filtration that contained a PS selective layer with 15-nm-diameter pores on top of a polysulfone-supporting membrane.[71] They used a film transfer method to place the block polymer film on top of the porous support (**Figure 1.9**). When the cylinders were perpendicularly aligned, the material was limited by lack of dimensional stability, crack formation, and poor adhesion to the underlying support.[72]

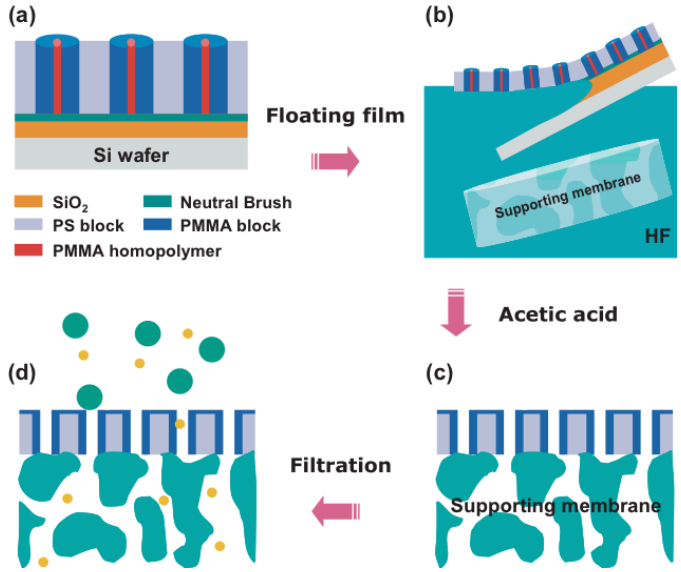

Figure 1.9. Strategy for fabrication of asymmetric nanoporous membranes used by Yang et al. image reproduced from Ref. 71.

In a distinct strategy, thin films made from poly(butadiene-*b*-2-vinyl pyridine-*b*-tertbutyl methacrylate) (BVT) terpolymers showed potential as tough selective layers for composite filtration membranes.[73] By selectively UV-crosslinking the polybutadiene matrix, Sperschneider *et al.* toughened their thin film without affecting the resulting perpendicular cylinder nanostructure. Because they could easily transfer the film off of a supporting NaCl plate onto another substrate without damaging the film, they suggested that these films could also be combined with a support layer to create a composite membrane.

In 2007, Peinemann *et al.* formulated a robust asymmetric membrane by combining block polymer self-assembly with a commercially employed non-solvent induced phase separation process.[74] The membrane, which is composed entirely of a poly(styrene-*b*-4-vinylpyridine) (PS-P4VP) block copolymer, exhibited a 250-nm-

thick nanoporous layer on top of a disordered support layer containing a much larger pore structure (**Figure 1.10**).

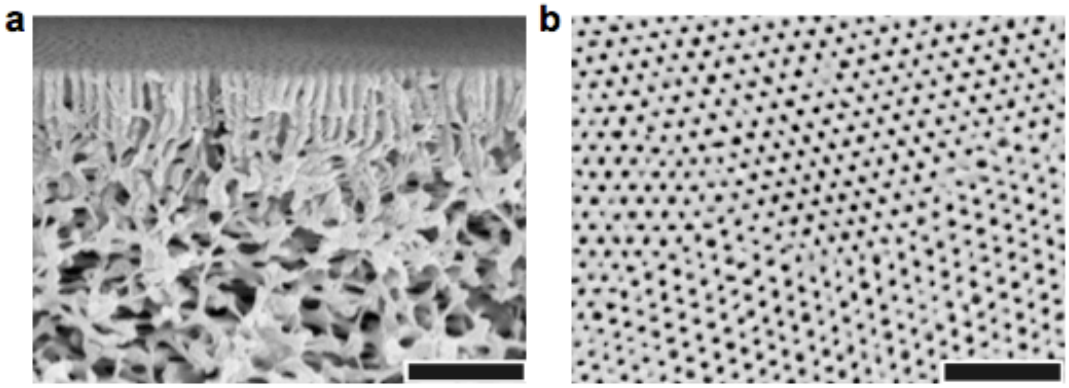

Figure 1.10. SEM images of phase inversion membrane prepared from PS-P4VP. Images borrowed from Reference 74. Scale bars equal 500 nm.

The use of more complex multiblock polymers, as described above, offers the potential for enhanced mechanical properties and also allows for simultaneous control of pore wall and matrix chemistries. For example, the previously mentioned PS-PDMA monoliths also contained tunable functionality in their design. In 2005, Rzayev *et al.* reported hydrophilic pore walls from a poly(styrene-*b*-dimethyl acrylamide-*b*-lactide) (PS-PDMA-PLA) terpolymer.[75] Hydrophilicity is attractive for filtration membranes because it can render them more fouling resistant. Etching the polylactide (PLA) exposed the PDMA midblock and rendered the pores hydrophilic. This PDMA block could be converted into PAA and subsequently modified using a variety of functionalized amines.[76] Mao *et al.* incorporated hydrophilic poly(ethylene oxide) (PEO) chains on the pore walls by preparing blends of poly(styrene-*b*-ethylene oxide) (PS-PEO) and PS-PLA diblock copolymers followed by etching of the PLA block.[77,78] Again, membrane hydrophilicity was

achieved by exploiting the miscibility and differing etch sensitivity of PEO and PLA. In 2006, Bailey *et al.* used an alternative, post-etch chemical transformation step to obtain functionalizable pore walls in a series of PS-PI-PLA block terpolymers that exhibited the core-shell cylinder morphology (**Figure 1.11**).[37] These examples showcase three different methods that can be used to incorporate desired functionality into a nanoporous membrane.

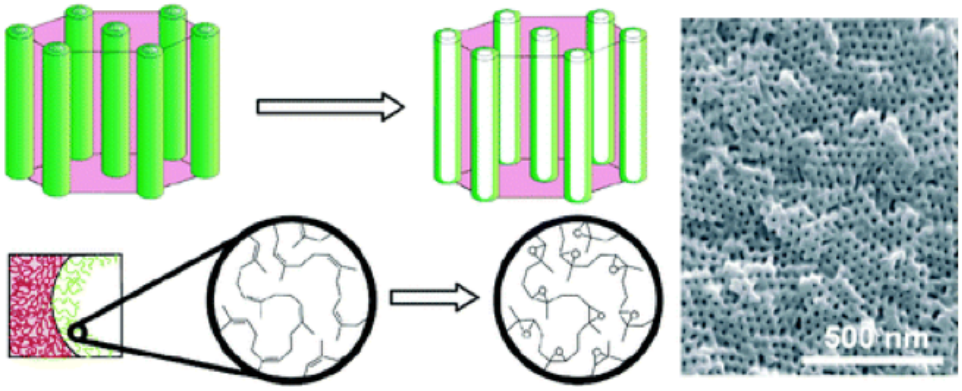

Figure 1.11. Image taken from Ref. [37] showing pore wall functunality before and after epoxidation of PI, left. SEM of nanoporous monolith after PLA removal, right.

More work is needed to develop practical fabrication process for thin film composite membranes that use block copolymers as the selective layer. Most nanoporous thin films for separation membranes have been made from polymers that form cylindrical morphologies. Such films often times must be solvent or thermally annealed after casting to achieve perpendicular orientation of cylinders.[79] Although these methods can be reliable, processes that are more appealing for large-scale membrane fabrication are desirable. For example, casting blends of

block copolymers with either a small amount of dissolved homopolymers or copolymers, as shown by Yang *et al.* and others, is a successful strategy for achieving perpendicular cylinder orientation in BCP films without the need for post-cast annealing steps. Work is also needed to reduce the overall number and complexity of fabrication steps required to prepare composite membranes. An attractive strategy may be to cast a selective layer directly onto a support layer. Recently, Phillip *et al.* demonstrated this strategy by casting a polystyrene-*block*-polylactide (PS-PLA) diblock copolymer film directly onto water-filled polyethersulfone support membrane (**Figure 1.12**).[63]

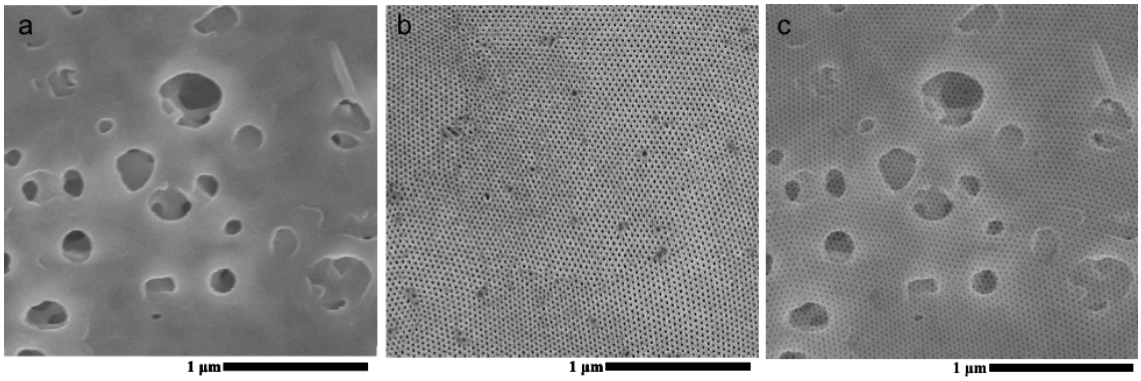

Figure 1.12. Membrane images adapted from the work of Philip et al (Ref. 63). Polyethersulfone support membrane, (a), top surface of nanoporous layer, (b), and overlaid images of images a and b, (c).

Block copolymers have also been used to develop chemically and thermally robust membranes. For example, Pitet *et al.* recently developed robust nanoporous polyethylene membranes exhibiting a bicontinuous structure (**Figure 1.13**).[80] These membranes are attractive precursors for water purification, battery separators or other demanding applications due to their high porosity and robust nature.

Bicontinuous structures such as these do not require separate pore alignment steps, but the increased tortuosity leads to lower permeabilities.

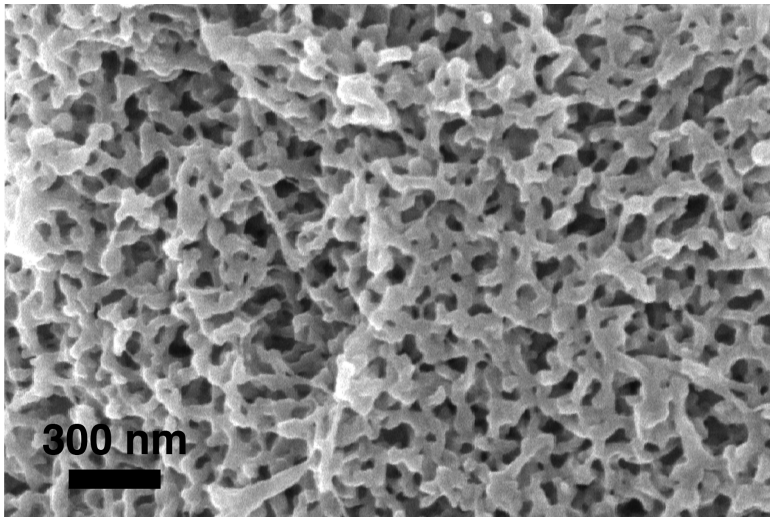

Figure 1.13. Bicontinuous nanoporous polyethylene membrane prepared from a block copolymer precursor. Reproduced with permission from Ref. 80. Copyright 2010 American Chemical Society.

1.3.3 Conclusions and Future Outlook

The progress highlighted here provides compelling evidence for the technological power and sophistication afforded by block copolymers. For example, the work by Yang *et al.* demonstrates how a nanoporous membrane prepared from a block copolymer can successfully be used to control diffusion of molecules of different sizes over a long time without membrane fouling. The works described above call attention to the outstanding performance of block copolymer membranes and how, with creative strategies, these materials can be made into useful separation devices. Such composite membranes can combine high flux, mechanical strength, and enhanced selectivity. Fine-tuning the design of block

copolymers for such membranes can also provide a wide range of material properties. As discussed here, multiple strategies are being pursued for the development of membranes with chemical, mechanical, and biological integrity. The possibilities for creating advanced separation membranes from block copolymers are truly exciting, and many look forward to the next set of advances in this technologically important arena.

1.4 Objective

Although AB diblock and ABC triblock copolymers can produce a wide array of nanoporous membranes, most are limited in that they produce membranes that cannot withstand the high applied pressures or handling needed in ultrafiltration and other applications.[11,70] Various efforts have been made to make polymer membrane materials that are tough and do not crack under the high applied pressure needed in ultrafiltration. Chemical or physical cross-linking of matrix polymer components can significantly improve the toughness of the membrane. Although there are examples of chemically cross-linked membranes, this present work is interested in the use of physically cross-linked block copolymer membranes.

The objective of this study is to explore the use of ABA thermoplastic elastomer based block copolymers to increase toughness in PLA containing block polymers. These block polymers could be used as tough nanoporous ultrafiltration membranes after film casting and removal of PLA. The objective is to make a tough

nanoporous ABA membrane from an ABAC tetrablock copolymer with C as a degradable block. The main ABAC system to be studied is poly(styrene-*b*-isoprene-*b*-styrene-*b*-lactide) (PS-PI-PS-PLA) tetrablock terpolymer.

Two ABAC systems have been studied to date: PS-PI-PS-PEO and poly(cyclohexylethylene-*b*-ethylene-*b*-yclohexylethylene) PCHE-PE-PCHE-PDMS. Both systems can be considered non-frustrated since the highest incompatibility in both tetrablock systems is between the two blocks that are not forced into contact—blocks B and C. Both ABAC systems exhibit interesting phase behavior that is different from linear ABC phase behavior. For example, core-shell cylinder morphologies were observed across a broad compositional range in two different systems. A short summary of the phase behavior observed is provided here.

A series of PS-PI-PS-PEO terpolymers with a 50/50 PS/PI volumetric ratio and f_{PEO} between 0 and 0.30 were investigated for their morphological behavior.[81] Below f_{PEO} = 0.07, the system was disordered. Between 0.07 and 0.09 f_{PEO}, liquid like packing of spheres were observed. Between 0.12 and 0.30 f_{PEO}, PS-PI-PS-PEO formed core(PEO)-shell(PS) cylinders. A cartoon showing the ABAC chain configuration in these morphologies is given in **Figure 1.14**.

In an asymmetric PS-PI-PS-PEO series, mostly hexagonally packed spheres were observed.[82] For a series of PS-PI-PS-PEO with 40:60 PS:PI volumetric ratio and f_{PEO} between 0 and 0.20, tetrablocks formed spheres packed on a simple hexagonal lattice. Core(PEO)-Shell(PS) cylinders were observed when f_{PEO} was 0.32. An unusual dodecagonal quasicrystalline morphology was observed after

heating below the order-disorder transition temperature (T_{ODT}) for a sphere forming tetrablock (f_{PEO} = 0.09; f_{PS} = 0.35; and f_{PI} = 0.65).[83]

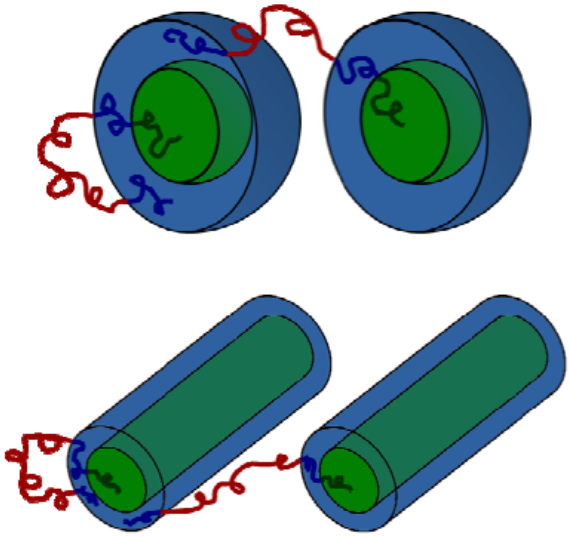

Figure 1.14. ABAC chain arrangement in core-shell spheres and cylinders. Spherical and cylindrical morphologies were observed across a broad compositional range for PS-PI-PS-PEO tetrablock terpolymers. Image was borrowed from Ref 81.

PCHE-PE-PCHE-PDMS tetrablock terpolymers also had behavior distinct from ABC terpolymers.[34] A series of tetrablocks with f_{PDMS} between 0 and 0.20 were prepared from a PCHE-PE-PCHE triblock with a 70/30 PE/PCHE volumetric ratio. An orthorhombic network (*Pnna* O^{52}) morphology consisting of PDMS spheres in a PCHE network was observed at f_{PDMS} of 0.09. At high f_{PDMS} core(PDMS)-shell(PCHE) cylinders were found up to 0.20 f_{PDMS}. Another series with 50:50 PE:PCHE volumetric ratio had slightly different phase behavior. This series formed PDMS spheres within PCHE lamellae between 0.13 and 0.19 f_{PDMS}. At higher f_{PDMS} (0.24-0.33) a three phase lamellae (LAM_3) morphology formed.

The interesting phase behavior observed in these two ABAC systems is inspiring for more research on ABAC terpolymers. The broad compositional range observed for core-shell cylinders is encouraging since it could mean similar morphological behavior also occurs in PS-PI-PS-PLA.

1.5 Thesis Overview

This thesis describes the synthesis and characterization of poly(styrene-*b*-isoprene-*b*-styrene-*b*-lactide) (PS-PI-PS-PLA) and poly(styrene-*b*-ethylene-co-ethylene-*alt*-propylene-*b*-styrene-*b*-lactide) (PS-PEEP-PS-PLA) tetrablock terpolymers. The bulk morphological behavior of PS-PI-PS-PLA tetrablocks was investigated using a combination of transmission electron microscopy (TEM), small-angle X-ray scattering (SAXS), differential scanning calorimetry (DSC) and scanning electron microscopy (SEM). Bulk mechanical properties were investigated using small scale tensile testing. Thin film morphology was characterized with SEM and atomic force microscopy (AFM). **Chapter 2** describes the morphological behavior of core-shell cylinder PS-PI-PS-PLA tetrablock terpolymers with 50/50 PS/PI volumetric ratio. This chapter also includes bulk mechanical properties, nanoporous results and the fabrication and characterization of a composite membrane with a nanoporous PS-PI-PS selective layer. **Chapter 3** covers a solvent annealing investigation of PS-PI-PS-PLA thin films with pure solvents and mixed solvents. Controlled solvent selectivity for PS and PLA blocks resulted in well-ordered nanoporous thin films. Blending of PLA homopolymer into films was also investigated. **Chapter 4** investigates the morphological and mechanical properties of a 70/30 PI/PS series of PS-PI-PS-PLA tetrablock terpolymers as well as the mechanical properties of the compositionally analogous PS-PEEP-PS-PLA tetrablock terpolymers.

1.6 References

(1) "Nanoporous" is a term used to describe materials with voids up to 100 nm in size. The official terminology used by IUPAC to describe the pore size of different materials ("microporous" for materials with voids less than 2 nm; "mesoporous" for materials with voids between 2 and 50 nm; and "macroporous" for materials with voids greater than 50 nm) is not adopted in this dissertation. The term "nanoporous" is generally accepted to include material with pore sizes up to 100 nm in size. (Corma, A. *Chemical Reviews* **1997**, *97*, 2373-2420.)

(2) Hillmyer, M. A. *Adv. Polym. Sci.* **2005**, *190*, 137-181.

(3) Hou, X.; Guo, W.; Jiang, L. *Chem. Soc. Rev.* **2011**, *40*, 2385-2401.

(4) Auriemma, F.; De Rosa, C. *Trop. J. Pharm. Res.* **2011**, *10*, 1-2.

(5) Duong, P. H. H.; Chung, T.-S. Jeyaseelan, K.; Armugam, A.; Chen, Z.; Yang, J.; Hong, M. *J. Membr. Sci.* **2012**, *409-410,* 34-43.

(6) Pimpin, A.; Srituravanich, W. *Eng. J.* **2011** *16* (1).

(7) Bates, F. S. Fredrickson, G. H. *Phys. Today* **1999**, *52*, 32.

(8) Park, C.; Yoon, J.; Thomas, E. L. *Polymer* **2003**, *44*, 6725–6760.

(9) Li, M.; Coenjarts, C.; Ober, C. K. Patternable Block Copolymers. In *Block Copolymers II, Advances in Polymer Science*; V. Abetz, Ed.; Springer: Heidelberg, Germany, 2005; 190, pp 183–226.

(10) Hamley, Ian. *The Physics of Block Copolymers.* Oxford University Press: Oxford, England, 1998. pp 1-87, 278-310.

(11) Olson, D. A.; Chen, L.; Hillmyer, M. A.; *Chemical Materials.* **2008**, 20, 869-890.

(12) Phillip, W.; Cussler, E.; O'Neill, B.; Amendt, M.; Hillmyer, M. Utilization of Block Copolymers as Ultrafiltration Membranes. Abstract for American Institute of Chemical Engineers Annual Meeting, **2008**. Philadelphia.

(13) Chen, L.; William, P. A.; Cussler, E. L.; Hillmyer, M. A. *Journal of American Chemical Society.* **2007**, 129, 13786-13787.

(14) Rzayev, J.; Hillmyer, M. A. *Macromolecules*. **2005**, 1, 3-5.

(15) Hamley, Ian. Developments in Block Copolymer Science and Technology. John Wiley & Sons, LTD: West Sussex, England, 2004. pp. 1-70, 127-152, 341-359.

(16) Hiemenz, P. C.; Lodge, T. P.; *Polymer Chemistry*, Second Edition; CRC Press, Taylor and Francis Group: Boca Raton, Fl, **2007**, pp 24-28, 117-135, 153, 247-283, 291- 296, 422-446, 472-497.

(17) Matsen, M.W.; Bates, F.S. *Macromolecules*. **1996**, 29, 7641-7644

(18) Meuler, A. J.; Hillmyer, M. A.; Bates, F. S. *Macromolecules Review* **2009**, *42*, 7221-7250.

(19) Kim, M. I.; Wakada, T.; Akasaka, S.; Nishitsuji, S.; Saijo, K.; Hasegawa, H.; Ito, K.; Takenaka, M. *Macromolecules* **2008**, *41*, 7667-7670.

(20) Matsen, M. *Journal of Chemical Physics.* **1999**, *111*, 7139-7146.

(21) Fredrickson, G.H.; Bates, F.S. *Annual Review of Materials Science.* **1996**, 26, 501-550.

(22) Matsen, M. *Journal of Chemical Physics*. **2000**, 113, 13, 5539-5545.

(23) Schmalz, H.; Boker, A.; Lange, R; Krausch, G.; Abetz, V. *Macromolecules.* **2001**, 34, 8720-8729

(24) Pearson, R.A.; Sue, H.-J.; Yee, A.F.; Toughening of Plastics: Advances in Modeling and Experiments. *ACS Symposium Series 759.* **2000**, Oxford University Press. Washington, D. C.

(25) Holden, G.; Bishop, E.T.; Legge, N.R.; *Journal of Polymer Science: Part C.* **1969**, 26, 37-57.

(26) Mahanthappa, M.K.; Hillmyer, M.A.; Bates, F.S. *Macromolecules.* **2008**, 41, 1341-1351.

(27) Kraton D SIS Properties Guide by Kraton.
http://www.kraton.com/Products/Kraton_D_SIS/

(28) Wang, R.; Xu, T. *Polymer.* **2007**, 48, 15, 4601-4608.

(29) Epps, T.H.; Cochran, E.W.; Bailey, T.S.; Waletzko, R.S.; Hardy, C.M.; Bates, F.S. *Macromolecules.* **2004**, 37, 8325-8341.

(30) Wang, R.; Hu, K.; Jiang, Z.; Zhou, D.; *Macromolecular Theory and Simulations.* **2005**, 14, 256-266.

(31) Bates, F.S.; Frederickson, G.H. *Annual Review Physical Chemistry.* **1990**, 42, 525-557.

(32) Shefelbine, T. A.; Vigild, M. E.; Matsen, M. W.; Hadjuk, D. A. Hillmyer, M. A.; Cussler, E. L.; Bates, F. S. *J. Am. Chem. Soc.* **1999**, *121*, 8457-8465.

(33) Castelleto, V.; Hamley, I. W. *Current Opin. Sol. Stat. and Mater. Sci.* **2004**, *8,* 426-438.

(34) Bluemle, M. Morphological Behavior of Linear ABC and ABAC Block Terpolymers. Ph.D. Dissertation, University of Minnesota, Minneapolis, Minnesota, USA, **2010**.

(35) Bailey, T. S. Morphological Behavior Spanning the Symmetric AB and ABC Block Copolymer States. Ph.D. Dissertation, University of Minnesota, Minneapolis, Minnesota, USA, **2001**.

(36) Bailey, T. S.; Pham, H. D.; Bates, F. S. *Macromolecules* **2001**, *34*, 6994-7008.

(37) Bailey, T. S.; Rzayev, J.; Hillmyer, M. A.*Macromolecules* **2006**, *39,* 8772-8781.

(38) Kudose, I. Kotaka, T. *Macromolecules* **1984,** *17*, 2325-2332.

(39) Matsushita, Y.; Tamura, M; Noda, I. *Macromolecules* **1994**, *27*, 3680-3682.

(40) Stadler, R.; Auschra, C.; Beckmann, J.; Krappe, U.; Voight-Martin, I.; Leibler, L. *Macromolecules* **1995**, *28*, 3080-3097.

(41) Krappe, U.; Stadler, R.; Voight-Martin, I. *Macromolecules* **1995**, *28*, 4558-4561.

(42) Breiner, U.; Krappe, U.; Abetz, V.; Stadler, R. *Macrmol. Chem. Phys.* **1997**, *198*, 1051-1083.

(43) Balsamo, V.; von Gyldenfeldt, F.; Stadler, R. *Macromolecules* **1999**, *32*, 1226-1232.

(44) Mogi, Y.; Mori, K.; Matsushita, Y.; Noda, I. *Macromolecules* **1992**, *25*, 5412-5415.

(45) Mogi, Y.; Kotsuji, H.; Kaneko, Y.; Mori, K.; Matsushita, Y.; Noda, I. *Macromolecules* **1992**, *25*, 5408-5411.

(46) Mogi, Y.; Nomura, M.; Kotsuji, H.; Ohnisi, K.; Matsushita, Y.; Noda, I. *Macromolecules* **1994**, *27*, 6755-6760.

(47) Bailey, T. S.; Hardy, C. M.; Epps, T. H., III; Bates, F. S. *Macromolecules* **2002**, *35*, 7007-1714.

(48) Epps, T. H., III; Cochran, E. W.; Hardy, C. M.; Bailey, T. S.; Waletzko, R. S.; Bates, F. S. *Macromolecules* **2004**, *37*, 7085-7088.

(49) Meuler, A. Thesis. Network Morphologies in Monodisperse and Polydisperse Multiblock Terpolymers Ph.D. Dissertation, University of Minnesota, Minneapolis, Minnesota, USA, **2009**.

(50) Zalusky, Andy. Nanoporous Materials From Ordered Polylactide-Containing Block Copolymer Templates. Ph.D. Dissertation, University of Minnesota, Minneapolis, Minnesota, USA, **2003**.

(51) Cochran, E. W.; Bates, F. S. *Phys. Rev. Lett.* **2004**, *93*, 087802(1-4).

(52) Hardy, C. M.; Bates, F. S.; Kim, M.-H.; Wignall, G. D. *Macromolecules* **2002**, *35*, 3189-3197.

(53) Chatterjee, J.; Jain, S.; Bates, F. S. *Macromolecules* **2007**, *40*, 2882-2896.

(54) Cleland, J.; Daugherty, A.; Mrsny, R. *Curr. Opin. Biotechnol.* **2001**, *12*, 212–219.

(55) Yang, S.; Yang, J.-A.; Kim, E.-S.; Jeon, G.; Oh, E. J.; Choi, K. Y.; Hahn, S. K.; Kim, J.K. *ACS Nano* **2010**, *4*, 3817-3822.

(56) Kukla, V. Kornatowski, J.; Demuth, D.; Girnus, I.; Pfeifer, H.; Rees, L. V. C.; Schunk, S.; Unger, K.; Karger, J. *Science* **1996**, *272*, 702–703.

(57) Martin, F.; Walczak, R.; Boiarski, A.; Cohen, M.; West, T.; Cosentino, C.; Ferrari, M. *J. Controlled Release* **2005**, *102*, 123–133.

(58) Rodwogin, Marc D.; Spanjers, Charles S.; Leighton, C.; Hillmyer, Marc A. *ACS Nano* **2010**, *4*, 725–732.

(59) Nuxoll, E. E.; Hillmyer, M. A.; Wang, R.; Leighton, C.; Siegel, R. A. *ACS Appl. Mater. Interfaces* **2009**, *4*, 888–893.

(60) Uehara, H. Kakiage, M.; Sekiya, M.; Sakuma, D. Yamonobe, T. Takano, N. Barraud, A.; Meurville, E.; Ryser, P. *ACS Nano* **2009**, *3*, 924–932.

(61) Schafer, A. I.; Davey, J. Ultrafiltration to Supply Drinking Water in International Development: A Review of Opportunities. *Appropriate Technologies for Environmental Protection in the Developing World.* Springer Science and Business Media B.V.: Edinburgh, UK, 2009; pp 151–168.

(62) Mehta, A.; Zydney, A. L. *J. Membr. Sci.* **2005**, *249*, 245–249.

(63) Phillip, W. A.; O'Neill, B.; Rodwogin, M.; Hillmyer, M. A.; Cussler, E. L. *ACS Appl. Mater.Interfaces* **2010**, *2*, 847–853.

(64) Li, X.; Fustin, C.-A.; Lefevre, N.; Gohy, J.-F.; De Feyter, S.; De Baerdemaeker, J.; Egger, W.; Vankelecom, I. F. J. *J. Mater. Chem*. **2010**, *20*, 4333–4339.

(65) Phillip, W. A. Block Polymer Membranes for Selective Separations. Ph.D. Dissertation, University of Minnesota, Minneapolis, Minnesota, USA, **2009**.

(66) Liu, G.; Ding, J.; Hashimoto, T.; Kimishima, K.; Winnik, F. M.; Nigam, S. *Chem. Mater.,* **1999**, *11*, 2233–2240.

(67) Cooney, D. T.; Hillmyer, M. A.; Cussler, E. L.; Moggridge, G. D. *Crystal. Rev.* **2006**, *12*, 13–24.

(68) Phillip, W. A.; Rzayev, J.; Hillmyer, M. A.; Cussler, E. L. *J. Membr. Sci.* **2006**, *286*, 144–152.

(69) Phillip, W. A.; Amendt, M.; O'Neill, B.; Chen, L.; Hillmyer, M. A.; Cussler, E. L. *ACS Appl. Mater. Interfaces* **2009**, *1*, 472–480.

(70) Chen, L.; Phillip, W. A.; Cussler, E. L.; Hillmyer, M. A. *J. Amer. Chem.l Soc. Commun.* **2007**, *129*, 13786–13787.

(71) Yang, S. Y.; Ryu, I.; Kim, H. Y.; Kim, J. K.; Jang, S. K.; Russell, T. P. *Adv. Mater.* **2006**, *18*, 709–712.

(72) Yang, S. Y.; Park, J.; Yoon, J.; Ree, M.; Jang, S. K.; Kim, J. K. *Adv. Funct. Mater.* **2008**, *18*, 1371-1377.

(73) Sperschneider, A.; Scacher, F.; Gawenda, M.; Tsarkova, L.; Muller, A. H. E.; Ulbricht, M.; Krausch, G.; Kohler, J. *Small* **2007**, *3*, 1056–1063.

(74) Peinemann, K.-V.; Abetz, V. Simon, P. F. W. *Nature* **2007**, *6*, 992–996.

(75) Rzayev, J.; Hillmyer, M. A. *Macromolecules* **2005**, *38*, 3–5.

(76) Rzayev, J.; Hillmyer, M. A. *J. Amer. Chem. Soc.* **2005**, *127*, 13373–13379.

(77) Mao, H.; Arrechea, P. L.; Bailey, T. S.; Johnson, B. J. S.; Hillmyer, M. A. *Faraday Discuss.* **2005**, *128,* 149–162.

(78) Mao, H.; Hillmyer, M. A. *Soft Matter* **2006**, *2*, 57–59.

(79) Vayer, M.; Hillmyer, M. A.; Dirany, M.; Thevenin, G.; Erre, R.; Sinturel, C. *Thin Solid Films* **2010**, *518*, 3710–3715.

(80) Pitet, L.; Amendt, M. A.; Hillmyer, M. A. *J. Amer. Chem. Soc.* **2010**, *132*, 8230–8231.

(81) Bluemle, M. J.; Zhang, J.; Lodge, T. P.; Bates, F. S. *Macromolecules Comm.* **2010**, *43*, 4449-4452.

(82) Zhang, J.; Sides, S.; Bates, F. S. *Macromolecules* **2012**, *45*, 256-265.

(83) Zhang, Z.; Bates, F. S. *J. Am. Chem. Soc.* **2012**, *134,* 7636-7639.

Chapter 2

PS-PI-PS-PLA Tetrablock Terpolymers for Tough Nanoporous Filtration Membranes*

Nanoporous poly(styrene-*b*-isoprene-*b*-styrene) (PS-PI-PS) was prepared from PS-PI-PS-PLA (PLA = poly(d,l-lactide)) tetrablock terpolymer precursors. Hydroxy end-functionalized PS-PI-PS was synthesized by sequential anionic polymerizations and used to initiate the ring-opening polymerization of d,l-lactide. A combination of small-angle x-ray scattering, transmission electron microscopy and scanning electron microscopy data support a core-shell cylinder morphology with PLA as the core component. The inherently robust mechanical properties associated with PS-PI-PS block copolymers provide the materials with enhanced flexibility and toughness compared to analogous nanoporous polystyrene samples prepared by etching of PS-PLA diblocks. Composite membranes containing nanoporous PS-PI-PS on top of microporous polyethersulfone (PES) were prepared by direct spin coating and also by a salt-plate coating/film-transfer strategy. Nanopores ($d_{pore} \approx 15$ nm) were created by a combination of reactive ion etching (RIE) and basic PLA hydrolysis. Resulting composite PS-PI-PS/PES membranes exhibited high selectivity and permeability comparable to that of commercial ultrafiltration membranes.

---

* Reproduced in part with permission from Jackson, E. A.; Lee, Y. M.; Hillmyer, M. A. Submitted to Macromolecules **November 2012.**

2.1 Introduction

Nanoporous materials are useful in catalysis, templating, water filtration, biomolecule separation and drug delivery applications.[1] While porous inorganic materials typically exhibit chemical, thermal and mechanical stability,[2] organic materials (e.g., polymers) offer enhanced chemical tunability and mechanical flexibility.[3-5] The generation of nanoporous organic materials from ordered block polymers has undergone tremendous development since the first report in 1988.[6] Block polymers can self-organize into well-ordered structures having nanoscopic domains with a uniform size distribution.[5,7,8] By removal of a sacrificial minority component, such ordered precursors are amenable to the preparation of a wide variety of nanoporous materials. The nanoscopic pores are well-suited for demanding separation applications (e.g., removal of viruses by size exclusion)[9] while the typically narrow pore-size distribution fosters remarkable selectivity.[10-12] Furthermore, block polymers can be designed to incorporate desired chemical, thermal, and mechanical attributes appropriate to specific applications.[8] There have been several reports describing the preparation of composite membranes with block polymer thin films as the selective layer and an underlying mechanical support with a much larger pore size. Such membranes have shown tremendous promise for use as implantable controlled drug delivery devices,[12-17] biofiltration,[9,11] and water filtration,[18-23] gas separation,[24,25] and battery or fuel cell membranes.[26,27]

One of the major challenges in implementing a nanoporous membrane from an ordered block polymer precursor is realizing mechanical integrity of the final

porous structure. This is especially important since many applications typically require flexible, thin (< 500 nm thick) films. Nanoporous materials have been prepared from both soft materials (i.e., low glass transition temperature, T_g) such as cross-linked polyisoprene (PI)[28] and rigid, high modulus materials like polystyrene (PS).[29] Pore-collapse is inevitable without a hard block (i.e., high T_g) like PS or a highly cross-linked matrix material. [28] Considering the relatively high entanglement molar mass of PS, low molar mass block polymers used for the preparation of nanoporous materials from ordered precursors typically gives monoliths and films that readily fracture under modest loads.[18] While cross-linking PS domains prior to creating the nanoporosity can lead to mechanical improvements,[30] the inflexibility of both native and crosslinked nanoporous PS thin films can be problematic for the formation of composite membranes.[31,32] For nanoporous materials made from block polymers with rubbery matrices, a significant degree of cross-linking is necessary to provide enough mechanical stability to maintain the nanoporous structure upon removal of the etchable component.[28,31,33] Thin film nanoporous membranes based on ABC triblock terpolymers have typically required chemical cross-linking of the rubbery matrix block as well.[34] Recently, a composite membrane has been reported by employing a thin film PS-PI-PLA terpolymer without chemical cross-linking.[35] After removal of PLA, the combination of the PS matrix and the PI pore walls in the nanoporous matrix provided sufficient mechanical stability in the thin film for ultrafiltration tests.[35]

Thermoplastic elastomers comprised of ABA triblock copolymers are tough plastic materials resulting from the combination of physical crosslinking between glassy domains formed during self-assembly and entanglement of the rubbery B midblock.[36] The strategy described in this chapter combines an established thermoplastic elastomer, poly(styrene)-*b*-poly(isoprene)-*b*-poly(styrene) (PS-PI-PS), with the chemically etchable aliphatic polyester polylactide (PLA), into a poly(styrene)-*b*-poly(isoprene)-*b*-poly(styrene)-*b*-poly(d,l-lactide) (PS-PI-PS-PLA) tetrablock terpolymer. Motivation stems from the hypothesis that, after removal of the PLA domains, a nanoporous scaffold of PS-PI-PS should have superior mechanical performance compared with non-cross-linked nanoporous PS or PS-PI.[35,36,37]

The architectural asymmetry in PS-PI-PS-PLA, an ABAC type block polymer, is expected to result in different phase behavior than the analogous ABC type terpolymers.[38,39,40] In seminal contributions by Bluemle et al.[38,39] on ABAC phase behavior, poly(styrene)-*b*-poly(isoprene)-*b*-poly(styrene)-*b*-poly(ethylene oxide) (PS-PI-PS-PEO) tetrablock terpolymers containing a 50:50 volumetric ratio of PI:PS behaved quite differently than PI-PS-PEO triblock terpolymers having similar composition.[39,41] Importantly, a core-shell cylinder (core PEO, shell PS and matrix PI) morphology could be accessed across a relatively wide compositional range (f_{PEO} = 0.14–0.30) in PS-PI-PS-PEO tetrablocks with $f_{PS} = f_{PI}$. The behavior of PS-PI-PS-PLA tetrablocks should be very similar considering that 1) the highly incompatible B and C blocks will avoid contact with each other and 2) the

asymmetric architecture will prefer curved interfaces.[39] Core-shell type morphologies should be accessible in PS-PI-PS-PLA over a similar compositional range as both are non-frustrated ABAC systems where $\chi_{BC} >> \chi_{AC} \approx \chi_{AB}$.

Here we describe the synthesis, morphological characterization and mechanical properties of core-shell cylinder forming PS-PI-PS-PLA tetrablock polymers (**Figure 2.1A**) and the preparation of a flexible, mechanically stable nanoporous PS-PI-PS membrane made therefrom. The strategy to obtain high permeability was to use a very thin nanoporous layer with a highly porous mechanically supportive layer in an asymmetric membrane. Specifically, selective composite membranes containing a thin nanoporous PS-PI-PS layer on a microporous polyethersulfone (PES) support (**Figure 2.1B**) were prepared by two separate methods. The first method was accomplished by spin coating PS-PI-PS-PLA polymers directly onto PES supports. Alternatively, a salt plate coating combined with film transfer method developed previously was employed.[35] Perpendicular PLA cylinders were trapped by spin coating from toluene with a small amount (5 wt%) of PLA homopolymer. Nanopores were then created through a combination of reactive ion etching (RIE) and a short PLA basic hydrolysis (**Figure 2.1A**). The resulting membrane showed high selectivity and permeability comparable to commercial filtration membranes.

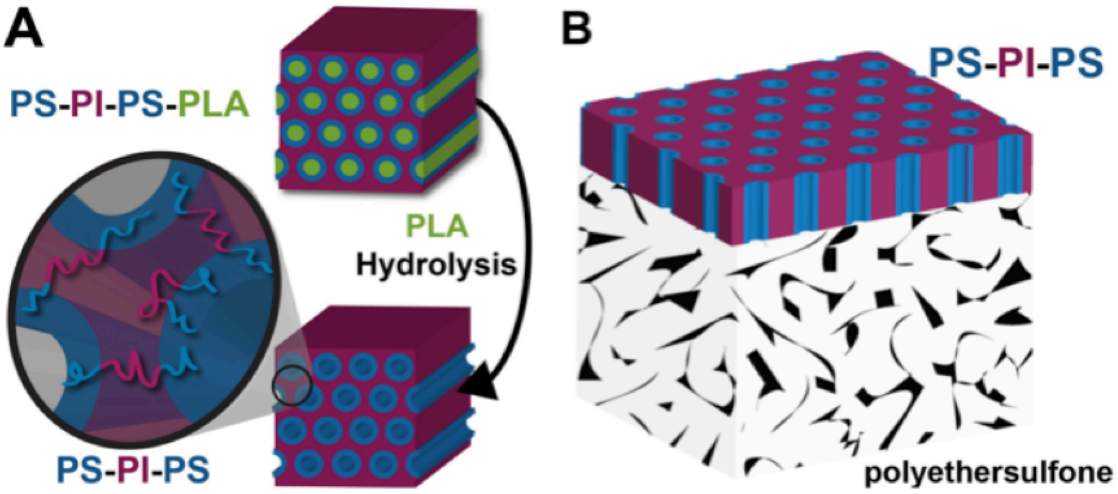

Figure 2.1. Illustration depicting the self-organization of a PS-PI-PS-PLA tetrablock terpolymer into the core-shell cylinder morphology followed by selective removal of PLA to generate a nanoporous thermoplastic elastomer (PS-PI-PS), (A); Illustration of a composite membrane containing a nanoporous PS-PI-PS layer coated on microporous polyethersulfone membrane support, (B).

2.2 Results

2.2.1 Synthesis and Molecular Characterization

Synthesis of Tetrablock Terpolymers. Three PS-PI-PS-PLA tetrablock terpolymers were synthesized by polymerization of d,l-lactide from one parent PS-PI-PS-OH triblock with symmetric composition (f_{PS} = f_{PI}) and PS blocks of approximately equal length synthesized by sequential anionic polymerization according to a previously reported procedure[41] (**Figure 2.2**).

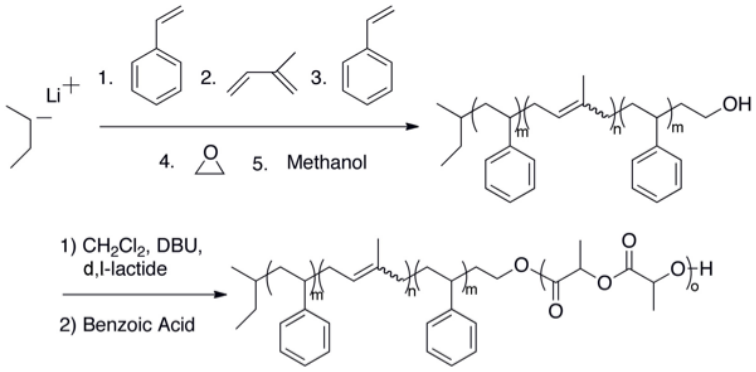

Figure 2.2. Synthetic scheme for PS-PI-PS-OH and PS-PI-PS-PLA polymers.

PS-PI-PS-OH composition, **Table 2.1**, was determined by a combination of ^{1}H nuclear magnetic resonance (NMR) spectroscopy (**Figure 2.3 and 2.4**) and size-exclusion chromatography (SEC) (**Figure 2.5**).[41] The parent triblock was then used to initiate ring-opening transesterification polymerization (ROTEP) of d,l-lactide catalyzed by 1,8-Diazabicycl[5.4.0]undec-7-ene (DBU).[42] The PLA molar mass was calculated using ^{1}H NMR spectroscopy (**Figure 2.6**) as described previously.[43] SEC analysis of the PS-PI-PS-PLA samples (**Figure 2.7**) indicated increasing molar mass with increasing PLA content and narrow, monomodal molar mass distributions ($Đ$ < 1.1 in all cases, see **Table 2.1**).

Table 2.1. Molecular characteristics of PS-PI-PS-OH precursor and PS-PI-PS-PLA polymers

		Volume Fraction *(f)* [a,b]						T_g [d] (°C)				
Sample ID	M_n [a,b] (kDa)	PI	PS	PLA	Đ [b]	D [c] (nm)	Morph - ology	PI	PS	PLA	e_b [e]	TS [f]
PS-PI-PS-OH	20.2	0.49	0.51	0	1.04	14	Lam	–58	65		370	6
PS-PI-PS-PLA(0.20)	26.9	0.39	0.41	0.20	1.06	28	CSC	–57	63	53	370	14
PS-PI-PS-PLA(0.21)	27.4	0.39	0.40	0.21	1.09	29	CSC	–57	63	53		
PS-PI-PS-PLA(0.25)	29.1	0.37	0.38	0.25	1.10	31	CSC	–57	63	53	450	16

[(a)]Estimated from a combination of ^{1}H NMR spectroscopy of final PS-PI-PS-OH triblock and size exclusion chromatography on a PS aliquot from the PS-PI-PS-OH synthesis. [(b)]Size exclusion chromatography (RI detector, PS standards, $CHCl_3$, 35 °C). [(c)]Small-angle X-ray scattering. [(d)]Differential Scanning Calorimetry [(e)]Elongation at break (e_b) determined by Tensile Tests [(f)]Tensile Strength (TS) measured by tensile tests.

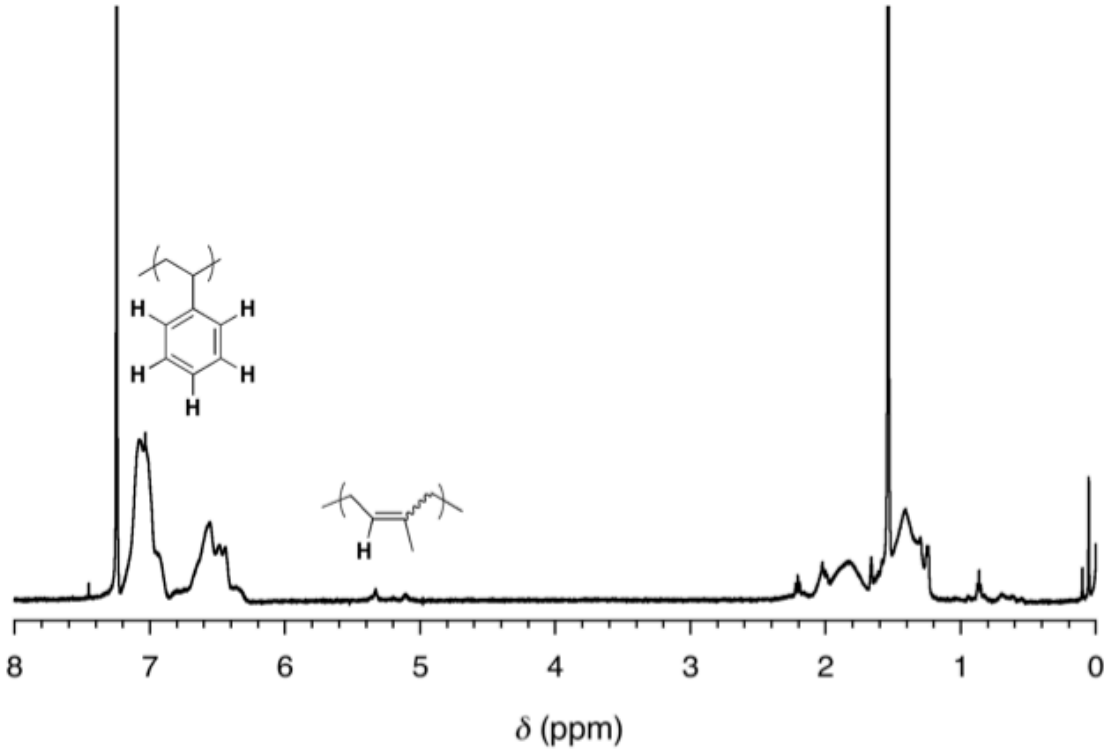

Figure 2.3. ^{1}H NMR spectrum taken immediately after addition of isoprene. First block of polystyrene was calculated from the polystyryl resonances between 6.2 and 7.2 ppm. Sec-butyl end group resonances between 0.6 and 1 ppm were used to calculate degree of polymerization of styrene. A small amount of polyisoprene is present because the aliquot was taken a few minutes after addition of isoprene monomer.

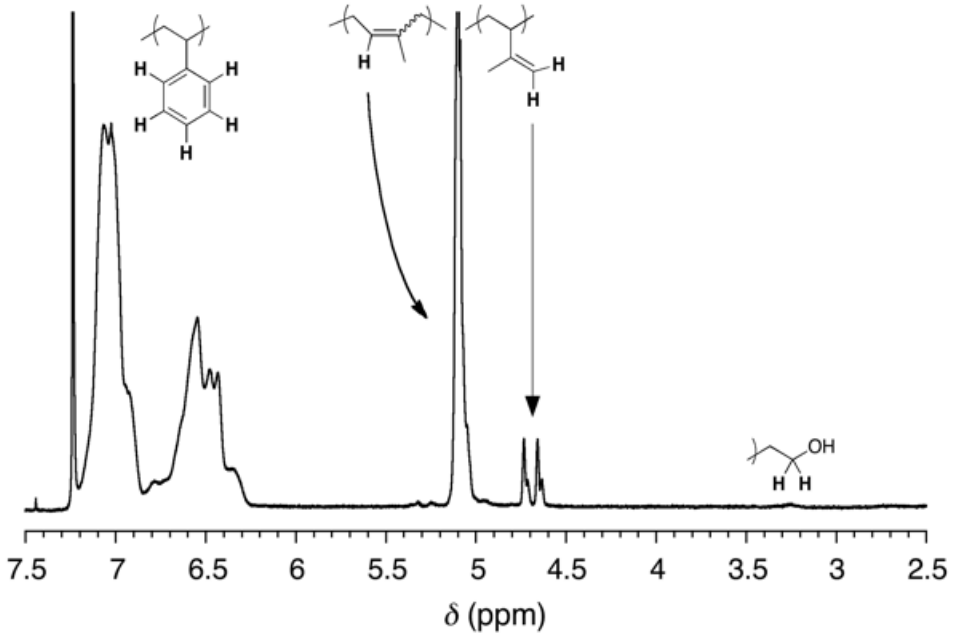

Figure 2.4. ^{1}H NMR spectrum of PS-PI-PS-OH in $CDCl_3$ at 25 °C. Mn was calculated by a combination of ^{1}H NMR end group analysis, SEC data of the PS first block aliquot based on PS standards. End group analysis by ^{1}H NMR was done using the end group found at the CH_2 resonances at 3.3 ppm and again with the sec-butyl end group at 0.5-0.9 ppm (not shown here). Molar mass calculated by end group analysis were in agreement within experimental error.

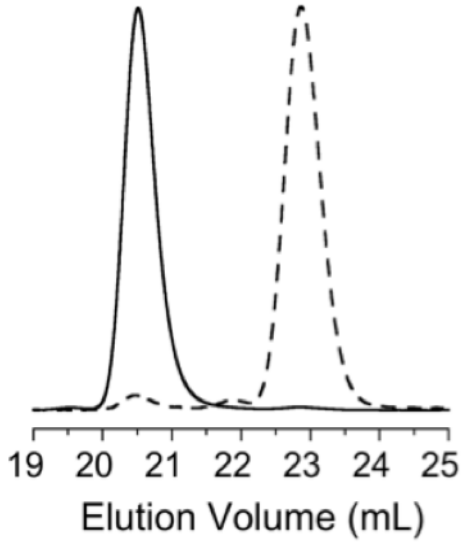

Figure 2.5. SEC traces for aliquot of taken after polymerization of the first block, PS, dashed line, and PS-PI-PS-OH triblock, solid black line. Small peaks at 22 mL at 20.5 mL in the aliquot trace are due to coupling of chains in the aliquot during removal from the reaction flask.

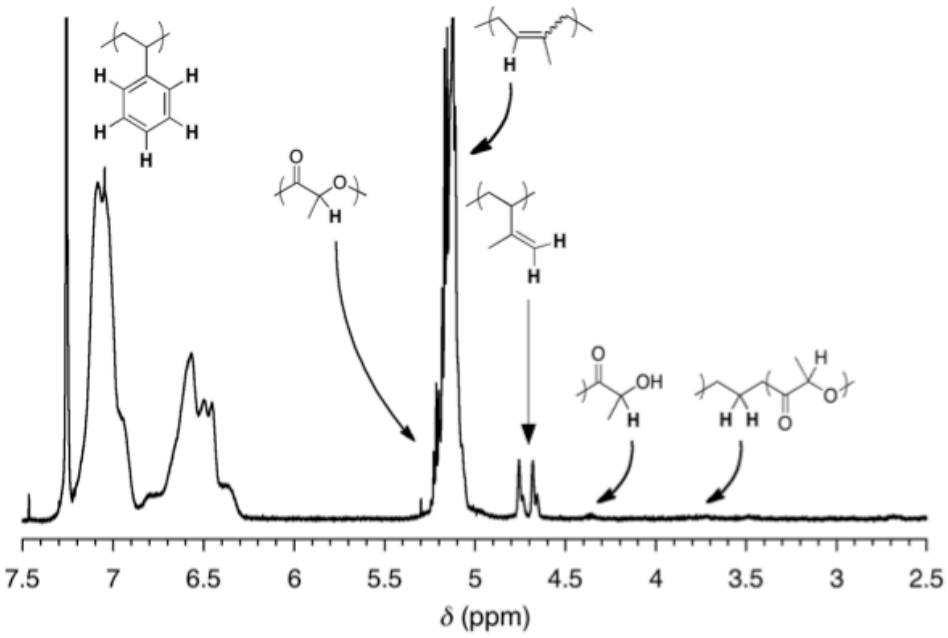

Figure 2.6. ^{1}H NMR spectrum of PS-PI-PS-PLA(0.20) in $CDCl_3$ at 25 °C. End group analysis was performed using the methylene resonance at 3.8 ppm and also with the sec-butyl end group at 0.5-0.9 ppm (not shown in this figure). Degree of polymerization calculated both ways gave identical molar mass for the PS-PI-PS-PLA tetrablock.

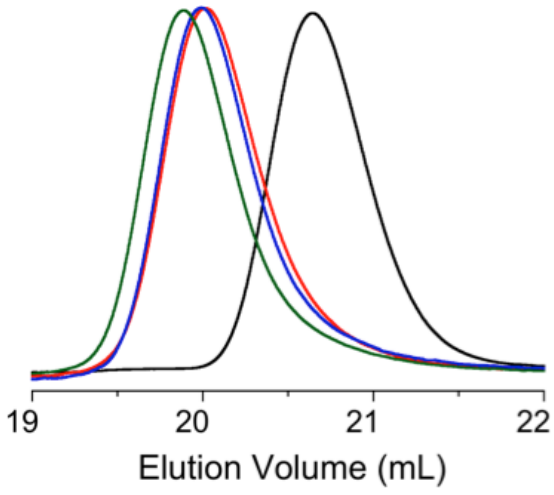

Figure 2.7. SEC traces for PS-PI-PS-OH triblock [black], SISL(0.19) [red], SISL(0.20) [blue], and SISL(0.25) [green].

2.2.2 Phase Behavior of PS-PI-PS and PS-PI-PS-PLA Polymers

Differential scanning calorimetry (DSC) was used to identify the glass transition temperatures of the PS, PI and PLA blocks (**Table 2.1**). Two inflections between 50 and 70 °C are present in the DSC curves of the tetrablocks (**Figures 2.8 and 2.9**) suggest that the PS and PLA blocks are microphase separated; $T_{g,PS}$ (~63 °C) is approximately 10 °C higher than $T_{g,PLA}$ (~53 °C).

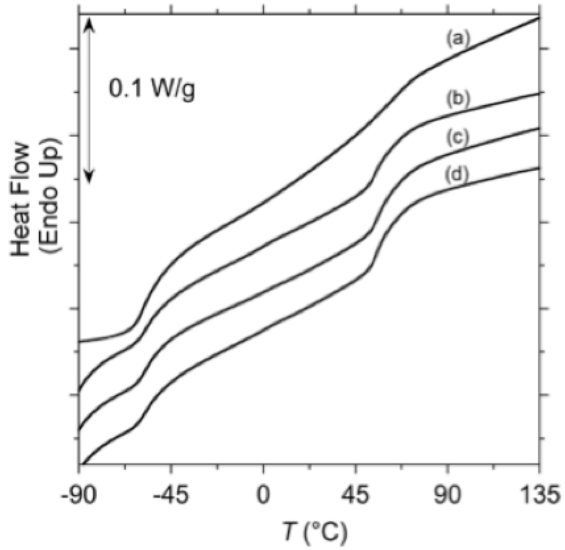

Figure 2.8. DSC curves for PS-PI-PS-OH, (a), PS-PI-PS-PLA(0.20), (b), PS-PI-PS-PLA(0.21), (c), PS-PI-PS-PLA(0.25), (d). Curves shifted vertically to show more clearly.

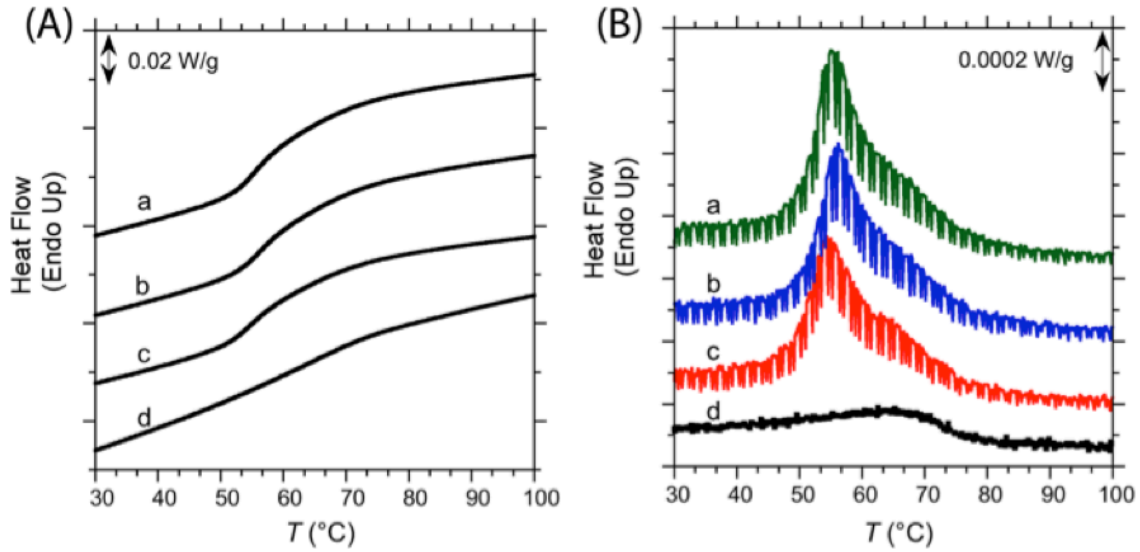

Figure 2.9. Raw data plot, (A) and derivative plot, (B) of DSC data for PS-PI-PS-OH and PS-PI-PS-PLA showing glass transition temperatures for PS and PLA blocks. Individual curves shown in each are (a) PS-PI-PS-PLA(0.25), (b) PS-PI-PS-PLA(0.21), (c) PS-PI-PS-PLA(0.20), and (d) PS-PI-PS-OH. Curves have been shifted vertically for clarity.

The morphologies formed by the PS-PI-PS and PS-PI-PS-PLA samples listed in **Table 2.1** were determined from a combination of small-angle X-ray scattering (SAXS) data and transmission electron microscopy (TEM) imaging. Powder samples (approximately 400–500 mg) of PS-PI-PS and PS-PI-PS-PLA were pressed into rectangular plaques and then processed using a channel-die at 150 °C to align the underlying morphologies into macroscopically oriented polymer "matchsticks" (stick dimensions $W \times H \times L$: 2 mm × 2 mm × 100 mm). 2D-SAXS was performed on small rectangular pieces ($W \times H \times L$: 2 mm × 2 mm × 5 mm), cut from the end of each sample.

The PS-PI-PS triblock exhibited lamellar morphology as expected with equal portions PS and PI (**Figure 2.10**). All three tetrablocks showed similar one-

dimensional (1D) and two-dimensional (2D) scattering patterns in the XY, XZ and YZ planes consistent with an aligned hexagonally packed cylindrical morphology (**Figure 2.11a-c**, **2.12a-c**).

A representative 1D-SAXS profile from the XY plane of channel-die aligned PS-PI-PS-PLA(0.21) reveals a primary scattering peak at q^* = 0.23 nm^{-1} (D = 27 nm) and higher order reflections that are consistent with hexagonal symmetry (**Figure 2.12**).

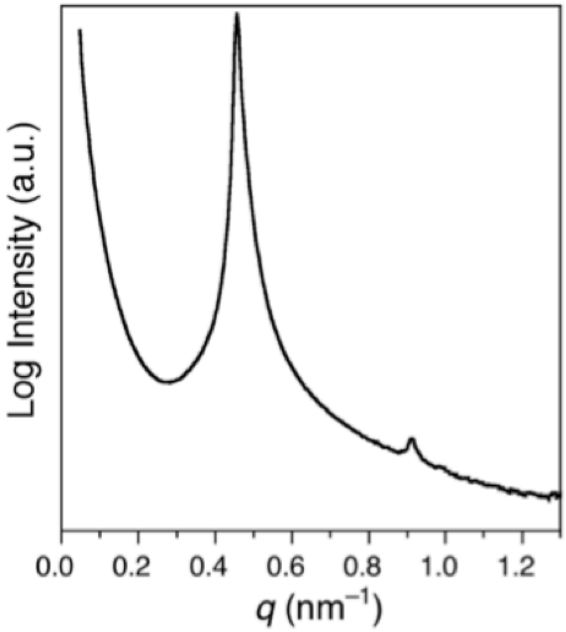

Figure 2.10. Room temperature 1D-SAXS data for PS-PI-PS [6-10-6] triblock after channel die alignment. SAXS and TEM are both consistent with an alternating lamellar morphology with a domain spacing of 14 nm (q^* = 0.44 nm^{-1}).

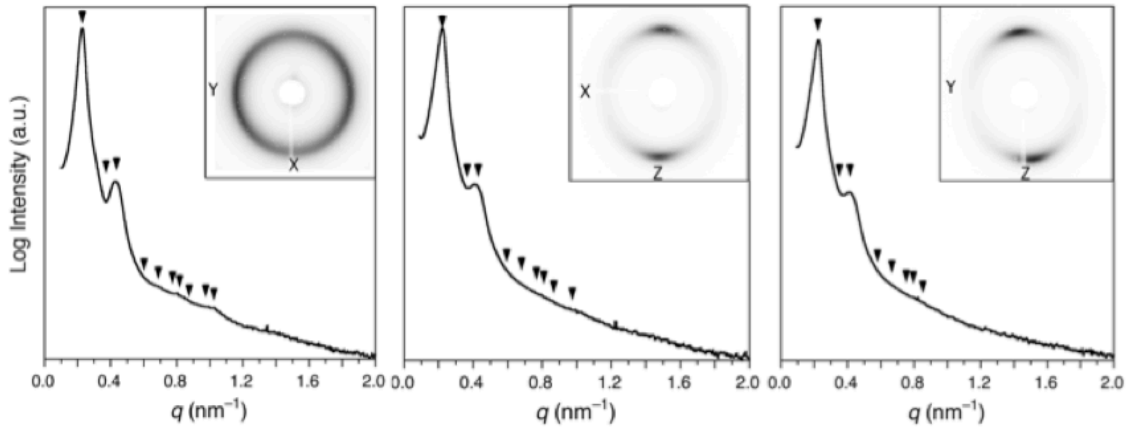

Figure 2.11. Room temperature 1D-SAXS data for channel-die aligned PS-PI-PS-PLA (0.20) with corresponding 2D-SAXS patterns. Scattering from the XY plane, *left*; XZ plane, *middle*; and the YZ plane, *right*. Triangles mark the following theoretical reflections for q/q* for hexagonally-packed cylinders: 1,√3: √4: √7: √9: √12: √13: √16: √19: and √25.

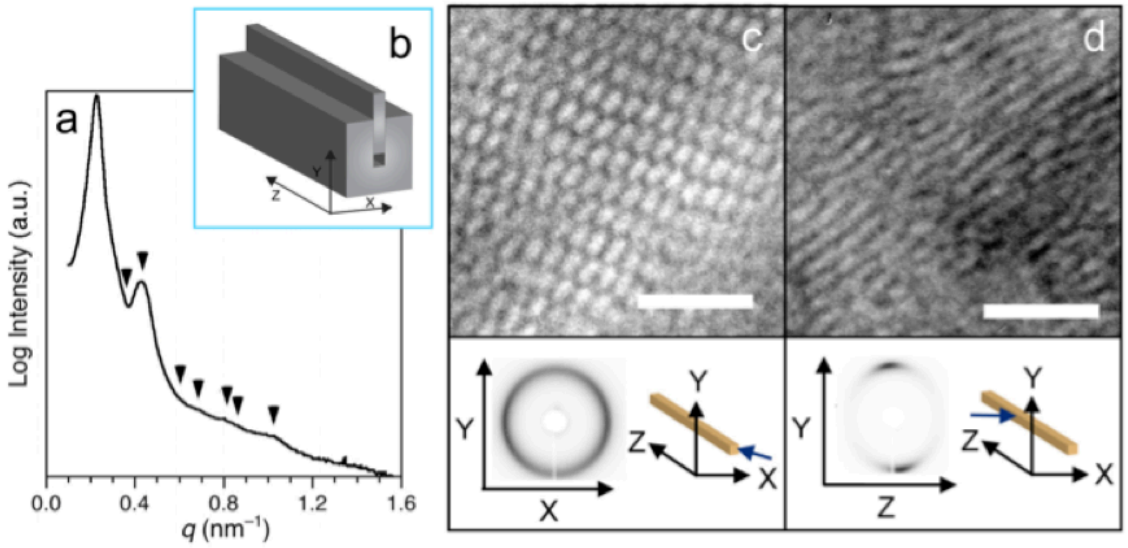

Figure 2.12. 1D-SAXS of PS-PI-PS-PLA polymer (f_{PLA} = 0.21) taken at 25 °C, after channel-die alignment at 150 °C, (a). Triangles indicate theoretical q/q^* ratios of √3: √4: √7: √9: √13: √16: and √25 associated with the hexagonal packed cylinder morphology. Cartoon of channel die apparatus, (b), showing direction of flow along z-axis. Morphology characterization of XY plane, (c) (*Bottom*, 2D SAXS patern; *Top*, TEM of XY face of microtomed channel-die stick). Morphology characterization of YZ plane, (d) (*Bottom*, 2D SAXS pattern; *Top*, TEM of YZ face of microtomed channel-die stick). Scale bars are 100 nm.

The 2D-scattering (**Figure 2.11**) from each of the three planes (XY, XZ and YZ planes) of PS-PI-PS-PLA (0.20) is consistent with scattering expected from an aligned cylindrical morphology. For a macroscopically aligned cylindrical morphology, incident radiation perpendicular to the direction of flow (i.e., perpendicular to the XZ or YZ planes) produces 2D-SAXS patterns with two distinct peaks in intensity at scattering vectors separated azimuthally by 180° (**Figure 2.13**).

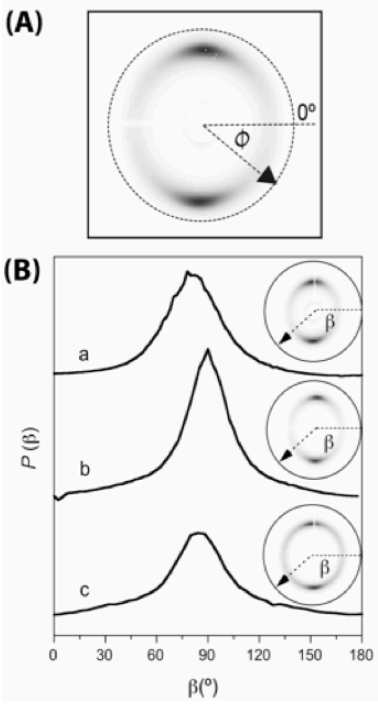

Figure 2.13. Representative diagram of integrated area used for each sample, (A); and normalized orientation distribution function (P(ß)) from channel-die aligned PS-PI-PS-PLAs polymers, (B), with f_{PLA} of (a) 0.20 (F_2 = 0.65) (b) 0.21 (F_2 = 0.77) and (c) 0.25 (F_2 = 0.72) .

Using the 2D-scattering pattern, analysis of the change in the intensity of primary scattering vector, q^*, with respect to azimuthal angle β was studied to determine the degree of cylinder alignment. The degree of alignment increases with

the value of the second-order orientation factor F_2, from 0 to 1 (i.e., isotropic to perfectly aligned, see below for details). A normalized orientation distribution function (P, eq. 1) was calculated followed by the calculation of F_2 for each 2D-SAXS pattern (eq. 2 and 3).

$$P(\beta) = \frac{I(q^*, \beta)q^{*2}}{\int_0^\pi I(q^*, \beta)q^{*2}sin\beta d\beta} \quad \text{(eq 1)}$$

$$F_2 = 1 - 3\langle cos^2\beta \rangle \quad \text{(eq 2)}$$

$$\langle cos^2\beta \rangle = \int_0^\pi cos^2\beta P(\beta) sin\beta d\beta \quad \text{(eq 3)}$$

Values of F_2 between 0.65 and 0.77 were calculated for channel-die aligned PS-PI-PS-PLA tetrablocks, consistent with a moderate degree of alignment parallel to the direction of flow.

Channel-die aligned samples were cryo-microtomed at –100 °C into ~ 60–70 nm thick slices and then stained with OsO_4 vapor (10 minutes) prior to TEM imaging to gain contrast between phases. TEM images of a representative channel-die aligned PS-PI-PS-PLA tetrablock (f_{PLA} = 0.21) are shown in **Figure 2.12c-d**. The structure is consistent with an "inverted" cylinder morphology where the majority domains PS and PLA (shown in white) form the cylinders and the minority domain, PI (stained black) forms the matrix. Bluemle recently reported inverted sphere and cylinder morphologies for PS-PI-PS-PEO tetrablock polymers when the PI midblock was the minority block.[39] The inverted core-shell cylinder structure of the PS-PI-PS-PLA tetrablocks is consistent with the morphology observed in PS-PI-

PS-PEO polymers having almost identical composition and molar mass.[39] The similar phase behavior in the PS-PI-PS-PEO and PS-PI-PS-PLA tetrablocks can be attributed to the A-B-A-C block architecture and the corresponding effect on the sequencing of the segment-segment interaction parameters ($\chi_{BC} >> \chi_{AC} \approx \chi_{AB}$; where A is PS, B is PI and C is PLA or PEO). For similarly structured non-frustrated A-B-C systems such as PI-PS-PEO[44] and PI-PS-PLA[45] (where $\chi_{AC} >> \chi_{BC} \approx \chi_{AB}$), inverted morphologies have not been reported. However, in A-B-C systems such as PS-PI-PEO,[41] PI-PS-PDMS[46], and some PS-PB-PMMA/PB-PMMA blends[47], where the midblock is highly incompatible with both outer blocks ($\chi_{BC} >> \chi_{AC} \approx \chi_{AB}$), compositionally inverted morphologies have been reported.

Figure 2.12c combines a TEM image of the XY plane with a 2-D x-ray scattering pattern from the same plane. Imperfect sample alignment during the microtome step resulted in a slight distortion of the hexagonal structure when visualized by TEM (**Figure 2.12c**). **Figure 2.12d** combines both the TEM image and the 2D SAXS pattern for the YZ plane, and both are consistent with an aligned structure. The 1-D scattering data (**Figure 2.12a**), TEM and 2-D scattering profiles of (**Figures 2.12c and 2.12d**) together point to an aligned hexagonally packed cylinder morphology. This hexagonally packed cylinder morphology is also evident in micrographs for tetrablocks with $f_{PS} = f_{PI}$ and f_{PLA} between 0.20 and 0.25 (**Figures 2.14 and 2.15**)

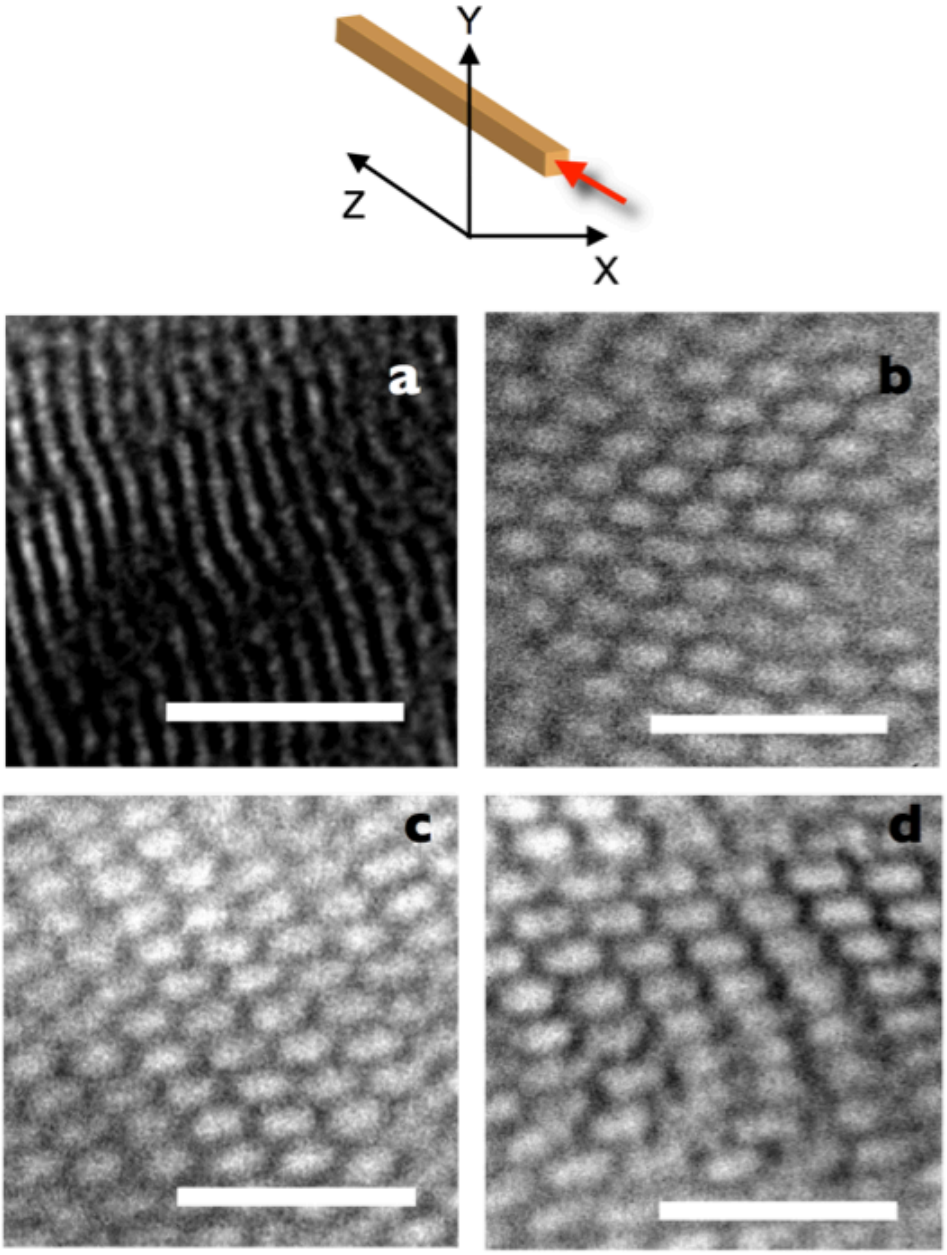

Figure 2.14. TEM of XY face of channel-die aligned polymers PS-PI-PS-OH (a), PS-PI-PS-PLA(0.20) (b), PS-PI-PS-PLA(0.21) (c), PS-PI-PS-PLA(0.25) (d). Samples were cryo-microtomed into ~60–70 nm thick samples at −100 °C and then stained with osmium tetroxide vapor for ~10 minutes before imaging. Black regions are due to stained polyisoprene domains. White domains contain both polystyrene and polylactide. Scale bars are 100 nm.

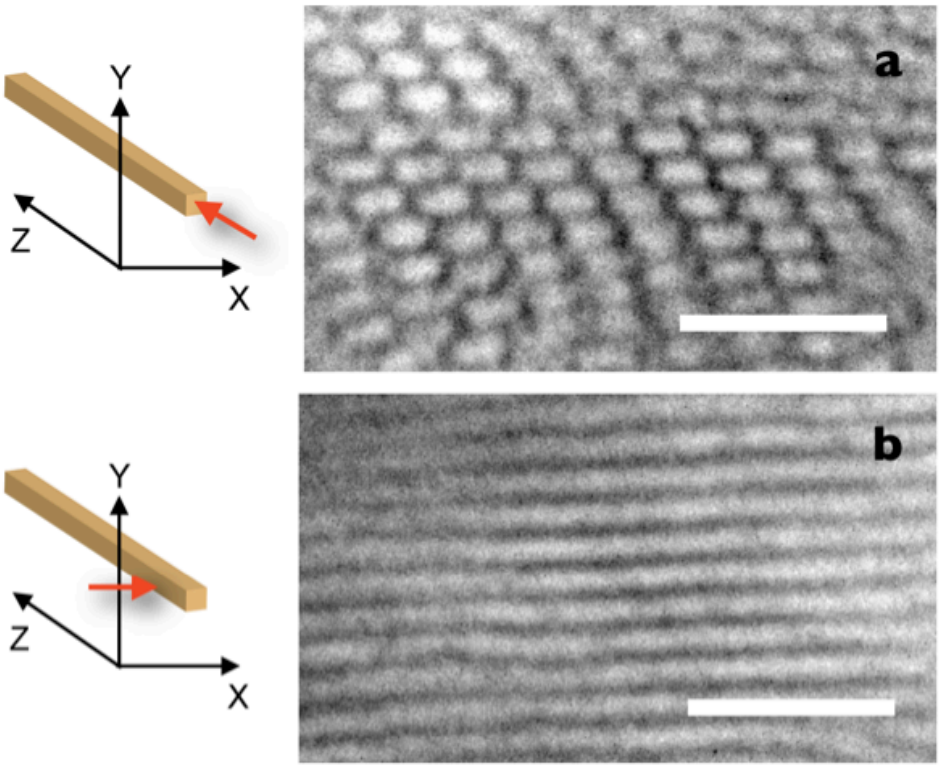

Figure 2.15. TEM of XY face of channel-die aligned polymers PS-PI-PS-PLA(0.25) (a), and TEM of YZ face of PS-PI-PS-PLA(0.25) (b). Samples were cryo-microtomed into ~60–70 nm thick samples at −100 ºC and then stained with osmium tetroxide (OsO_4) for ~10 minutes before imaging. Black regions are due to stained polyisoprene domains. White domains contain both polystyrene and polylactide. Scale bars are 100 nm. Image (a) is the same image as Figure 2.14d but is repeated here for comparison to YZ face.

2.2.3 Thin Film Morphology

PS-PI-PS-PLA polymers were drop cast from a dilute solution of toluene onto Formvar coated TEM grids and stained with OsO_4. The as-cast specimens also exhibited a cylinder structure of white PS and PLA domains within a dark PI matrix (**Figures 2.16 and 2.17**). In these as-cast films, there were regions of parallel cylinder orientation, regions of perpendicular orientation and also mixed regions

(**Figure 2.17**). These variable structures were hypothesized to arise due to different evaporation rates and film thickness variations across the TEM grid. In some thinner sections of the film (**Figure 2.16**) where the polymer adopts a parallel orientation, contrast between PS (white) and PLA (grey) domains showed the core(PLA)-shell(PS) structure. To further confirm the core-shell cylinder morphology, we used scanning electron microscopy (SEM) of PLA etched samples as discussed below.

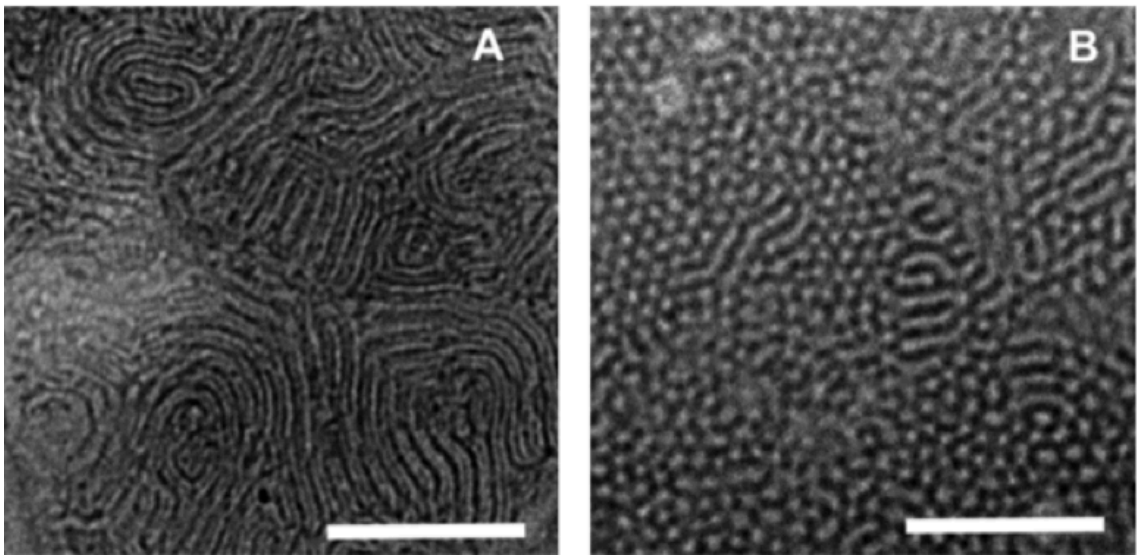

Figure 2.16. TEM of OsO_4 stained film of PS-PI-PS-PLA(0.20) drop cast onto TEM grid from 0.1 wt % toluene solution, (A and B). Different regions of the film showed different cylinder orientation: some parallel, as in (A), and some perpendicular and parallel, as shown in (B). The high contrast in image (A) shows 3 distinct domains: Black is polyisoprene, white is polystyrene and the light grey between the white polystyrene domains is polylactide. The slight contrast between PS and PLA is due to the inherent different in electron density between PS and PLA since neither are stained with OsO_4. Less contrast is evident for the perpendicular regions. Film was stained with OsO_4 for ~10 minutes before imaging. Black regions are due to stained polyisoprene domains. Scale bars are 300 nm.

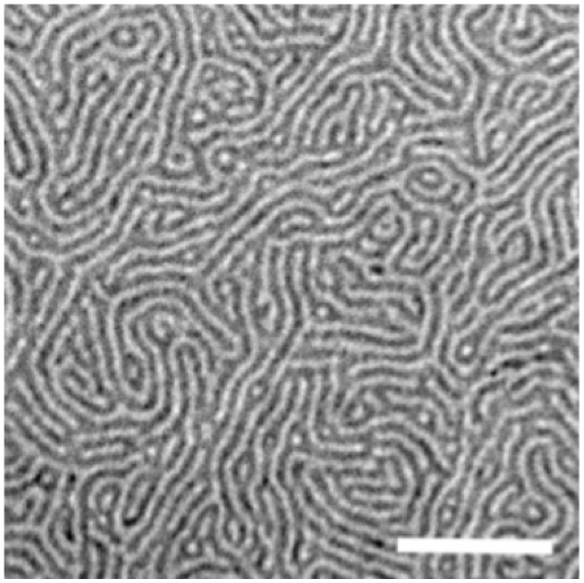

Figure 2.17. TEM of film of PS-PI-PS-PLA(0.19) drop cast onto TEM grid from 0.1 wt % toluene solution. Film was stained with OsO_4 for ~10 minutes before imaging. Black regions are due to stained PI domains. Scale bar is 300 nm.

2.2.4 Tensile Properties of PS-PI-PS and PS-PI-PS-PLA Polymers

Representative engineering stress vs. percent strain curves of PS-PI-PS-PLA(0.20) and PS-PI-PS-PLA(0.25) (**Figures 2.18 and 2.19**) demonstrate that these materials consistently behave as tough materials with average elongations at break (ε_b) near 450% strain (**Table 2.1**). Thus we expect nanoporous materials derived from these polymers to be more robust than nanoporous PS or PS-PI-PS monoliths.

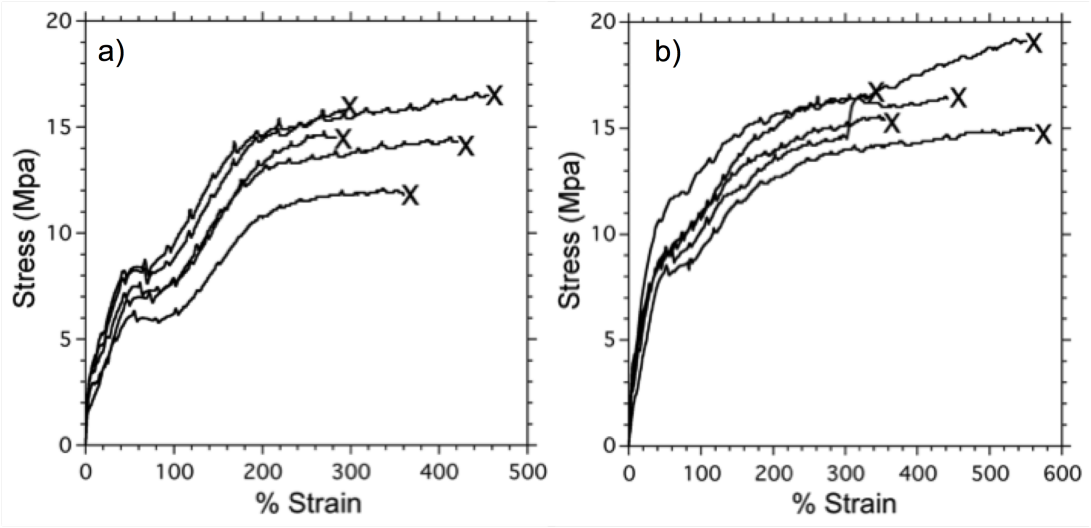

Figure 2.18. Stress vs Strain data for pressed rectangles of PS-PI-PS-PLA(0.20), (a); Stress vs Strain data for PS-PI-PS-PLA(0.25), (b). X marks point at which the sample broke.

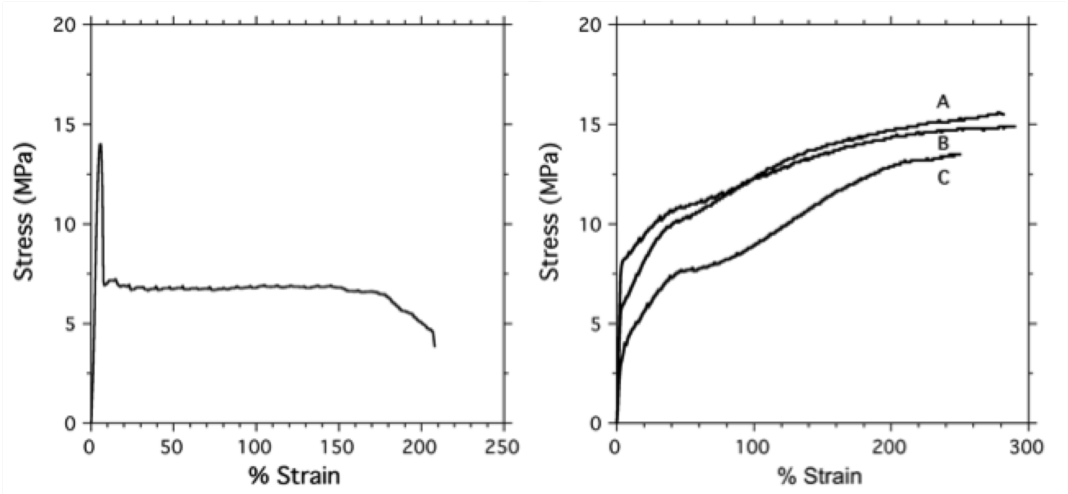

Figure 2.19. Stress versus % Strain data for pressed dogbones. Left, PS-PI-PS precursor; Right, PS-PI-PS-PLA(0.21), (A), PS-PI-PS-PLA(0.20), (B), and PS-PI-PS-PLA(0.25), (C). Dogbones of PS-PI-PS-PLA tetrablocks did not break. The highest % strain in plot B represents the limit of extension in the small tensile tester. Figure 2.18 Contains results from smaller samples that could be stretched long enough to break using the small scale tensile tester.

2.2.5 Basic Hydrolysis of PLA from Bulk PS-PI-PS-PLA

PLA can be etched from monoliths of PS-PLA and most other PLA containing block polymers using a basic solution (0.5 M NaOH) of 60:40 (v:v) water:methanol at 65 °C.[43] To prevent PS pore-wall collapse during degradation of PS-PI-PS-PLA samples, the etching solution temperatures were kept at room temperature because of the relatively low T_g of the PS shell (~63 °C). A small amount of sodium dodecyl sulfate (SDS) was added to increase compatibility between the etching solution and the hydrophobic PS pore walls, ensuring complete infiltration.[43] Initial attempts to remove PLA involved submerging a small cube cut from a channel-die aligned sample into a dilute basic solution (0.5M NaOH, 60:40 (v:v) water:methanol, 0.1 wt % SDS) for one week.

PS-PI-PS-PLA cubes etched at room temperature had pores that were visible by SEM (**Figure 2.20**) but very limited removal of PLA; SEC and ^{1}H NMR results suggested that not all of the PLA had been removed from room temperature etched samples. It was hypothesized that despite the addition of 0.1 wt% SDS, the hydrophilic etching solution could not reach very far into the pores likely due to the hydrophobic nature of the matrix combined with imperfect cylinder alignment (alignment ~70%). Despite the inability to remove all of the PLA from the bulk samples, it was expected that nanopores would be more accessible in thin films.

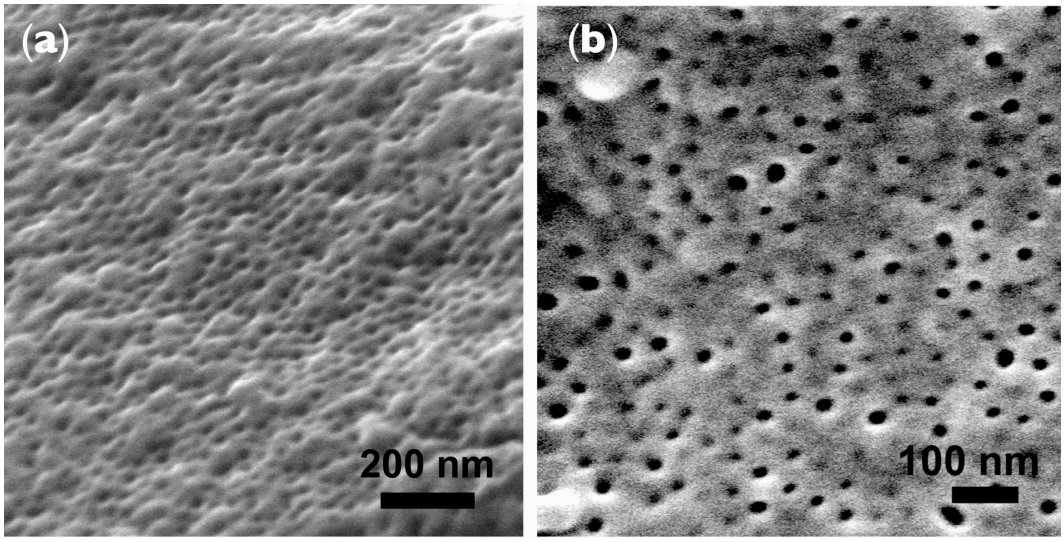

Figure 2.20. SEM images of XY face of etched channel-die aligned PS-PI-PS-PLA(0.20) after etching at room temperature with 60/40 water/methanol in 0.5 M NaOH with 0.1 wt% SDS.

2.2.6 Composite Membrane Preparation

Figure 2.1b illustrates the composite membrane structure we prepared. For the supporting material, we used a polyethersulfone (PES) membrane (**Figure 2.24**) with an average pore diameter of 117 nm ± 103 nm (from Imagej™ analysis of a 133 μm^2 binarized SEM image, (**Figure 2.21**) and a reported molar mass cut-off of 1,000 kDa). Composite membrane structures were prepared using two strategies: 1) by directly spin coating the PS-PI-PS-PLA polymer onto a water filled PES support (**Figure 2.22**),[19,35] and 2) by spin coating onto a salt plate, dissolving the salt plate and then transferring the film to the PES supporting material (**Figure 2.23**).[9,48]

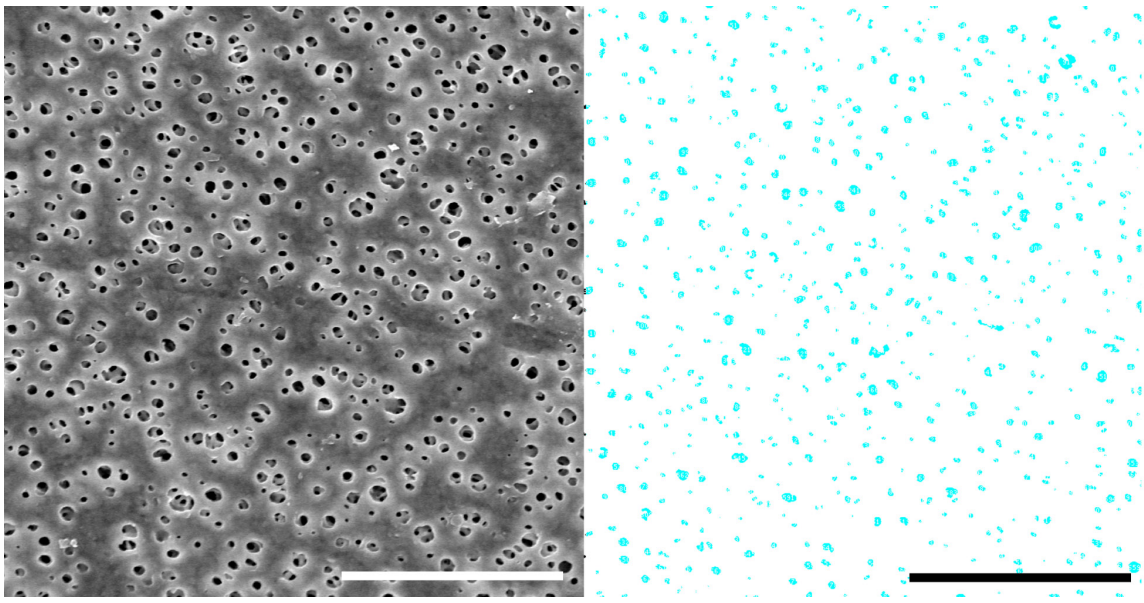

Figure 2.21. Real (*left*) and Binary (*right*) SEM images of support surface. Right image was used to estimate average pore size and pore surface area. Scale bars are both 4 micron.

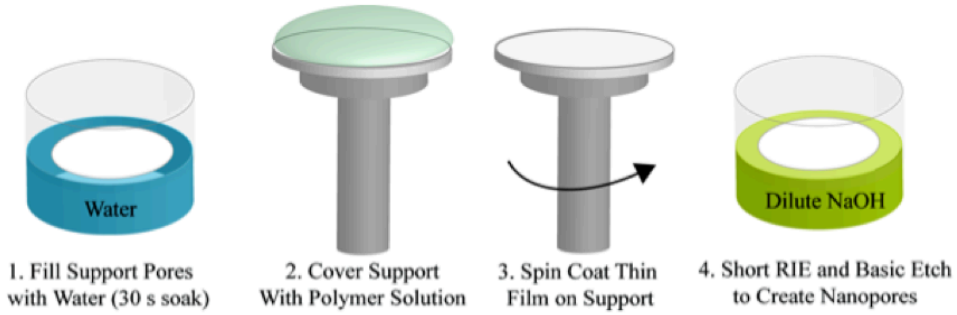

Figure 2.22. Procedure for direct coating onto PES support by spin coating.

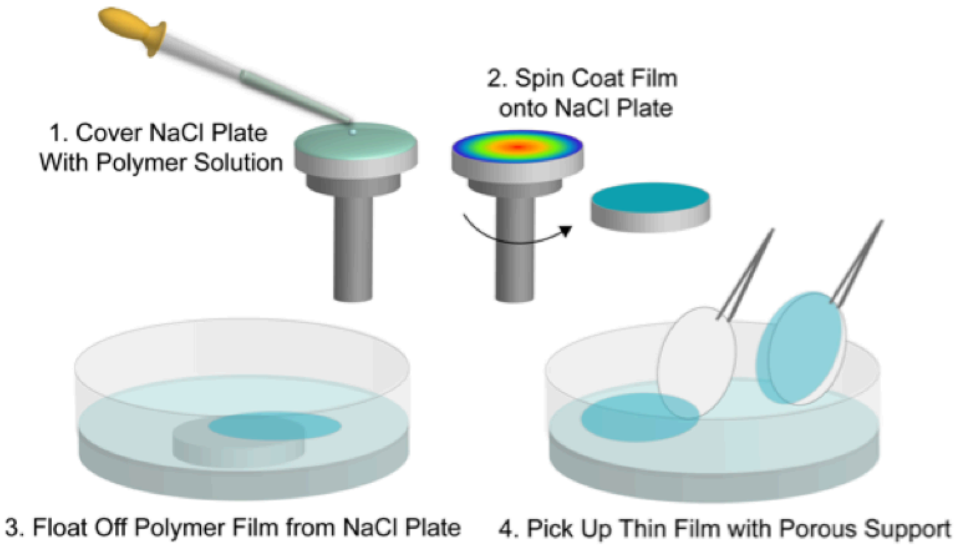

Figure 2.23. Procedure for coating via the salt plate transfer method.

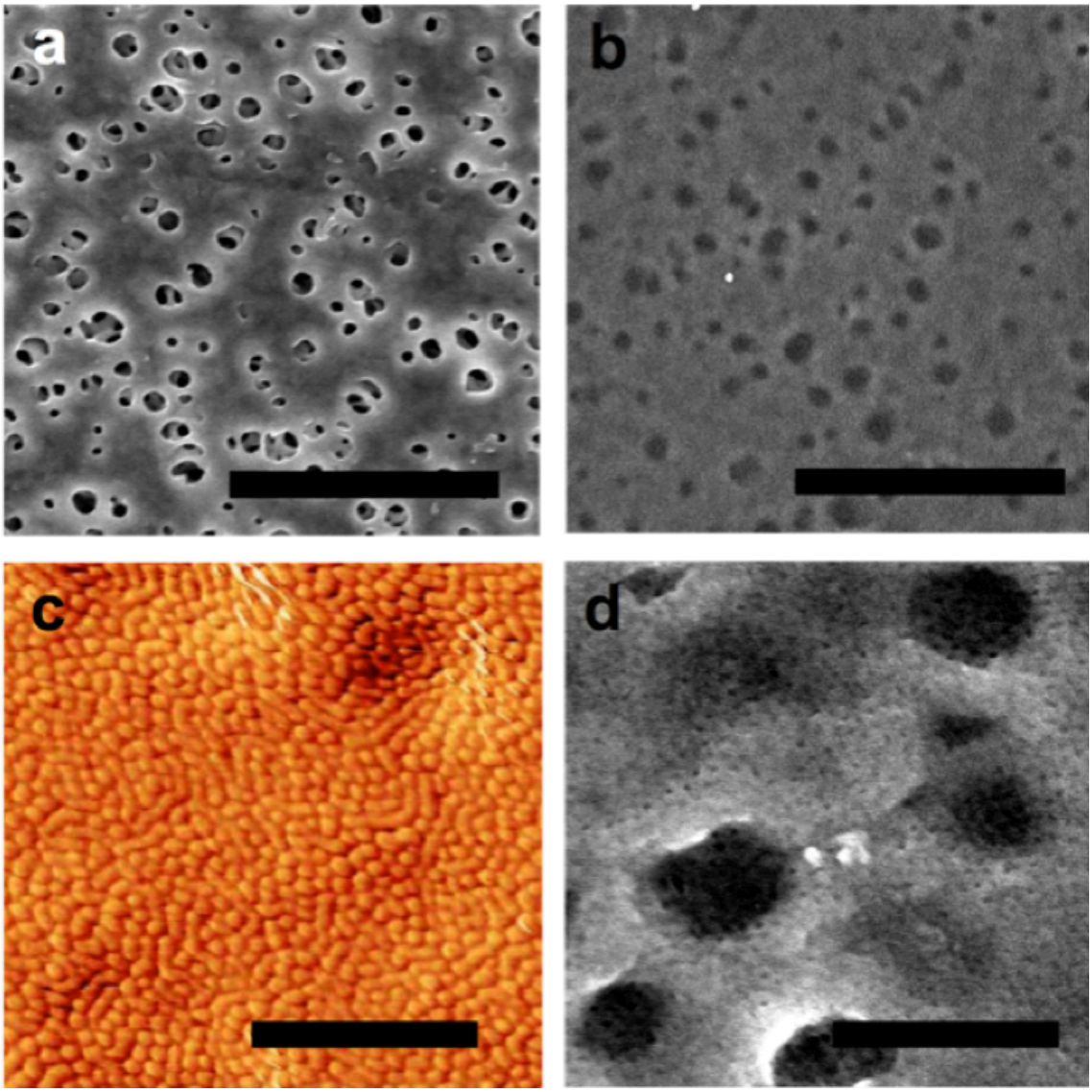

Figure 2.24. Composite membrane prepared by direct coating of tetrablock onto a PES support: SEM of bare microporous PES, (a); SEM of PS-PI-PS-PLA(0.21)/PLA blend coated PES Support after direct spin coating, (b); Tapping mode AFM phase image of surface of spin coated film coated on of PES support, (c); We observed similar results using pure PS-PI-PS-PLA tetrablocks. SEM of nanoporous selective layer after PLA hydrolysis, (d). Scale bars for images a and b are 3 micron. Scale bars for c and d are 500 nm.

The right combination of polymer solvent and PES filling liquid was necessary to successfully create a fully coated PES support through the direct coating method. The combination that resulted in complete coverage of the support and also avoided polymer precipitation during the coating process was a non-polar organic solvent with a polar immiscible liquid in the support. Importantly, a filling liquid that does not affect the block polymer morphology during the coating process is essential. Furthermore, it must be easily removed after coating. Water worked well as a polar filling liquid for the PES support and toluene (**Figure 2.24b** and **Figure 2.25a**) or chlorobenzene (**Figure 2.25b**) as the PS-PI-PS-PLA solvent gave the most complete coverage. The worst coverage was found with water miscible PS-PI-PS-PLA solvents, such as THF (**Figure 2.25c**).

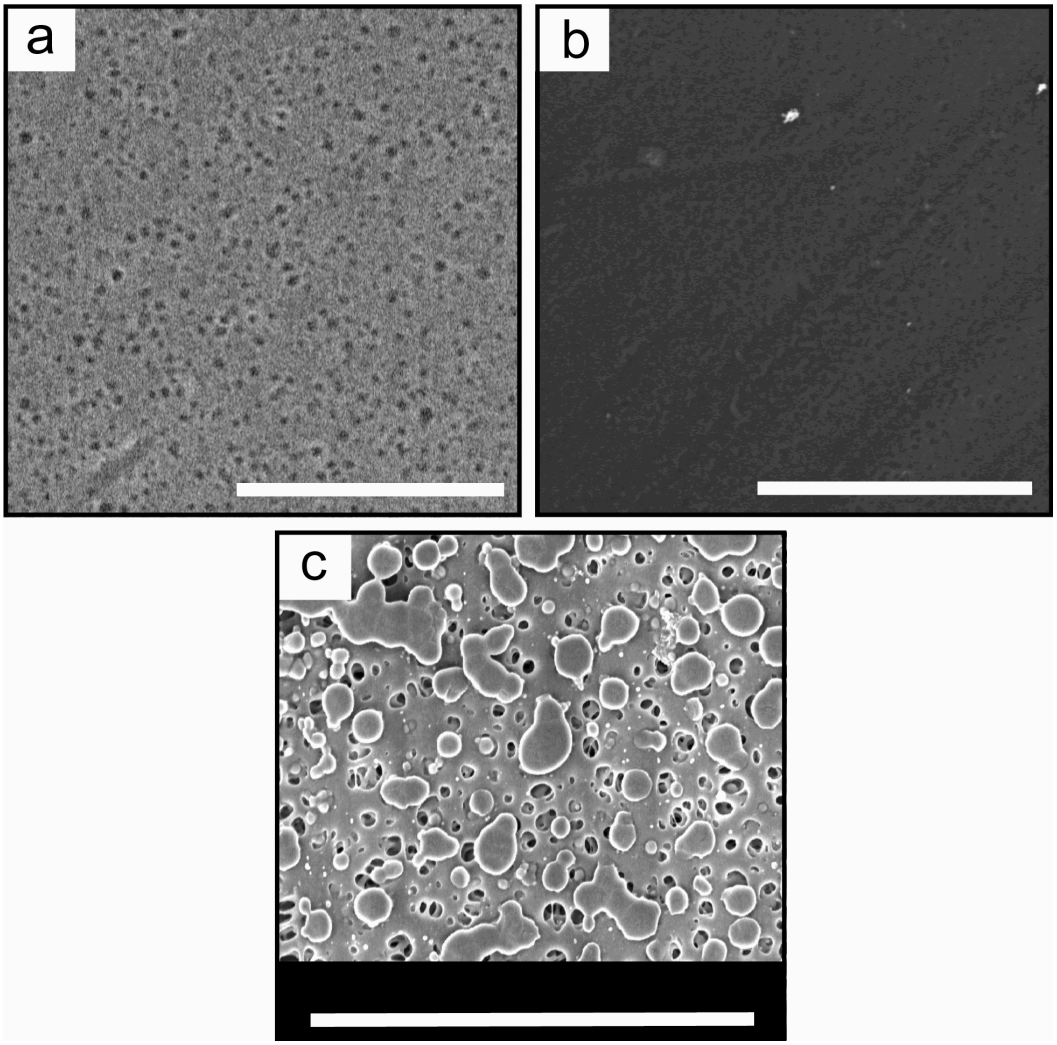

Figure 2.25. SEM images of composite membrane surfaces after spin coating from toluene solution (a), chlorobenzene solution (b), THF solution (c). Scale bars are 7.5 micron.

It was recently demonstrated that spin coating a similar PS-PI-PLA triblock polymer from chlorobenzene resulted in perpendicular cylinder orientation.[35,48] This method was employed on the tetrablock terpolymers and it was found that a uniform defect free film coating was accessible. However, the block polymer film at the air-polymer interface showed parallel cylinders by AFM for PS-PI-PS-PLA. Instead, it was found that with toluene, a relatively neutral solvent for PS, PI and

PLA, a mixture of parallel and perpendicularly orientated cylinders was achieved (**Figure 2.26a**) and also good thin film coverage of the PES support (**Figure 2.24b**).

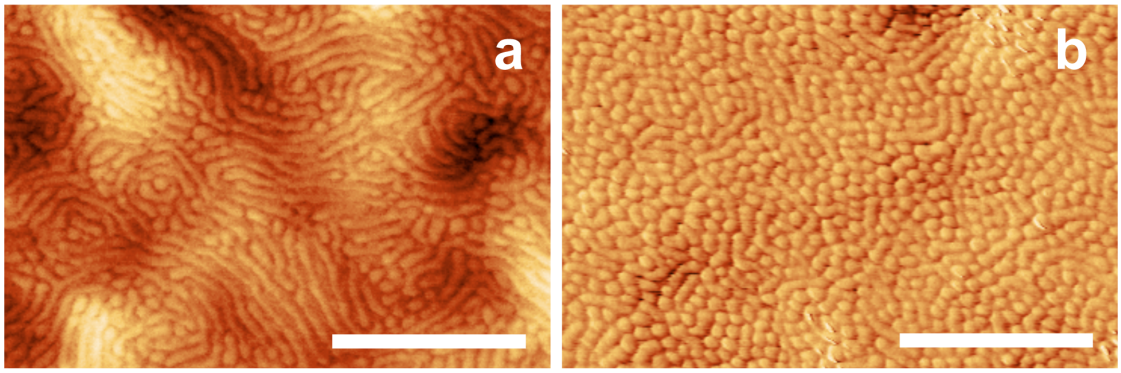

Figure 2.26. Tapping mode AFM images of surface of PS-PI-PS-PLA(0.21), (a); and PS-PI-PS-PLA(0.21)/PLA, (b), films spin coated onto water filled PES support from toluene. Scale bars are 500 nm.

Addition of homopolymer of the minority block in cylinder forming diblock copolymers can enhance the directionality of ordering in the film.[49,50] The confinement of a homopolymer that has a molar mass slightly larger than the respective copolymer block causes stretching of homopolymer chains along the long axis of the cylindrical domains to overcome confinement to a domain that is smaller than the radius of gyration (R_g) of the homopolymer.[50] As solvent is removed, confined yet elongated homopolymer chains develop into perpendicular copolymer/homopolymer cylindrical domains with higher regularity than for the copolymer alone.[50] To test this hypothesis, a small amount (5 wt% of total polymer) of PLA homopolymer was added to induce perpendicular orientation during solvent evaporation in spin coating. PLA homopolymer with a molar mass of 10 kg mol^{-1} was chosen, slightly larger than PLA block in the tetrablock (7 kg mol^{-1}). The

molar mass ratio (alpha) of (homopolymer)/(PLA block) for our blend is ~1.4 which is near the estimated ideal ratio of 1.5 needed for maximum perpendicular enhancement from the confinement of homopolymer in cylindrical domains suggested by Jeong et al.[50] PS-PI-PS-PLA spin coated films contained mixed orientation of cylinders (**Figure 2.26a**). Films spin coated from a 95/5 wt/wt PS-PI-PS-PLA(0.21)/PLA blend (2 wt % of polymer overall in toluene; total $f_{PLA\text{-}Blend}$ = 0.24) contained mostly perpendicularly oriented cylinders at the surface by AFM (**Figure 2.26b**). The addition of homopolymer to block polymer films has been used previously in nanoporous block polymer membranes to tune pore size.[51] While the main intention for the PLA homopolymer in our case was to induce perpendicular orientation, one can imagine that it could also be used to control pore size.

Using a solution of PS-PI-PS-PLA, PLA and toluene for the film casting process, ordered thin films were prepared in composite membranes. Directly coated composite membranes were prepared by spin coating a 2.3 wt% solution of 95/5 wt/wt PS-PI-PS-PLA/PLA blend in toluene onto water filled polyethersulfone (PES) membranes (**Figure 2.24a**). The water filled support was then attached to a spin coater (**Figure 2.22**) and coated with enough solution to fully cover the substrate without overflowing the PES surface. Once fully covered with the polymer solution, PES supports were spun at 2000 rpm and left to dry for at least one hour before removing. Surfaces of resulting membranes after coating are shown in **Figure 2.24b and 2.24c**.

For composite membranes prepared by the salt plate method (described in more detail in **Figure 2.23**), the same toluene solution was dispensed onto a sodium chloride (NaCl) plate and spun at 2000 rpm. After drying, the salt plate was separated from the polymer film by dissolving in water for a few minutes. The thin film was then lifted out of the water by scooping up the film from below with the supporting.

Early attempts to remove PLA by basic hydrolysis without reactive ion etching (RIE) resulted in few nanopores on the surface by SEM. As we expect that this was due to a surface wetting layer, dried composite membranes were exposed to 15 seconds of reactive ion etching (RIE) to remove any surface wetting layer of PS or PI blocking the PLA domains. After RIE, composite membranes were then exposed to a dilute solution of sodium hydroxide in water (0.05 M NaOH) for 45 minutes to hydrolyze the PLA domains. Afterwards, composite membranes were rinsed with pure water for 20 minutes to remove any residual lactic acid or salts. SEM micrographs of the surfaces of representative composite membranes after RIE and PLA hydrolysis demonstrate the nanopores created through this etching process (**Figure 2.24d**, directly coated membrane; **Figure 2.27**, for the salt plate method). The average pore size was estimated as 15 nm from SEM micrographs of the surface of the composite membranes after PLA removal.

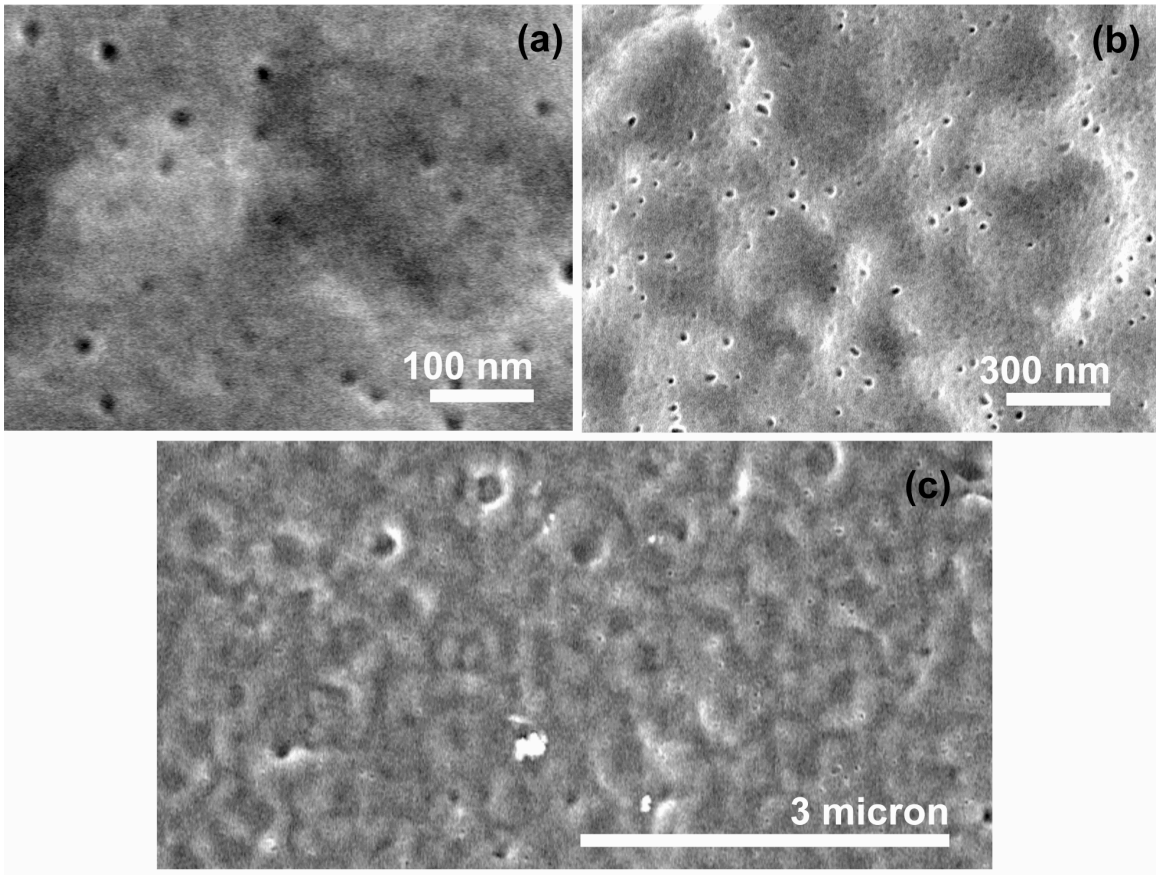

Figure 2.27. SEM images for surface of membrane prepared by salt plate method. SEM images were taken after base etching and flux test. High magnification, (a), medium magnification, (b), and lower magnification, (c).

2.2.7 Composite Membrane Evaluation

Results from flow experiments of pure water are shown in **Figure 2.28**. Permeability was measured as 96.9 L $m^{-2}h^{-1}bar^{-1}$ (**Figure 2.28a**) for a membrane prepared by the salt plate method and 53.7 L $m^{-2}h^{-1}bar^{-1}$ for a directly coated membrane (**Figure 2.29**). While, the permeability for either membrane is less than expected for the ideal composite membrane of nanoporous PS-PI-PS on the PES support, they are both comparable to commercial ultrafiltration membranes.[52,53]

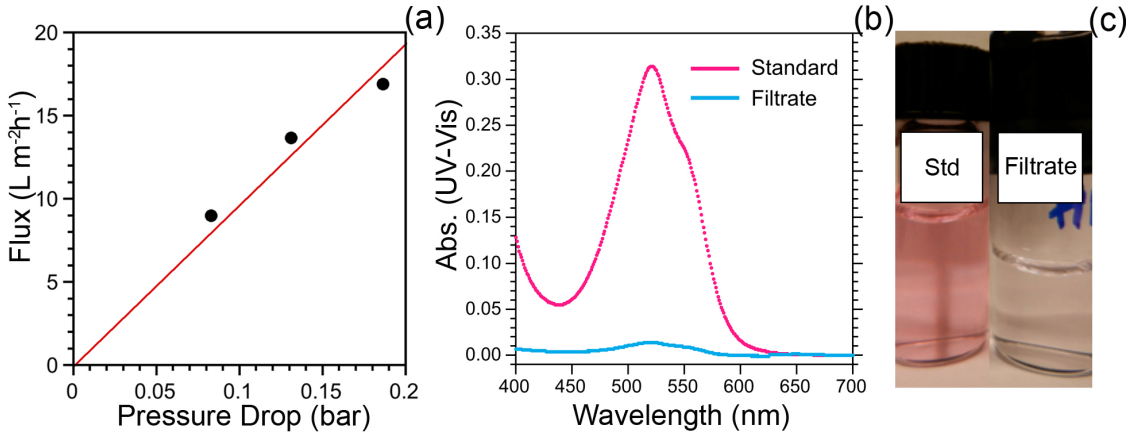

Figure 2.28. Permeability data from a composite PS-PI-PS/PES membrane, (a). Permeability of 96.9 L $m^{-2}h^{-1}bar^{-1}$ was found from the slope of the linear fit (red). UV-vis Absorbance results, (b), for standard fluorescent dextran solution (dark pink) and filtrate(blue). Photograph of standard (Std) and filtrate solutions, (c).

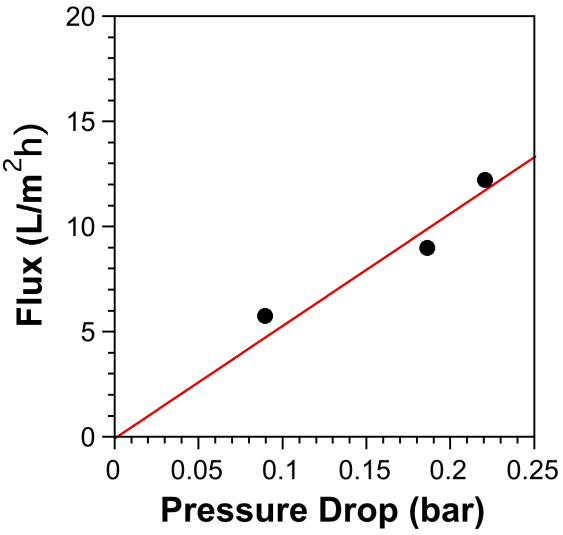

Figure 2.29. Permeability for directly coated membrane.

This theoretical permeability for an ideal membrane was calculated using the Hagen-Poiseuille fluid flow through a cylindrical pore[54]

$$\nu = \frac{\varepsilon}{\tau}\left(\frac{d^2\Delta P}{32\mu l}\right) \tag{1}$$

where the fluid velocity, ν, is dependent on pore diameter, d, film thickness, l, void fraction, e, tortuosity, τ, and liquid viscosity, μ. Without the PES support, the ideal permeability for water through the PS-PI-PS selective layer should be 5075 L $m^{-2}h^{-1}bar^{-1}$ using a e = 0.24; l = 100 nm; τ = 1 (assuming perfect perpendicular cylinder alignment); $\mu = 1\times10^{-8}$ bar s (water); and ΔP = 1 bar. Accounting for the porosity of the underlying support (0.06, estimated from support surface SEM image by ImageJ™ analysis of binary image, **Figure 2.21**), it was estimated that the permeability of a composite with an ideal selective layer would be 365 L $m^{-2}h^{-1}bar^{-1}$

assuming no resistance to flow from the underlying support. If it is assumed that the discrepancy between predicted and observed permeability is entirely due to the actual versus predicted pore density, then the fraction of PLA domains rendered "fully" porous can be assumed to be equivalent to the ratio of the observed to predicted permeabilities. By this analysis, ~27% of predicted pores are open for the salt plate method membrane and ~15% of pores open for the directly coated membrane. From SEM image analysis of composite membranes after etching, the percent of thin film surface area covered by nanopores at the upper surface is estimated to be ~5% for both the salt plate coated the directly coated films (equivalent to ~21 % of PLA domains open, which falls between the 27 and 15% by permeability estimation).

Considering that the PES support has a measured permeability of 3435 L $m^{-2}h^{-1}bar^{-1}$, we expect the composite membrane permeability to be a fraction of that value. If we assume all PLA domains above support pores were removed during etching, the resulting pore density on the surface of the membrane should be the PLA fraction of the selective layer (f_{PLA} = 0.24) times the void fraction of the support (0.06), or 0.0144 (1.4% of the surface area of the film). After multiplying by 0.24, the ideal volume fraction of pores in the top layer, by the measured PES permeability, the result is similar, 824 L $m^{-2}h^{-1}bar^{-1}$. This assumes that the block polymer layer is so thin that flux through the length of its pores should have no contribution to the overall permeability.[55] The only contribution we are considering is the actual surface area of pores in the thin film that connect to the underlying

support. Based on SEM image analysis, nanopores cover ~5% of the thin film surface area for the salt plate films and ~2.5 % of the thin film surface area for directly coated membranes (equivalent to ~21% and 10.5% of potential pores open, respectively for salt plate and direct coating). This reduction in surface area should bring down the permeability to 172 L $m^{-2}h^{-1}bar^{-1}$ for the salt plate coating and 86 L $m^{-2}h^{-1}bar^{-1}$ for the directly coated membrane if we assume the surface porosity matches the porosity within the thin film layer and that the thickness of the thin film contributes minimal to no resistance to the overall permeability of the composite membrane.[55] These estimations are relatively close to the measured values.

Tetramethylrhodamine-isothiocyanato-dextrans (TRITC-Dex) have been used in biological research mainly for studying permeability and transport in biological tissues and vessels.[56] Recently they have been used for accurate UF membrane selectivity characterization.[57, 58] TRITC-Dex was chosen as the solute for our rejection analysis because its concentration could be determined consistently and reproducibly by UV-Vis spectroscopic analysis for concentrations ranging from 0 to 0.5 mg/mL (where TRITC-Dex substitution is 0.001-0.0008 mol TRITC per mol of dextran). Although we did not test for fouling, limited fouling is expected for a neutral TRITC-Dex and a neutral membrane.[57]

A dilute solution of TRITC-Dex, M_w = 155 kg/mol, in water (0.5 mg/mL) was prepared and added to the filtration cell. Based on reported sizes, the 155 kg/mol TRITC-Dex should have an hydrodynamic radius (R_h) of about 17 nm in

diameter when dissolved in water.[56,59] The dextran solution was flushed through the membrane under a pressure of 0.2 bar and a stirring speed of 600 rpm. The filtrate was collected and analyzed by UV-vis to determine dextran concentration. UV-vis absorption of TRITC-Dex was found at λ_{max} = 521 nm in the standard solution, consistent with previously reported values for TRITC-Dex in water.[60,61] The UV-vis absorptions for the standard solution, pure water and intermediate concentrations of TRITC-Dex in water were also measured for comparison and calibration (**Figure 2.30**). **Figure 2.28b** shows the absorption data for the filtrate and standard solution. The pure water was measured as the baseline in the experiment. The percent rejection was calculated from the difference between the 0.5 mg mL^{-1} standard solution peak intensity (pink curve) and the filtrate (blue curve) intensity at λ_{max} = 521 nm. Samples were analyzed by UV-vis spectroscopy three separate times and less than 1% difference in absorbance was observed between sets of data. Using this method we observed an average rejection of 96.9 % for the 155 kg mol^{-1} M_w TRITC-Dextran. Furthermore, the absorption data for dextran solution passed through the support alone (**Figure 2.31**) shows no dextran rejection. This indicates that the 96.9 % rejection for the composite membrane is solely due to the nanoporous thin film coating.

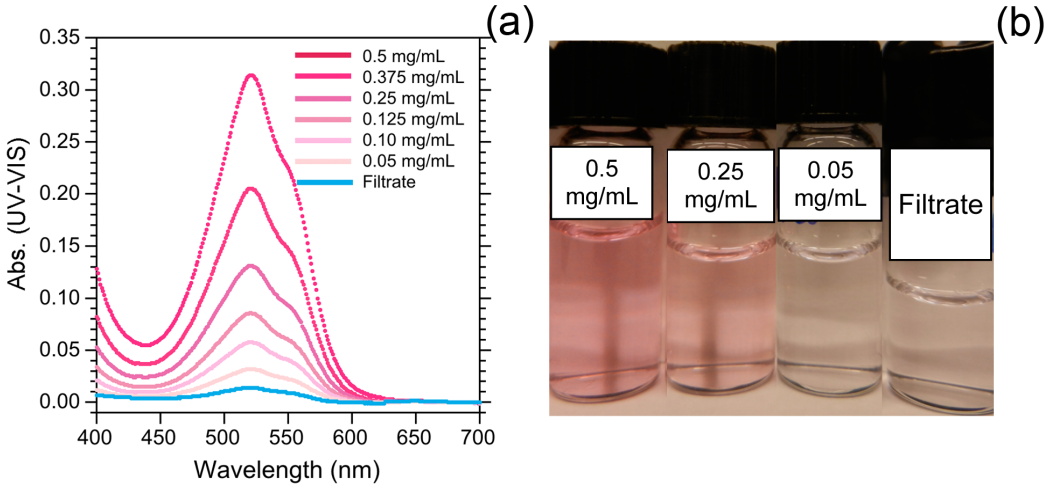

Figure 2.30. UV-vis absorbance data for TRITC-Dex standard solutions and filtrate, (a). Photograph of TRITC-dextran solutions with decreasing pink color intensity with decreasing TRITC-dextran concentration, (b).

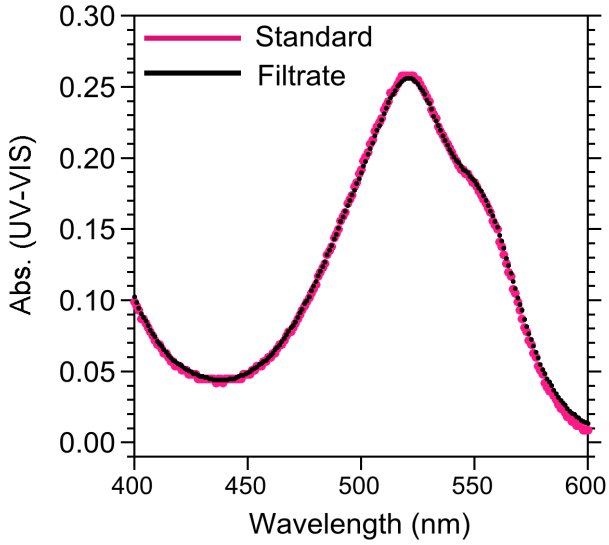

Figure 2.31. UV-vis absorbance data for PES support cut-off test.

2.3 Conclusions

By creating a block polymer containing 3 chemically distinct polymers, into a tetrablock ABAC architecture, we were able to prepare a material with two unique features. Both nanoporosity and mechanical stability were combined through use of a PS-PI-PS-PLA tetrablock terpolymer. Our work demonstrates another example of material enhancements that can result from the incorporation of more complex multiblock polymers. Nanoporous PS-PI-PS materials prepared here exhibit tensile properties superior to nanoporous polymers prepared from comparable AB diblocks or ABC triblocks. Furthermore, we demonstrated that we could combine this polymer with a microporous supportive PES layer into a mechanically stable composite nanoporous filtration membrane. We demonstrated the synthesis, morphological characterization and composite membrane results for core-shell cylinder PS-PI-PS-PLA tetrablock terpolymers. Nanoporous composite membranes could be made by both a direct coating method and a salt plate film transfer method. Membranes contained ~100 nm thick selective layers with cylindrical pores 15 nm in diameter with a narrow pore size distribution. The addition of a small amount of homopolymer PLA allowed us to enhance the perpendicular alignment of PLA cylinders during the spin coating process. We were able to prepare a nanoporous film by a short RIE followed by a short basic PLA hydrolysis step. Composite membranes demonstrated high selectivity (97% rejection of 17 nm TRITC-Dex) and permeability (97 L $m^{-2}h^{-1}bar^{-1}$) comparable to that of commercial membranes.

2.4 Experimental Details

Materials

Styrene (99%, 10-15 ppm 4-*tert*-butylcatechol inhibitor, Aldrich) was purified by one distillation from calcium hydride (90-95%, Aldrich) and a successive distillation from butylmagnesium chloride (~3mL/50g styrene, 2.0 M solution in diethyl ether, Aldrich) under a static vacuum of 10-20 mTorr. Isoprene (99%, 100 ppm *p-tert*-butylcatechol inhibitor, Aldrich) was purified by two successive vacuum distillations from *n*-butyllithium (~3 mL/50 g isoprene, 2.5 M solution in hexanes, Aldrich). Ethylene oxide (99.5+%, compressed gas, Aldrich) was distilled once from butylmagnesium chloride (1 mL/10 mL ethylene oxide). Cyclohexane was purified by passage through activated alumina and a supported copper redox catalyst under high-purity argon in home-built columns. *Sec*-Butyllithium (1.3 M solution in cyclohexane, Aldrich) was used as received. The 50/50 (v:v) methanol/isopropanol solution used for reaction termination was degassed with nitrogen prior to use. d,l-Lactide was recrystallized from ethyl acetate and stored under nitrogen in a glovebox before use. All other chemicals were used as received without purification.

Characterization

^{1}H NMR Spectroscopy experiments were performed at room temperature on a Varian Inova 500 instrument operating at 500 MHz. Solutions of polymer were prepared in $CDCl_3$ at a concentration of approximately 15 mg/mL. All spectra were obtained at 25 °C after 32 transients using a relaxation delay of 5 s with chemical shifts reported as d (ppm) relative to the ^{1}H signals of $CHCl_3$ at 7.27 ppm.

Size-exclusion chromatography (SEC) was used to characterize the dispersity (Đ) and molar mass evolution for the PS aliquot, PS-PI-PS-OH triblock, PS-PI-PS-PLA tetrablocks and PLA etched PS-PI-PS-PLA monoliths. Samples were prepared at

concentrations between 1-5 mg/mL in $CHCl_3$. SEC was performed at 35 °C using three Plgel 5μm Mixed-C columns in series with an available molar mass range of 400–400 000 g mol^{-1}. The columns are contained in a Hewlett-Packard (Agilent Technologies) 1100 series liquid chromatograph equipped with a Hewlett-Packard 1047A refractive index detector. Molar mass and Đ values are reported with respect to polystyrene standards obtained from Polymer Laboratories.

Differential scanning calorimetric (DSC) analysis was performed on a Q1000 instrument from TA Instruments calibrated with an Indium standard. The samples were heated to 150 ºC and then subsequently cooled to –100 °C followed by heating again to 150 °C. Samples were heated and cooled at a rate of 10 °C min^{-1}. Presented data and glass transitions temperature measurements were taken from the second heating ramp. Data analysis (T_g) was performed on TA Instruments Universal Analysis software.

Small-angle X-ray scattering (SAXS) experiments were performed at the Sector 5-ID-D beamline of the Advanced Photon Source (APS) at Argonne National Laboratories, maintained by the Dow-Northwestern-Dupont Collaborative Access Team (DNDCAT). The source produces X-rays with 0.84 Å wavelength. For our experiments, the sample to detector distance was fixed to 4.042 m and the detector radius was 81 mm. Scattering intensity was monitored using a Mar 165 mm diameter CCD detector operating with a resolution of 2048 by 2048. The two dimensional scattering patterns were azimuthally integrated to afford one-dimensional profiles presented as spatial frequency (q) versus scattered intensity.

For Transmission Electron Microscopy (TEM), ultrathin sections (ca. 70 nm) of the polymer films were cut using a Reichert UltraCut S Ultramicrotome with a Model FC-S addition at -100 ºC. Thin sections were placed on 300 mesh copper grids and subsequently stained with OsO_4 vapor for ~10 min by exposure to a 4%

aqueous solution. TEM analysis was performed on a JEOL JEM-1210 transmission electron microscope operating at 100 kV equipped with a Gatan Multiscan CCD camera.

Tensile tests were performed using small rectangular samples of the polymers that were cut from a sample pressed for 10 minutes at 150 ºC under 1000 psi. The samples had the approximate dimensions of 0.5 mm (T) × 3 (W) × 7 mm (L). The tensile measurements were performed on a Rheometrics Scientific MiniMat instrument. Samples were extended lengthwise uniaxially 15.0 mm min^{-1}.

Scanning Electron Microscopy (SEM): Etched and dried tetrablocks were coated with 3 nm of Pt via direct Pt sputter coating prior to imaging with SEM. SEM was performed on a Hitachi S-900 FE-SEM at 2 kV.

Atomic Force Microscopy (AFM): AFM surface morphological analysis was performed using an Agilent 5500 environmental SPM plus inverted light microscopy with Olympus tapping mode at ambient conditions using commercial silicon TM tips (Veeco Instruments).

Ellipsometry: Ellipsometry was performed using a J. A. Woolam, EC-2000 ellipsometer, with incident angles of 60 and 75°, and laser wavelengths between 400 and 1100 nm

Filtration Test: Water flow rate experiments were performed in a small dead-end ultrafiltration cell (Amicon 8010 filtration cell, membrane diameter 25 mm, volume 10 mL, stirring speed 600 rpm). Solute rejection tests were performed using 0.5 mg mL^{-1} TRITC-Dex solutions in HPLC grade water at a stirring speed of 600 rpm and pressure of 0.2 bar. Concentration of the collected solutions was determined with UV-vis spectrometry. UV-vis absorption spectra for all solutions were determined

on a Spectronic Genesys 5 spectrometer over a wavelength range of 300–1000 nm. Solution spectra were obtained in a 1 cm polystyrene cuvette. HPLC grade water was used as the baseline for all measurements. UV absorbance (at λ_{max} = 521 nm) vs. TRITC-Dex concentration was calibrated with TRITC-Dex solutions of varying concentration (0, 0.05, 0.1, 0.125, 0.25, 0.375 and 0.5 mg/mL). Calibration was performed three times.

Representative Synthesis of PS-PI-PS-OH The synthesis of the PS-PI-PS-OH triblock precursor was done using the previously established method described by Bailey et al. (Bailey, T. S.; Pham, H. D.; Bates, F. S. *Macromolecules* **2001**, *34*, 6994–7008.) For the synthesis performed here sequential anionic polymerization of styrene (19.91 g), isoprene (35.87 g) and then styrene (21.79 g) was initiated by *sec*-butyllithium (2.636 mL, 1.3 M) in cyclohexane under ~5 PSI positive pressure of argon. After polymerization a 150 fold excess of ethylene oxide (18.43 mL) was added to cap the growing PS-PI-PS chain ends with one unit of ethylene oxide. All glassware was dried in a 105 °C oven overnight and flame-dried under vacuum before use. Yield = 75.7 g (97.6%). SEC (PS standards): PS fragment M_n = 5,700 kg/mol, M_w/M_n = 1.04, PS-PI-PS-OH M_n (by ^{1}H NMR spectroscopy and SEC of PS fragment.) = 21.3 kg mol-1, M_w/M_n = 1.05. ^{1}H NMR (ppm downfield from TMS): 6.20-7.26 (b, -(C_6H_5)), 4.90-5.30 (b,-CH_2-C*H*=C(CH_3)-CH_2-), 4.60-4.90 (b, CH_2=C(CH_3)-), 3.5-3.7 (m, -CH_2-OH), 0.84-2.40 (b, CH_2=C(CH_3)-C(R)*H*CH_2-,-CH_2-CH=C(CH_3)-CH_2-, and C_6H_5-C(R)*H*-CH_2-), 0.5-0.78 (m, -CH_3, initiator fragment).

Representative Synthesis of PS-PI-PS-PLA. Polymerizations of d,l-lactide initiated by the PS-PI-PS-OH parent triblock were performed according to a procedure previously reported by Rzayev et al. for the polymerization of l-lactide catalyzed with diazabicyclo[5.4.0]undec-7ene (DBU). The procedure for PS-PI-PS-PLA (0.20) is given below as a representative synthesis for PS-PI-PS-PLA tetrablocks. PS-PI-PS-OH (1.00 g) and d,l-lactide (0.475 g) were dissolved in dry

methylene chloride (10 mL) in a glass scintillation vial in a nitrogen glovebox. DBU (7 μL) was then added to initiate the polymerization. The vial was then sealed with a Teflon lined screw cap, removed from the glove box and placed on a stir plate. Polymerizations were run for 60 minutes at room temperature in order to reach around 80% conversion of d,l-lactide. After 60 minutes, a small amount of benzoic acid (~5-10 mg) was added to terminate the reaction. The polymer was precipitated with methanol, filtered and dried in vacuo (50 °C for 48 h). Yield = 1.13 g (77% d,l-lactide conversion). M_n (by ^{1}H NMR spectroscopy) = 27.5 kg mol^{-1}, PDI (PS standards): M_w/M_n = 1.07. ^{1}H NMR (ppm downfield from TMS): 6.20-7.26 (b, -CH(C_6H_5)), 4.90-5.30 (b, -CH_2-C*H*=C(CH_3)-CH_2-), 4.98-5.28 (b, -C(O)C*H*(CH_3)O-), 4.60-4.90 (b, -CH_2=C(CH_3)-), 4.30-4.42 (m, -C(O)C*H*(CH_3)OH), 3.95-4.15 (b, -CH_2CH_2-O-), 2.60-2.75 (bd, -C(O)CH(CH_3)O*H*), 0.84-2.40 (b, CH2=C(CH_3)-C(R)*H*-CH_2-, -CH_2-CH=C(CH_3)-CH_2-, -C(O)CH(CH_3)O-, and C_6H_5-C(R)*H*-CH_2-), 0.5-0.78 (m, -CH_3, initiator fragment).

Degradation Conditions: Channel die aligned samples were cryo-cut into 3 x 3 x 1.5 mm cubes before being subjected to etching conditions. Prior to etching each sample was placed in a dewar of liquid nitrogen for 1 minute and then immediately broken in half. In all degradation experiments, PS-PI-PS-PLA cubes were allowed to react in dilute basic conditions without stirring for one month. A series of basic solutions with solvents of different polarities was tested to find improved degradation conditions. The five solutions tested all contained 0.5 M NaOH, 0.1 wt % SDS and one of the following five solvents or solvent mixtures: 1) Water 2) 40:60 (v:v) Methanol: Water 3) 70:30 (v:v) Methanol:Water 4) Methanol 5) Ethanol. Cubes were also placed in one of the five corresponding control solutions (same as etching solutions but without NaOH) for 1 month. All samples were rinsed (~20 seconds) with the control solutions, deionized water and then directly dissolved in chloroform for SEC analysis. SEM verified the formation of nanopores after basic

etching at room temperature. Ethanolic and methanolic etching solutions proved superior to more hydrophilic etching solutions in removing PLA.

2.5 References

(1) Bernards, D. A.; Desai, T. A. *Soft Matter* **2010**, *6*, 1621–1631.

(2) Logar, N. Z.; Kaucic, V. *Acta Chim. Slov.* **2006**, *53*, 117–135.

(3) Hillmyer, M. A. In *Block Copolymers II*; Abetz, V., Ed.; Advances in Polymer Science Series; Springer: Berlin/Heidelberg 2005; Vol. 190, pp 137–181.

(4) Olson, D. A.; Chen, L.; Hillmyer, M. A. *Chem. Mater.* **2008**, *20*, 869–890.

(5) Hamley, I. W. *Nanotechnology* **2003**, *14*, R39–R54.

(6) Lee, J. S.; Hirao, A.; Nakahama, S. *Macromolecules* **1988**, *21*, 274–276.

(7) Abetz, V.; Simon, P. F. W. In *Block Copolymers I*; Springer-Verlag Berlin: Berlin, 2005; Vol. 189, p 125–212.

(8) Bates, F. S.; Fredrickson, G. H. *Phys. Today,* **1999**, *52*, 32–38.

(9) Yang, S. Y.; Park, J.; Yoon, J.; Ree, M.; Jang, S. K.; Kim, J. K. *Adv. Func. Mater.* **2008**, *18*, 1371–1377.

(10) Jackson, E. A.; Hillmyer, M. A. *ACS Nano* **2010**, *4*, 3548–3553.

(11) Yang, S. Y.; Ryu, I.; Kim, H. Y.; Kim, J. K.; Jang, S. K.; Russell, T. P. *Adv. Mater.* **2006**, *18*, 709–712.

(12) Yang, S. Y.; Yang, J. A.; Kim, E. S.; Jeon, G.; Oh, E. J.; Choi, K. Y.; Hahn, S. K.; Kim, J. K. *ACS Nano* **2010**, *4*, 3817–3822.

(13) Bernards, D. A.; Desai, T. A. *Adv. Mater.* **2010**, *22*, 2358–2362.

(14) Nuxoll, E. E.; Hillmyer, M. A.; Wang, R. F.; Leighton, C.; Siegel, R. A. *ACS Appl. Mater. & Interfaces* **2009**, *1*, 888–893.

(15) Uehara, H.; Kakiage, M.; Sekiya, M.; Sakuma, D.; Yamonobe, T.; Takano, N.; Barraud, A.; Meurville, E.; Ryser, P. *ACS Nano* **2009**, *3*, 924–932.

(16) Siegel, R. A.; Gu, Y. D.; Lei, M.; Baldi, A.; Nuxoll, E. E.; Ziaie, B. *J. Controlled Release* **2010**, *141*, 303–313.

(17) Lo, K. H.; Chen, M. C.; Ho, R. M.; Sung, H. W. *ACS Nano* **2009**, *3*, 2660–2666.

(18) Phillip, W. A.; O'Neill, B.; Rodwogin, M.; Hillmyer, M. A.; Cussler, E. L. *ACS Appl. Mater. & Interfaces.* **2010**, *2*, 847–853.

(19) Li, X. F.; Fustin, C. A.; Lefevre, N.; Gohy, J. F.; De Feyter, S.; De Baerdemaeker, J.; Egger, W.; Vankelecom, I. F. J. *J. Mater. Chem.* **2010**, *20*, 4333–4339.

(20) Schacher, F.; Ulbricht, M.; Muller, A. H. E. *Adv. Funct. Mater.* **2009**, *19*, 1040–1045.

(21) Peinemann, K.-V.; Abetz, V.; Simon, P. F. W. *Nat. Mater.* **2007**, *6*, 992–996.

(22) Schacher, F.; Rudolph, T.; Wieberger, F.; Ulbricht, M.; Muller, A. H. E. *ACS Appl. Mater. & Interfaces* **2009**, *1*, 1492–1503.

(23) Nunes, S. P.; Sougrat, R.; Hooghan, B.; Anjum, D. H.; Behzad, A. R.; Zhao, L.; Pradeep, N.; Pinnau, I.; Vainio, U.; Peinemann, K.-V. *Macromolecules* **2010**, *43*, 8079–8085.

(24) Liu, G.; Ding, J.; Stewart, S. *Angew. Chem., Int. Ed.* **1999**, *38*, 835–838.

(25) Yave, W.; Car, A.; Funari, S. S.; Nunes, S. P.; Peinemann, K. V. *Macromolecules* **2010**, *43*, 326–333.

(26) Pitet, L. M.; Amendt, M. A.; Hillmyer, M. A. *J. Am .Chem. Soc.* **2010**, *132*, 8230–8231.

(27) Uehara, H.; Yoshida, T.; Kakiage, M.; Yamanobe, T.; Komoto, T.; Nomura, K.; Nakajima, K.; Matsuda, M. *Macromolecules* **2006**, *39*, 3971–3974.

(28) Cavicchi, K. A.; Zalusky, A. S.; Hillmyer, M. A.; Lodge, T. P. *Macromol. Rapid Commun.* **2004**, *25*, 704–709.

(29) Zalusky, A. S.; Olayo-Valles, R.; Wolf, J. H.; Hillmyer, M. A. *J. Am. Chem. Soc.* **2002**, *124*, 12761–12773.

(30) Chen, L.; Hillmyer, M. A. *Macromolecules* **2009**, *42*, 4237–4243.

(31) Hansen, M. S.; Vigild, M. E.; Berg, R. H.; Ndoni, S. *Polym. Bull.* **2004**, *51*, 403–409.

(32) Guo, F. X.; Andreasen, J. W.; Vigild, M. E.; Ndoni, S. *Macromolecules* **2007**, *40*, 3669–3675.

(33) Zhou, N.; Bates, F. S.; Lodge, T. P. *Nano Lett.* **2006**, *6*, 2354–2357.

(34) Sperschneider, A.; Scacher, F.; Gawenda, M.; Tsarkova, L.; Muller, A. H. E.; Ulbricht, M.; Krausch, G.; Kohler, J. *Small* **2007**, *3*, 1056–1063.

(35) Querelle, S.; Jackson, E. A.; Hillmyer, M. A.; Cussler, E. *In preparation.*

(36) Kricheldorf, H. R.; Quirk, R. P.; Holden, G. *Thermoplastic elastomers*; 3rd ed.; Hanser Gardner Publications: Cincinnati, 2004.

(37) Walker, B. M.; Rader, C. P. *Handbook of thermoplastic elastomers*; 2nd ed.; Van Nostrand Reinhold: New York, 1988.

(38) Bluemle, M. J.; Fleury, G.; Lodge, T. P.; Bates, F. S. *Soft Matter* **2009**, *5*, 1587–1590.

(39) Bluemle, M. J.; Zhang, J. W.; Lodge, T. P.; Bates, F. S. *Macromolecules* **2010**, *43*, 4449–4452.

(40) Bates, F. S.; Hillmyer, M. A.; Lodge, T. P.; Bates, C. M.; Delaney, K. T.; Fredrickson, G. H. *Science*, **2012**, *336*, 434–440.

(41) Bailey, T. S.; Pham, H. D.; Bates, F. S. *Macromolecules* **2001**, *34*, 6994–7008.

(42) Lohmeijer, B. G. G.; Pratt, R. C.; Leibfarth, F.; Logan, J. W.; Long, D. A.; Dove, A. P.; Nederberg, F.; Choi, J.; Wade, C.; Waymouth, R. M.; Hedrick, J. L. *Macromolecules* **2006**, *39*, 8574–8583.

(43) Bailey, T. S.; Rzayev, J.; Hillmyer, M. A. *Macromolecules* **2006**, *39*, 8772–8781.

(44) Chatterjee, J.; Jain, S.; Bates, F. S.; *Macromolecules* **2007**, *40*, 2882–2896.

(45) Zalusky, A. S. Nanoporous Materials From Ordered Polylactide-Containing Block Copolymer Templates. Ph. D. Dissertation, University of Minnesota, Twin Cities, 2003.

(46) Hardy, C. M.; Bates, F. S.; Kim, M. H.; Wignall, G. D. *Macromolecules* **2002**, *35*, 3189–3197.

(47) Goldacker, T.; Abetz, V. *Macromolecules* **1999**, *32*, 5165–5167.

(48) Kubo, T.; Wang, R. F.; Olson, D. A.; Rodwogin, M. A.; Hillmyer, M. A. *Appl. Phys. Lett.* **2009**, *93*, 133112(1–3).

(49) Kim, S. Y.; Misner, M. J.; Russell, T. P. *Adv. Mater.* **2004**, *16*, 2119–2123.

(50) Jeong, U.; Ryu, D. Y.; Kho, D. H.; Kim, J. K.; Goldbach, J. T.; Kim, D. H.; Russell, T. P. *Adv. Mater*. **2004**, *16*, 533–536.

(51) Phillip, W. A.; Dorin, R. M.; Werner, J.; Hoeks, E. M. V.; Wiesner, U.; Elimelech, M. *Nano Lett.* **2011**, *11*, 2892–2900.

(52)Dow Ultrafiltration Operating Specifications. http://www.dowwaterandprocess.com/products/uf/op_spec.htm (accessed November 20, 2012)
Dow reports that their UF membranes, which contain a nominal pore diameter of 30 nm, work at a flux of 40-120 L $m^{-2}h^{-1}$.

(53) Hyflux Gurgle Tap Filter Webpage. http://www.hyfluxshop.com/Lists/TechSpec/Gurgle%20F38_F380905-02[1].pdf (accessed September 3, 2012). Hyflux reports a flux of 48 L $m^{-2}h^{-1}$ for a small residential UF tap filter that contains a membrane pore diameter of 15 nm.

(54) Dullien, F. A. L. In Porous media: fluid transport and pore structure; Academic Press: San Diego, 1992; pp 574.

(55) Phillip, W. A. Block Polymer Membranes for Selective Separations. Ph. D. Dissertation, University of Minnesota, 2009. p. 167.

(56) TdB Consultancy Website. www.tdbcons.se/tdbcons2/attachment/tritc_dextran.pdf (accessed November 20, 2012).

(57) Mulherkar, P. van Reis, R. *J. Membr. Sci.* **2004**, *236*, 171-182.

(58) Bakhshayeshi, M. et al. *J. Membr. Sci.* **2011,** *379*, 239-248,

(59) Pharmacos Webpage on Dextran Properties. http://www.dextran.net/dextran-physical-properties.html (accessed November 20, 2012).

(60) Ow, H.; Larson, D. R.; Srivastava, M.; Baird, B. A.; Webb, W. W.; Wiesner, U. *Nano Lett.* **2004**, *5*, 113-117.

(61) Pedone, A.; Bloino, J.; Monti, S.; Prampolini, G.; Barone, V. *Phys. Chem. Chem. Phys.* **2009**, *12*, 1000-1006.

Chapter 3

Solvent Vapor Annealing of PS-PI-PS-PLA and PS-PI-PS-PLA/PLA Films

This chapter describes solvent vapor annealing treatments used to control the orientation of nanostructures produced in thin films of a tetrablock terpolymer and a tetrablock/homopolymer blend. The ABAC polymer used was a poly(styrene-*b*-isoprene-*b*-styrene-*b*-d,l-lactide) (PS-PI-PS-PLA) tetrablock terpolymer previously determined to adopt a core(PLA)-shell(PS) cylinder morphology in the bulk. Perpendicular alignment of PLA cylinders was observed in PS-PI-PS-PLA films when a mixed solvent environment was used. Perpendicular alignment was achieved regardless of film thickness by inclusion of 5 wt % homopolymer PLA. Tapping mode atomic force microscopy (AFM) was used to visualize film surface morphologies. Subsequent reactive ion etching (RIE) and basic hydrolysis of PLA produced 15 nm pores in a PS-PI-PS matrix. Nanoporosity was confirmed by scanning electron microscopy (SEM) images and the vertical continuity of pores was confirmed by cross-sectional SEM analysis.

3.1 Introduction

3.1.1 Solvent Vapor Annealing Study of PS-PI-PS-PLA Films

Ordered block copolymer (BCP) thin films have received much attention as ideal tools for a variety of nanotechnology applications.[1,2,3,4,5,6] For example, self-assembled BCP films have led to improvements in high-density information storage media,[7,8,9,10] nanoporous membranes,[11,12,13,14,15] nano-objects,[16] photonic band-gap materials,[17] semi-conductors,[18,19] magnetic storage materials,[20] and others.[21,22] Many of these applications rely on thin films containing cylindrical or lamellar morphologies.[23,24] For membranes and other templating applications, it is generally desired that films contain sacrificial domains that fully transverse the film and can be selectively removed to produce pores.

In this chapter, the thin film alignment of a poly(styrene-*b*-isoprene-*b*-styrene-*b*-d,l-lactide) (PS-PI-PS-PLA) tetrablock terpolymer is discussed. The block polymer contains a volume fraction of PLA (f_{PLA}) of 0.21 and adopts a core(PLA)-shell(PS) hexagonally packed cylinder morphology in the bulk (see **Chapter 2**).[25] ABAC polymers have been shown to exhibit interesting phase behavior in the bulk but have not been studied in thin films.[26,27,28,29] Motivation to study thin films of this polymer arose from the combination of the inherent mechanical toughness provided by the physically crosslinked PS-PI-PS blocks and the nanoporosity generated after selectively etching the PLA block. Tough, well-ordered nanoporous films are attractive materials for high performance filtration membranes, pattern

transfer masks, and other applications.[27] PLA has found great utility as a sacrificial block in many block polymer systems in bulk[30,31,32,33] and thin films[8,34,35,36,37,38,39,40,41] due to the efficiency of PLA hydrolysis. Also, because of the high interaction parameter between PI and PLA, ultra-small domains can theoretically be prepared (<10 nm). The combination of mechanical integrity, etchable domains, and small domain sizes makes PS-PI-PS-PLA an overall attractive precursor for size-selective membranes and also for generating other nanomaterials. These attributes encouraged an investigation into how to prepare well-ordered films from PS-PI-PS-PLA. It is possible to obtain perpendicular PLA orientation through spin coating, as was shown for PS-PLA[35,42] PS-PI-PLA[39,40,41,43], and PS-PI-PS-PLA[25]. However, spin coating can be undesirable for membrane and templating applications since it does not allow enough time for morphology organization throughout the film and can trap domain size inhomogeneities. The microstructure of PS-PI-PLA and PS-PI-PS-PLA films was a mixture of perpendicular and parallel cylinders in previous reports because spin coating was used.[25,43] This translated to less than ideal porosity in PLA-etched films.

Strategies that have been employed to control block polymer structure in thin films include thermal annealing, solvent annealing, electrical field alignment, and controlled solvent evaporation.[21] Simulation and experiments have shown that the film morphology of cylinder and lamellar forming diblock copolymers is dependent on the relative interfacial interactions of the blocks and the commensurability between the film thickness and block polymer domain spacing.[44]

To control the orientation of domains, the interfacial preference of the constituent blocks must be controlled during annealing so that it is energetically favorable for all blocks to be at the interfaces. If it is not favorable, the preferential interaction of one constituent with a surface can lead to selective enrichment of that block at the substrate-polymer (or air-polymer) interface. Such circumstances favor orientation of cylindrical or lamellar microdomains parallel with the substrate surface. Various techniques have been used to control the interfacial preference of polymer blocks during alignment to favor perpendicular orientation.

Solvent vapor annealing (SVA) is one useful technique that can promote well-ordered perpendicular arrays of AB and ABC[45] block polymers.[1,2,3,4,5,38] Unlike thermal annealing, SVA allows one to control and tune the air- and film surface-polymer environment.[38,46] Additionally, the technique is a relatively fast alignment procedure that can facilitate organization/alignment of domains in block polymers with high interaction parameters and/or high molecular weights.[47] Recently mixed solvent SVA has been employed to more finely tune the surface environment to specific block polymer systems to induce desired morphological alignment or alter overall morphology.[48,49,50,51,52,53]

Controlled SVA is especially well suited for PLA containing films. While thermal annealing has been used to orient PLA cylinders in PS-PLA, thermal degradation of PLA[54,55] prevents the use of thermal annealing for other PLA-containing block polymers requiring high temperatures (> 200 °C) or long

annealing times (high T_g, high molecular weight or high incompatibility block polymers).

Controlled SVA was implemented to create a relatively neutral film surface interface. The intention was to find the best solvent condition for achieving perpendicular cylinder orientation using a fast solvent annealing process. Films were annealed in toluene, chloroform, tetrahydrofuran (THF) and solvent mixtures containing THF and acetone. Annealing in Toluene, chloroform and THF consistently produced films with parallel cylinder orientation. Increasing the polarity of the solvent with addition of different amounts of acetone led to different film morphologies. Perpendicular cylinder orientation was consistently obtained with a 70/30 vol/vol mixture of THF and acetone at film thicknesses near the tetrablock domain spacing (L_0 = 28.6 nm). Above 50% acetone solvent concentration, films no longer formed perpendicular orientation. To achieve perpendicular orientation at any thickness, a homopolymer additive strategy was employed. A small amount of homopolymer has been shown to stabilize perpendicular orientation and increase order across films with hexagonally or tetragonally packed cylinders.[56,57] Thickness-independent perpendicular orientation of PLA-cylinders was obtained reproducibly through solvent annealing of films containing a blend of 95 wt% PS-PI-PS-PLA and 5 wt% homopolymer PLA. Well-ordered, PS-PI-PS porous films were reproducibly obtained after a short RIE and subsequent PLA hydrolysis step.

3.2 Results

Thin films of core(PLA)-shell(PS) cylinder forming PS-PI-PS-PLA terpolymers (number average molar mass M_n = 27 kg mol^{-1}, polydispersity, Đ, = 1.09; volume fractions f_{PS} = 0.40, f_{PI} = 0.39, f_{PLA} = 0.21; f_{PS} divided equally between blocks; domain spacing L_0 = 28.6 nm) were first spin coated onto hydrophobically treated Si wafers from dilute solutions in chlorobenzene. The hexamethyl disilazane (HMDS) treatment was done to improve compatibility between the Si wafer ($E_{surf}^{HMDS\text{-}Si}$ = 43 mJ/m^2)[58] and the polymer blocks (E_{surf}^{PI} = 32 mJ/m^2; $E_{surf}^{PS} \approx E_{surf}^{PLA} \approx$ 40 mJ/m^2)[41].

An AFM image of representative spin coated film of PS-PI-PS-PLA is shown in **Figure 3.1**. For all films, initial film thickness (T_0) after spin coating was measured using ellipsometry. Tapping mode Atomic Force Microscopy (AFM) was used to gain contrast between soft PI domains and the harder PS and PLA domains in film surface images (PI domains appear darker relative to PS and PLA).

Spin coated films show a microphase-separated structure of cylindrical light domains in a dark matrix, consistent with PS/PLA cylinders in a PI matrix. The apparent structures (**Figure 3.1**) are consistent with a non-equilibrium mixed cylinder orientation due to fast evaporation of solvent during spin coating.

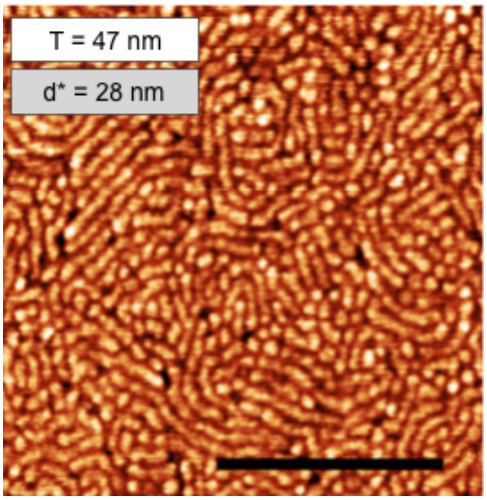

Figure 3.1. Representative AFM image of the surface of PS-PI-PS-PLA (f_{PLA} = 0.21) film spin coated from chlorobenzene. Scale bar is 500 nm.

Films were exposed to a variety of solvent vapors. Solvent selectivity for the polymer blocks can be estimated from the solubility parameters of polymers and solvents used. **Table 3.1** lists the Hansen Solubility Parameters for each polymer block and solvent used in this study.[59] The Hansen Solubility Parameters describe how well one material can dissolve another. The more alike the solubility parameters between a solvent and a polymer, the more likely the polymer will dissolve in that solvent. Generally, the solubility parameter increases in value with increasing polarity materials. The order of polarity for the polymer blocks is as follows: PI is the least polar (16.6 $MPa^{1/2}$), PS is intermediate (19.3 $MPa^{1/2}$) and PLA is most polar (20.6 $MPa^{1/2}$).

Table 3.1. Polymer and Solvent Solubility Parameters[59]

Polymer	Hansen Solubility Parameter, $[MPa]^{½}$	Solvent	Hansen Solubility Parameter, $[MPa]^{½}$
PI	16.6	Toluene	18.2
PS	18.4	Chloroform	19.0
PLA	20.6	THF	19.4

Films were solvent annealed for either 5 or 20 min in a home-built chamber (**Figure 3.2**) to facilitate a controlled solvent environment. Films were swollen with solvent vapor by using a constant flow of N_2 gas (3.8 L min^{-1}) through the solvent reservoir. Solvent was removed quickly after a set time by closing off the solvent line to the sample chamber (valve C, **Figure 3.2**) and quickly purging the sample chamber with clean N_2 gas (valve B, **Figure 3.2**). Afterwards, film surface morphologies of annealed films were analyzed using tapping mode AFM. Some films were etched with sodium hydroxide (NaOH) to remove PLA and then imaged by scanning electron microscopy (SEM).

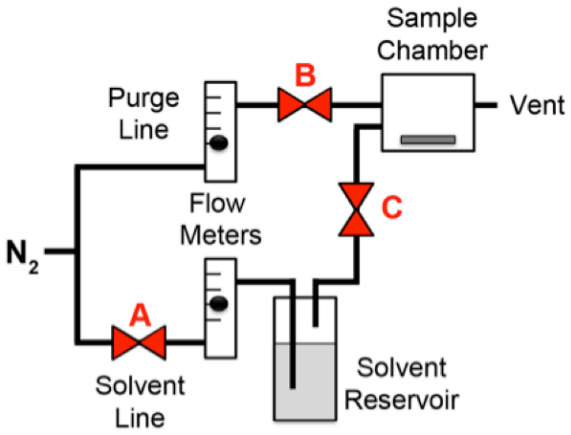

Figure 3.2. Solvent Annealing Chamber. Red letters indicate valves A, B and C.

3.2.1 Solvent Annealing in Good Solvents for PS and PI:

Based on the solubility parameters (listed in **Table 3.1**), toluene, chloroform and THF should be better solvents for PS and PI than for PLA. Of these solvents, the least polar toluene (18.2 $MPa^{1/2}$) is least compatible with PLA (20.6 $MPa^{1/2}$). Due to the success of chloroform in aligning PI-PLA[38] and THF to align PS-PLA[42], those two solvents, along with toluene, were explored for PS-PI-PS-PLA.

After annealing, parallel cylinder orientation was observed consistently in all PS-PI-PS-PLA films. Representative AFM images after solvent annealing for 5 minutes are given in **Figure 3.3a-c**. The measured spacing between parallel cylinders from the AFM images is close to the bulk cylinder-cylinder (cyl-cyl) spacing (33 nm) for images in **Figure 3.3**. Islands and holes were observed across film surfaces when the film thickness was not commensurate with the domain spacing. Islands contained parallel orientation as well. Films annealed for longer times (20 or 40 min) also had parallel orientation (not shown).

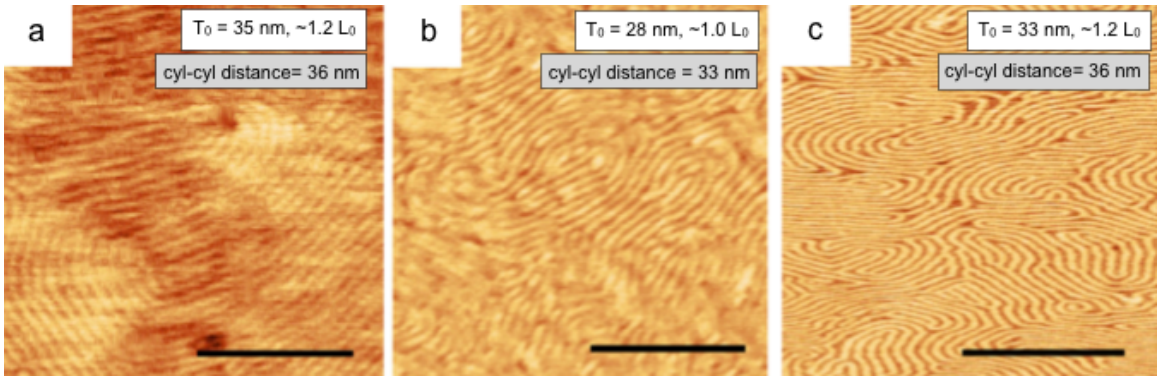

Figure 3.3. PS-PI-PS-PLA(0.21) films solvent annealed in chloroform (a), toluene (b) and THF (c). Films were annealed in solvent vapor for 5 minutes (a-c). Listed principal domain spacings, d*, represent the lateral distance between parallel domains at the surface (Scale bars = 500 nm).

Parallel orientation was also evident by SEM. A representative SEM image is shown in **Figure 3.4**. Samples were immersed in 0.25 M sodium hydroxide (NaOH) solutions of 60/40 (vol/vol) water/methanol containing 0.1 wt% sodium dodecylsulfate for 45 minutes prior to imaging.

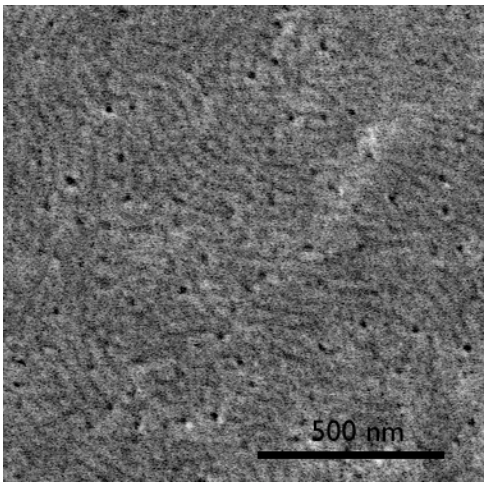

Figure 3.4. THF Annealed PS-PI-PS-PLA film after exposure to NaOH solution. Toluene and Chloroform annealed films also showed either featureless films or parallel cylinders.

SAXS data of PS-PI-PS-PLA dissolved in toluene showed ordered structures for polymer solutions containing 50% polymer and 75% polymer (**Figure 3.5**). At 25%, scattering was consistent with a disordered microphase separated structure. The principal domain spacing (d*) for 50% and 75% polymer is consistent with the bulk domains spacing, ~28 nm. As the solvent concentration increases, the sample disorders without change in the domain spacing. This suggests that toluene is a relatively neutral[60] or theta solvent for the tetrablock overall.[61] Domain spacing is expected to increase when the solvent is selective for one or more blocks or

decrease if the solvent is good for the entire polymer. Instead no change is observed. However, in this case, no change in domain spacing occurred.

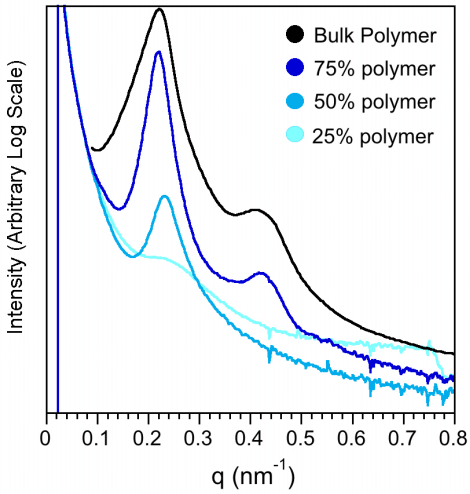

Figure 3.5. SAXS of PS-PI-PS-PLA swollen with toluene. SAXS was measured for mixtures containing 25%, 50% and 75% polymer. With increasing amount of toluene, the swollen polymer transitions from the bulk core(PLA)-shell(PS) structure to a disordered structure.

A schematic of a possible swollen film structure adopted by the tetrablock is shown in **Figure 3.6**. Because of the high incompatibility between PI and PLA, it is expected that the core(PLA)-shell(PS) arrangement of polymer chains should persist when the solvent is more favorable for PI and PS than for PLA. We believe that the films contain ~50% solvent or less at short times based on related film thickness data for solvent annealed PS-PLA copolymer films in our group. The SAXS data suggests that the tetrablock does not disorder until the solution contains ~25% or less polymer. While this data is not *in situ* swollen film data, it does suggest that tetrablock films swollen in toluene are not disordered below 75% solvent concentration.

A cartoon was created to explain the formation of parallel cylinders from a swollen film is shown in **Figure 3.6**. In the swollen film, PS and PI chains protect the PLA chains from solvent and PI contact. Whether they exist as micelles with PLA cores (at high solvent concentration) or as another microphase separated structure, PS and PI chains should surround PLA chains in the swollen film. As solvent is removed, the core-shell structure should fully develop with the PI phase surrounding core(PLA)-shell(PS) domains. Parallel orientation occurs due to the preference for PI/PS chains to be at the film/solvent vapor interface while PLA domains can hide within PS and PI.

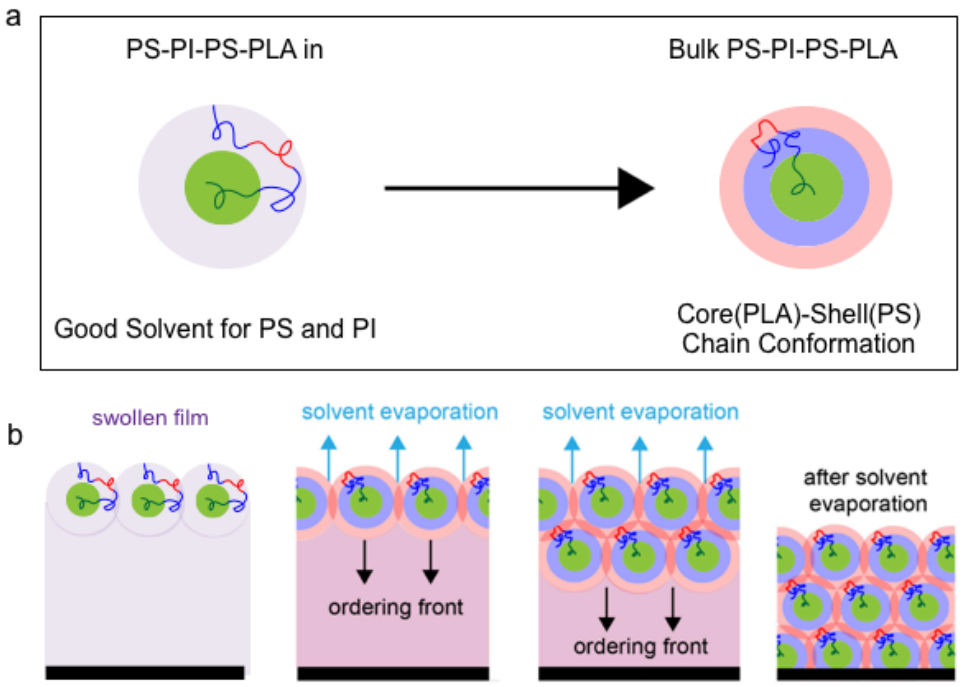

Figure 3.6. Formation of parallel cylinders from a solvent that is good for PI and PS but poor for PLA. Hypothetical polymer chain conformation in swollen film, left, and dried film, right, (a). Parallel cylinder formation is created from an ordered front that propagates through the film during solvent evaporation, (b). PLA forms the interior of swollen structure (e.g. cylinder, sphere) to avoid poor solvent and PI contact.

3.2.2 Solvent Annealing in Good Solvents for PS and PLA

Results from the previous solvents suggest that a more neutral solvent atmosphere may be necessary to obtain perpendicular orientation of PLA cylinders. Acetone (solubility parameter = 20.3 $MPa^{1/2}$) has been shown to be a good solvent for PLA.[42] Increasing the solvent polarity can have two main effects: 1, it can increase the preference for PLA to be at the film surface; and 2, it can increase the effective volume fraction of PLA in the swollen film. Likewise, increasing the polarity of the solvent can decrease the relative energetic preference for the least polar, PI, chains to be at the film surface/vapor interface.

Research on PS-PLA diblock copolymer films has shown that for PS and PLA, acetone (20.3 $MPa^{1/2}$) is selective for PLA (20.6 $MPa^{1/2}$) while THF (19.4 $MPa^{1/2}$) is slightly selective for PS (18.4 $MPa^{1/2}$).[42] Based on this previous work, PS-PI-PS-PLA films were solvent annealed in mixed solvent vapor containing THF and acetone. To finely tune the solvent polarity, the amount of acetone was varied; THF/acetone solvent mixtures contained 30%, 50% or 70% acetone by volume.

Figure 3.7 shows a summary of AFM phase images for surfaces of films annealed in THF and acetone mixtures. Perpendicular cylinder orientation was observed with 30% acetone and 50% acetone. However, the 30% acetone annealed films contained more hexagonally ordered domains than the 50% acetone annealed films. This was evident by AFM (representative surface images shown in **Figure 3.7a-b**). Films annealed in 50% acetone had more grain defects and contained a mixture of perpendicular and short parallel cylinders at the film surface. Films

annealed in 70% acetone contained either an interpenetrating network (**Figure 3.7c**) or a mixture of parallel and perpendicular cylinders (**Figure 3.7d**) depending on the film thickness.

Basic hydrolysis was used to remove PLA after solvent annealing. Samples were immersed in 0.25 M sodium hydroxide (NaOH) solutions of 60/40 (vol/vol) water/methanol containing 0.1 wt % sodium dodecylsulfate. SEM images in **Figure 3.7e-f** show the resulting surface morphology for films after base etching of PLA. Films annealed in the 30% and 50% acetone solvent mixtures had hexagonally packed nanopores after etching. With 70% acetone, the swollen PLA volume fraction was increased enough to cause the film morphology to change altogether. NaOH etched films from the 70% acetone system contained porous structures consistent with a PLA network structure at 1.2 L_0 (**Figure 3.7g**) and a perforated lamellar morphology at ~1.8 L_0 (**Figure 3.7h**).

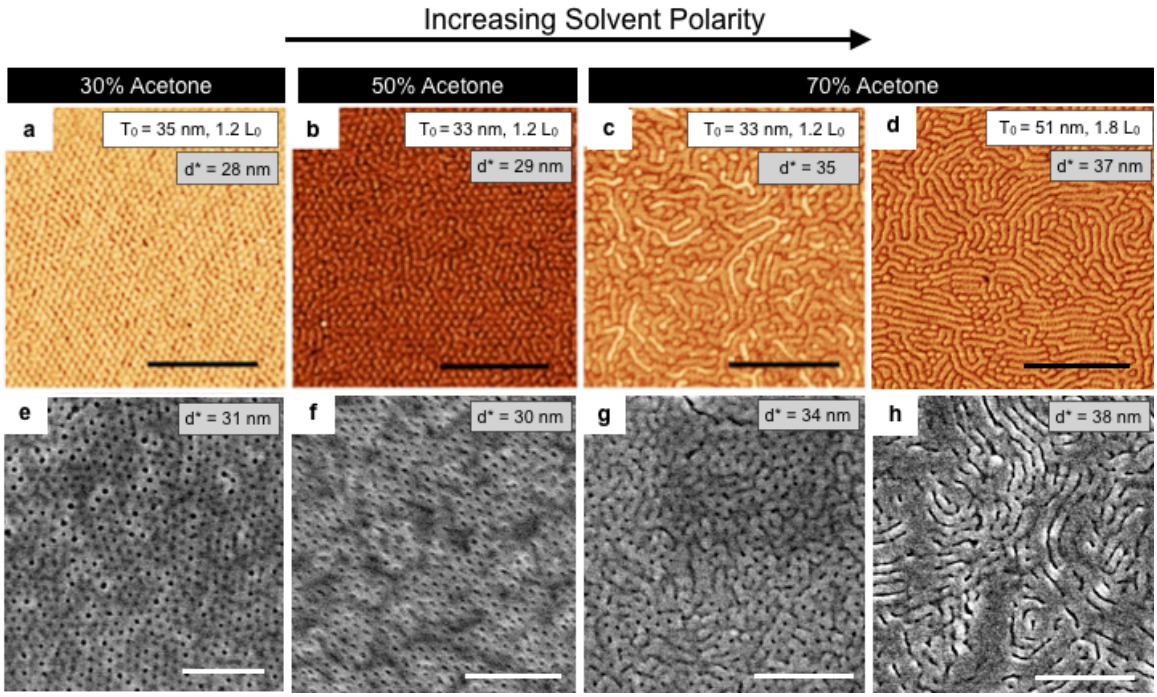

Figure 3.7. AFM images of PS-PI-PS-PLA(f_{PLA} = 0.21) films solvent annealed in THF/acetone mixtures with 30% acetone (a); 50% acetone (b) and 70% acetone (c and d). SEM images of the annealed films after base etching of PLA are shown below the corresponding AFM images (e-f). (Black scale bars= 500 nm; White scale bars = 300 nm).

The THF/Acetone mixture with 30% acetone is a good solvent for both PS and PLA but slightly poor for PI based on the reported solubility parameters. Films adopted either perpendicular or parallel cylinder orientation (depending on film thickness) after annealing for 5 minutes. For film thicknesses between 28-30 nm (T~L_0), mostly perpendicular cylinder orientation was observed. As the film thickness was increased from 28 to 60 nm (1 to 2 L_0), films contained a progressively higher amount of parallel orientation of cylinders across the film surface (**Figure 3.8**). Films thicker than 60 nm (~$2L_0$) contained only parallel cylinder orientation. The larger spacing in thicker films is relatively consistent with

the larger cyl-cyl spacing (bulk cyl-cyl spacing = 33 nm) expected from parallel cylinders (cyl-cyl spacing is 37-39 nm in thin film).

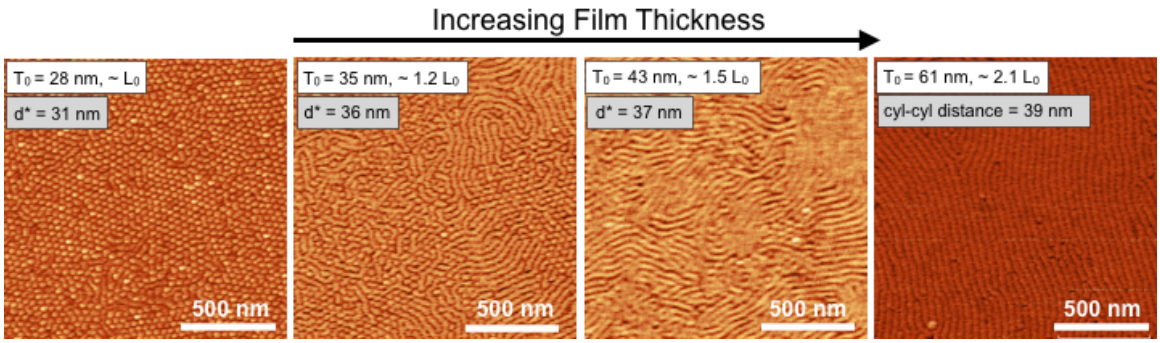

Figure 3.8. PS-PI-PS-PLA(f_{PLA} = 0.21) films after solvent annealing in the 30% acetone mixture.

Solvent annealing for longer time resulted in parallel cylinder orientation for the 30% and 50% acetone solvent mixtures (**Figure 3.9**). The change to parallel at longer time suggests that the cylinder orientation is time dependent. The swollen film thickness can also change over time during solvent annealing which could lead to a different swollen film structure. However, we do not have measurements to clarify this. For the 70% acetone system, the observed morphology was very similar after 5 or 20 min (**Figure 3.7c** and **Figure 3.9c**).

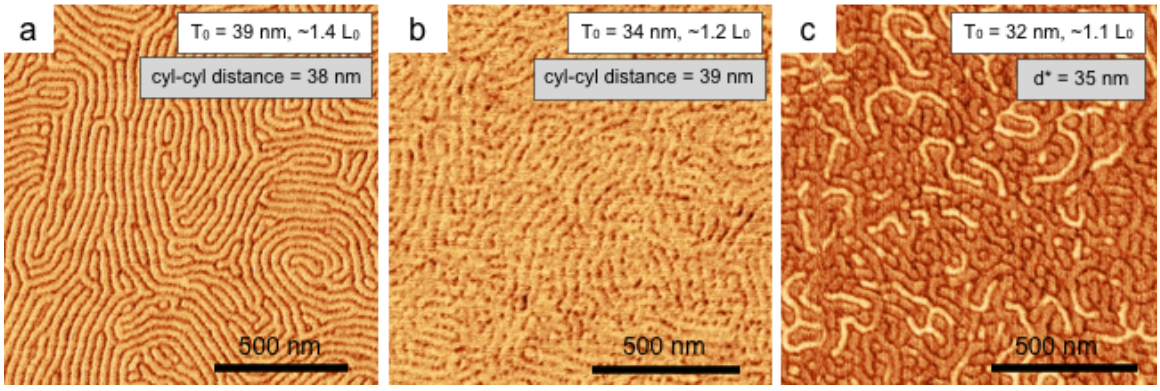

Figure 3.9. Films solvent annealed for 20 min in thf/acetone solvent mixtures containing 30% acetone, (a), 50% acetone, (b), and 70% acetone, (c).

SAXS data from solutions of PS-PI-PS-PLA in the 70/30 vol/vol THF/acetone mixture can provide some insight into the swollen film morphology. **Figure 3.10** is consistent with a disordered structure at 50% polymer and a highly ordered structure at 75% polymer. Scattering from the 75% solution is consistent with an ordered cylinder phase with a principal domain spacing of 27 nm ($q^* = 0.23\ nm^{-1}$). A slight decrease in the domain spacing suggests there is reduced segregation between blocks (28.6 nm bulk vs. 27 nm 75% polymer solution). Also, the 70/30 vol/vol THF/acetone solvent system can disorder the tetrablock at a lower solvent concentration than toluene (50% vs. 75% solvent). These results show that the 70/30 vol/vol THF/acetone mixture can more effectively mediate the interfacial tensions between the blocks in the swollen film. Because of this, we can argue that this solvent mixture is better for annealing PS-PI-PS-PLA than toluene and other good solvents for PS/PI. The thin film results show that this more

effective solvent provides a more favorable environment for the formation of perpendicular cylinders.

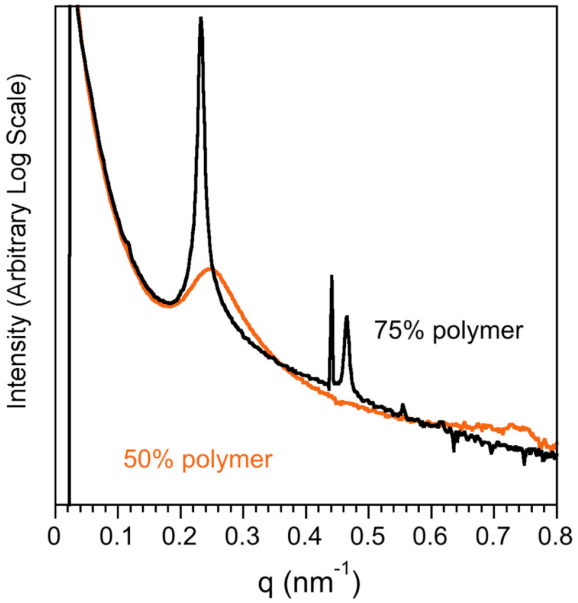

Figure 3.10. SAXS of PS-PI-PS-PLA swollen with 70/30 vol/vol THF/Acetone mixture. SAXS was measured for mixtures containing 25%, 50% and 75% polymer. Scattering from 75% polymer mixture, black curve, exhibits scattering consistent with cylinders or lamellae. Scattering from 50% mixture shows a disordered structure. Not shown: 25% mixture did not scatter. The sharp peak at ~0.44 nm^{-1} is an artifact in the scattering data.

3.2.3 Conclusions from Solvent Annealing of PS-PI-PS-PLA

Solvent vapor annealing with THF, toluene and chloroform gave parallel cylinder orientation consistently. By increasing the polarity with 30% or 50% acetone in a THF/acetone mixture, perpendicular cylinder orientation could be achieved. At higher acetone concentration, however, cylinders did not orient perpendicular to the substrate. The best solvent atmosphere for achieving well-ordered perpendicular cylinder domains was the 30% acetone and 70% THF mixture. However, as the film thickness was increased (T ~$2L_0$ or greater), this

solvent system was no longer effective in producing perpendicular cylindrical domains. This is a common observation in cylinder forming copolymer thin films.[66,63,62] Even with neutral interfaces (substrate and surface/air) for the polymer blocks, parallel orientation can often occur. Theory and simulations have predicted that perpendicular arrays of cylinders should be obtainable at all thickness when neutral interfaces are used.[63] However, such a result has never been observed experimentally. As copolymer film thickness increases, perpendicular orientation is generally more difficult to obtain. Furthermore, copolymers with non-zero interfacial tension between blocks, such as those in PS-PI-PS-PLA, are more difficult to orient even with neutral interfaces (substrate and film surface).[63] In order to achieve perpendicular orientation in thicker films, an alternative method was used. This method is discussed in the following section.

3.2.4 Blending with PLA Homopolymer

Balancing interfacial tensions does not guarantee perpendicular orientation for cylindrical and lamellar morphologies.[21] One successful strategy to overcome this limitation is to use a homopolymer additive. Homopolymer/copolymer blends have allowed thickness independent perpendicular cylinder orientation in films for a variety of copolymer systems.[62,63,64] When an appropriately sized homopolymer for the minority block is used, perpendicular orientation can be enhanced vertically and organization can be enhanced laterally. This effect is achieved when only a small amount of homopolymer is used since higher homopolymer concentration will lead to macrophase separation.

The homopolymer additive strategy was effective for achieving perpendicular orientation in the following copolymer systems: PS-PMMA/PMMA,[62] PS-P4VP/PS,[65] PS-PEO/PEO and PS-PEO/PMMA,[66] PS-PI-PS/PS,[63] and PS-PB-PS/PS.[67] The confinement of the homopolymer to the center of the domain, rather than fully dispersed within the domain, tends to enhance the extent of perpendicular orientation of cylindrical domains. This effect is optimized when the molecular weight ratio between the homopolymer and corresponding copolymer block is equal to 1.5. This is due to the asymmetric elongation of homopolymer chains along the long axis of a cylindrical domain caused by the mismatch in the PLA homopolymer/PLA block chain lengths.

Maybe most appropriate to the PS-PI-PS-PLA tetrablock films, is the work related to PS-PI-PS and PS-PB-PS triblocks. For these systems, perpendicular PS cylinder orientation was achieved by using the appropriate molecular weight and concentration of PS homopolymer.[63,67] Because of the success of homopolymer in both AB diblock and ABA copolymer cylinder films, we hypothesized that a small amount of homopolymer PLA might also enhance formation of perpendicular orientation of PLA cylinders in PS-PI-PS-PLA films.

Polymer films were prepared from spin coating dilute solutions of 95/5 wt/wt PS-PI-PS-PLA/PLA homopolymer from chlorobenzene onto HMDS modified Si wafers (at 1500, 2000 and 3000 rpm). The PLA homopolymer used had a molecular weight M_n = 10 kg mol^{-1}. This homopolymer was specifically chosen

due to the molecular weight ratio of 1.4 (near the ideal 1.5 ratio) between homopolymer PLA and the PLA block (M_n homo PLA/ M_n PLA Block = 1.4)

Spin coated films containing the PS-PI-PS-PLA/PLA (95/5 wt/wt) blend were solvent annealed for 5 min in a 70/30 mixture of THF/acetone (the best system for the PS-PI-PS-PLA tetrablock). Surface AFM images of solvent annealed PS-PI-PS-PLA/PLA blended films are shown in **Figure 3.11**. PS-PI-PS-PLA/PLA blended films exhibit a perpendicular orientation at all thicknesses between 30 and 100 nm.

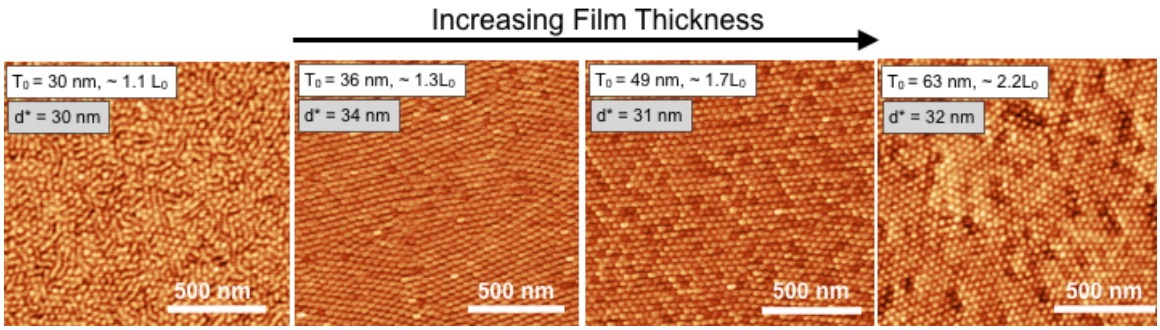

Figure 3.11. PS-PI-PS-PLA(f_{PLA} = 0.20)/PLA 95/5 wt/wt blend after solvent annealing in a 70/30 v/v THF/acetone mixture. In each row, film thickness increases from left to right.

To confirm reproducibility, PS-PI-PS-PLA/PLA blended films were solvent annealed in the 70/30 vol/vol THF/acetone atmosphere multiple times on multiple days. On each day, samples were annealed for 2, 5 and 10 minutes. For each annealing time, films of three different thicknesses were annealed. Representative sets of results from 5 different days of experiments are shown in **Figure 3.12** and **Figure 3.13**. Perpendicular cylinder orientation was observed for all films solvent annealed for 2 (**Figure 3.12a–c**) or 5 (**Figure 3.12d–f**) minutes. After 10 minutes of

annealing (**Figure 3.12g–i**), most films contained perpendicular orientation while one rather thick 99 nm film showed parallel orientation (**Figure 3.12i**). The most well ordered perpendicular arrays resulted from solvent annealing for 5 minutes where ordered grains as wide as 2 or 3 square microns across were seen.

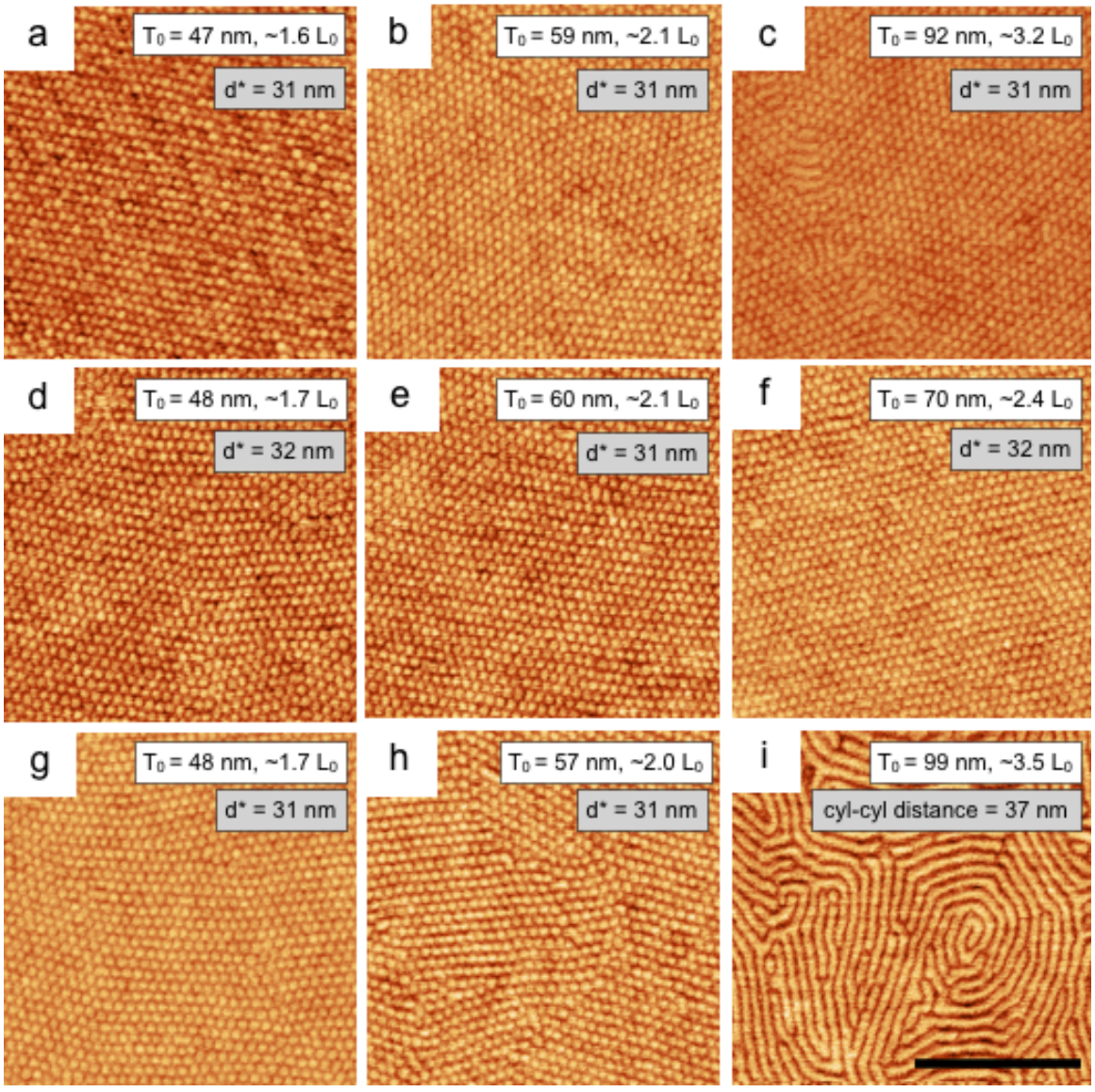

Figure 3.12. PS-PI-PS-PLA(f_{PLA} = 0.21)/PLA blend films solvent annealed in a 70/30 vol/vol THF/acetone mixture for either 2 (a-c), 5 (d-f) or 10 (g-i) min after spin coating with 1.5 wt % solution in chlorobenzene at 1500, 2000 or 3000 rpm. Scale bar is 500 nm.

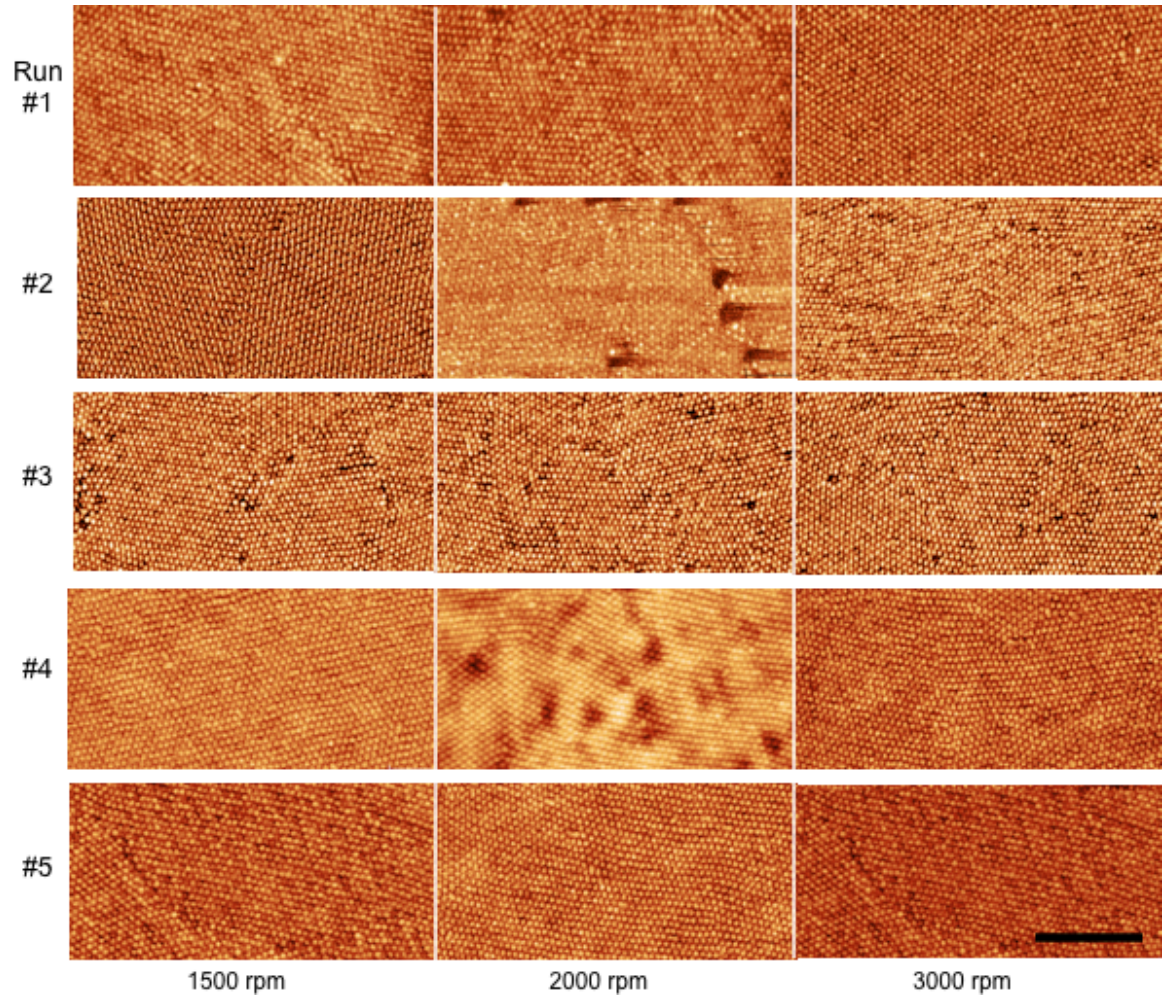

Figure 3.13. 5 representative sets of films solvent annealed in 70/30 v/v THF/acetone mixture for 5 minutes after spin coating with 1.5 wt % solution in chlorobenzene at 1500, 2000 or 3000 rpm. Average film thicknesses for films prepared from 1.5 wt % solution were 48 ±1 nm for 3000 rpm, 59 ± 2 nm for 2000 rpm and 76 ±12 for 1500 rpm. Scale bar is 500 nm.

3.2.5 Nanoporous Films:

Basic hydrolysis was used to remove PLA after solvent annealing. Samples were immersed in 0.25 M NaOH solutions of 60/40 (vol/vol) water/methanol containing 0.1 wt % sodium dodecylsulfate. Pores with a diameter of 15 nm were

visible on the films surface after basic hydrolysis by SEM (**Figure 3.14e**). Cross-sectional SEM analysis confirmed that nanopores span the entire film thickness for film thicknesses up to 100 nm (**Figure 3.14c, 3.14f** and **Figure 3.15**). Thicker films were not prepared.

On the film surface, only about half of the expected pore volume was evident by SEM due to an un-etchable wetting layer on parts of the surface (**Figure 3.14b**). To remove the wetting layer, an Oxygen (O_2) plasma reactive ion etch (RIE) step was used. A representative film surface after RIE is shown in **Figure 3.14d**. It was determined that a short ~6-8 sec RIE was sufficient to remove the surface wetting layer for all films. Following the RIE step, films were exposed to basic hydrolysis to remove newly exposed PLA domains. SEM images show well-ordered hexagonally packed nanopores (**Figure 3.14e–f**) 15 nm in diameter after RIE followed by basic hydrolysis. The underlying morphology is clearly well-organized hexagonally packed PLA cylinders (**Figure 3.15**). The structure is apparent across the entire film surfaces after RIE and basic hydrolysis (representative film surface with large area shown in **Figure 3.16**). This was consistent for all films (annealed 5 minutes or less) etched by RIE and basic hydrolysis **Figure 3.14–3.16**).

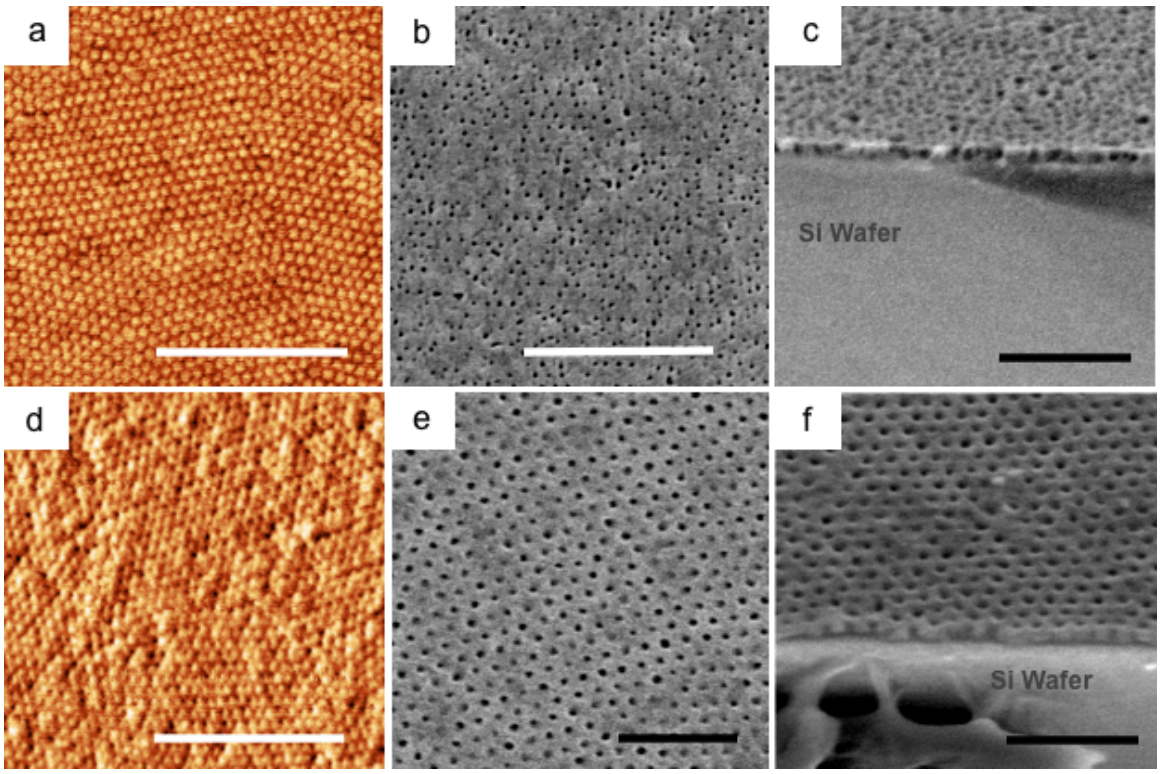

Figure 3.14. PS-PI-PS-PLA(f_{PLA} = 0.21) /PLA (95/5 wt/wt polymer blend) film spin coated from 2 wt % solution at 3000 rpm. Solvent annealed in 70/30 mixture of the/acetone for 5 minutes (thickness = 48 nm). Images show PS-PI-PS-PLA/PLA film after solvent annealing, (a), after basic etching (b and c), after RIE without basic etching (d), after RIE and basic etching (e and f). Cross sectional images show perpendicular cylinder orientation (c and f). (White scale bars = 500 nm; Black scale bars = 200 nm.) Domain spacing for image (a) is 32 nm.

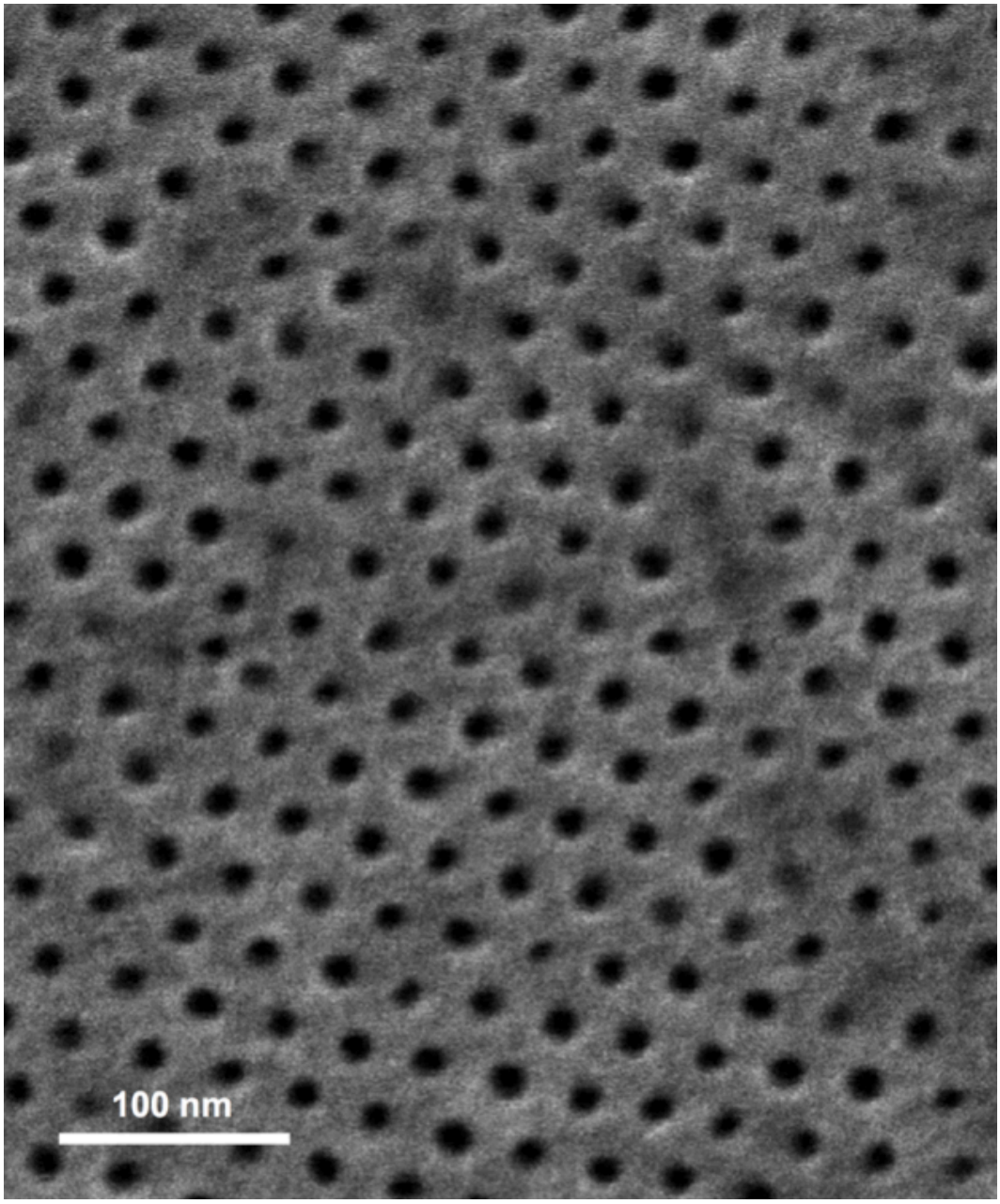

Figure 3.15. SEM image of PS-PI-PS-PLA(f_{PLA} = 0.21) /PLA (95/5 wt/wt polymer blend) 90 nm thick film after solvent annealing, RIE and PLA removal.

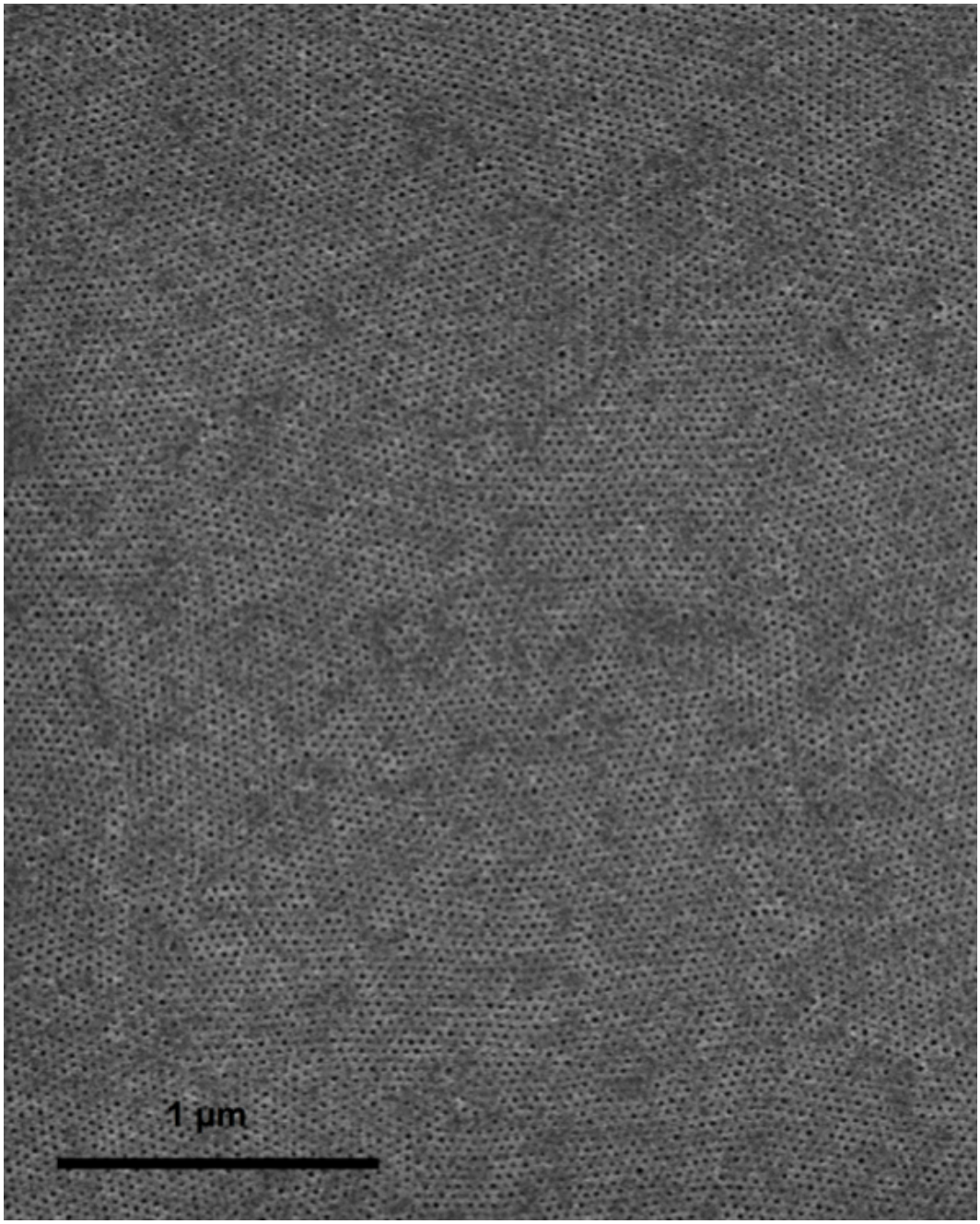

Figure 3.16. SEM image of a PS-PI-PS-PLA(f_{PLA} = 0.21)/PLA (95/5 wt/wt polymer blend)film after solvent annealing, RIE and PLA removal. Film thickness is 90 nm.

SEM cross-sectional analysis of etched films showed that perpendicular cylinders spanned the entire film thickness for thin, moderate and thicker films (**Figure 3.14c, 3.14f** and **3.17**). Perpendicular orientation was observed above the critical domain spacing (~28 nm) (by AFM surface image, **Figure 3.14**) up to the at least ~100 nm thick films (cross section shown in **Figure 3.17**). Perpendicular orientation may be possible in thicker films as well, however the thickest films prepared were ~100 nm.

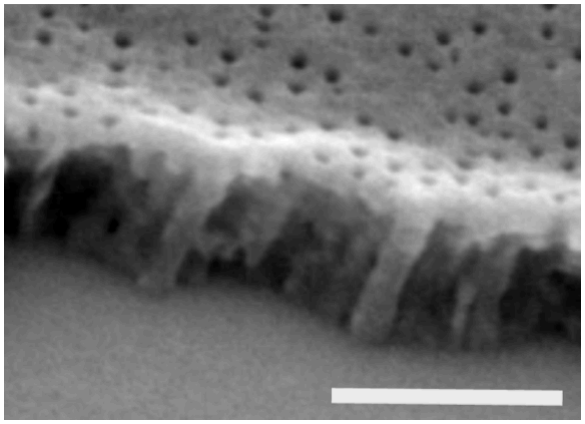

Figure 3.17. SEM image of cross-section of porous PS-PI-PS-PLA(f_{PLA} = 0.21)/PLA (95/5 wt/wt polymer blend) film showing vertical cylindrical pores. (scale bar = 200 nm). T_0 = 99 nm.

SEM images of the bottom surface of the film after basic hydrolysis of PLA (**Figure 3.18**) provide further evidence that the pores span the film thickness and reach the underlying substrate. The PLA etched polymer film and Si wafer were separated by first coating the top of the polymer film in a thin layer of room temperature setting epoxy and by second immersing the epoxy coated film in a liquid nitrogen for at least one minute. By doing this, the epoxy/block polymer film portion could be separated from the Si wafer naturally or with just a slight tap of the

wafer on a hard surface. The image shown in **Figure 3.18** shows pores that were formed from etching from the surface of the film before the film was transferred from Si wafer to epoxy. The bottom surface contains a mixture of larger domains and smaller dots like the surface of the film before RIE. The smaller domains at the top and bottom interface are likely due to PLA homopolymer (see discussion below).

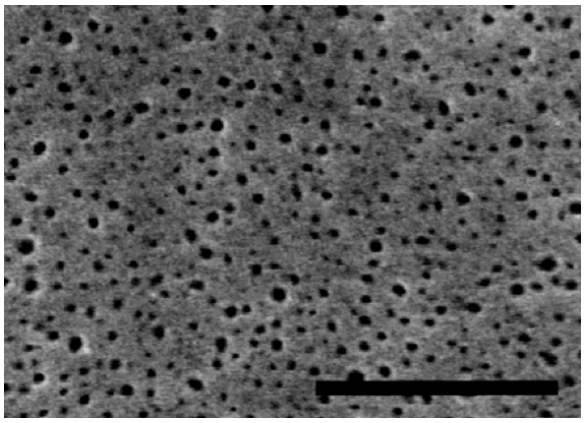

Figure 3.18. Representative SEM image of back side of etched PS-PI-PS-PLA(f_{PLA} = 0.21) /PLA (95/5 wt/wt polymer blend) film. The back side of the film was imaged by SEM after being removed from a Si wafer. (scale bar = 500 nm)

3.2.6 Role of Homo PLA in Perpendicular Cylinder Orientation

All PS-PI-PS-PLA(f_{PLA} = 0.21)/PLA blend films with perpendicular orientation showed an interesting hexagonal secondary structure (**Figure 3.19**). This was true for every film that was annealed for 2 or 5 minutes. With high magnification AFM and SEM of stained films, small features between cylinders are apparent (**Figure 3.19a**). In the AFM images of the blend, light colored "lines" connect the hexagonally packed cylinders laterally across the film. This was not observed in any PS-PI-PS-PLA films (**Figure 3.20a-b**).

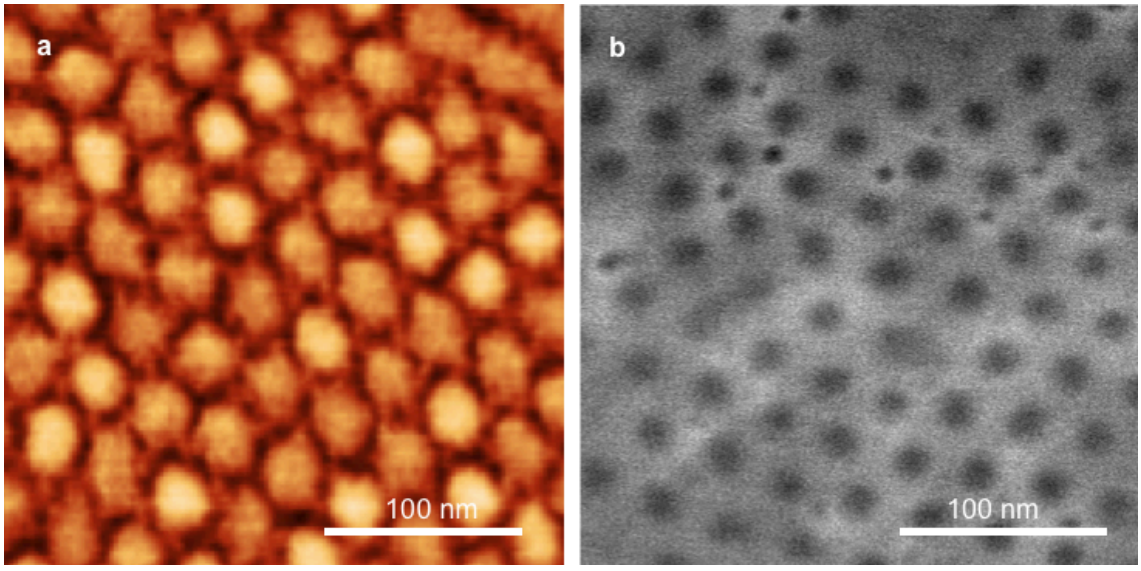

Figure 3.19. PS-PI-PS-PLA(f_{PLA} = 0.21) /PLA (95/5 wt/wt polymer blend) film after solvent annealing in a 70/30 THF/Acetone environment for 5 minutes. a) Tapping mode AFM phase image. Lighter domains are associated with stiffer blocks while the darker domains are due to the softer blocks. B) SEM of RuO_4 stained film. Dark spots in SEM are due to unstained PLA domains. T_0 = 48 nm; d* = 32 nm.

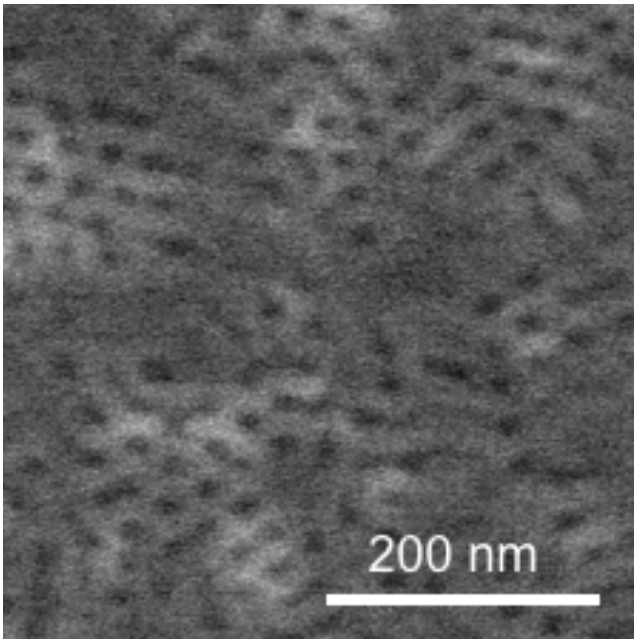

Figure 3.20. PS-PI-PS-PLA(f_{PLA} = 0.21) film solvent annealed in 70/30 THF/Acetone Environment for 5 minutes. Image is an SEM of a RuO_4 stained film. Dark domains are due to unstained PLA domains. T_0 = 28 nm. d* = 31 nm.

To further investigate this morphology, solvent annealed films were stained with ruthenium tetraoxide (RuO_4) and imaged by SEM. All films were stained with ruthenium RuO_4 for 4 minutes prior to imaging. RuO_4 can stain both PS and PI domains while leaving PLA unstained. In the SEM images, unlike in TEM, the stained PS and PI regions actually appear light in the SEM image due to the stronger secondary electron signal from the heavy metal domains. Because of this, the darkest regions in the SEM (**Figure 3.19b** and **3.20b**) are due to the unstained PLA domains.

SEM images of PS-PI-PS-PLA/PLA blend films after solvent annealing (**Figure 3.19b**) contain a cylindrical PLA morphology with smaller domains of PLA interstitially placed. For the blend, the surface of the film is not a perfect array

of small dots and large PLA cylinders. Instead, it is an irregular surface with some regions rich in hexagonal packing and others that are featureless. The featureless areas, like those in PLA-etched SEM images above, are due to a uniform polymer layer lining the surface. Since these regions are the same color as the PS and PI regions (**Figure 3.19b**), these regions contain one or more of those blocks (PS and/or PI). For these films, the hexagonal domain spacing measured was 27 nm, slightly smaller than the tetrablock film domain spacing. In comparison, the PS-PI-PS-PLA films without PLA homopolymer contain a hexagonal structure consistent with the bulk core(PLA)-shell(PS) cylinder morphology (**Figure 3.20**.

The surface morphology observed by SEM after base-etching of PLA was similar to the AFM and SEM images of un-etched PS-PI-PS-PLA/PLA films. Small holes centered between hexagonally packed pores were apparent across the film surface after only base etching (**Figure 3.21a-c**). The pore diameter of the small features is ~8 nm while the diameter of the larger pores is 15 nm. A simplified cartoon interpretation of the wetting layer structure seen by SEM is shown in **Figure 3.21d**.

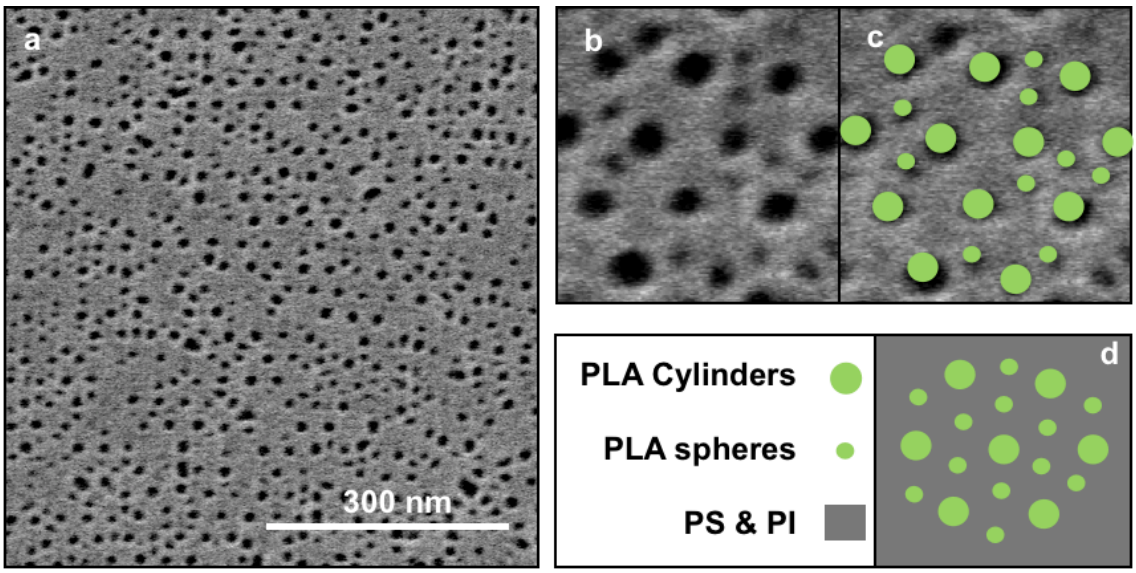

Figure 3.21. SEM of a representative PS-PI-PS-PLA(0.21)/PLA blend film after solvent annealing in 70/30 vol/vol THF/Acetone for 5 minutes. SEM of film surface after base etching, (a); Magnified portion of a, (b); Image b overlaid with green dots over pores, (c); Cartoon rendition of suspected surface arrangement of PLA domains for PS-PI-PS-PLA/PLA films seen in SEM images, (d).

When blend films were exposed to RIE and stained (no base etching) only the larger hexagonal domains are apparent (**Figure 3.22a**). The same hexagonally packed structure was evident after RIE and base etching (**Figure 3.22b**). The domain spacing after RIE was measured as 27 nm for both stained and PLA-etched films. The PLA domains had a diameter of 15 nm for stained films and 13 nm after etching (decreased size of pore in etched due to ~2 nm of Pt coating on etched surface for SEM imaging). The interstitial packing of homopolymer occurred only at the film interfaces. Smaller holes between hexagonally packed domains were never observed after RIE in surface or cross section SEM images.

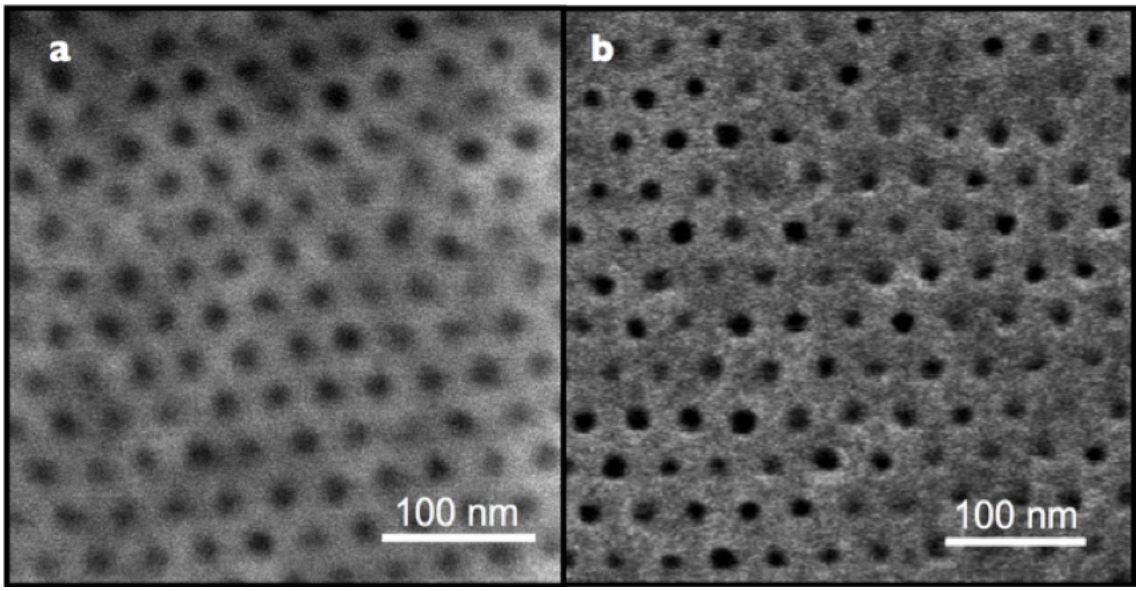

Figure 3.22. SEM images of PS-PI-PS-PLA(f_{PLA} = 0.21) /PLA (95/5 wt/wt polymer blend) film after solvent annealing in a 70/30 THF/Acetone environment for 5 minutes. SEM image of RuO_4 stained blend film after RIE, (a). Dark domains are due to unstained PLA domains. SEM image of the same film after RIE and base etching, (b). T_0 = 48 nm.

There have been a few reported cases where an added homopolymer actually fills in the insterstitial regions between cylinders.[56] For example, in poly(styrene-*b*-methyl methacrylate) (PS-PMMA) films where PMMA formed the cylindrical phase, added homopolymer PS was found to enhance perpendicular orientation of PMMA (and vice versa for PS cylinder forming diblocks) cylinders by filling in the interstitial regions (**Figure 3.23**). In this report they argued that the homopolymer chains of the corresponding majority block provided an increase of conformational entropy in copolymer chains. In other words, if PS homopolymer chains filled in the more distant regions of the matrix, then PS chains of the copolymer did not have to stretch as far to reach those more remote triangular

regions. They reported that addition of homopolymer effectively lowered the energy required for the formation of the perpendicular cylindrical morphology. As a result, improved ordering resulted both laterally and vertically in the PS-PMMA films.

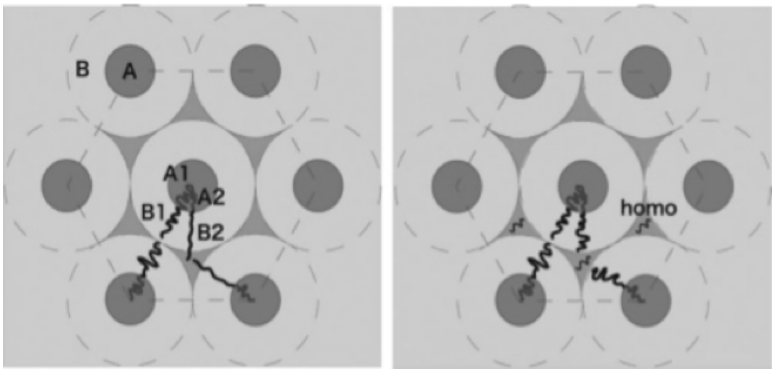

Figure 3.23. Image taken from Ref 56. Proposed chain packing of AB diblock copolymer, left, and the corresponding blend of AB diblock and B homopolymer. The black homopolymer chains in the right image can fill in the triangular regions between cylindrical domains while B chains must stretch in the left image. With homopolymer added, the black diblock B block chains do not have to stretch to fill the more distant interstitial regions.

It appears that a similar phenomenon occurs at the surface of the PS-PI-PS-PLA/PLA films. All films containing PLA homopolymer that were annealed for 5 minutes or less had perpendicular orientation regardless of film thickness. All of those films contained an interstitial structure of smaller PLA domains between larger PLA cylinders at the film surface. For all of those films, perpendicular PLA cylinder orientation existed below the surface. By segregating in the interstitial regions in the films surface, the PLA homoplymer can provide increased conformational entropy to tetrablock chains at the surface by filling in where

tetrablock chains would otherwise have to stretch across. The added homopolymer counteracts the tendency for the films to adopt parallel orientation above L_0. The homopolymer essentially serves as a "buffer" against parallel orientation and allows perpendicular orientation regardless of film thickness. The homopolymer blending was only investigated for the 70/30 vol/vol THF/Acetone mixture. The effect of the homopolymer in other solvent systems would also be interesting to investigate. The observed phenomenon may be special only to the specific solvent system employed.

3.3 Conclusions on PS-PI-PS-PLA/PLA Films

The most effective solvent system for achieving perpendicular PLA cylinders was a 70/30 vol/vol THF/acetone mixture. Less polar solvents produced parallel orientation and more polar solvents led to other film morphologies.

The addition of 5 wt % PLA homopolymer allowed thickness independent perpendicular orientation of PLA cylinders in films up to 100 nm thick and improved lateral ordering of hexagonally packed grains. This was due in part to 1) a neutral solvent atmosphere and 2) the incorporation of homopolymer PLA.

Multiple runs on separate days all resulted in perpendicular cylinder orientation for films annealed for 2 or 5 minutes confirming the reproducibility of this procedure. Well-ordered hexagonally packed 15 nm pores were created after RIE and basic hydrolysis of PLA. Vertical pores spanning the entire thickness of etched films were observed by SEM confirming perpendicular orientation was developed throughout the depth of the films.

3.4 Experimental Details

Materials

The PS-PI-PS-PLA polymer used in this work had a total molecular weight of 27 kg mol^{-1} (Mn(PS) = 11 kg mol^{-1}, Mn (PI) = 9 kg mol^{-1}, Mn (PLA) = 7 kg mol^{-1}) and polydispersity Đ of 1.09.[36] Synthetic details regarding the preparation of this multiblock terpolymer were reported previously. The tetrablock PS-PI-PS-PLA polymer used in this study adopts a hexagonally packed core(PLA)-shell(PS) cylinder morphology in the bulk. Domain spacing in the bulk, L_0, was 28.6 nm by SAXS. Using a PS volume fraction of 0.40 and a PLA volume fraction of 0.21, a 33.0 nm cylinder center-center distance was estimated from SAXS. In addition, a PS cylinder diameter of 23.5 nm and PLA cylinder diameter of 13.8 nm were also estimated from SAXS using the equation for cylindrical domains ($f_{polymer}=2\pi/(\sqrt{3})(R/D)^2$); where R = radius and D = domain spacing.

Homopolymer PLA was prepared by ROTEP of d,l-lactide from benzyl alcohol using $Sn(Oct)_2$ as the catalyst. The measured M_n was 10 kg mol^{-1} and PDI of 1.08 measure by GPC.

Annealing solvents were dried over activated molecular sieves (3 Å for Acetone, 4 Å for thf, toluene and chloroform) for 48 h prior to solvent annealing to remove water. Solvents were filtered through 0.45 μm Pall PTFE Acrodisc syringe filters before polymer dissolution. All polymer solutions were filtered through 0.45 μm Pall PTFE Acrodisc syringe filters before spin coating and used within 1 d after preparation. All other reagents were purchased from Sigma Aldrich and were used as received.

Wafer Hydrophobic Modification. HMDS treatment of Si wafers was achieved by sonicating wafers in solvents (acetone, then methanol) for 15 min each, rinsing with

isopropanol, immersing in a 1:5 (v/v) HMDS:toluene solution for 16 h, followed by rinsing wafers with toluene and blow drying with house nitrogen (N_2) gas.

Spin Coating. Both PS-PI-PS-PLA and the 95/5 (w/w) PS-PI-PS-PLA/PLA blend were spin coated from 1.0% or 1.5% (w/v) chlorobenzene solutions onto HMDS treated Si wafers at ambient conditions. Spin coating was preformed at 1500, 2000 and 3000 rpm for 60 s to generate a range of film thicknesses.

Thin Film Solvent Vapor Annealing. Solvent vapor annealing of films was performed immediately after spin coating. The experimental setup for solvent annealing is presented in **Figure 3.2**. To remove any atmospheric humidity or solvent vapors, the entire solvent annealing chamber (including solvent reservoir) was purged with N_2 gas for 30 minutes before use. Before each experiment, the solvent reservoir was filled with 150 mL of solvent (either toluene, chloroform, thf or a mixture of thf and acetone) and then sealed off from the sample chamber and atmosphere. Spin coated films were then placed inside the sample chamber and purged with N_2 gas for 10 minutes. After purging, N_2 gas was then redirected to the solvent line and the valve between the solvent reservoir and sample chamber was opened to introduce solvent vapor into the sample chamber.

Solvent absorption was observed by change in film color after a few seconds. Using a N_2 flow rate of 3.8 L/min, solvent vapor was passed through the sample chamber for 2, 5, 10 or 20 min. Higher flow rates oversaturated the films with solvent and caused dissolution of polymer from the Si wafer. After a specified time, solvent was removed from films immediately by redirecting the N_2 flow from the solvent line to the purge line.

RIE Etching. Surface wetting layers from annealed films were removed by reactive ion etching (RIE) on an STS etcher model 320. Films were exposed to oxygen (O_2) plasma at 30 mTorr with power of 60 W for 6-8 s.

Hydrolysis. Samples were immersed in a 0.25 M sodium hydroxide solution containing 40/60 (v/v) methanol/water containing 0.1 wt % of sodium dodecylsulfate for 45 min without stirring. After removing from solution, films were rinsed with a 40/60 (v/v) methanol/water solution for 10 minutes, rinsed briefly with water and then dried with N_2 gas.

Thin Film Analysis

Ellipsometry. Film thickness was measured by a surface and thin film spectroscopic ellipsometer VASE from J.A. Wollam Co., Inc.

Atomic Force Microscopy (AFM). Tapping mode AFM was performed on an Agilent 5500 environmental Scanning Probe Microscope.

Scanning electron microscopy (SEM). SEM imaging was performed on a Hitachi S-900 field emission gun scanning electron microscope (FE-SEM). For best resolution and least sample charging, SEM analysis was performed at 2 kV on films coated with 2-3 nm of Pt. For cross-sectional SEM, PLA etched films were immersed in liquid N_2 for 1-2 min before fracturing in the liquid N_2 bath. Prior to SEM, samples were coated for 13 minutes at a coating rate of 0.2 nm Pt/min with a VCR High Resolution Indirect Ion-Beam Sputter Coater.

For the observation of bottom surface, epoxy resin (EpoFix resin and hardener from Struenrs) was covered on top surface of polymer film and then cured for 24 h. Polymer film was detached from Si wafer substrate in liquid nitrogen to expose the bottom side of the etched film.

Molecular Characterization

^{1}H NMR Spectroscopy. All experiments were performed at 25 ^{o}C on a Varian Inova (500 MHz) instrument with polymer solutions in $CDCl_3$. Chemical shifts were determined as δ (ppm) relative to the ^{1}H signals of $CHCl_3$ at 7.27 ppm.

Size-exclusion chromatography (SEC). SEC was used to determine the molecular weight and PDI of PLA homopolymer. SEC was performed on a Hewlett-Packard (Agilent Technologies) 1100 series liquid chromatography equipped with a Hewlett-Packard 1047A refractive index detector. Samples were prepared at concentrations between 1 - 5 mg/mL in $CHCl_3$, and run at 35 °C with $CHCl_3$ as an eluent through three Plgel 5μm Mixed-C columns in series with an available molecular weight range of 400 – 400,000 g/mol. Molecular weights and molecular weight dispersities were estimated by polystyrene standards purchased from Polymer Laboratories.

3.5 References

(1) Albert, J. N. L.; Epps, T. H., III *Mater. Today* **2010**, *13*, 191-226.

(2) Segalman, R. A.; *Mater. Sci. Eng., R* **2005**, *48*, 191-226.

(3) Hamley, I. W. *Nanotechnology* **2003**, 24*,* R39-R54.

(4) Fasolka, M. J.; Mayes, A. M.; *Annu. Rev. Mater. Res.* **2001**, *31*, 323-355.

(5) Darling, S. B.; *Prog. Polym. Sci.* **2007**, *32*, 1152.

(6) Tseng, Y-C.; Darling, S. B.; *Polymers*, **2010**, *2*, 470-489.

(7) Stoykovich, M. P.; Nealey, P. F. *Materials Today* **2006**, *9*, 20.

(8) Park, M., et al., *Science* **1997** *276*, 1401.

(9) Park, S., et al., *ACS Nano* **2008**, *2*, 766.

(10) Ruiz, R., et al., *Science* **2008**, *321*, 936.

(11) Peinemann, K.-V.; Abetz, V.; Simon, P. F. W. *Nature* **2007**, *6*, 992–996.

(12) Phillip, W. A.; O'Neill, B.; Rodwogin, M.; Hillmyer, M. A.; Cussler, E. L. *ACS Appl. Mater. Interfaces* **2010**, *2*, 847–853.

(13) Yang, S. Y.; Ryu, I.; Kim, H. Y.; Kim, J. K.; Jang, S. K.; Russell, T. P. *Adv Mater.* **2006**, *18*, 709-712.

(14) Sperschneider, A.; Scacher, F.; Gawenda, M.; Tsarkova, L.; Muller, A. H. E.; Ulbricht, M.; Krausch, G.; Kohler, J. *Small* **2007**, *3*, 1056–1063.

(15) Yang, S.; Yang, J.-A.; Kim, E.-S.; Jeon, G.; Oh, E. J.; Choi, K. Y.; Hahn, S. K.; Kim, J. K. *ACS Nano* **2010**, *4*, 3817–3822.

(16) Simon PFW, Ulrich R, Spiess HW, Wiesner U. *Chem. Mater.* **2001,** *13,* 3464.

(17) Fink, Y.; Urbas, A. M.; Bawendi, M. G.; Joannopoulos, J. D.; Thomas, E. L. *J. Lightwave Technology* **1999**, *17*, 1963-1969.

(18) Black, C. T.; Guarini, K. W.; Milkove, K. R.; Baker, S. M.; Russell, T. P.; Tuominen, M. T. *Appl. Phys. Lett.* **2001**, *79*, 409-411.

(19) Black, C. T.; Ruiz, R.; Breyta, G.; Cheng, J. Y.; Colburn, M. E.; Guarini, K. W.; Kim, H. C.; Zhang, Y. *IBM Journal of Research and Development* **2007**, *51*, 605-633.

(20) Xia, G.; Wang, S.; Jeong, S-J. *Nanotechnology* **2010**, *21*, 1-5.

(21) Hawker, C. J.; Russell, T. P.; *MRS Bull*. **2005**, *30*, 952.

(22) Park, C.; Yoon, J.; Thomas, E. L; *Polymer* **2003**, *44*, 6725-6760.

(23) Hillmyer, M.A. *Adv. Polym. Sci.* **2005**, *190*, 137-181.

(24) Bang, J.; Jeong, U.; Ryu, D.Y.; Russell, T.P.; Hawker, C.J. *Adv. Mater.* **2009**, *21*, 4769–4792

(25) Jackson, E. A.; Lee. Y.; Hillmyer, M. A. *Submitted to Macromolecules* **2012.**

(26) Bluemle, M. J.; Fleury, G.; Lodge, T. P.; Bates, F. S. *Soft Matter* **2009**, *5*, 1587-1590.

(27) Zhang, J.; Bates, F. *J. Am. Chem. Soc.* **2012**, *134*, 7636-7639.

(28) Zhang, J.; Sides, S.; Bates, F. *Macromolecules* **2012**, *45*, 256-265.

(29) Bluemle, M. J.; Zhang, J.; Lodge, T. P.; Bates, F. S. *Macromolecules* **2010**, *43*, 4449-4452.

(30) Zalusky, A. S.; Olayo-Valles, J. H.; Taylor, C. J.; Hillmyer, M. A. *Macromolecules* **2001**, *123*, 1519.

(31) Zalusky, A. S.; Olayo-Valles, R.; Wolf, J. H.; Hillmyer, M. A. *J. Am. Chem. Soc.* **2002**, *124*, 12761.

(32) Phillip, W.A.; Rzayev, J.; Hillmyer, M.A.; Cussler, E.L. *J. Membr. Sci.* **2006**, *286*, 144-152.

(33) Pitet, L. M.; Amendt, M. A.; Hillmyer, M. A. *J. Am. Chem. Soc.* **2010**, 132, 8230–8231.

(34) Phillip, W.A.; O'Neill, B.; Rodwogin, M.; Hillmyer, M.A.; Cussler, E.L. *ACS Appl. Mater. Interfaces* **2010**, *2*, 847-853.

(35) Olayo-Valles, R.; Guo, S.W.; Lund, M.S.; Leighton, C.; Hillmyer. M.A. *Macromolecules* **2005**, *38*, 10101-10108.

(36) Ho, R.-M.; Tseng, W.-H.; Chiang, Y.-W.; Lin, C.-C.; Ko, B.-T.; Huang, B.-H. *Polymer* **2005**, *46*, 9362-9377.

(37) Nuxoll, E.E.; Hillmyer, M.A.; Wang, R.F.; Leighton, C.; Siegel, R.A. *ACS Appl. Mater. Interfaces* **2009**, *1*, 888-893.

(38) Cavicchi, K.A.; Russell, T.P. *Macromolecules* **2007**, *40*, 1181-1186.

(39) Baruth, A.; Rodwogin, M. D.; Erickson, M. J.; Hillmyer, M. A.; Leighton, C. ACS *Appl. Mater. and Interfaces* **2011**, *3*, 3472-3481.

(40) Guo, S.; Rzayev, J.; Bailey, T.S.; Zalusky, A.S.; Olayo-Valles, R.; Hillmyer, M.A. *Chem. Mater.* **2006**, *18*, 1719-1721.

(41) Kubo, T.; Wang, R.F.; Olson, D.A.; Rodwogin, M.; Hillmyer, M.A.; Leighton, C. *Appl. Phys. Lett.* **2008**, *93*, 133112.

(42) Vayer, M.; Hillmyer, M.A.; Dirany, M.; Thevenin, G; Erre, R.; Sinturel, C. *Thin Solid Films* **2010**, *518*, 3710-3715.

(43) Querelle, S. Jackson, E. A. Hillmyer, M. A. *In preparation.*

(44) Cavicchi, K. A.; Berthiaume, K. J.; Russell, T. P. *Polymer* **2005**, *46*, 11635-11639.

(45) Bang, J.; Kim, S. H.; Drockenmuller, E.; Misner, M. J.; Russell, T. P.; Hawker, C. J. *J. Am. Chem. Soc.* **2006**, *128*, 7622-7629.

(46) Elbs, H.; Fukunaga, K.; Stadler, R.; Sauer, G.; Magerle, R.; Krausch, G. *Macromolecules* **1999**, *32*, 1204-1211.

(47) Albert, J. N. L.; Bogart, T. D.; Lewis, R. L.; Beers, K. L.; Fasolka, M. J.; Hutchinson, J. B.; Vogt, B. D.; Epps, T. H. *Nano Lett.* **2011**, *11*, 1351-1357.

(48) Jung, Y. S.; Ross, C. A. *Adv. Mater.* **2009**, *21*, 2540–2545.

(49) Kim, S. H.; Misner, M. J.; Xu, T.; Kimura, M.; Russell, T. P. *Adv. Mater.* **2004**, *16*, 226–231.

(50) Bang, J.; Kim, B. J.; Stein, G. E.; Russell, T. P.; Li, X.; Wang, J.; Kramer, E. J.; Hawker, C. J. *Macromolecules* **2007**, *40*, 7019–7025.

(51) Park, S.; Kim, B.; Xu, J.; Hofmann, T.; Ocko, B. M.; Russell, T. P. *Macromolecules* **2009**, *42*, 1278-1284.

(52) Gotrik, K. W.; Hannon, A. F.; Son, J. G.; Keller, B.; Alexander-Katz, A.; Ross, C. A. *ACS Nano* **2012**, *6*, 8052–8059.

(53) Lee, D. H.; Park, S.; Gu, W.; Russell, T. P. *ACS Nano* **2011**, *5*, 1207–1214.

(54) Garlotta, D. *J. Polym. & Environ.* **2001**, *9*, 63-84.

(55) Gupta, M. C.; Deshmukh, V. G. *Colloid & Polymer Sci.* **1982**, *260*, 514-517.

(56) Kitano, H. et al. *Langmuir*, **2007**, *23*, 6404-6410.

(57) Yamauchi, L.; Akasaka, S.; Hasegawa, H.; Iatrou, H.; Hadjichristidis, N.; *Macromolecules,* **2005**, *38*, 8022.

(58) Lim, S. C.; Kim, S. H.; Lee, J. H.; Kim, M. K.; Kim, D. J.; Zyung, T. *Synth. Met.* **2005**, *148,* 75-79.

(59) Polymer Handbook, 4th ed.; Brandup, J.; Immergut, E. H., Grulke, E., Abe, A., Bloch, D. R., Eds.; John Wiley & Sons; New York, 1999, 2005.

(60) Hanley, K. J.; Lodge, T. P. *Macromolecules*, **2000**, *33*, 5918-5931.

(61) Hiemenz, P. C.; Lodge, T. P.; *Polymer Chemistry*, Second Edition; CRC Press, Taylor and Francis Group: Boca Raton, Fl, **2007**, pp 24-28, 117-135, 153, 247-283, 291- 296, 422-446, 472-497.

(62) Jeong, U; Ryu, D.Y.; Kho, D.H.; Kim, J.K.; Goldbach, J.T.; Kim, D.H.; Russell, T.P. *Adv. Mater.* **2004**, *16*, 533-536.

(63) Ahn, D.U.; Sancaktar, E. *Adv. Funct. Mater.* **2006**, *16*, 1950-1958.

(64) Mykhaylyk, T.A.; Mykhaylyk, O.O.; Collins, S.; Hamley, I.W. *Macromolecules* **2004**, *37*, 3369-3377.

(65) Shibayama, M.; Hasegawa, H.; Hashimoto, T.; Kawai, H. *Macromolecules* **1982**, *15*, 274-280.

(66) Kim, S. H.; Misner, M. J.; Xu, T.; Kimura, M.; Russell, T. P. *Adv. Mater.* **2004**, *16*, 226–231.

(67) Park, D.S; Sancaktar, E. *Current Nanoscience*, **2012**, *8*, 244-248.

Chapter 4

Asymmetric PS-PI-PS-PLA & PS-PEEP-PS-PLA Tetrablock Terpolymers*

This chapter describes the preparation, morphology and tensile behavior of poly(styrene-*b*-isoprene-*b*-styrene-d,l-lactide) (PS-PI-PS-PLA) and poly(styrene-*b*-ethylene-*r*-ethylene-*alt*-propylene-*b*-styrene-*b*-d,l-lactide) (PS-PEEP-PS-PLA) tetrablock terpolymers. Hydroxy end-functionalized PS-PI-PS and PS-PEEP-PS were used to initiate ring-opening polymerizations of d,l-lactide to obtain a series of polymers with varying PLA composition. Tensile Behavior of PS-PI-PS-PLA tetrablocks and corresponding PS-PEEP-PS-PLA analogs was also investigated. Morphological behavior of PS-PI-PS-PLA tetrablocks was also studied using SAXS and TEM.

* This chapter presents work done in collaboration with Dr. David Olson.

4.1 Introduction

The PS-PI-PS-PLA tetrablocks discussed in **Chapter 2** had strikingly tougher mechanical properties than the compositionally symmetric PS-PI-PS precursor. Upon the addition of only 20-25% PLA, the tetrablocks exhibited tensile strength (14-16 MPa) of almost triple that of the PS-PI-PS triblock precursor (6 MPa). Because of this encouraging result, we were motivated to look into the effect of addition of small amounts of PLA on the mechanical properties of more common ABA thermoplastic elastomers.

The more common commercially available ABA thermoplastic elastomers (TPEs) typically have asymmetric A/B composition (~15−30% A) and higher overall molecular weight (50−150 kg mol^{-1}). Many TPEs contain PS domains as a minority phase (~15-30% PS) in a rubbery matrix such as poly(butadiene) (PB), polyisoprene (PI) or hydrogenated low T_g blocks such as poly(ethylene-butylene) (PEB) or poly(ethylene-*alt*-propylene) (PEP). Such TPEs have been used as adhesives and in materials for automobiles, medical devices, diapers, footwear and many more consumer products. The world demand for TPEs is increasing and as is poised to reach 5.6 million metric tons by 2015.[1]

This chapter describes two sets of ABAC tetrablock terpolymers synthesized from ABA triblocks with asymmetric composition. Poly(styrene-*b*-isoprene-*b*-styrene-d,l-lactide) (PS-PI-PS-PLA) tetrablock terpolymers (**Scheme 4.1**) with PLA volume fraction ranging from 0 to 20% were synthesized from a hydroxyl end-

functionalized PS-PI-PS triblock precursor with a 70:30 volume ratio of PI to PS. These PS-PI-PS-PLA tetrablocks were synthesized and analyzed for morphological behavior through a collaboration with Dr. David Olson.

Compositionally analogous poly(styrene-*b*-ethylene-*r*-ethylene-*alt*-propylene-*b*-styrene-*b*-d,l-lactide) (PS-PEEP-PS-PLA) tetrablock terpolymers (**Scheme 4.1**) were also prepared from a hydroxyl end-functionalized PS-PEEP-PS triblock received from the Kuraray Company.

Tensile behavior of all tetrablocks was investigated. This chapter describes the effect PLA volume fraction on mechanical properties of PS-PI-PS-PLA and PS-PEEP-PS-PLA tetrablocks.

Scheme 4.1. Chemical Structures for PS-PI-PS-PLA and PS-PEEP-PS-PLA

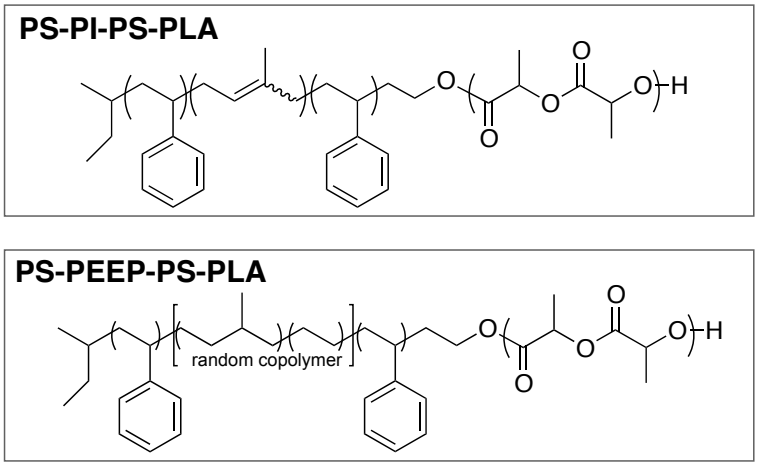

4.2 Synthesis of Tetrablocks

4.2.1 PS-PI-PS-OH

The PS-PI-PS-OH triblock precursor was synthesized by sequential anionic polymerization using the previously established method described by Bailey et al.[2] The triblock was synthesized by Dr. David Olson. Sequential anionic polymerization of styrene (19.91 g), isoprene (35.87 g) and then styrene (21.79 g) was initiated by *sec*-butyllithium (2.636 mL, 1.3 M) in cyclohexane under ~5 PSI positive pressure of argon (**Scheme 4.2**).

Scheme 4.2. Synthesis of PS-PI-PS-OH

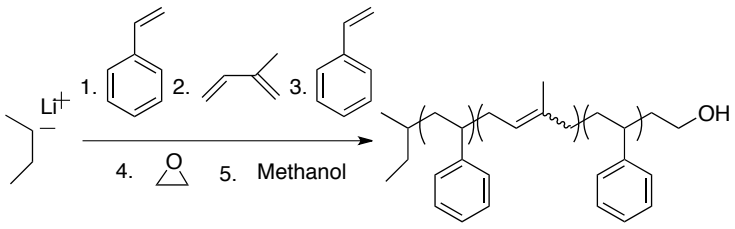

After polymerization, 150-fold excess of ethylene oxide (18.43 mL) was added to cap the growing PS-PI-PS chain ends with one unit of ethylene oxide. The reaction was terminated with nitrogen purged acidic methanol. The terminated polymer was precipitated into a 1:1 methanol:isopropanol solution. The precipitated polymer was then dried in a 45−50 °C vacuum over for 48 hours to remove solvent. This reaction yielded 75.5 g of triblock for a 97.2% yield. The ^{1}H NMR spectrum of the resulting polymer is shown in **Figure 4.1**. The molecular

weight, M_n, determined by ^{1}H NMR spectroscopy was 69.5 kg mol^{-1}. SEC results for the triblock and aliquots from the first and second blocks are shown in **Figure 4.2**. The triblock molecular weight dispersity, **Đ**, was 1.08 relative to PS standards. The molecular weight of the three blocks, determined using a combination of SEC and ^{1}H NMR spectroscopy, was 11.4 kg mol^{-1}, 46.1 kg mol^{-1}, 12.0 kg mol^{-1} for blocks PS-block-1, PI and PS-block-2 respectively. This polymer is denoted as PS-PI-PS-OH [11-46-12] in **Table 4.1**.

Table 4.1. PS-PI-PS-PLA and PS-PEEP-PS-PLA Tetrablocks

Sample ID	f_{PI}[a]	f_{PS}[a]	f_{PLA}[a]	M_n[b]	Đ[c]
PS-PI-PS-OH [11-46-12]*	*0.70*	*0.30*	*0.00*	*69.5*	*1.08*
PS-PI-PS-PLA* [11-46-12-3]	0.65	0.28	0.06	75.6	1.12
PS-PI-PS-PLA* [11-46-12-6]	0.62	0.27	0.11	81.7	1.09
PS-PI-PS-PLA [11-46-12-11]	0.59	0.26	0.15	85.7	1.10
PS-PI-PS-PLA [11-46-12-20]	0.54	0.25	0.19	91.2	1.11

*Polymers synthesized by Dr. David Olson. [a]Volume fractions are calculated from published densities at 140 °C (ρ_{PI} = 0.830[3] ρ_{PS} = 0.969[21], ρ_{PLA} = 1.154[4]). [b]Determined from ^{1}H NMR end group analysis. [c]Determined from SEC measurements.

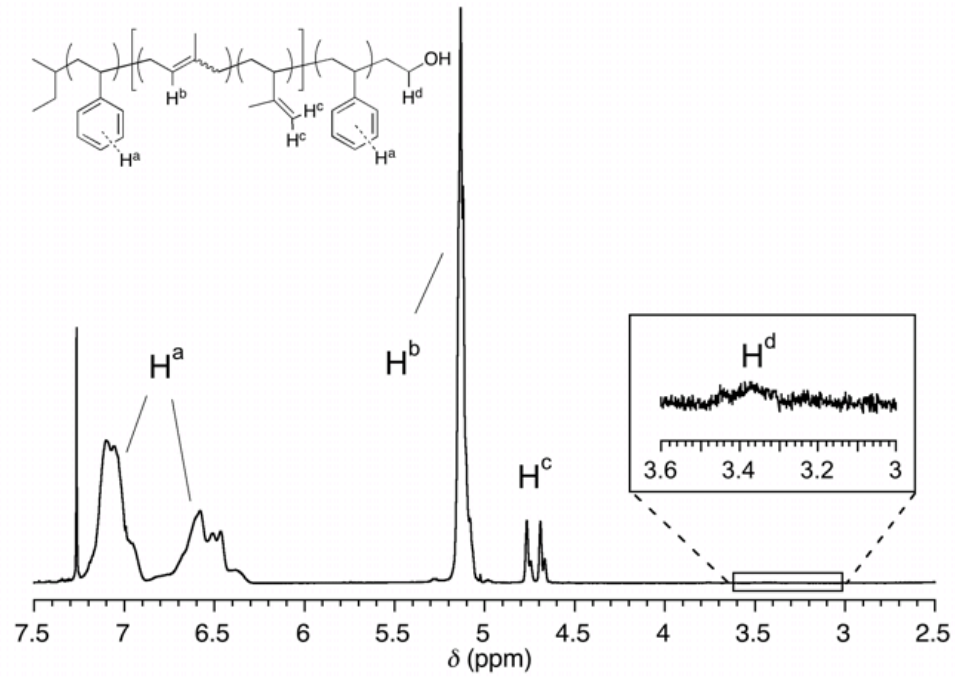

Figure 4.1. ^{1}H NMR spectrum of hydroxyl terminated **PS-PI-PS-OH** (11-46-12) dissolved in $CDCl_3$ (7.26 ppm). ^{1}H NMR (ppm downfield from TMS): 6.20-7.26 (b, -(C_6H_5)), 4.90-5.30 (b, -CH_2-C*H*=C(CH_3)-CH_2-), 4.60-4.90 (b, CH_2=C(CH_3)-), 3.5-3.7 (m, -CH_2-OH), 0.84-2.40 (b, CH_2=C(CH_3)-C(R)*H*CH_2-,-CH_2-CH=C(CH_3)-CH_2-, and C_6H_5-C(R)*H*-CH_2-), 0.5-0.78 (m, -CH_3, initiator fragment).

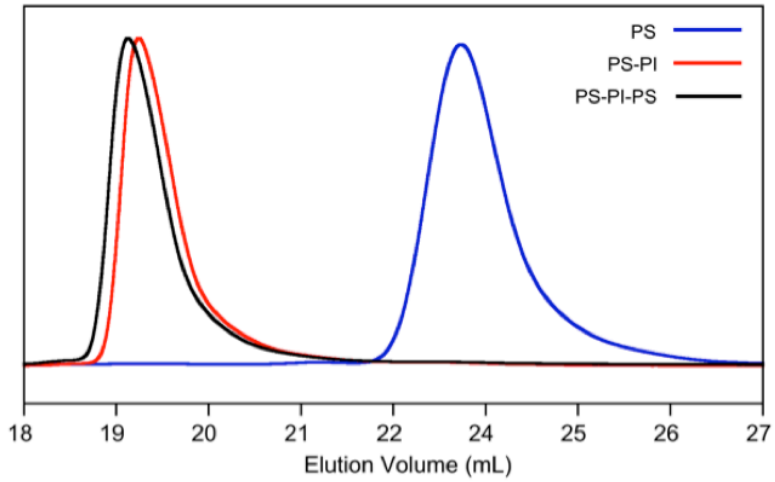

Figure 4.2. SEC of PS block 1 aliquot, blue (PDI of 1.06); PS-PI aliquot, red (PDI of 1.07); and PS-PI-PS triblock, black (PDI of 1.08).

4.2.2 Synthesis of PS-PI-PS-PLA from PS-PI-PS-OH

PS-PI-PS-PLA tetrablocks were synthesized by two different methods. For the first method, original PS-PI-PS-PLA polymers were synthesized by polymerization of d,l-lactide initiated by the parent triblock using triethyl aluminum ($AlEt_3$) as the catalyst (**Scheme 4.3**). In a typical PS-PI-PS-PLA synthesis, a 2 g sample of PS-PI-PS-OH was added to a sealable pressure flask and brought into a glove box. Inside the glove box, 9 mL of toluene was added to the flask and the mixture was stirred overnight at room temp to dissolve the polymer. Once dissolved, 0.05 mL of 1.0 M $AlEt_3$ was added to the flask and allowed to stir overnight at room temperature. The next day, 0.198 g of d,l-lactide was added to the flask. The flask was sealed, removed from the glove box and then placed in a 90 °C oil bath. The reaction was allowed to stir at 90 °C for 12 h. Finally, the reaction was terminated with 2 mL of 0.5 M HCl and then precipitated into methanol. The resulting tetrablocks were filtered and then dried in a vacuum oven at 45−50 °C for 48 hours to remove residual solvent. Molecular weight, PDI and volume fractions were obtained from ^{1}H NMR and SEC characterization. A representative polymerization resulted in a yield of 2.55 g (77% d,l-lactide conversion), M_n of 91.2 kg mol^{-1} (by ^{1}H NMR spectroscopy), and molecular weight dispersity of 1.13 relative to PS standards.

Scheme 4.3. Synthesis of PS-PI-PS-PLA with Triethyl Aluminum

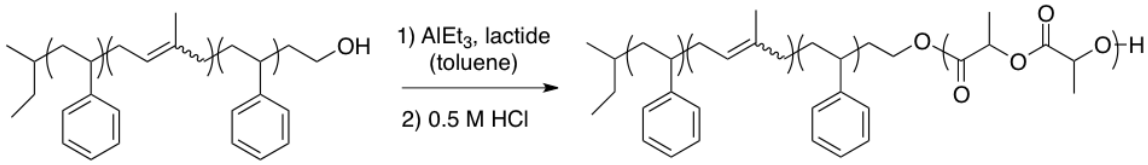

For the second method, polymerizations of d,l-lactide were catalyzed with diazabicyclo[5.4.0]undec-7-ene (DBU) (**Scheme 4.4**). In a representative synthesis, 8.40 g of PS-PI-PS-OH triblock and 1.817 g of d,l-lactide were dissolved in ~30 mL dry methylene chloride in a glass scintillation vial in a nitrogen glovebox. DBU (20 μL) was then added to activate the polymerization. The vial was then sealed with a Teflon lined screw cap, removed from the glove box and placed on a stir plate. After stirring at room temperature for 60 minutes, a small amount of benzoic acid (~5-10 mg) was added to terminate the reaction. The polymer was precipitated with methanol, filtered and dried in a vacuum oven (50 °C for 48 h). A representative polymerization resulted in a 96% yield (9.91 g).

Scheme 4.4. Synthesis of PS-PI-PS-PLA with DBU

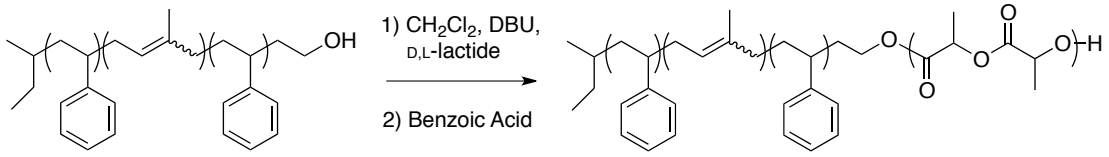

Indication of lactide polymerization was observed by the presence of at peak at 4.4 ppm in each tetrablock spectrum (**Figure 4.3**). A shift of the –**CH2**-OH resonance in the triblock from 3.3 ppm to 3.8 ppm in the tetrablock indicates the

addition of PLA to the hydroxyl end of triblock (–**CH2**-O-PLA). This shift was observed in all tetrablocks. The degree of polymerization of lactide was estimated by comparison of the *sec*-butyl end group resonances (0.8-0.9 ppm) and the methine protons –**CH2**-O-PLA (3.8 ppm) to the PLA backbone resonances, -C(=O)-**CH**(CH3)-O- (~5.17 ppm). This degree of polymerization was also confirmed by comparison to aromatic PS resonances (6.20-7.26 ppm).

SEC results for all PS-PI-PS-PLA tetrablocks are presented in **Figure 4.4**. A decrease in elution volume with increasing molecular weight was observed for all tetrablocks prepared from reactions with increasing amount of lactide.

Four PS-PI-PS-PLA tetrablocks were synthesized using these methods. Molecular, dispersity and block fractions for all prepared tetrablocks are listed in **Table 4.1**.

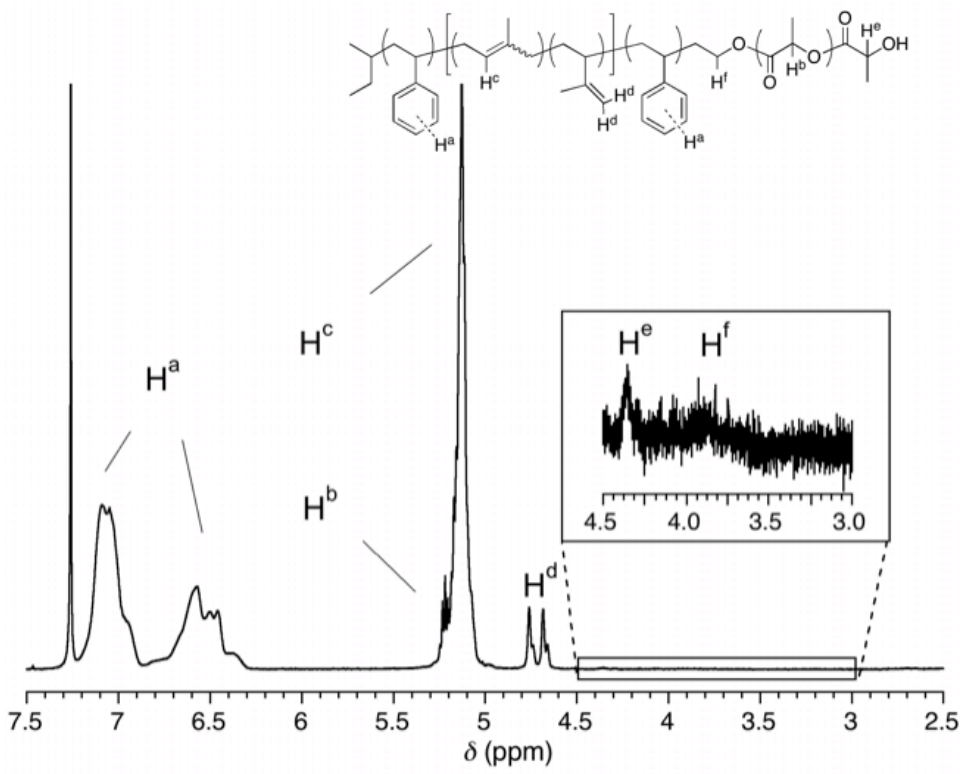

Figure 4.3 ^{1}H NMR spectrum of **PS-PI-PS-PLA** (f_{PLA} = 0.19) dissolved in $CDCl_3$ (7.26 ppm). No resonances were observed at 3.3 ppm suggesting that all PS-PI-PS-OH was converted to PS-PI-PS-PLA. Ratio of H^f to H^e is 2 to 1. ^{1}H NMR (ppm downfield from TMS): 6.20-7.26 (b, -CH(C_6H_5)), 4.90-5.30 (b, -CH_2-C*H*=C(CH_3)-CH_2-), 4.98-5.28 (b, -C(O)C*H*(CH_3)O-), 4.60-4.90 (b, -CH_2=C(CH_3)-), 4.30-4.42 (m, -C(O)C*H*(CH_3)OH), 3.95-4.15 (b, -CH_2CH_2-O-), 2.60-2.75 (bd, -C(O)CH(CH_3)O*H*), 0.84-2.40 (b, CH2=C(CH_3)-C(R)*H*-CH_2-, -CH_2-CH=C(CH_3)-CH_2-, -C(O)CH(CH_3)O-, and C_6H_5-C(R)*H*-CH_2-), 0.5-0.78 (m, -CH_3, initiator fragment).

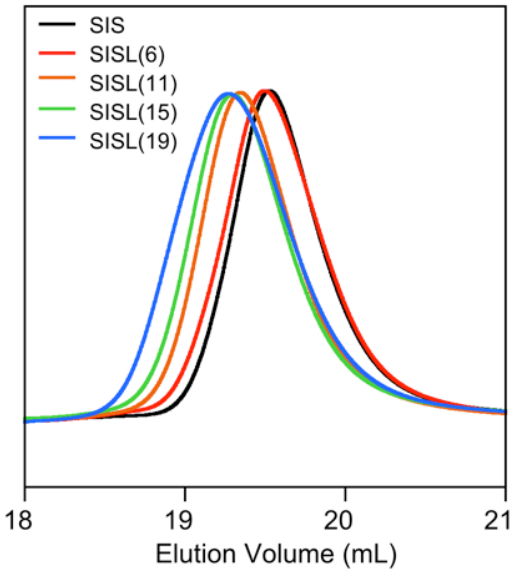

Figure 4.4. SEC traces of PS-PI-PS-OH and PS-PI-PS-PLA tetrablocks prepared therefrom.

Differential Scanning Calorimetry (DSC) was used to determine the thermal transitions in the triblock and tetrablocks (**Figure 4.5**). Thermograms represent the second heat at a rate of 10 °C min^{-1} and a cooling rate of 20 °C min^{-1}. The triblock had glass transition temperatures (T_g's) of 90 °C for PS and −60 °C for PI blocks. were apparent for all polymers. For the tetrablocks the PS T_g decreased slightly to ~80 °C while the PI T_g was essentially unchanged from the triblock (−60 °C). In addition the tetrablocks contained a T_g due from the PLA block at ~53 °C. The strength of T_g for the PLA block increased with increasing size of the PLA block. The presence of three separate T_g's indicated the blocks were microphase separated.

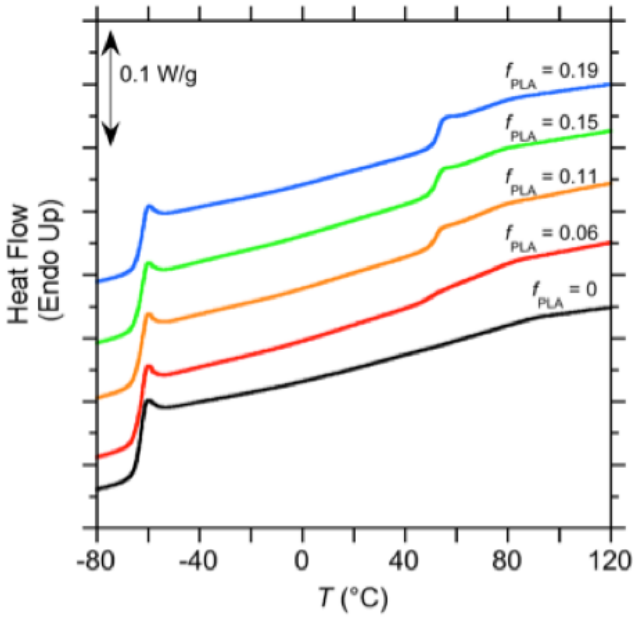

Figure 4.5. Differential Scanning Calorimetry (DSC) of PS-PI-PS-OH triblock and PS-PI-PS-PLA tetrablocks with varying volume fractions of PLA.

4.2.3 Synthesis of PS-PEEP-PS-PLA from PS-PEEP-PS-OH

In addition to PS-PI-PS-PLA tetrablocks, analogous poly(styrene-*b*-ethylene-*co*-ethylene-*alt*-propylene-*b*-styrene-*b*-lactide (PS-PEEP-PS-PLA) tetrablocks terpolymers were prepared with a chemically saturated B block, PEEP (**Table 4.2**). The midblock was prepared by copolymerization of butadiene and isoprene monomers and then hydrogenated. Use of a saturated elastomer phase for the rubbery B midblock can result in materials with longer stability, since the saturated elastomer is much less susceptible to oxidative degradation. Also, it is more resistant to UV and high temperature.[6] The resulting higher stability materials are more attractive for many applications including membranes.[5]

Septon polymers are a commercially available line of midblock-hydrogenated thermoplastic elastomers produced by the Kuraray Company that have been shown to have improved stability compared to analogous unsaturated TPEs.[6] Using the commercially available hydroxylated PS-PEEP-PS precursor supplied by Kuraray, PS-PEEP-PS-PLA tetrablock could easily be prepared by the intiation of lactide polymerization from the hydroxyl chain end.

The ^{1}H NMR spectrum for the PS-PEEP-PS triblock (**Figure 4.6**) contains resonances from aromatic PS and a small amount (<1 %) of remaining unsaturated resonances from the midblock (δ ~4.7 and 5.2 ppm).[7]

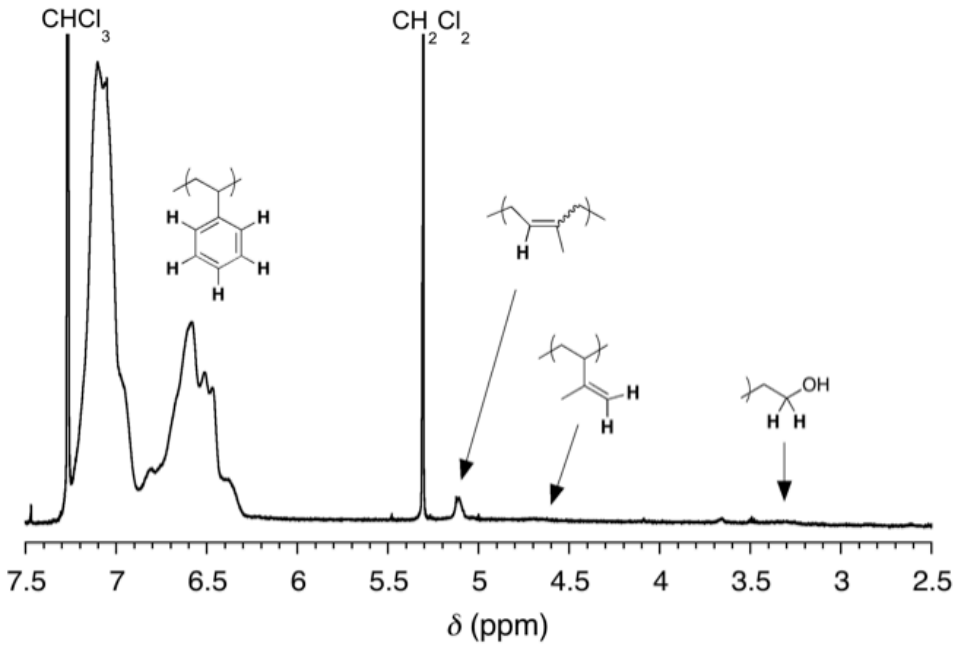

Figure 4.6. ^{1}H NMR spectrum of PS-PEEP-PS-OH triblock in $CDCl_3$.

Polymerizations of d,l-lactide were catalyzed with DBU using conditions reported above for PS-PI-PS-PLA (**Scheme 4.5**).

Scheme 4.5. Synthesis of PS-PEEP-PS-PLA

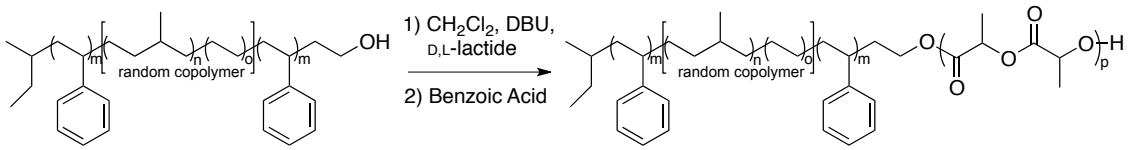

Despite the different triblock initiator, PS-PEEP-PS-PLA tetrablocks were prepared in essentially the same way as PS-PI-PS-PLA tetrablocks. Presence of peaks at δ 5.17 ppm and δ 4.4 ppm in the ^{1}H NMR spectrum of tetrablocks indicated polymerization of lactide. A representative spectrum is described in **Figure 4.7**.

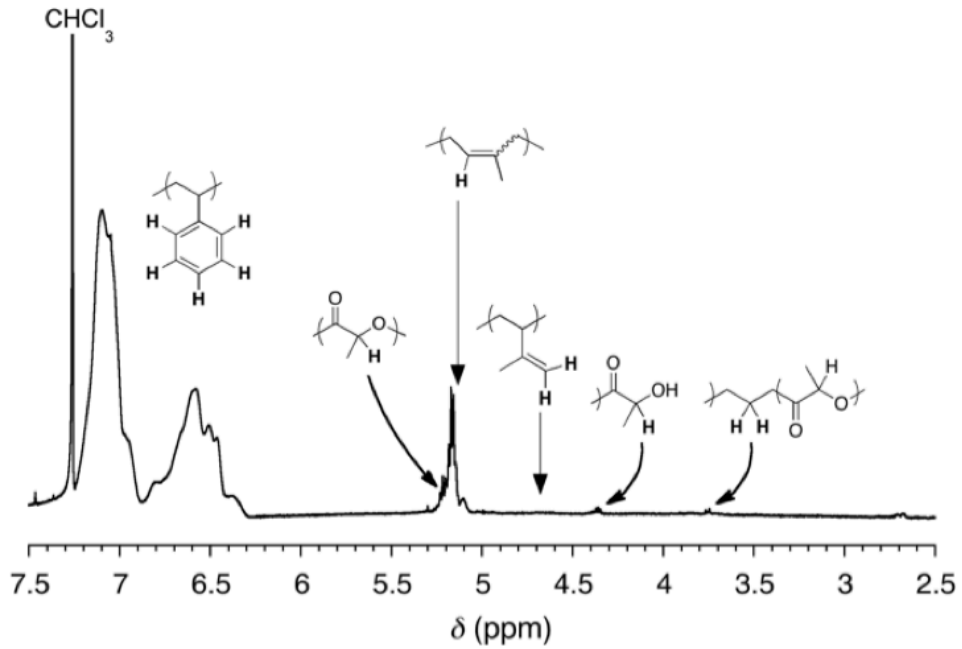

Figure 4.7. ^{1}H NMR spectrum of representative PS-PEEP-PS-PLA triblock (PS-PEEP-PS-PLA with f_{PLA} = 0.05) in $CDCl_3$.

SEC results for all PS-PEEP-PS-PLA tetrablocks are presented in **Figure 4.8**. Results show increasing molecular weight (decreasing elution volume) with increasing amount of lactide used for each polymerization. All tetrablocks had monomodal molecular weight distributions with molecular weight dispersities between 1.09 and 1.15. A summary of the PS-PEEP-PS-PLA tetrablocks is presented in Table 4.2. Six tetrablocks were prepared with f_{PLA} between 0.05 and 0.40 and molecular weights between 67 and 146 kg mol^{-1}.

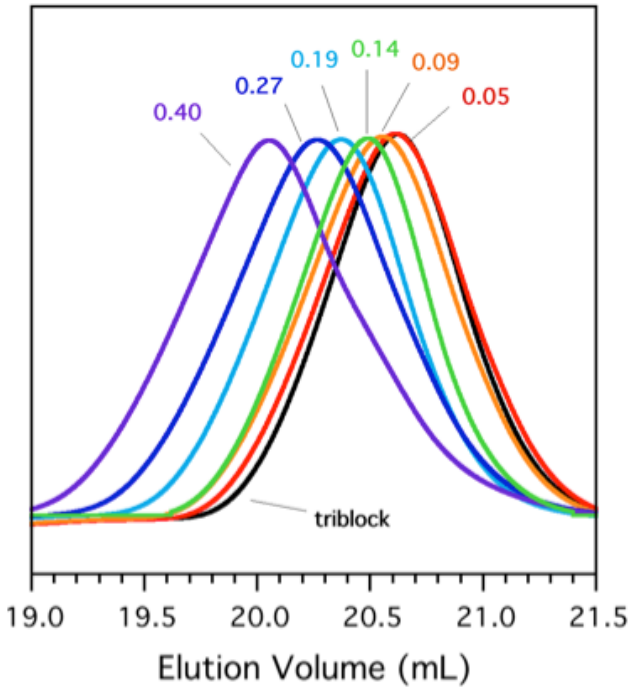

Figure 4.8. Gel Permeation Chromatography (GPC) of PS-PEEP-PS-OH triblock and PS-PEEP-PS-PLA tetrablocks with varying volume fractions of PLA.

Table 4.2. PS-PEEP-PS-PLA Molecular Characterization Data

Sample ID [kg mol^{-1} per block]	f_{PEEP}[a]	f_{PS}[a]	f_{PLA}[a]	M_n[b]	Đ[c]
PS-PEEP-PS-OH [9-47-9]	*0.67*	*0.28*	*0.00*	65.2	*1.07*
PS-PEEP-PS-PLA [9-47-9-5]	0.70	0.25	0.05	67.4	1.09
PS-PEEP-PS-PLA [9-47-9-9]	0.67	0.23	0.10	71.3	1.09
PS-PEEP-PS-PLA [9-47-9-13]	0.64	0.22	0.14	76.2	1.09
PS-PEEP-PS-PLA [9-47-9-20]	0.60	0.21	0.19	84.9	1.09
PS-PEEP-PS-PLA [9-47-9-33]	0.53	0.19	0.28	98.3	1.11
PS-PEEP-PS-PLA [9-47-9-59]	0.41	0.15	0.40	124.5	1.15

[a]Volume fractions are calculated from published densities at 140 °C (ρ_{PEEP} = 0.855[8] g/cm^3 ρ_{PS} = 0.969[21], ρ_{PLA} = 1.154[9]). [b]Determined from ^{1}H NMR end group analysis. [c]Determined from SEC measurements.

DSC data shows that the PEEP midblock contains some crystallinity (**Figure 4.9).** Because the midblock is a random copolymer of polyethylene (PE) and poly(ethylene-alt-propylene) (PE-*alt*-PP), there should be difference run lengths of PE and PP throughout the midblock.[10,11,12] The breadth in the DSC peak between ~ −60 and +20 °C is due to different run lengths of monomers within the copolymer block.

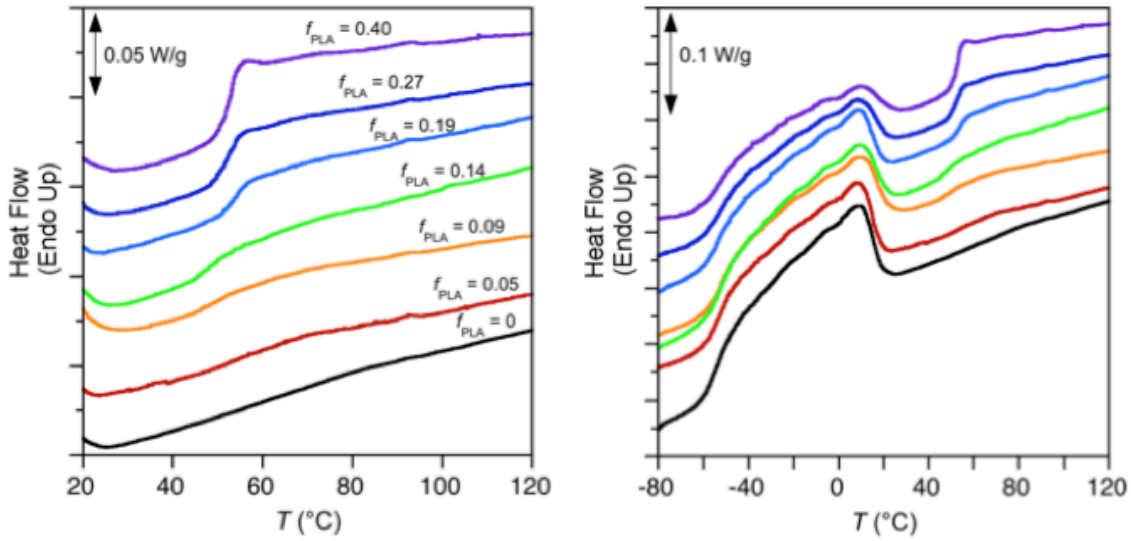

Figure 4.9. DSC Thermograms for PS-PEEP-PS and PS-PEEP-PS-PLA Tetrablocks. Region showing glass transitions for PLA and PS, left. Plot showing all thermal transitions for PS, PLA and PI, right.

4.3 Tensile Testing of PS-PI-PS-PLA and PS-PEEP-PS-PLA

4.3.1 Results

Tensile tests were performed using small rectangular samples of the polymers that were cut from a sample pressed for 10 minutes at 150 °C under 1000 psi. The samples had the approximate dimensions of 0.5 mm (T) × 3 (W) × 4 mm (L). The tensile measurements were performed on a Rheometrics Scientific MiniMat instrument. Samples were extended lengthwise uniaxially at 15.0 mm min^{-1}. A summary of the mechanical properties for PS-PI-PS-PLA and PS-PEEP-PS-PLA tetrablocks and their triblock precursors can be found listed in **Table 4.3** and plotted in **Figure 4.10**. Values listed represent the average results for at least five tensile tests for each polymer.

Table 4.3. Tensile Properties of PS-PI-PS-PLA and PS-PEEP-PS-PLA Tetrablocks.

Polymer (100 × f_{PLA})	f_{PLA}	Young's Modulus E ± sd (MPa)	Ultimate Tensile Strength σ_B ± sd (MPa)	Strain at Break ϵ_B ± sd (%)	Toughness ± sd (10^7 Nm/m^2)
PS-PI-PS (0)	0	16 ± 8	15 ± 2	2090 ± 320	12 ± 3
PS-PI-PS-PLA (6)	0.06	9 ± 6	5 ± 1	1040 ± 400	4 ± 2
PS-PI-PS-PLA (11)	0.11	7 ± 1	16 ± 3	2010 ± 500	11 ± 6
PS-PI-PS-PLA (15)	0.15	5 ± 1	17 ± 6	1010 ± 380	7 ± 6
PS-PI-PS-PLA (19)	0.19	3.0 ± 0.1	17 ± 8	1100 ± 250	4 ± 2
PS-PEEP-PS (0)	0	33 ± 16	29 ± 6	1280 ± 180	13 ± 5
PS-PEEP-PS-PLA (5)	0.05	7 ± 2	30 ± 6	830 ± 80	8 ± 2
PS-PEEP-PS-PLA (9)	0.09	25 ± 5	32 ± 5	900 ± 90	9 ± 3
PS-PEEP-PS-PLA (14)	0.14	16 ± 2	33 ± 5	750 ± 200	11 ± 5
PS-PEEP-PS-PLA (19)	0.19	16 ± 4	25 ± 4	680 ± 230	7 ± 4
PS-PEEP-PS-PLA (27)	0.27	70 ± 19	29 ± 4	790 ± 170	12 ± 4
PS-PEEP-PS-PLA (40)	0.40	219 ± 85	35 ± 10	720 ± 180	16 ± 7

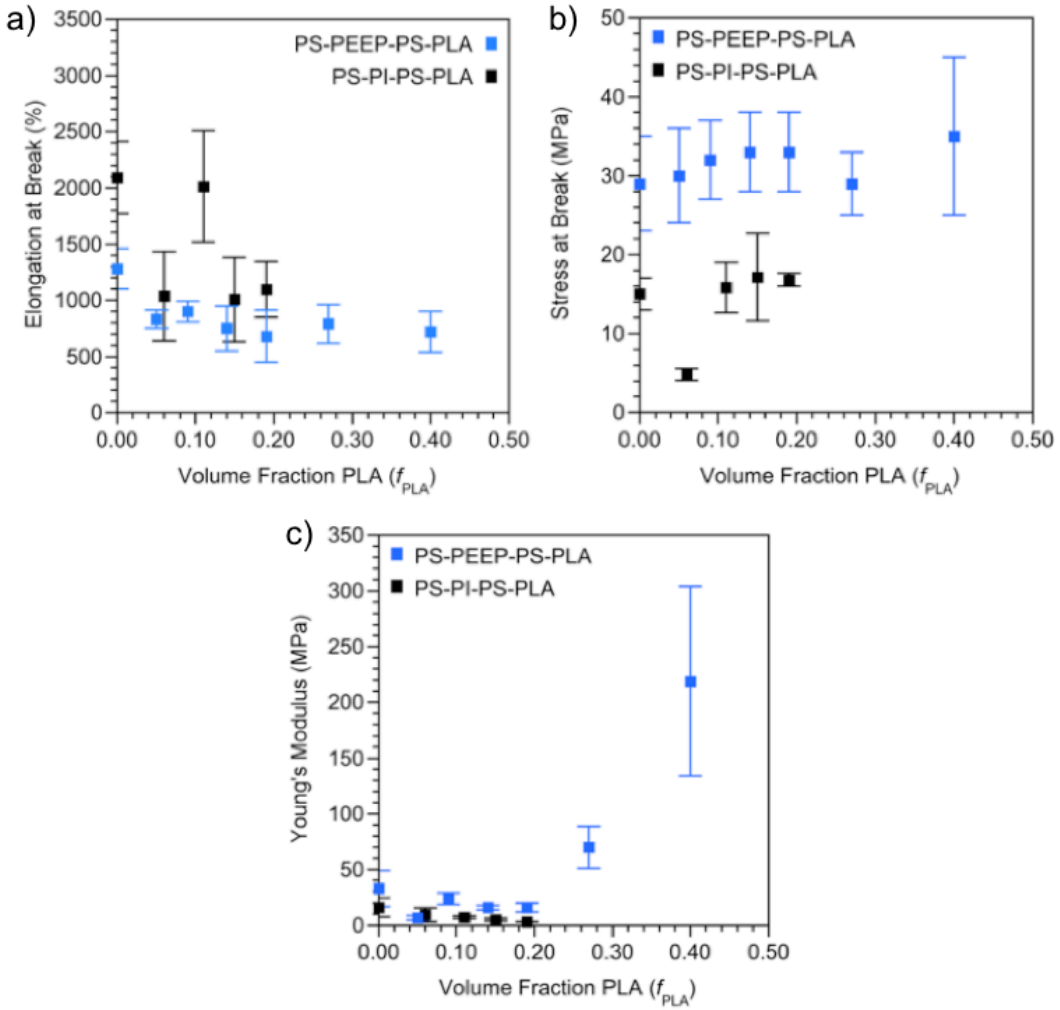

Figure 4.10. Average mechanical property results for PS-PI-PS-PLA and PS-PEEP-PS-PLA tetrablocks: average elongation at break, a); average stress at break, b); average Young's Modulus, c). Error bars represent standard deviations based on at least 5 different experiments.

A comparison between the tensile results of the triblocks can highlight the general differences between the two series. Both the ABA and ABAC polymers have slightly different mechanical properties due to the different B blocks. The PS-PI-PS triblock had tensile behavior typical of an ABA TPE: a high elongation at break (ϵ_B) of ~2000%, a stress at break (σ_B) of 15 MPa and a Young's modulus (E) of

16 MPa.[13] In comparison, PS-PEEP-PS had 1) a stress at break that was twice as high as PS-PI-PS (29 MPa vs 15 MPa); 2) a young's modulus that was twice as high as PS-PI-PS; and 3) a somewhat lower elongation at break than PS-PI-PS (1200% vs. 2000 %). The same general trend was observed in the corresponding tetrablocks for each series.

Representative tensile curves (average values presented in **Table 4.3** and **Figure 4.10**) for PS-PI-PS-PLA tetrablocks and PS-PEEP-PS-PLA tetrablocks are presented in **Figure 4.11**. For both ABAC systems, addition of f_{PLA} between 0.05 and ~0.15-0.19 actually led to a decrease in toughness. For PS-PI-PS-PLA, tetrablocks with f_{PLA} between 0.05 and 0.15 had decreased values for young's modulus, strain at break, ultimate tensile strength and toughness in comparison to those of the PS-PI-PS triblock precursor. At 0.15 and 0.19 f_{PLA}, the ultimate tensile strength improved slightly in comparison to the triblock precursor.

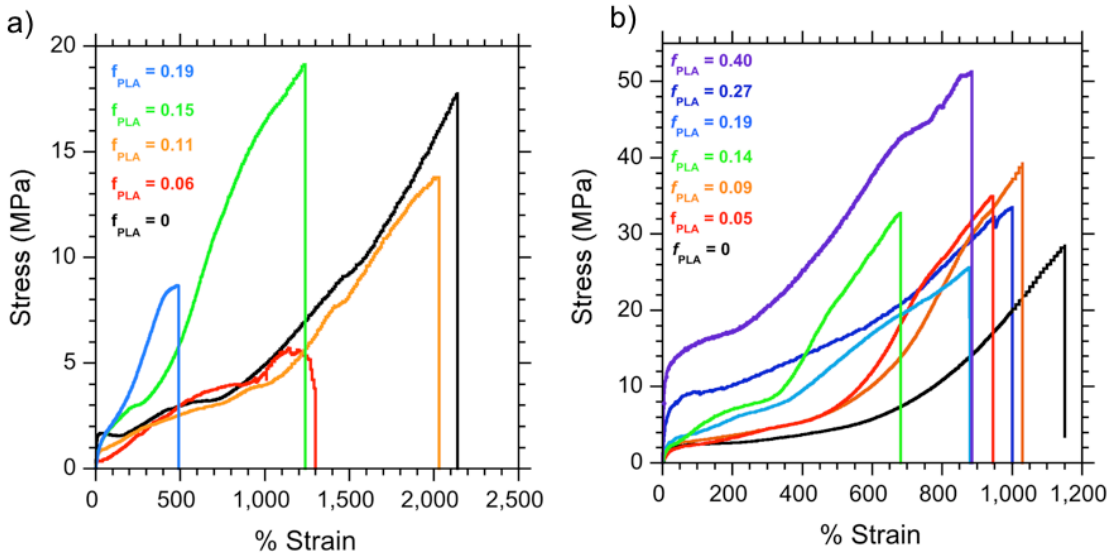

Figure 4.11. Representative tensile behavior for the PS-PI-PS triblock and PS-PI-PS-PLA tetrablocks, a). Representative tensile test results for PS-PEEP-PS triblock and PS-PEEP-PS-PLA tetrablock terpolymers (f_{PLA} between 0 and 0.40), b).

For PS-PEEP-PS-PLA, a f_{PLA} between 0.05 and 0.19 resulted in decreased strain at break, young's modulus and toughness compared to the triblock. However, once f_{PLA} was increased to 0.27, significantly improved properties were observed. The most significant change observed was in the young's modulus. The PS-PEEP-PS-PLA tetrablock with f_{PLA} = 0.27 had a young's modulus over 2 times that of the triblocks precursor (70 MPa vs. 33 MPa). The tetrablock with f_{PLA} = 0.40 had even better performance; the young's modulus was almost 7 times that of the triblock (219 MPa vs. 33 MPa) and the ultimate tensile strength was higher than the triblock precursor (35 MPa vs. 29 MPa for triblock).

4.3.2 Conclusions on Tetrablock Mechanical Properties

In summary, despite our expectation that a small PLA block could lead to improved mechanical properties in common TPEs, mechanical properties of tetrablocks of each series actually became worse with addition of small amounts of PLA. The mechanical properties improved only when the f_{PLA} was equal to 0.20 or higher. In terms of the rubbery content, properties improved only when the $f_{midblock}$ (f_{PI} or f_{PEEP}) was ~0.55 or below and the volume fraction of glassy blocks (PS and PLA) combined was ~0.45 or above.

Block polymer tensile properties can depend on factors such as morphology, composition, molecular weight, block chain architecture and interaction parameters between domains.[14,15] Morphology can have a significant influence on mechanical

properties.[19] In the next section, we present some of the morphological behavior of PS-PI-PS-PLA tetrablocks in an effort to address the different mechanical properties observed for an ABA triblock (PS-PI-PS) and corresponding ABAC (PS-PI-PS-PLA) tetrablock terpolymers.

4.4 Morphology

4.4.1 Introduction

The following section presents phase behavior of the PS-PI-PS-PLA tetrablocks with PLA content ranging from 0 to 19% by volume. Small angle X-ray scattering (SAXS) and transmission electron microscopy (TEM) were used to elucidate morphology and domain spacing (d*). Dynamic mechanical spectroscopy was used to determine order-disorder transition temperatures (T_{ODT}'s). Some of this work was done in collaboration with Dr. David Olson.

To help determine the triblock and tetrablock ordered morphologies, polymers were aligned using a channel-die alignment procedure (see **Chapter 2** for more details). The channel-die setup and corresponding coordinate axes are presented in **Figure 4.12** for reference. An example channel-die aligned matchstick of polymer is also presented with coordinate axes (**Figure 4.12**).

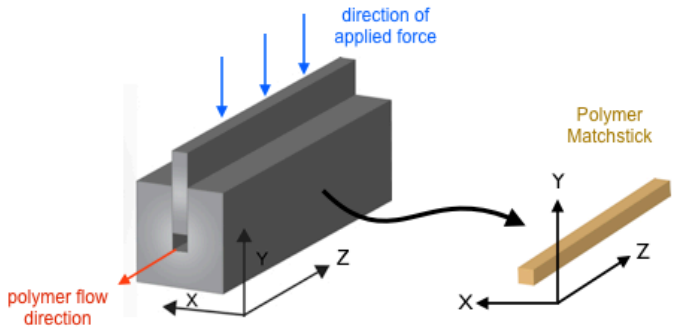

Figure 4.12. Channel-die alignment setup and resulting polymer matchstick with coordinate axes shown.

A summary of observed morphological data for PS-PI-PS and PS-PI-PS-PLA tetrablocks is summarized in **Table 4.4**. While the PS-PI-PS-OH triblock exhibited a hexagonally packed cylinder (HEX) morphology, addition of varying amounts of PLA led to the following morphologies: PLA spheres in PS cylinders with f_{PLA} = 0.06; and core(PLA)-shell(PS) cylinders (CSC) for tetrablocks with f_{PLA} = 0.15 and 0.19.

Table 4.4. Morphology Data for PS-PI-PS-PLA Tetrablock Terpolymers

Sample ID	f_{PLA}	M_n	Phase	d^*, nm[a]	T_{ODT}[b]
PS-PI-PS-OH [11-46-12]	*0.00*	*69.5*	HEX	25	250
PS-PI-PS-PLA [11-46-12-3]	0.06	75.6	Cyl with Spheres	31	>250
PS-PI-PS-PLA [11-46-12-6]	0.11	81.7	unknown	unknown	>250
PS-PI-PS-PLA [11-46-12-11]	0.15	85.7	CSC	41	>250
PS-PI-PS-PLA [11-46-12-20]	0.19	91.2	CSC	43	>250

[a]Determined from SAXS results. [b]Determined from DMS temperature ramps.

4.4.2 Hexagonally Packed Cylinders (HEX) (f_{PLA} = 0)

The PS-PI-PS triblock was assigned the HEX phase based on a combination of SAXS and TEM data. **Figure 4.13** shows one-dimensional (1D) and two-dimensional (2D) SAXS data for a channel die aligned PS-PI-PS matchstick (**Figure 4.13a**). The sample was aligned at 150 ºC for one hour (**Figure 4.12** shows channel die setup with directional axes). Two-point scattering data (180º apart) in **Figure 4.13a** is evident along the direction of flow. This is indicative of scattering from the long axis of cylindrical or lamellar domains (from the YZ or XZ planes). Scattering from the XY plane, **Figure 4.13a**, is consistent with an isotropic arrangement of domains. Scattering in the 1D-integrated SAXS plot, **Figure 4.13c**, is consistent with hexagonal symmetry with a principal domain spacing (d*) of 25 nm. Together with the 2D scattering data, the hexagonal cylinder morphology can be assigned to the PS-PI-PS triblock. The reason for lack of hexagonal scattering in the 2D XY image can be attributed to imperfect alignment across the XY plane.

The TEM image in **Figure 4.13c** supports the cylinder assignment. The light regions correspond to unstained PS domains while the dark regions are due to OsO_4 stained PI. This sample was dropcast (0.5 wt%) onto a formvar TEM grid from toluene.

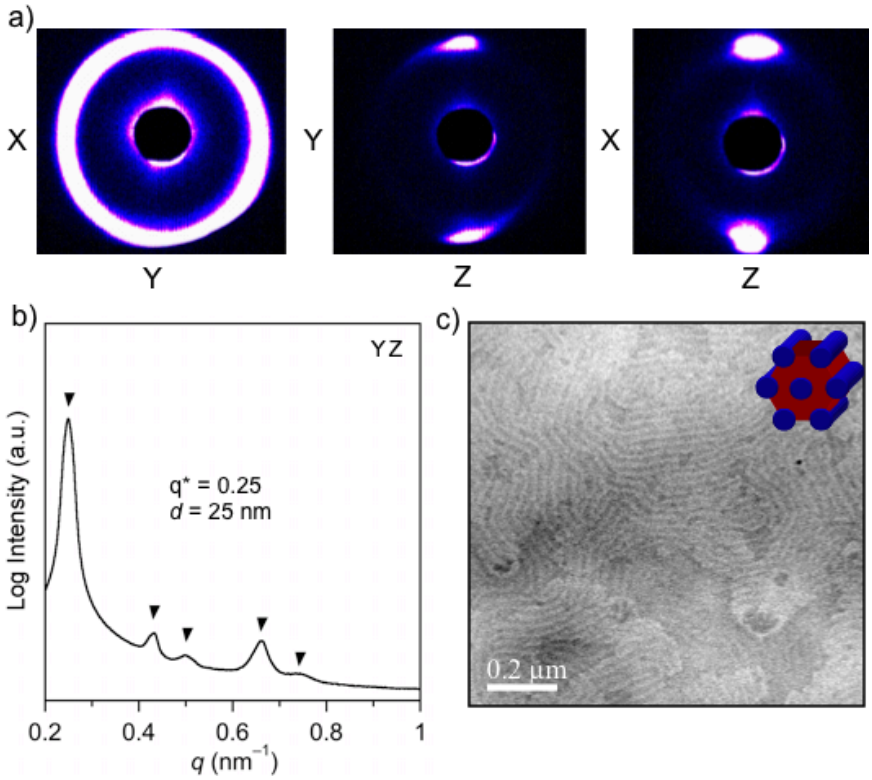

Figure 4.13. 2D SAXS of PS-PI-PS triblock taken in the XY, YZ and XZ plane of channel die aligned sample, (a); representative 1D integrated SAXS data for channel die aligned PS-PI-PS sample (YZ plane scattering is shown, other 1D integrated data show same pattern), (b). Triangles mark q/q* reflections of √1, √3, √4, √7 and √9. Sample was annealed at 80 °C for 2 minutes prior to scan. TEM of PS-PI-PS [11-46-12] drop cast onto Formvar coated TEM grid from a 0.5 wt% toluene solution, (c). Tetrablock film in (c) was stained with OsO_4. SAXS data prepared by Dr. David Olson.

4.4.3 PS-PI-PS-PLA Tetrablocks After Pressing

Like the samples prepared for tensile tests, tetrablocks were pressed for 10 minutes at 150 °C under 1000 psi. **Figure 4.14** shows SAXS of tetrablocks after pressing. The domain spacing increased with increasing volume fraction of PLA. All polymers had very broad scattering curves with no discernible second order peaks.

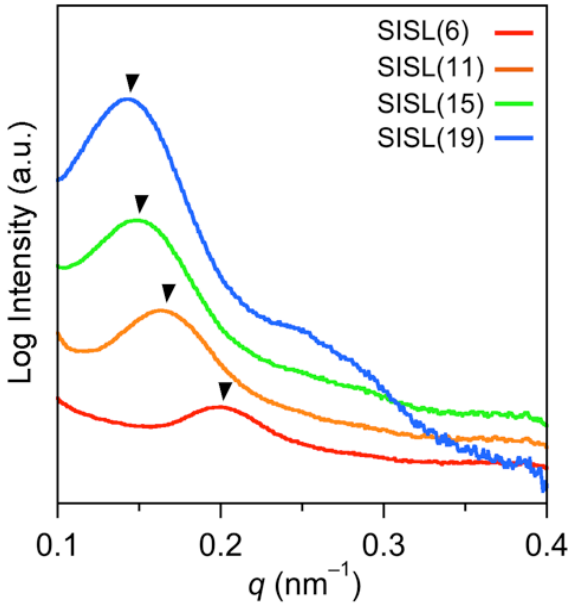

Figure 4.14. Bulk SAXS of PS-PI-PS-PLA tetrablocks after pressing.

4.4.4 Core-Shell Cylinders (CSC) (f_{PLA} = 0.15−0.19)

A core(PLA)-shell(PS) cylinder morphology (CSC) was observed for PS-PI-PS-PLA tetrablock terpolymers with f_{PLA} = 0.15. One-dimensional integrated SAXS (**Figure 4.15a**) does not provide much clarity for determination of the morphology due to the broad scattering results. The channel-die aligned sample had a domain spacing of 41 nm. **Figure 4.15** shows 2D scattering results for the channel-die aligned tetrablock. 2D Scattering patterns in the XZ and YZ planes are consistent with cylindrical domains aligned along the Z-axis. Isotropic scattering in the XY planes is consistent with isotropic arrangement of ordered grains across the XY plane.

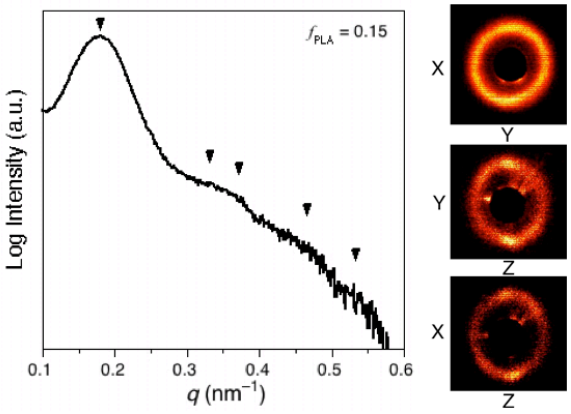

Figure 4.15. SAXS of channel die aligned PS-PI-PS-PLA(f_{PLA} = 0.15). Left, 1D integrated SAXS trace (d* = 41 nm); Right, 2D SAXS patterns from three planes of aligned sample. Triangles mark theoretical q/q* reflections for hexagonal symmetry: √1, √3, √4, √7, √9.

TEM images in **Figure 4.16** are consistent with an ordered core-shell cylinder (CSC) morphology for the tetrablock with f_{PLA} = 0.15. Sections stained with OsO_4 contain hexagonal white domains within a dark stained PI matrix

(**Figure 4.16a**). The measured diameter of these features is ~27 nm. This size is close to the estimated size (29 nm) based on domain spacing from SAXS (41 nm) and the volume fraction of PS (0.26) and PLA (0.15). Short range ordering of domains across the XY plane in the TEM images is consistent with the isotropic 2D SAXS results (**Figure 4.15**). **Figure 4.16b-c** contains images of PS-PI-PS-PLA with f_{PLA} = 0.15 after staining with ruthenium tetroxide (RuO_4). The white features are due to unstained PLA domains. **Figure 4.16c** shows the long axis of white unstained PLA cylinders that extend along the Z axis.

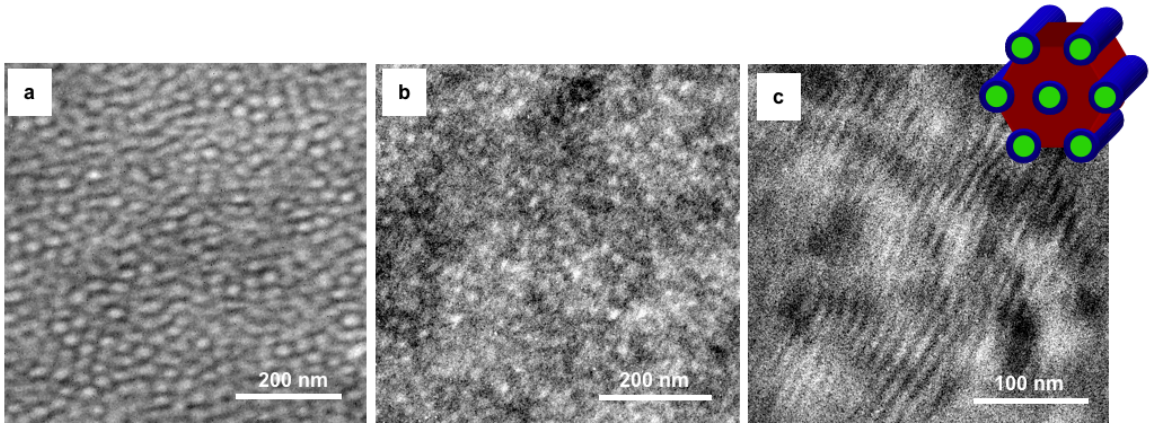

Figure 4.16. Transmission electron micrographs of XY face of channel die aligned PS-PI-PS-PLA (f_{PLA} = 0.15). The sample was cryomicrotomed at -100 °C. XY face of PS-PI-PS-PLA(15), (a). XY face of PS-PI-PS-PLA(f_{PLA} = 0.15), (b), and YZ face of PS-PI-PS-PLA(f_{PLA} = 0.19), (c). Section shown in image (a) was stained with a 4 wt% solution of OsO_4 for 10 minutes prior to TEM. Images (b) and (c) are of sections stained with a 0.5 wt % solution of RuO_4 for 20 minutes before imaging.

Channel-die aligned samples of the tetrablock with f_{PLA} = 0.15 were exposed to basic solutions to chemically etch the PLA domains. The following etching methods gave varying results: method 1) 1 week in a 0.5 Molar sodium hydroxide (0.5 M NaOH) 60/40 v/v Water/Methanol solution at 25 °C; method 2) 1 week,

25 ºC, in a 0.5 M NaOH 60/40 v/v Water/Methanol solution with 0.1 wt% sodium dodecyl sulfate (SDS); and method 3) 1 week, 50 ºC, 0.5 M NaOH 60/40 v/v Water/Methanol solution with 0.1 wt% SDS. Based on mass loss, SEM and GPC results, the most effective method was method 2: 1 week at 25 ºC with 0.1 wt% SDS surfactant. SEM images from the resulting monoliths are shown in **Figure 4.17**.

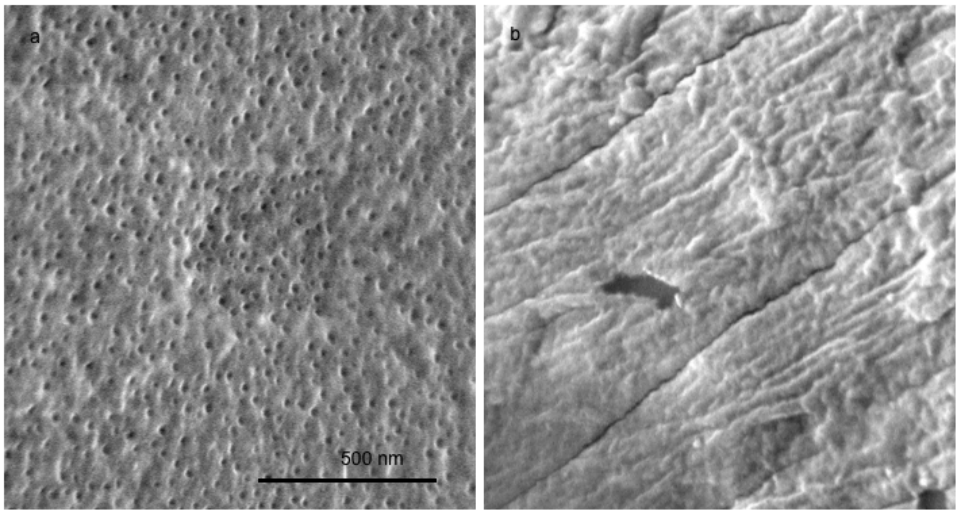

Figure 4.17. SEM image of channel die aligned PS-PI-PS-PLA(f_{PLA} = 0.15) after base etching. XY face after base etching, (a); YZ face after base etching, (b). Cylinder pore diameter measure from SEM equaled 22 nm.

Pores consistent with cylinder "ends" were visible on the XY face. Average pore diameter was 20 nm. Long, high-aspect ratio domains consistent with etched cylindrical domains were visible from the YZ face. However, the sample did not have pores visible across the entire surface. This suggests that some PLA domains were inaccessible to the etching solution. GPC results show that not much PLA was method from any etching method (**Figure 4.18**). Etching resulted in 20% mass loss (bulk tetrablock w_{PLA} = 0.14) however the error is expected to be high in the

mass measurement because the sample mass was only a few milligrams. Using a higher temperature for etching should increase the reaction rate and lead to higher PLA degradation, however this was not the case for samples etched at 50 °C.

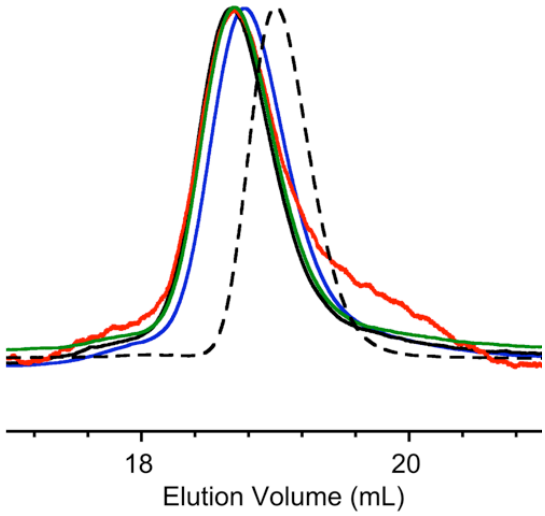

Figure 4.18. SEC traces for polymers PS-PI-PS-PLA(15), **black**, and PS-PI-PS triblock, dashed **black**. Traces for base etched PS-PI-PS-PLA(0.15) are shown for method 1 (green), method 2 (red), and method 3 (blue).

A similar SAXS and TEM data were also observed for PS-PI-PS-PLA tetrablock terpolymers with f_{PLA} = 0.19. We suspect this polymer also adopts a poorly aligned core(PLA)-shell(PS) cylinder morphology. **Figure 4.19** contains TEM and SAXS data for the channel die aligned tetrablock. For this tetrablock, the domain spacing was 43 nm. The TEM image of the XY face contains hexagonally packed white features like **Figure 4.16a**. The expected diameter of the core(PLA)-shell(PS) cylinders is 30 nm. This was estimated from the domain spacing (43 nm from SAXS) and the sum of the volume fractions of PS (0.25) and PLA (0.19). The

diameter of the white circular features in the TEM image are ~30-31 nm in diameter. The 2D saxs data in XZ and YZ planes (**Figure 4.19c**) is also consistent a structure such as cylinders aligned along the Z axis. The broad scattering in the 1D integrated SAXS pattern is similar to the 1D for PS-PI-PS-PLA(0.15) and the amount of order visible in the TEM image.

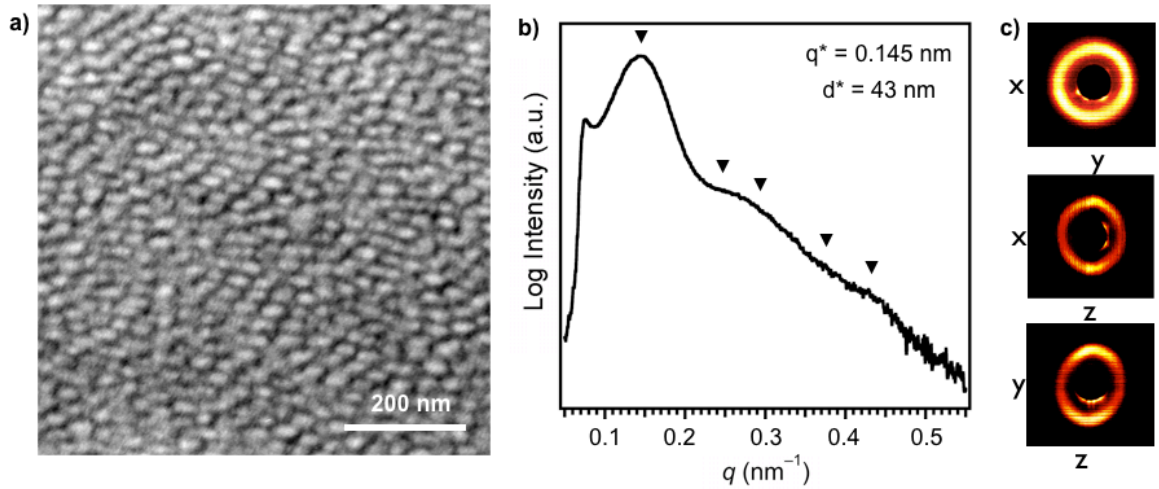

Figure 4.19. Morphology data for channel-die aligned PS-PI-PS-PLA(0.19): TEM of XY face, a). Sections for TEM stained with OsO_4. 1D integrated SAXS data for aligned sample, b). 2D SAXS images, c).

4.4.5 PLA Spheres in PS Cylinders (f_{PLA} = 0.06)

The morphology of the PS-PI-PS-PLA with f_{PLA} = 0.06 was investigated by Dr. David Olson. The tetrablock was aligned using both channel die and reciprocating shear. SAXS and TEM of a channel die aligned sample show evidence of a microphase-separated structure with little alignment (**Figure 4.20a-c**). 1D data is again consistent with a poorly ordered hexagonal structure (**Figure 4.20a**) having a domain spacing of 31 nm with isotropic scattering in the 2D image consistent with a poorly aligned structure. The TEM image (**Figure 4.20c**) contains

circular white features (PS and PLA) within a black, PI, matrix. The white domains appear hexagonally packed in some small regions and have a diameter of ~18 nm. The estimated diameter of a cylinder containing both PS and PLA is 19 nm (estimated from d* =31 nm and total volume fraction = 0.34). However, a clear image of the morphology was not discernible after the channel-die alignment method.

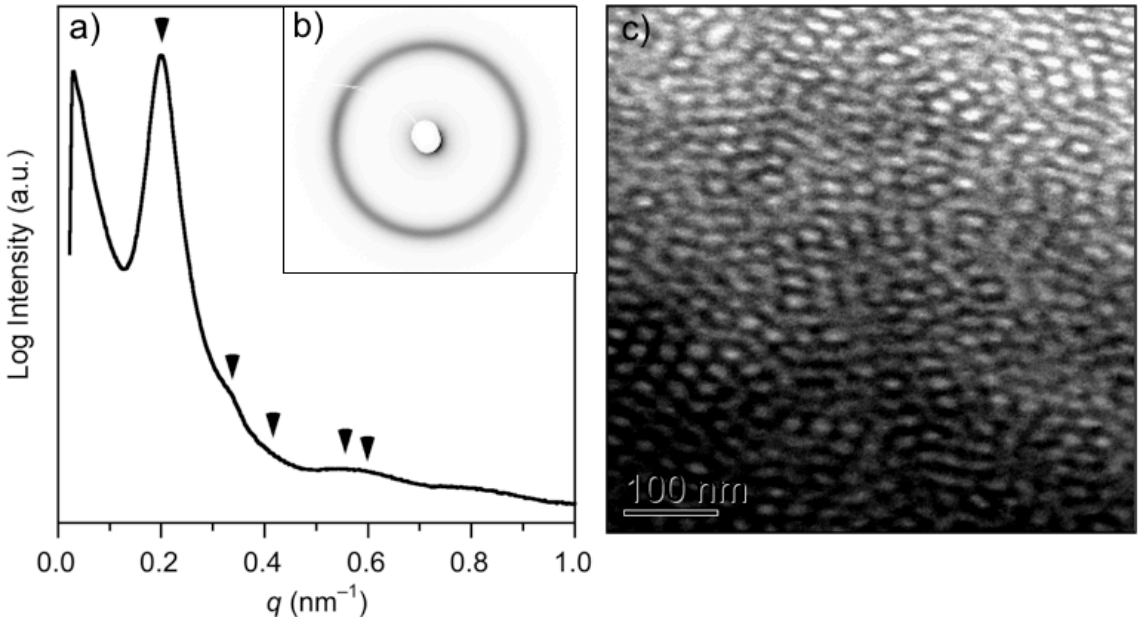

Figure 4.20. Integrated 1D SAXS of PS-PI-PS-PLA(f_{PLA} = 0.06) after channel die alignment (q* = 0.20; d = 31.4 nm), (a), where triangles mark theoretical first few q/q* reflections for hexagonal symmetry (1, √3, √4, √7 and √9). 2D raw image showing isotropic scattering in XY plane, (b). TEM image of XY face after channel die alignment, (c). Both SAXS and TEM experiments were performed by Dr. David Olson.

Improved alignment was achieved with reciprocating shear alignment (**Figure 4.21a**). 2D SAXS reflections in **Figure 4.21b** are 90º apart in the XY plane and 91º in the YZ plane-consistent with a BCC-like packing. However, the packing

in the XZ plane is more consistent with hexagonal symmetry. The reflections in the integrated 1D SAXS profile (**Figure 4.21c**) for the XZ plane are consistent with root √2q* and root √3q* which can be indicative of spherical structure. Due to the hexagonal 2D scattering in the XY plane, the first three reflections for hexagonal symmetry (1, √3, √4, and √7) are also marked for comparison in the 1D plot (**Figure 4.21c**). To further clarify this morphology, TEM analysis was also pursued.

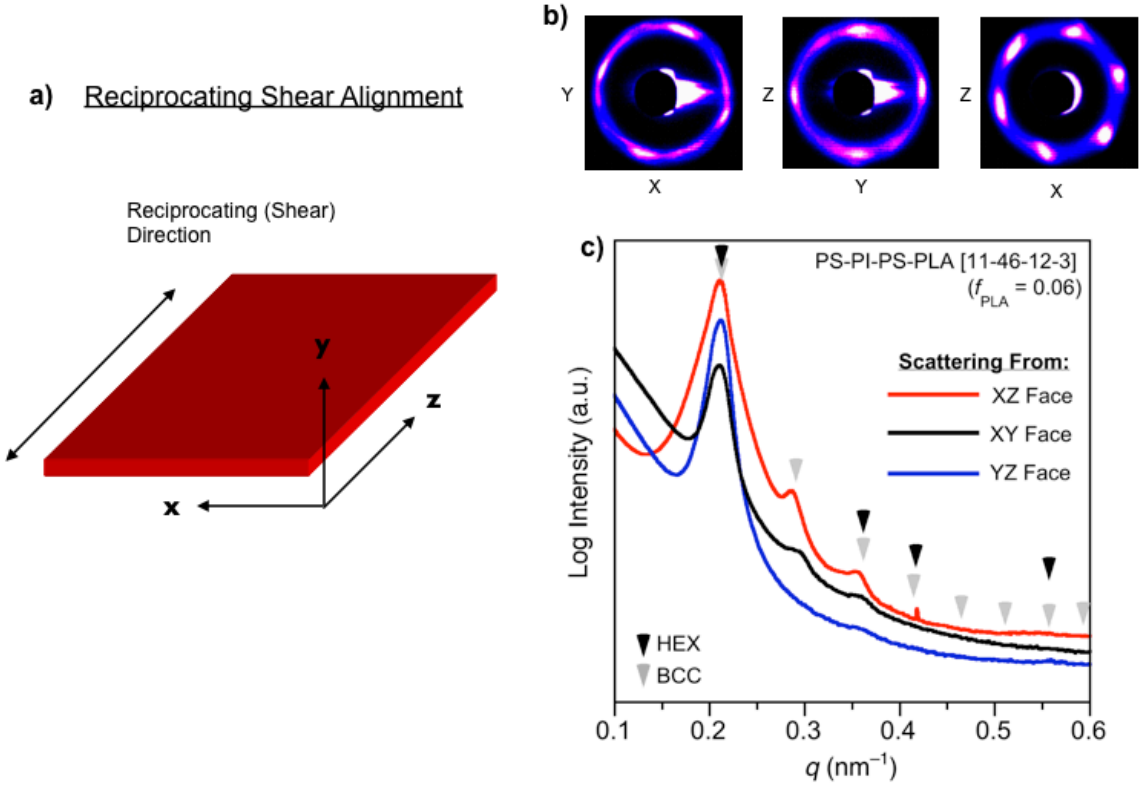

Figure 4.21. Reciprocating shear alignment diagram with coordinate axes shown, (a). 2D images of scattering from each plane of PS-PI-PS-PLA(f_{PLA} = 0.06) aligned by reciprocating shear, (b); Integrated 1D SAXS after reciprocating shear alignment from each of the three planes, (c). Black triangles mark theoretical first few q/q* reflections for hexagonal symmetry (1, √3, √4, and √7). Grey Triangles mark theoretical reflections for BCC ((1, √2, √3, √4, √5, √6, √7 and √8) Domain spacings were 31.6, 31.6 and 32.6 nm respectively for the XY, YZ and XZ faces. Reciprocating shear experiments done by Dr. David Olson.

TEM images of the PS-PI-PS-PLA with f_{PLA} = 0.06 sample after shear alignment (**Figure 4.22**) show a structure with light domains that resemble spheres within cylinders. **Figures 4.22a-b** show TEM images of the long axis of cylindrical domains. The spherical PLA domains appear discrete within the cylinders in **Figure 4.22b** and cause the PS cylinders to undulate in diameter. The formation of small PLA domains makes sense based on the volume fraction of PLA (f_{PLA} = 0.06). However, it is not completely clear whether the PLA domains are discrete spheres or connected within the PS cylinders.

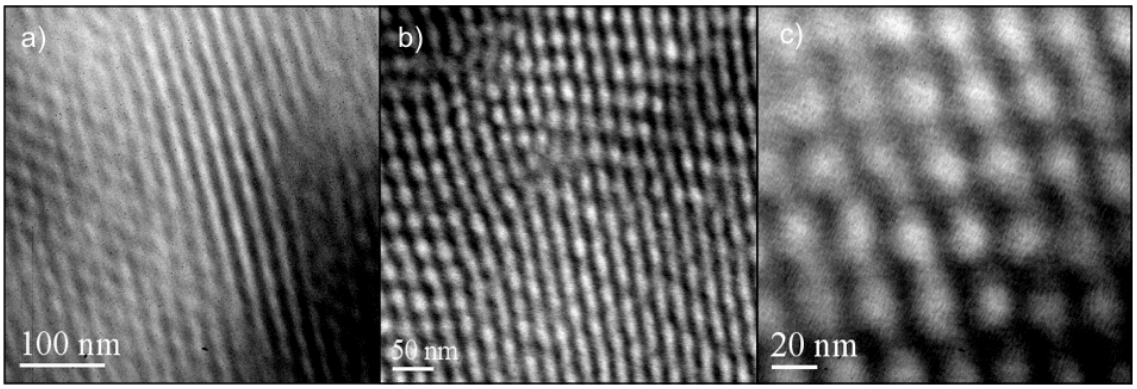

Figure 4.22. TEM images of PS-PI-PS-PLA(f_{PLA} = 0.06) after shear alignment. Samples were microtomed at -120 ºC and stained with OsO_4 prior to imaging. Images are taken from sections cut from the XY face, (a), YZ face, (b), and XZ face, (c). TEM images taken by Dr. David Olson.

A drawing of a tentative sphere in cylinder morphology is shown in **Figure 4.23**. These drawings are based on the structures observed in TEM images and spacings and symmetry from SAXS data. Two different structures show the packing of spheres in different planes. This packing is based on the apparent morphology

from the TEM image. The TEM image in **Figure 4.22b** shows both types of sphere packing within the cylindrical domains.

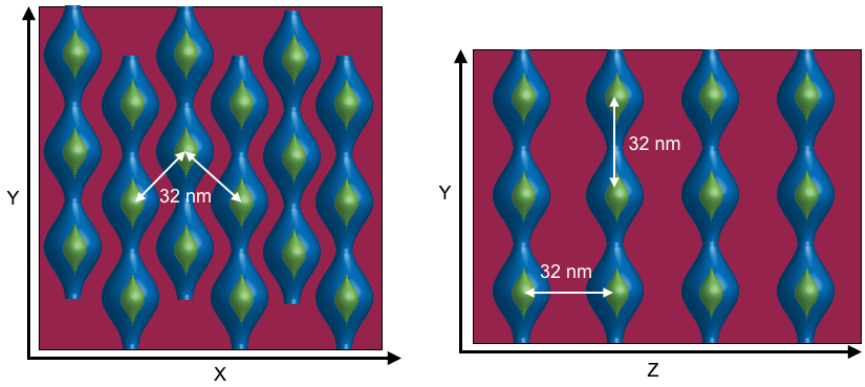

Figure 4.23. Proposed morphology for PS-PI-PS-PLA(f_{PLA} = 0.06). Morphology contains of small PLA "beads" [green] within PS cylinders [blue] in a PI matrix [red]. Left image shows packing of beads in XY plane. Right image shows PLA bead packing in YZ plane. Spacings marked on the cartoons are based on domain spacings from 2D SAXS of the shear-aligned sample.

Undulating cylindrical structures have been studied for AB copolymer systems. They have been reported near order-order transitions and order-disorder transitions for diblock copolymers.[16,17] A similar ABC morphology was observed by Breiner et al. for a linear ABC terpolymer.[18] A poly(styrene-*b*-butadiene-*b*-methyl methacrylate) (PS-PB-PMMA) triblock terpolymer adopted an undulating core(PMMA)-shell(PB) cylinder morphology at f_{PS} = 0.64, f_{PB} = 0.21 and f_{PMMA} = 0.15. The undulations were reportedly due to the high incompatibility between the interface of the adjacent core(PMMA) and shell(PB) domains. A key difference between this triblock and the tetrablock is that the blocks with the highest incompatibility are not directly linked in the tetrablock.

4.5 Discussion on PS-PI-PS-PLA Tetrablock Morphologies

The tensile results indicate the addition of PLA to PS-PI-PS led to decreased elongation at break, decreased young's modulus and decreased overall toughness for all PS-PI-PS-PLA tetrablocks. Since there are many variables involved (molecular weight, architecture, composition) one cannot unambiguously attribute the mechanical behavior of these polymers strictly to the morphologies they adopt.[19] However, a comparison of the mechanical properties and morphologies can still highlight some major differences that may affect the mechanical behavior.

Generally, addition of PLA led polymer with microstructures that were more difficult to align than the triblock precursor. The increased molecular weight and incompatibility between blocks led poorly ordered structures even after channel-die alignment. The pressed, un-aligned samples had no discernible second order scattering peaks. Since the tensile tests were performed on un-aligned samples, the results represent tensile behavior of samples with isotropic arrangement of microphase-separated domains.

First, we draw a comparison between the CSC PS-PI-PS-PLA tetrablock with f_{PLA} = 0.15 and the PS-PI-PS triblock precursor. PS-PI-PS-PLA samples with f_{PLA} of 0.15 had higher stress at break but lower elongation at break (ϵ_B) than the PS-PI-PS triblock. While both polymers exhibit hexagonally packed cylinder morphologies, the tetrablock contains core(PLA)-shell(PS) cylinders while the triblock contains just PS cylinders. Since the mechanical properties are related to the cross-linking of the PS domains in both polymers, the state of PS chains are

important to the mechanical behavior. While the triblock had PS cylinders that were 14 nm in diameter, the cylindrical shells of PS in the CSC tetrablock were 29 nm in diameter. The actual width of the PS shell from outer to inner edge was only 6 nm in the tetrablock. The addition of PLA actually led to a decrease in PS domain width. With a smaller size PS width (6 nm), the free PS chain ends (not attached to PLA) are confined into a smaller space than the free PS chain ends in the triblock. This structural change to PS domain is a substantial difference between the two polymers. The depressed PS T_g (~80 °C) attributed to a confined PS layer[20] in the tetrablock terpolymer may have influence on the mechanical behavior. It is suspected that the relatively poor performance of the tetrablock terpolymer could be a consequence of the PS confinement.

Increasing the f_{PLA} to 0.19 led to a core-shell cylinder structure and a further decrease in the Young's modulus and the toughness. With a f_{PLA} of 0.19, the Young's modulus (3 MPa) and toughness (4 MPa) were about half those observed for the tetrablock with f_{PLA} = 0.15. The stress at break was similar at 17 MPa. This high ultimate tensile strength for both CSC samples suggests that continuity in the PLA domains increased the ultimate tensile strength. Both CSC tetrablocks had higher ultimate tensile stength (17 MPa) than the triblock (15 MPa).

The addition of a small amount of PLA in PS-PI-PS-PLA(f_{PLA} = 0.06) produced the lowest toughness (4 Nm/m^2) and stress at break (5 MPa). The lower toughness of these materials, compared to the triblock and other tetrablocks, may be due to the short PLA chains. The small amount of PLA causes the PS domains

to either pinch or bulge. Pinched regions are likely points of higher stress and could be a reason why this sample fails at lower stress and strain compare to all of the other PS-PI-PS-PLA samples.

Investigation of additional model multiblock terpolymers is required to unambiguously determine the origin of the dramatically different mechanical performance in these tetrablock terpolymers.

4.6 Conclusions

PS-PI-PS-PLA and PS-PEEP-PS-PLA Tetrablock terpolymers were synthesized from asymmetric triblock precursors with 70 to 30 volumetric ratio of rubbery midblock to PS end blocks. Tensile properties were investigated and found to depend on the volume fraction of PLA. Generally PS-PEEP-PS-PLA tetrablocks had higher stress at break and lower elongation at break than the analogous PS-PI-PS-PLA tetrablocks due to the PEEP midblock. In both systems, tetrablocks with higher PLA composition (>15% PLA) had tensile behavior consistent with continuous microphase-separated glassy domains. When the f_{PLA} was between 0.15 and 0.19, PS-PI-PS-PLA tetrablocks formed a core(PLA)-shell(PS) cylinder morphology. The continuous cylindrical domains led to increased ultimate tensile strength but decreased elongation at break and young's modulus compared to the PS-PI-PS triblock. PS-PEEP-PS-PLA samples with $f_{PLA} > 0.27$ had much tougher mechanical properties than all other tetrablocks. The improved properties could be due to a more continuous PLA phase at higher $f_{PLA.}$

4.7 Experimental Details

Materials. Styrene (99%, 10-15 ppm 4-*tert*-butylcatechol inhibitor, Aldrich) was purified by one distillation from calcium hydride (90-95%, Aldrich) and a successive distillation from butylmagnesium chloride (~3mL/50g styrene, 2.0 M solution in diethyl ether, Aldrich) under a static vacuum of 10-20 mTorr. Isoprene (99%, 100 ppm *p-tert*-butylcatechol inhibitor, Aldrich) was purified by two successive vacuum distillations from *n*-butyllithium (~3 mL/50 g isoprene, 2.5 M solution in hexanes, Aldrich). Ethylene oxide (99.5+%, compressed gas, Aldrich) was distilled once from butylmagnesium chloride (1 mL/10 mL ethylene oxide). Cyclohexane was purified by passage through activated alumina and a supported copper redox catalyst under high-purity argon in home-built columns. *Sec*-Butyllithium (1.3 M solution in cyclohexane, Aldrich) was used as received. The 50/50 (v:v) methanol/isopropanol solution used for reaction termination was degassed with nitrogen prior to use. d,l-Lactide was recrystallized from ethyl acetate and stored under nitrogen in a glovebox before use. The hydroxylated SEEPS precursor used was received from Kuraray Polymers. Butylated hydroxytoluene (BHT) was removed from SEEPS before lactide polymerization by dissolution in THF followed by precipitation into methanol. All other chemicals were used as received without purification.

Size Exclusion Chromatography (SEC) PS-PI-PS, PS-PI-PS-PLA, PS-PEEP-PS and PS-PEEP-PS-PLA samples were prepared at concentrations between 1-5 mg/mL in chloroform ($CHCl_3$). SEC was performed at 35 °C using three Plgel 5µm Mixed-C columns in series with an available molecular weight range of 400–400 000 g mol–1. The columns are contained in a Hewlett-Packard (Agilent Technologies) 1100 series liquid chromatograph equipped with a Hewlett-Packard 1047A refractive index detector. Molecular weight and Đ values are reported with

respect to polystyrene standards obtained from Polymer Laboratories. SEC with CHCl3 was used to characterize the dispersity (Đ) and molecular weight evolution for the PS aliquot, PS-PI-PS-OH triblock, PS-PI-PS-PLA tetrablocks and PLA etched PS-PI-PS-PLA monoliths.

^{1}H NMR Spectroscopy experiments were performed at room temperature on a Varian Inova 500 instrument operating at 500 MHz. Solutions of polymer were prepared in deuterated chloroform ($CDCl_3$) at a concentration of approximately 20 mg mL^{-1}. All spectra were obtained at 25 °C after 32 transients using a relaxation delay of 5 s with chemical shifts reported as δ (ppm) relative to the ^{1}H signals of $CHCl_3$ at 7.27 ppm.

Channel Die Alignment was used to aid morphological alignment. In a typical alignment, a polymer sample is first molded into flat pieces by pressing a polymer in a mold above the polymers melting temperature for 5 minutes at 1000 psi. The pressed pieces are removed from the mold and placed in the center of the channel die. A thin metal plate is placed partially inside the channel. The entire setup is placed inside a hot press and allowed to warm to press temperature. The temperature of the press is set above the glass transition temperatures of the individual blocks of the block copolymer but below the order-disorder temperature so that when the polymer is aligned it flows into an ordered state rather than disordered state.

Once hot, the press plates are gradually closed together pressing the thin metal plate inside the channel down on the polymer at approximated a few millimeters every 5-10 minutes. Eventually, once a thin 1.5 mm high stick of polymer has been pressed the setup is cooled, removed from the press and annealed in a vacuum oven for 48 hours.

Small-Angle X-ray Scattering (SAXS) experiments were performed at the Sector 5-ID-D beamline of the Advanced Photon Source (APS) at Argonne National

Laboratories, maintained by the Dow-Northwestern-Dupont Collaborative Access Team (DNDCAT). The source produces X-rays with 0.84 Å wavelength. For our experiments, the sample to detector distance was fixed to 4.042 m and the detector radius was 81 mm. Scattering intensity was monitored using a Mar 165 mm diameter CCD detector operating with a resolution of 2048 by 2048. The two dimensional scattering patterns were azimuthally integrated to afford one-dimensional profiles presented as spatial frequency (q) versus scattered intensity.

Transmission Electron Microscopy (TEM) ultrathin sections (ca. 70 nm) of the polymer samples were cut using a Reichert UltraCut S Ultramicrotome with a Model FC-S addition at -100 ºC. Thin sections were placed on 300 mesh copper grids and subsequently stained with either OsO_4 or RuO_4 vapor for 10 min by exposure to a 4% aqueous solution. TEM analysis was performed on a JEOL JEM-1210 transmission electron microscope operating at 100 kV equipped with a Gatan Multiscan CCD camera.

Dynamic Mechanical Spectroscopy (DMS) experiments were conducted on Rheometric Scientific ARES strain-controlled rheometer using 25 mm plates. Samples were pressed with 2 tons of force for 5 minutes at 100 °C prior to tests. Isochronal experiments were performed with a constant frequency of 1 rad/sec with a heat or cool rate of 2 °C/min. The sample was heated from 80 °C to 260 °C and then cooled to 85 °C. This test can find the temperature where a morphological transition occurs. Discontinuous changes in the elastic G' (ω) and loss G" (ω) moduli indicate the change in either one morphology to another in an order-order transition (OOT) or the change from an ordered morphology to a disordered state (order-disorder transition or ODT).

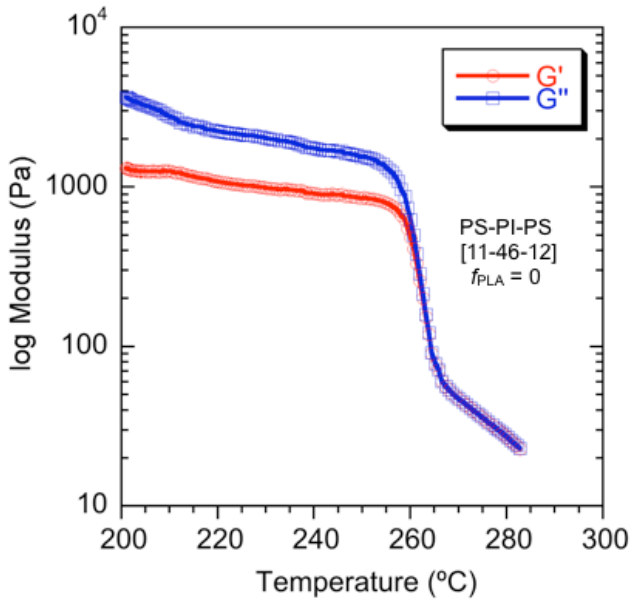

Figure 4.24. Temperature ramp for PS-PI-PS [11-46-12]. T_{ODT} at ~250ºC is evident by the discontinuous drop in the moduli (G' and G").

Channel Die Alignment: All channel die alignments were either performed at 150 ºC or 200 ºC. Samples were aligned over the course of ~45 min to 1 h.

Reciprocating Shear Alignment: Samples were shear aligned at either 160 or 180 ºC for 24 h under an argon atmosphere. Plate movement amplitude was 3.3 mm. A full cycle was completed in 6.4 s.
The PS-PI-PS triblock was aligned at 200 ºC. PS-PI-PS-PLA(0.06) was aligned at 160 ºC. PS-PI-PS-PLA(11) was aligned at 180 ºC.

Differential Scanning Calorimetry (DSC) analysis of PS-PI-PS and PS-PI-PS-PLA polymers was performed on a Q1000 instrument from TA Instruments calibrated with an Indium standard. The samples were heated to 150 ºC and then subsequently cooled to –100 °C followed by heating again to 150 °C. Samples were heated and cooled at a rate of 10 °C min^{-1}. Presented data and glass transitions

temperature measurements were taken from the second heating ramp. Data analysis (T_g) was performed on TA Instruments Universal Analysis software.

DSC analysis of PS-PEEP-PS-PLA polymers was performed on a Discovery DSC instrument from TA Instruments calibrated with an Indium standard. The samples were heated to 150 °C and then subsequently cooled to –80 °C followed by heating again to 150 °C. Samples were heated and cooled at a rate of 10 °C min^{-1}. Presented data and glass transitions temperature measurements were taken from the second heating ramp. Data analysis (T_g) was performed on TA Instruments Trios Software.

4.8 References

(1) Rubber World Website.
http://www.rubberworld.com/RWmarket_report.asp?id=679 (accessed Jan. 18, 2013)

(2) Bailey, T. S.; Pham, H. D.; Bates, F. S. *Macromolecules* **2001**, *34*, 6994-7008

(3) Fetters, L. J.; Lohse, D. J.; Richter, D.; Witten, T. A.; Zirkel, A. *Macromolecules* **1994**, 27, 4639–4647.

(4) Witzke, D. R.; Narayan, R.; *Macromolecules* **1997**, *30*, 7075-7085.

(5) Pitet, L. M.; Amendt, M. A; Hillmyer, M. A. *J. Am. Chem. Soc.* **2010**, *132*, 8230-8231.

(6)Kuraray Company Septon Division Website.
http://www.septon.info/en/septon/list_septon.html (accessed January 2, 2013)

(7) Kuraray Product Literature Provided with PS-PEEP-PS triblock.

(8) Fetters, L. J.; Lohse, D. J.; Richter, D.; Witten, T. A.; Zirkel, A. *Macromolecules* **1994**, 27, 4639–4647.

(9) Witzke, D. R.; Narayan, R.; *Macromolecules* **1997**, *30*, 7075-7085.

(10) Inci, B.; Wagener, K. B. *JACS* **2011**, *133*, 11872-11875.

(11) Rojas, G.; Inci, B.; Wei, Y.; Wagener, K. B. *JACS* **2009**, *131*, 17376-17386.

(12) Smith, J. A.; Brzezinska, K. R.; Valenti, D. J.; Wagener, K. B. *Macromolecules* **2000**, *33*, 3781-3794.

(13) Frick, E. M.; Zalusky, A. S.; Hillmyer, M. A. *Biomacromolecules* **2003**, *4*, 216-223.

(14) Meuler, A. J. Network Morphologies in Monodisperse and Polydisperse Multiblock Terpolymers. Ph. D. Dissertation, University of Minnesota, Twin Cities, 2009.

(15) Zhu, Y.; Burgaz, E.; Gido, S. P.; Staudinger, U.; Weidisch, R.; Uhrig, D.; Mays, J. M. *Macromolecules* **2006**, *39*, 4428-4436.

(16) Floudas, G.; Pakula, T.; Velis, G.; Sioula, S.; Hadjichristidis, N. *J. Chem. Phys.* **1998**, *108,* 6498.

(17) Ryu, C. Y.; Lodge, T. P. *Macromolecules* **1999**, *32*, 7190-7201.

(18) Breiner, V.; Krappe, U.; Abetz, V.; Stadler, R. *Macromol. Chem. Phys.* **1997***, 198,* 1051-1083.

(19) Qiao, L.; Hahn, S. F.; Winey, K. I. *Ind. Eng. Chem. Res.* **2006**, *45*, 5598-5602.

(20) Kim, S.; Roth, C. B.; Torkelson, J. M. *J. Polymer Sci.: Part B: Polymer Phys.* **2008**, *46*, 2754-2764.

Bibliography

Abetz, V.; Simon, P. F. W. In *Block Copolymers I*; Springer-Verlag Berlin: Berlin, 2005; Vol. 189, p 125–212.

Ahn, D.U.; Sancaktar, E. *Adv. Funct. Mater.* **2006**, *16*, 1950-1958.

Albert, J. N. L.; Bogart, T. D.; Lewis, R. L.; Beers, K. L.; Fasolka, M. J.; Hutchinson, J. B.; Vogt, B. D.; Epps, T. H. *Nano Lett.* **2011**, *11*, 1351-1357.

Albert, J. N. L.; Epps, T. H., III *Mater. Today* **2010**, *13*, 191-226.

Auriemma, F.; De Rosa, C. *Trop. J. Pharm. Res.* **2011**, *10*, 1-2.

Bailey, T. S. Morphological Behavior Spanning the Symmetric AB and ABC Block Copolymer States. Ph.D. Dissertation, University of Minnesota, Minneapolis, Minnesota, USA, **2001**.

Bailey, T. S.; Hardy, C. M.; Epps, T. H., III; Bates, F. S. *Macromolecules* **2002**, *35*, 7007-1714.

Bailey, T. S.; Pham, H. D.; Bates, F. S. *Macromolecules* **2001**, *34*, 6994-7008

Bailey, T. S.; Rzayev, J.; Hillmyer, M. A. *Macromolecules* **2006**, *39*, 8772–8781.

Bakhshayeshi, M. et al. *J. Membr. Sci.* **2011,** *379*, 239-248,

Balsamo, V.; von Gyldenfeldt, F.; Stadler, R. *Macromolecules* **1999**, *32*, 1226-1232.

Bang, J.; Jeong, U.; Ryu, D.Y.; Russell, T.P.; Hawker, C.J. *Adv. Mater.* **2009**, *21*, 4769–4792

Bang, J.; Kim, B. J.; Stein, G. E.; Russell, T. P.; Li, X.; Wang, J.; Kramer, E. J.; Hawker, C. J. *Macromolecules* **2007**, *40*, 7019–7025.

Bang, J.; Kim, S. H.; Drockenmuller, E.; Misner, M. J.; Russell, T. P.; Hawker, C. J. *J. Am. Chem. Soc.* **2006**, *128*, 7622-7629.

Baruth, A.; Rodwogin, M. D.; Erickson, M. J.; Hillmyer, M. A.; Leighton, C. ACS *Appl. Mater. and Interfaces* **2011**, *3*, 3472-3481.

Bates, F. S.; Fredrickson, G. H. *Phys. Today,* **1999**, *52*, 32–38.

Bates, F. S.; Hillmyer, M. A.; Lodge, T. P.; Bates, C. M.; Delaney, K. T.; Fredrickson, G. H. *Science*, **2012**, *336*, 434–440.

Bates, F.S.; Frederickson, G.H. *Annual Review Physical Chemistry.* **1990**, 42, 525-557.

Bernards, D. A.; Desai, T. A. *Adv. Mater.* **2010**, *22*, 2358–2362.

Bernards, D. A.; Desai, T. A. *Soft Matter* **2010**, *6*, 1621–1631.

Black, C. T.; Guarini, K. W.; Milkove, K. R.; Baker, S. M.; Russell, T. P.; Tuominen, M. T. *Appl. Phys. Lett.* **2001**, *79*, 409-411.

Black, C. T.; Ruiz, R.; Breyta, G.; Cheng, J. Y.; Colburn, M. E.; Guarini, K. W.; Kim, H. C.; Zhang, Y. *IBM Journal of Research and Development* **2007**, *51*, 605-633.

Bluemle, M. J.; Fleury, G.; Lodge, T. P.; Bates, F. S. *Soft Matter* **2009**, *5*, 1587–1590.

Bluemle, M. J.; Zhang, J. W.; Lodge, T. P.; Bates, F. S. *Macromolecules* **2010**, *43*, 4449–4452.

Bluemle, M. Morphological Behavior of Linear ABC and ABAC Block Terpolymers. Ph.D. Dissertation, University of Minnesota, Minneapolis, Minnesota, USA, **2010**.

Breiner, U.; Krappe, U.; Abetz, V.; Stadler, R. *Macrmol. Chem. Phys.* **1997**, *198*, 1051-1083.

Castelleto, V.; Hamley, I. W. *Current Opin. Sol. Stat. and Mater. Sci.* **2004**, *8,* 426-438.

Cavicchi, K. A.; Berthiaume, K. J.; Russell, T. P. *Polymer* **2005**, *46*, 11635-11639.

Cavicchi, K. A.; Zalusky, A. S.; Hillmyer, M. A.; Lodge, T. P. *Macromol. Rapid Commun.* **2004**, *25*, 704–709.

Cavicchi, K.A.; Russell, T.P. *Macromolecules* **2007**, *40*, 1181-1186.

Chatterjee, J.; Jain, S.; Bates, F. S. *Macromolecules* **2007**, *40*, 2882-2896.

Chen, L.; Hillmyer, M. A. *Macromolecules* **2009**, *42*, 4237–4243.

Chen, L.; William, P. A.; Cussler, E. L.; Hillmyer, M. A. *Journal of American Chemical Society.* **2007**, 129, 13786-13787.

Cleland, J.; Daugherty, A.; Mrsny, R. *Curr. Opin. Biotechnol.* **2001**, *12*, 212–219.

Cochran, E. W.; Bates, F. S. *Phys. Rev. Lett.* **2004**, *93*, 087802(1-4).

Cooney, D. T.; Hillmyer, M. A.; Cussler, E. L.; Moggridge, G. D. *Crystal. Rev.* **2006**, *12*, 13–24.

Corma, A. *Chemical Reviews* **1997**, *97*, 2373-2420.

Darling, S. B.; *Prog. Polym. Sci.* **2007**, *32*, 1152.

Dow Ultrafiltration Operating Specifications. http://www.dowwaterandprocess.com/products/uf/op_spec.htm (accessed November 20, 2012)

Dullien, F. A. L. In Porous media: fluid transport and pore structure; Academic Press: San Diego, 1992; pp 574.

Duong, P. H. H.; Chung, T.-S. Jeyaseelan, K.; Armugam, A.; Chen, Z.; Yang, J.; Hong, M. *J. Membr. Sci.* **2012**, *409-410,* 34-43.

Elbs, H.; Fukunaga, K.; Stadler, R.; Sauer, G.; Magerle, R.; Krausch, G. *Macromolecules* **1999**, *32*, 1204-1211.

Epps, T. H., III; Cochran, E. W.; Hardy, C. M.; Bailey, T. S.; Waletzko, R. S.; Bates, F. S. *Macromolecules* **2004**, *37*, 7085-7088.

Epps, T.H.; Cochran, E.W.; Bailey, T.S.; Waletzko, R.S.; Hardy, C.M.; Bates, F.S. *Macromolecules.* **2004**, 37, 8325-8341.

Fasolka, M. J.; Mayes, A. M.; *Annu. Rev. Mater. Res.* **2001**, *31*, 323-355.

Fetters, L. J.; Lohse, D. J.; Richter, D.; Witten, T. A.; Zirkel, A. *Macromolecules* **1994**, 27, 4639–4647.

Fink, Y.; Urbas, A. M.; Bawendi, M. G.; Joannopoulos, J. D.; Thomas, E. L. *J. Lightwave Technology* **1999**, *17*, 1963-1969.

Floudas, G.; Pakula, T.; Velis, G.; Sioula, S.; Hadjichristidis, N. *J. Chem. Phys.* **1998**, *108,* 6498.
Fredrickson, G.H.; Bates, F.S. *Annual Review of Materials Science.* **1996**, 26, 501-550.

Frick, E. M.; Zalusky, A. S.; Hillmyer, M. A. *Biomacromolecules* **2003**, *4*, 216-223.

Garlotta, D. *J. Polym. & Environ.* **2001**, *9*, 63-84.

Goldacker, T.; Abetz, V. *Macromolecules* **1999**, *32*, 5165–5167.

Gotrik, K. W.; Hannon, A. F.; Son, J. G.; Keller, B.; Alexander-Katz, A.; Ross, C. A. *ACS Nano* **2012**, *6*, 8052–8059.

Guo, F. X.; Andreasen, J. W.; Vigild, M. E.; Ndoni, S. *Macromolecules* **2007**, *40*, 3669–3675.

Guo, S.; Rzayev, J.; Bailey, T.S.; Zalusky, A.S.; Olayo-Valles, R.; Hillmyer, M.A. *Chem. Mater.* **2006**, *18*, 1719-1721.

Gupta, M. C.; Deshmukh, V. G. *Colloid & Polymer Sci.* **1982**, *260*, 514-517.

Hamley, I. W. *Nanotechnology* **2003**, *14*, R39–R54.

Hamley, Ian. Developments in Block Copolymer Science and Technology. John Wiley & Sons, LTD: West Sussex, England, 2004. pp. 1-70, 127-152, 341-359.

Hamley, Ian. *The Physics of Block Copolymers.* Oxford University Press: Oxford, England, 1998. pp 1-87, 278-310.

Hanley, K. J.; Lodge, T. P. *Macromolecules*, **2000**, *33*, 5918-5931.

Hansen, M. S.; Vigild, M. E.; Berg, R. H.; Ndoni, S. *Polym. Bull.* **2004**, *51*, 403–409.

Hardy, C. M.; Bates, F. S.; Kim, M. H.; Wignall, G. D. *Macromolecules* **2002**, *35*, 3189–3197.

Hawker, C. J.; Russell, T. P.; *MRS Bull*. **2005**, *30*, 952.

Hiemenz, P. C.; Lodge, T. P.; *Polymer Chemistry*, Second Edition; CRC Press, Taylor and Francis Group: Boca Raton, Fl, **2007**, pp 24-28, 117-135, 153, 247-283, 291- 296, 422-446, 472-497.

Hillmyer, M. A. *Adv. Polym. Sci.* **2005**, *190*, 137-181.

Hillmyer, M. A. In *Block Copolymers II*; Abetz, V., Ed.; Advances in Polymer Science Series; Springer: Berlin/Heidelberg 2005; Vol. 190, pp 137–181.

Hillmyer, M.A. *Adv. Polym. Sci.* **2005**, *190*, 137-181.

Ho, R.-M.; Tseng, W.-H.; Chiang, Y.-W.; Lin, C.-C.; Ko, B.-T.; Huang, B.-H. *Polymer* **2005**, *46*, 9362-9377.

Holden, G.; Bishop, E.T.; Legge, N.R.; *Journal of Polymer Science: Part C.* **1969**, 26, 37-57.

Hou, X.; Guo, W.; Jiang, L. *Chem. Soc. Rev.* **2011**, *40*, 2385-2401.

http://www.kraton.com/Products/Kraton_D_SIS/

http://www.rubberworld.com/RWmarket_report.asp?id=679 (accessed Jan. 18, 2013)

http://www.septon.info/en/septon/list_septon.html (accessed January 2, 2013)
Hyflux Gurgle Tap Filter Webpage. http://www.hyfluxshop.com/Lists/TechSpec/Gurgle%20F38_F380905-02[1].pdf (accessed September 3, 2012).

Inci, B.; Wagener, K. B. *JACS* **2011**, *133*, 11872-11875.

Jackson, E. A.; Hillmyer, M. A. *ACS Nano* **2010**, *4*, 3548–3553.

Jackson, E. A.; Lee. Y.; Hillmyer, M. A. *Submitted to Macromolecules* **2012.**

Jeong, U; Ryu, D.Y.; Kho, D.H.; Kim, J.K.; Goldbach, J.T.; Kim, D.H.; Russell, T.P. *Adv. Mater.* **2004**, *16*, 533-536.

Jung, Y. S.; Ross, C. A. *Adv. Mater.* **2009**, *21*, 2540–2545.

Kim, M. I.; Wakada, T.; Akasaka, S.; Nishitsuji, S.; Saijo, K.; Hasegawa, H.; Ito, K.; Takenaka, M. *Macromolecules* **2008**, *41*, 7667-7670.

Kim, S. H.; Misner, M. J.; Xu, T.; Kimura, M.; Russell, T. P. *Adv. Mater.* **2004**, *16*, 226–231.

Kim, S. Y.; Misner, M. J.; Russell, T. P. *Adv. Mater.* **2004**, *16*, 2119–2123.

Kim, S.; Roth, C. B.; Torkelson, J. M. *J. Polymer Sci.: Part B: Polymer Phys.* **2008**, *46*, 2754-2764

Park, C.; Yoon, J.; Thomas, E. L. *Polymer* **2003**, *44*, 6725–6760.

Xia, G.; Wang, S.; Jeong, S-J. *Nanotechnology* **2010**, *21*, 1-5.

Kitano, H. et al. *Langmuir*, **2007**, *23*, 6404-6410.

Krappe, U.; Stadler, R.; Voight-Martin, I. *Macromolecules* **1995**, *28*, 4558-4561.

Kricheldorf, H. R.; Quirk, R. P.; Holden, G. *Thermoplastic elastomers*; 3rd ed.; Hanser Gardner Publications: Cincinnati, 2004.

Kubo, T.; Wang, R. F.; Olson, D. A.; Rodwogin, M. A.; Hillmyer, M. A. *Appl. Phys. Lett.* **2009**, *93*, 133112(1–3).

Kubo, T.; Wang, R.F.; Olson, D.A.; Rodwogin, M.; Hillmyer, M.A.; Leighton, C. *Appl. Phys. Lett.* **2008**, *93*, 133112.

Kudose, I. Kotaka, T. *Macromolecules* **1984,** *17*, 2325-2332.

Kukla, V. Kornatowski, J.; Demuth, D.; Girnus, I.; Pfeifer, H.; Rees, L. V. C.; Schunk, S.; Unger, K.; Karger, J. *Science* **1996**, *272*, 702–703.

Kuraray Product Literature Provided with PS-PEEP-PS triblock.

Lee, D. H.; Park, S.; Gu, W.; Russell, T. P. *ACS Nano* **2011**, *5*, 1207–1214.

Lee, J. S.; Hirao, A.; Nakahama, S. *Macromolecules* **1988**, *21*, 274–276.

Li, M.; Coenjarts, C.; Ober, C. K. Patternable Block Copolymers. In *Block Copolymers II, Advances in Polymer Science*; V. Abetz, Ed.; Springer: Heidelberg, Germany, 2005; 190, pp 183–226.

Li, X.; Fustin, C.-A.; Lefevre, N.; Gohy, J.-F.; De Feyter, S.; De Baerdemaeker, J.; Egger, W.; Vankelecom, I. F. J. *J. Mater. Chem*. **2010**, *20*, 4333–4339.

Lim, S. C.; Kim, S. H.; Lee, J. H.; Kim, M. K.; Kim, D. J.; Zyung, T. *Synth. Met.* **2005**, *148,* 75-79.

Liu, G.; Ding, J.; Hashimoto, T.; Kimishima, K.; Winnik, F. M.; Nigam, S. *Chem. Mater.,* **1999**, *11*, 2233–2240.

Liu, G.; Ding, J.; Stewart, S. *Angew. Chem., Int. Ed.* **1999**, *38*, 835–838.

Lo, K. H.; Chen, M. C.; Ho, R. M.; Sung, H. W. *ACS Nano* **2009**, *3*, 2660–2666.

Logar, N. Z.; Kaucic, V. *Acta Chim. Slov.* **2006**, *53*, 117–135.

Lohmeijer, B. G. G.; Pratt, R. C.; Leibfarth, F.; Logan, J. W.; Long, D. A.; Dove, A. P.; Nederberg, F.; Choi, J.; Wade, C.; Waymouth, R. M.; Hedrick, J. L. *Macromolecules* **2006**, *39*, 8574–8583.

Mahanthappa, M.K.; Hillmyer, M.A.; Bates, F.S. *Macromolecules.* **2008**, 41, 1341-1351.
Mao, H.; Arrechea, P. L.; Bailey, T. S.; Johnson, B. J. S.; Hillmyer, M. A. *Faraday Discuss.* **2005**, *128,* 149–162.

Mao, H.; Hillmyer, M. A. *Soft Matter* **2006**, *2*, 57–59.

Martin, F.; Walczak, R.; Boiarski, A.; Cohen, M.; West, T.; Cosentino, C.; Ferrari, M. *J. Controlled Release* **2005**, *102*, 123–133.

Matsen, M. *Journal of Chemical Physics.* **1999**, *111*, 7139-7146.

Matsen, M. *Journal of Chemical Physics*. **2000**, 113, 13, 5539-5545.

Matsen, M.W.; Bates, F.S. *Macromolecules*. **1996**, 29, 7641-7644

Matsushita, Y.; Tamura, M; Noda, I. *Macromolecules* **1994**, *27*, 3680-3682.

Mehta, A.; Zydney, A. L. *J. Membr. Sci.* **2005**, *249*, 245–249.

Meuler, A. J. Network Morphologies in Monodisperse and Polydisperse Multiblock Terpolymers. Ph. D. Dissertation, University of Minnesota, Twin Cities, 2009.

Meuler, A. J.; Hillmyer, M. A.; Bates, F. S. *Macromolecules Review* **2009**, *42*, 7221-7250.

Mogi, Y.; Kotsuji, H.; Kaneko, Y.; Mori, K.; Matsushita, Y.; Noda, I. *Macromolecules* **1992**, *25*, 5408-5411.

Mogi, Y.; Mori, K.; Matsushita, Y.; Noda, I. *Macromolecules* **1992**, *25*, 5412-5415.

Mogi, Y.; Nomura, M.; Kotsuji, H.; Ohnisi, K.; Matsushita, Y.; Noda, I. *Macromolecules* **1994**, *27*, 6755-6760.

Mulherkar, P. van Reis, R. *J. Membr. Sci.* **2004**, *236*, 171-182.

Mykhaylyk, T.A.; Mykhaylyk, O.O.; Collins, S.; Hamley, I.W. *Macromolecules* **2004**, *37*, 3369-3377.

Nunes, S. P.; Sougrat, R.; Hooghan, B.; Anjum, D. H.; Behzad, A. R.; Zhao, L.; Pradeep, N.; Pinnau, I.; Vainio, U.; Peinemann, K.-V. *Macromolecules* **2010**, *43*, 8079–8085.

Nuxoll, E. E.; Hillmyer, M. A.; Wang, R. F.; Leighton, C.; Siegel, R. A. *ACS Appl. Mater. & Interfaces* **2009**, *1*, 888–893.

Olayo-Valles, R.; Guo, S.W.; Lund, M.S.; Leighton, C.; Hillmyer. M.A. *Macromolecules* **2005**, *38*, 10101-10108.
Olson, D. A.; Chen, L.; Hillmyer, M. A. *Chem. Mater.* **2008**, *20*, 869–890.

Ow, H.; Larson, D. R.; Srivastava, M.; Baird, B. A.; Webb, W. W.; Wiesner, U. *Nano Lett.* **2004**, *5*, 113-117.

Park, C.; Yoon, J.; Thomas, E. L; *Polymer* **2003**, *44*, 6725-6760.

Park, D.S; Sancaktar, E. *Current Nanoscience*, **2012**, *8*, 244-248.

Park, M., et al., *Science* **1997** *276*, 1401.

Park, S., et al., *ACS Nano* **2008**, *2*, 766.

Park, S.; Kim, B.; Xu, J.; Hofmann, T.; Ocko, B. M.; Russell, T. P. *Macromolecules* **2009**, *42*, 1278-1284.

Pearson, R.A.; Sue, H.-J.; Yee, A.F.; Toughening of Plastics: Advances in Modeling and Experiments. *ACS Symposium Series 759.* **2000**, Oxford University Press. Washington, D. C.

Pedone, A.; Bloino, J.; Monti, S.; Prampolini, G.; Barone, V. *Phys. Chem. Chem. Phys.* **2009**, *12*, 1000-1006.

Peinemann, K.-V.; Abetz, V. Simon, P. F. W. *Nature* **2007**, *6*, 992–996.

Pharmacos Webpage on Dextran Properties. http://www.dextran.net/dextran-physical-properties.html (accessed November 20, 2012).

Phillip, W. A. Block Polymer Membranes for Selective Separations. Ph. D. Dissertation, University of Minnesota, 2009. p. 167.

Phillip, W. A.; Amendt, M.; O'Neill, B.; Chen, L.; Hillmyer, M. A.; Cussler, E. L. *ACS Appl. Mater. Interfaces* **2009**, *1*, 472–480.

Phillip, W. A.; Dorin, R. M.; Werner, J.; Hoeks, E. M. V.; Wiesner, U.; Elimelech, M. *Nano Lett.* **2011**, *11*, 2892–2900.

Phillip, W. A.; O'Neill, B.; Rodwogin, M.; Hillmyer, M. A.; Cussler, E. L. *ACS Appl. Mater. & Interfaces.* **2010**, *2*, 847–853.

Phillip, W. A.; Rzayev, J.; Hillmyer, M. A.; Cussler, E. L. *J. Membr. Sci.* **2006**, *286*, 144–152.

Phillip, W.; Cussler, E.; O'Neill, B.; Amendt, M.; Hillmyer, M. Utilization of Block Copolymers as Ultrafiltration Membranes. Abstract for American Institute of Chemical Engineers Annual Meeting, **2008**. Philadelphia.

Phillip, W.A.; O'Neill, B.; Rodwogin, M.; Hillmyer, M.A.; Cussler, E.L. *ACS Appl. Mater. Interfaces* **2010**, *2*, 847-853.

Phillip, W.A.; Rzayev, J.; Hillmyer, M.A.; Cussler, E.L. *J. Membr. Sci.* **2006**, *286*, 144-152. Pimpin, A.; Srituravanich, W. *Eng. J.* **2011** *16* .

Pitet, L. M.; Amendt, M. A; Hillmyer, M. A. *J. Am. Chem. Soc.* **2010**, *132*, 8230-8231.

Polymer Handbook, 4th ed.; Brandup, J.; Immergut, E. H., Grulke, E., Abe, A., Bloch, D. R., Eds.; John Wiley & Sons; New York, 1999, 2005.

Qiao, L.; Hahn, S. F.; Winey, K. I. *Ind. Eng. Chem. Res.* **2006**, *45*, 5598-5602.

Querelle, S.; Jackson, E. A.; Hillmyer, M. A.; Cussler, E. *In preparation.*

Rodwogin, Marc D.; Spanjers, Charles S.; Leighton, C.; Hillmyer, Marc A. *ACS Nano* **2010**, *4*, 725–732.

Rojas, G.; Inci, B.; Wei, Y.; Wagener, K. B. *JACS* **2009**, *131*, 17376-17386.

Rubber World Website.

Ruiz, R., et al., *Science* **2008**, *321*, 936.

Ryu, C. Y.; Lodge, T. P. *Macromolecules* **1999**, *32*, 7190-7201.

Rzayev, J.; Hillmyer, M. A. *J. Amer. Chem. Soc.* **2005**, *127*, 13373–13379.

Rzayev, J.; Hillmyer, M. A. *Macromolecules* **2005**, *38*, 3–5.

Rzayev, J.; Hillmyer, M. A. *Macromolecules*. **2005**, 1, 3-5.

Schacher, F.; Rudolph, T.; Wieberger, F.; Ulbricht, M.; Muller, A. H. E. *ACS Appl. Mater. & Interfaces* **2009**, *1*, 1492–1503.

Schacher, F.; Ulbricht, M.; Muller, A. H. E. *Adv. Funct. Mater.* **2009**, *19*, 1040–1045.

Schafer, A. I.; Davey, J. Ultrafiltration to Supply Drinking Water in International Development: A Review of Opportunities. *Appropriate Technologies for Environmental Protection in the Developing World.* Springer Science and Business Media B.V.: Edinburgh, UK, 2009; pp 151–168.

Schmalz, H.; Boker, A.; Lange, R; Krausch, G.; Abetz, V. *Macromolecules.* **2001**, 34, 8720-8729

Segalman, R. A.; *Mater. Sci. Eng., R* **2005**, *48*, 191-226.

Shefelbine, T. A.; Vigild, M. E.; Matsen, M. W.; Hadjuk, D. A. Hillmyer, M. A.; Cussler, E. L.; Bates, F. S. *J. Am. Chem. Soc.* **1999**, *121*, 8457-8465.

Shibayama, M.; Hasegawa, H.; Hashimoto, T.; Kawai, H. *Macromolecules* **1982**, *15*, 274-280.

Siegel, R. A.; Gu, Y. D.; Lei, M.; Baldi, A.; Nuxoll, E. E.; Ziaie, B. *J. Controlled Release* **2010**, *141*, 303–313.

Simon PFW, Ulrich R, Spiess HW, Wiesner U. *Chem. Mater.* **2001,** *13,* 3464.

Smith, J. A.; Brzezinska, K. R.; Valenti, D. J.; Wagener, K. B. *Macromolecules* **2000**, *33*, 3781-3794.

Sperschneider, A.; Scacher, F.; Gawenda, M.; Tsarkova, L.; Muller, A. H. E.; Ulbricht, M.; Krausch, G.; Kohler, J. *Small* **2007**, *3*, 1056–1063.

Stadler, R.; Auschra, C.; Beckmann, J.; Krappe, U.; Voight-Martin, I.; Leibler, L. *Macromolecules* **1995**, *28*, 3080-3097.

Stoykovich, M. P.; Nealey, P. F. *Materials Today* **2006**, *9*, 20.

TdB Consultancy Website. www.tdbcons.se/tdbcons2/attachment/tritc_dextran.pdf (accessed November 20, 2012).

Tseng, Y-C.; Darling, S. B.; *Polymers*, **2010**, *2*, 470-489.

Uehara, H. Kakiage, M.; Sekiya, M.; Sakuma, D. Yamonobe, T. Takano, N. Barraud, A.; Meurville, E.; Ryser, P. *ACS Nano* **2009**, *3*, 924–932.

Uehara, H.; Yoshida, T.; Kakiage, M.; Yamanobe, T.; Komoto, T.; Nomura, K.; Nakajima, K.; Matsuda, M. *Macromolecules* **2006**, *39*, 3971–3974.

Vayer, M.; Hillmyer, M. A.; Dirany, M.; Thevenin, G.; Erre, R.; Sinturel, C. *Thin Solid Films* **2010**, *518*, 3710–3715.

Walker, B. M.; Rader, C. P. *Handbook of thermoplastic elastomers*; 2nd ed.; Van Nostrand Reinhold: New York, 1988.

Wang, R.; Hu, K.; Jiang, Z.; Zhou, D.; *Macromolecular Theory and Simulations.* **2005**, 14, 256-266.

Wang, R.; Xu, T. *Polymer.* **2007**, 48, 15, 4601-4608.

Witzke, D. R.; Narayan, R.; *Macromolecules* **1997**, *30*, 7075-7085.

Yamauchi, L.; Akasaka, S.; Hasegawa, H.; Iatrou, H.; Hadjichristidis, N.; *Macromolecules,* **2005**, *38*, 8022.

Yang, S. Y.; Park, J.; Yoon, J.; Ree, M.; Jang, S. K.; Kim, J. K. *Adv. Func. Mater.* **2008**, *18*, 1371–1377.

Yang, S. Y.; Ryu, I.; Kim, H. Y.; Kim, J. K.; Jang, S. K.; Russell, T. P. *Adv. Mater.* **2006**, *18*, 709–712.
Yang, S. Y.; Yang, J. A.; Kim, E. S.; Jeon, G.; Oh, E. J.; Choi, K. Y.; Hahn, S. K.; Kim, J. K. *ACS Nano* **2010**, *4*, 3817–3822.

Yave, W.; Car, A.; Funari, S. S.; Nunes, S. P.; Peinemann, K. V. *Macromolecules* **2010**, *43*, 326–333.

Zalusky, A. S.; Olayo-Valles, J. H.; Taylor, C. J.; Hillmyer, M. A. *Macromolecules* **2001**, *123*, 1519.

Zalusky, A. S.; Olayo-Valles, R.; Wolf, J. H.; Hillmyer, M. A. *J. Am. Chem. Soc.* **2002**, *124*, 12761.

Zalusky, Andy. Nanoporous Materials From Ordered Polylactide-Containing Block Copolymer Templates. Ph.D. Dissertation, University of Minnesota, Minneapolis, Minnesota, USA, **2003**.

Zhang, J.; Bates, F. *J. Am. Chem. Soc.* **2012**, *134*, 7636-7639.

Zhang, J.; Sides, S.; Bates, F. *Macromolecules* **2012**, *45*, 256-265.

Zhang, Z.; Bates, F. S. *J. Am. Chem. Soc.* **2012**, *134,* 7636-7639.

Zhou, N.; Bates, F. S.; Lodge, T. P. *Nano Lett.* **2006**, *6*, 2354–2357.

Zhu, Y.; Burgaz, E.; Gido, S. P.; Staudinger, U.; Weidisch, R.; Uhrig, D.; Mays, J. M. *Macromolecules* **2006**, *39*, 4428-4436.

Appendix A

Tape Casting of PS-PI-PS-PLA

This appendix describes draw down coating of PS-PI-PS-PLA using a controlled solvent system. Large area films were prepared with perpendicular PLA cylinder orientation.

A.1 Draw Down Coating

A draw down coating machine (**Figure A.1**) was used to prepare films of PS-PI-PS-PLA on 4 inch Si wafers. A solvent chamber was made prepared and used for a controlled solvent casting environment. The solvent chamber was fitted with a nitrogen inlet line, a glass cover and two small holes for copper wire attachments. In a typical experiment, a wire wound rod was attached to the motorized draw down bar via two copper wires. A Si wafer was taped to a plastic sheet placed under the solvent chamber box. The wire wound rod was centered at the far edge of the Si wafer. Before casting a film, the solvent box was purged by first covering the box with the thick glass slide and then purging with Nitrogen gas for 5 minutes. After 5 minutes, a polymer solution was dispersed by syringe onto the silicon wafer either directly in front of the rod in a line or by filling the surface of the wafer with a larger volume of solvent.

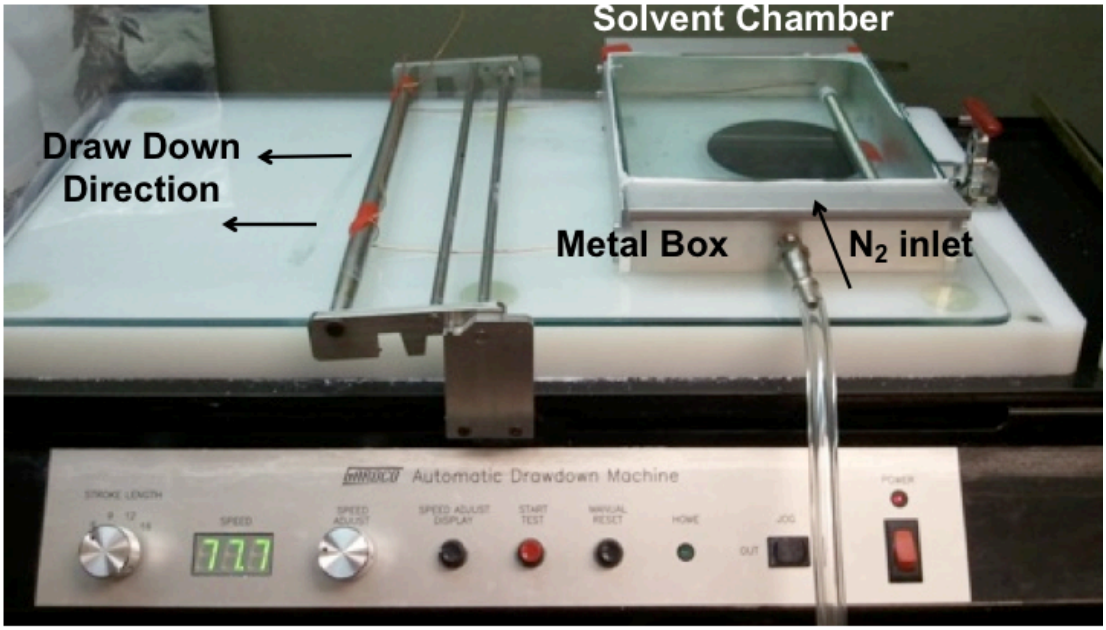

Figure A. 1. Draw down casting setup with automatic drawdown machine, controlled solvent chamber, wire-wound rod and Si wafer.

After dispensing the polymer solution, the drawdown mechanism was initiated and the wire wound rod was pulled across the Si substrate. A top view of the drawdown setup is shown in **Figure A.2**. The quality of film coating (by eye) varied depending on the type of solvent and evaporation rate, how much solvent, the placement of the rod onto the wafer and how level the substrate and rod were in the plane of coating.

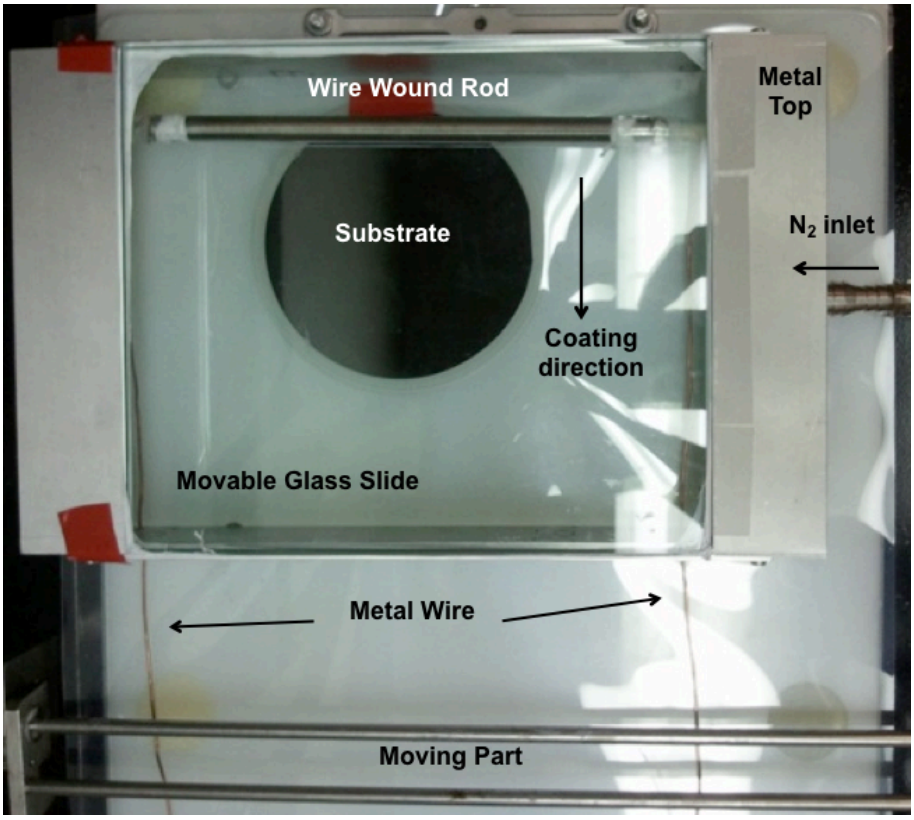

Figure A.2. Top view of drawdown setup.

The optimal results were acquired when the following procedure was used. First, the chamber box (with Si wafer inside) was purged with N_2 for 5 minutes. Second, 1 mL of the PS-PI-PS-PLA/PLA blend solution was dispensed across the entire surface of the Si wafer. The optimal solution used was a 1-1.15 wt% solution of PS-PI-PS-PLA/PLA (95/5 wt/wt) in a 70/30 vol/vol THF/Acetone mixture. For the drawdown rod, a small #2.5 size wire wound rod (equivalent to a 6.4 μm wet film thickness) provided uniform thin films after solvent evaporation. A very low gentle flow of nitrogen across the films surface during the drawdown procedure increased the solvent evaporation rate and led to improved uniformity across the film.

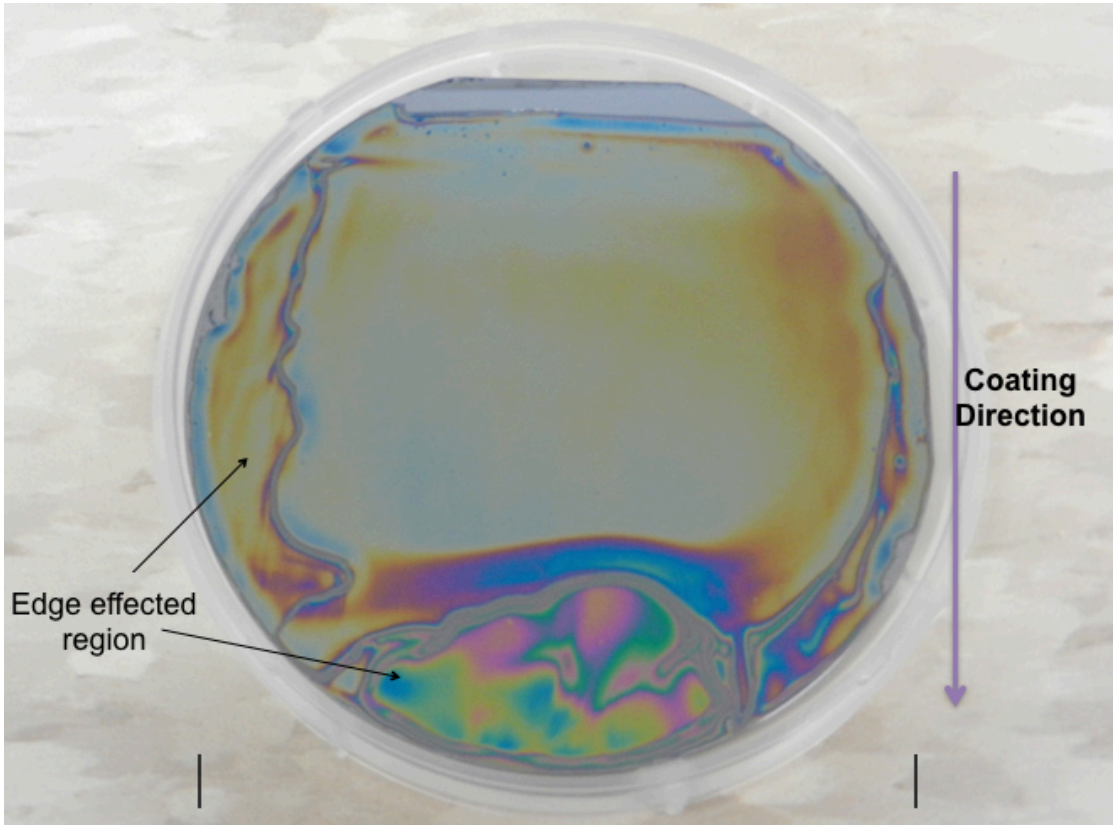

Figure A.3. Surface of Si wafer (HMDS modified) after draw down using above procedure. A large portion of the Si wafer is covered with a uniformly colored film (indicative of relatively uniform thickness).

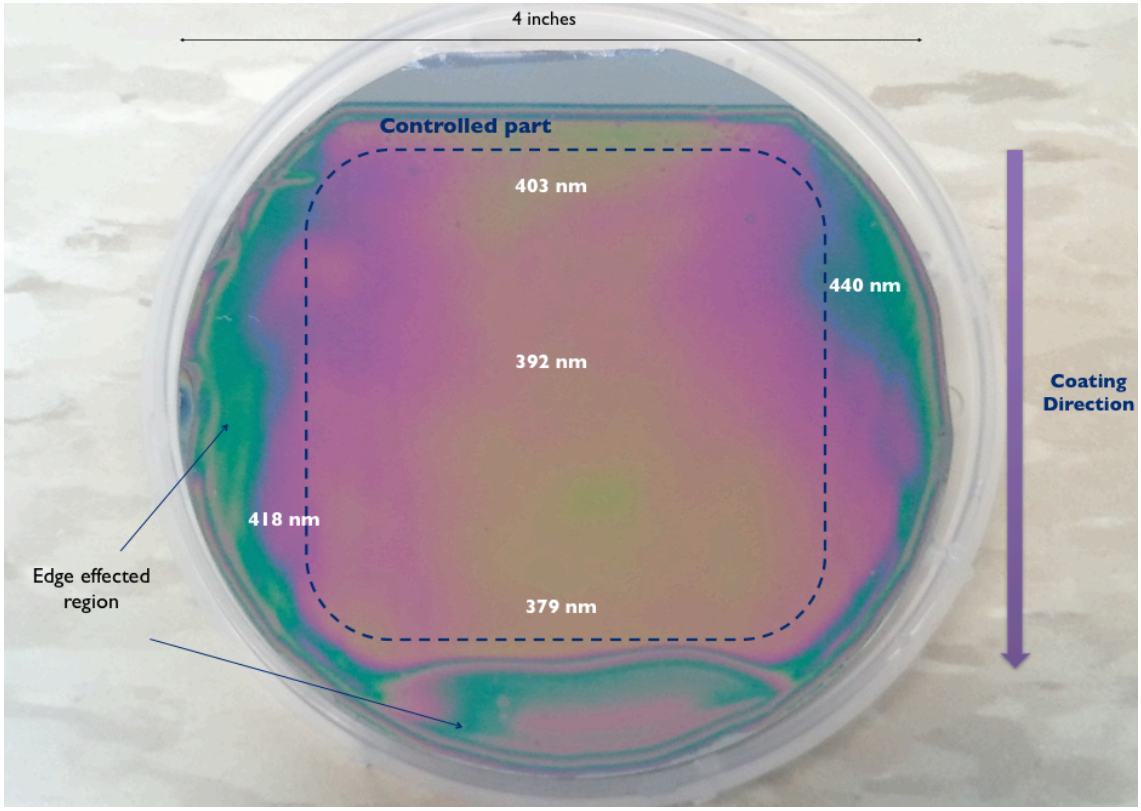

Figure A.4. Surface of Si wafer (HMDS modified) after draw down using above procedure. A large portion of the Si wafer is covered with a uniformly colored film (indicative of relatively uniform thickness).

AFM analysis of the block polymer microstructure provided evidence that the specific solvent condition led to perpendicular orientation of cylindrical domains. The specific solvent mixture was used after previous experiment with a controlled solvent annealing chamber (See **Chapter 3**). The above procedure worked well at both the macroscale (**Figure A.3** and **Figure A.4**) and nanoscale (**Figure A.5**). The polymer film coated Si wafer was broken into 12 pieces and each piece was analyzed by tapping mode AFM (**Figure A.5**). Each portion of the film, regardless of thickness, contained hexagonally ordered domains, which are consistent with perpendicular cylindrical domains. Based on similar results in solvent annealed films, these domains were thought to be perpendicular PLA cylinders. Perpendicular orientation was apparent even the thickest portions of the films (up

to 229 nm). Film thicknesses noted in **Figure A.5** were measured by ellipsometry. A large scale AFM image is shown in **Figure A.6**.

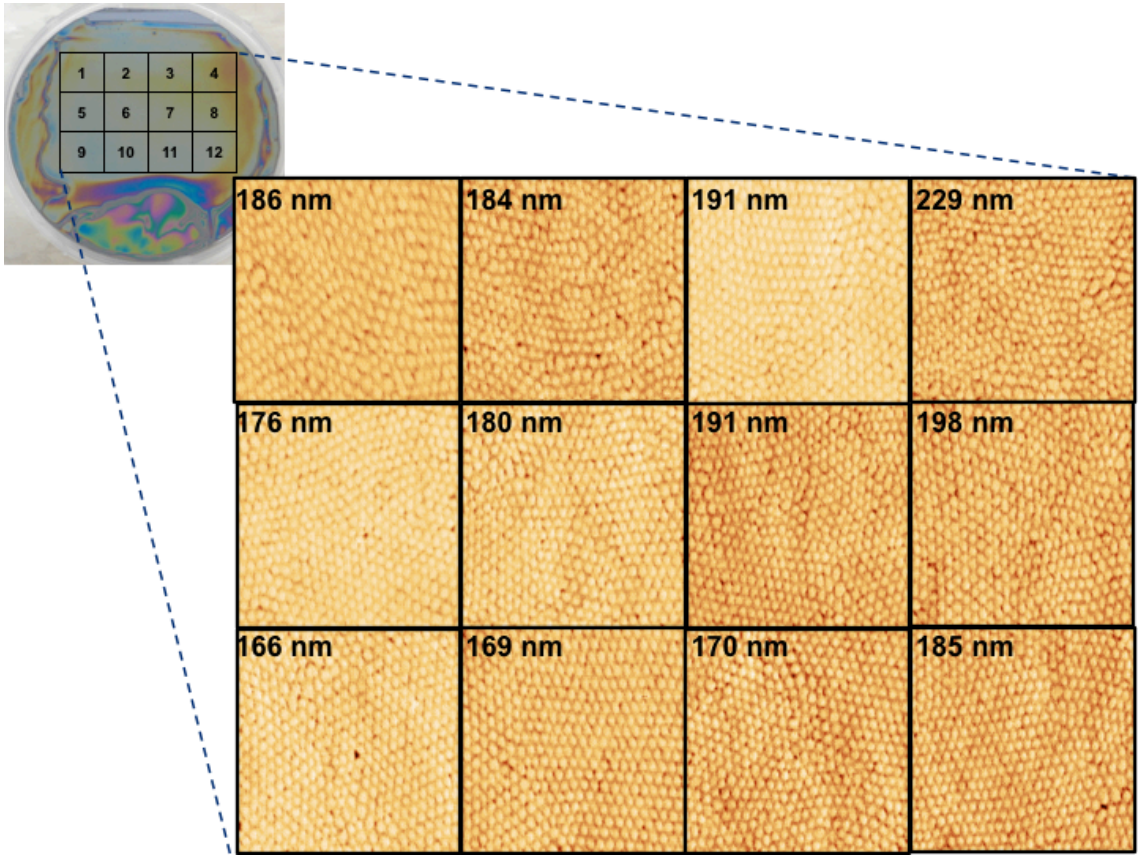

Figure A.5. AFM results for film prepared by drawdown procedure. Corresponding portions of the large coated wafer are displayed in the grid covering the Si wafer image.

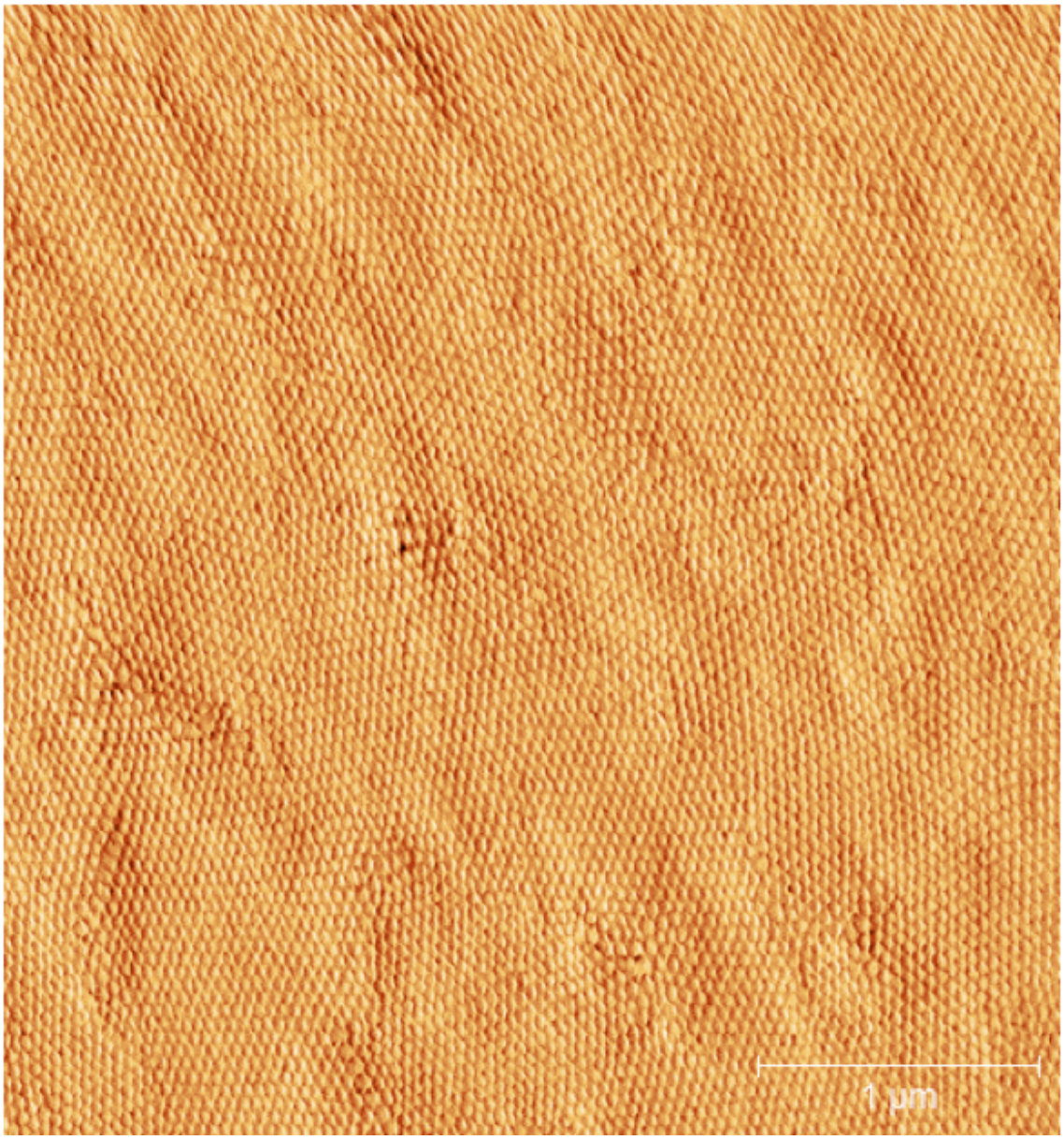

Figure A.6. Large Scale tapping mode AFM image showing the consistent hexagonal structure across the film.

Using the same etching procedure that was outlined in Chapter 3 (RIE plus base etching), drawdown films were base-etched to remove PLA and create nanopores. SEM images after etching show that hexagonally packed pores across the surface of the film (**Figure A.7**). The microtructure is consistent with the porous cylinder

morphology observed in **Chapter 3**. Despite wrinkles or thickness variations in the film, the hexagonal porous structure is still prevalent and the film remains intact. No ripping or tears were present suggesting that the films are mechanically robust. This is an encouraging result. This casting procedure could be applied to prepare a large area nanoporous membrane. The particular solvent system is not amenable to the composite coating method using in **Chapter 2** since THF and acetone are miscible with water. Another strategy would be required to be able to cast films from THF and acetone and creating a uniform coating on top of a porous support.

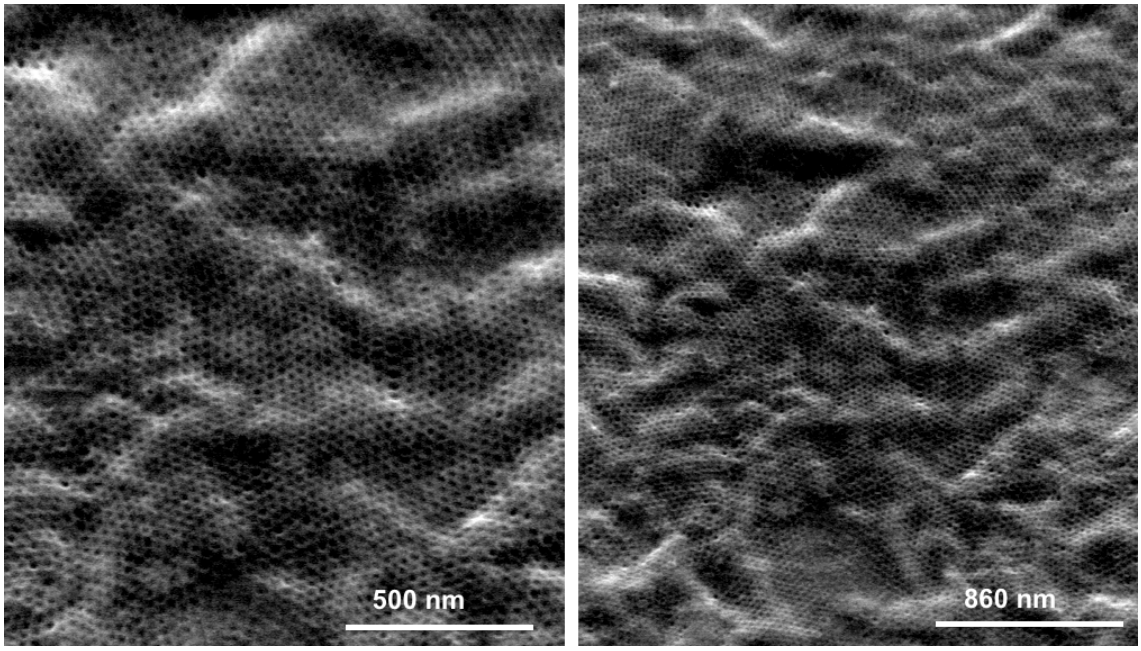

Figure A.7. SEM images of drawdown coated films after RIE and base etching.